2008

Solid-Phase Synthesis of Asymmetrically Substituted Phthalocyanines

Sultan Sibel Erdem
Louisiana State University and Agricultural and Mechanical College, serdem1@lsu.edu

SOLID-PHASE SYNTHESIS OF ASYMMETRICALLY SUBSTITUTED PHTHALOCYANINES

A Dissertation

Submitted to the Graduate Faculty of the
Louisiana State University and
Agricultural and Mechanical College
In partial fulfillment of the
Requirements for the degree of
Doctor of Philosophy

In

The Department of Chemistry

By
Sultan Sibel Erdem
B. S., Marmara University, 2001
May, 2009

Acknowledgments

During my graduate study at Louisiana State University, I am indebted to great number of people. Initially, I want to express my sincere gratitude to my advisor Professor Robert P. Hammer. There are no words that can describe my gratitude and respect that I have towards to him. I truly appreciate his exceptional support, encouragement, guidance and patience throughout my graduate career. His continuous encouragement and belief in me kept me up on my feet. Not only his depth of knowledge in the field of chemistry but also his positive attitude and work ethics have inspired me ever since I have joined his research group. It was a great privilege and honor to work under his supervision. I also would like to thank Dr. Irina V. Nesterova for her invaluable assistance with spectroscopic and chromatographic analyses and sharing her knowledge with me. I would like to thank Dr. Frank Fronczek for the crystallography work and Mr. Tim Jenson for performing cell studies. I would like to thank my committee members, Dr. M. Graca H. Vicente, Dr. Doug Gilman, Dr. Randall W. Hall and Dr. Beilie Ge for taking time to read this dissertation. I also thank Dr. Steven A. Soper and Dr. M. Graca H. Vicente for financial support through their grants from the National Science Foundation and National Institutes of Health. I also thank former and current members of Hammer research group, especially Gregory T. McCandless, Dr. Marcus A. Etienne and Dr. Jia Wang for their valuable friendship and making me feel like I am home here**.** I also want to thank Cyrus K. Bett for our valuable discussions about peptide synthesis.

Special thanks go to my spouse, Mustafa Erdem, for his endless support, encouragement and belief in me ever since he stepped in my life. I deeply appreciate his encouragement to study abroad and his great concern of my career. Without him, I would not succeed. In closing, I want to thank my parents and my brother for their tireless support from thousands miles away.

Table of Contents

Acknowledgments..…….....ii

List of Abbreviations and Symbols…….....v

Abstract…….....viii

Chapter
1 Introduction…….....1
1.1 Phthalocyanines…….1
1.1.2 Synthesis of Phthalocyanines……..3
1.1.3 Polymer Supports…….……..…….5
1.1.4. Applications of Phthalocyanines……6
1.2 Objective of the Project……7
1.3 References……..8

2 Solution Phase Synthesis of Phthalonitrile Precursors and Phthalocyanines…….. 12
2.1 Introduction……..12
2.2 Results and Discussion……11
2.2.1 Synthesis of Phthalonitriles Bearing Carboxylate, Amine and Nitro Groups……13
2.2.2 Synthesis of Polyethyleneglycol Substituted Phthalonitriles……...…….17
2.2.3 Solution-Phase Synthesis of Phthalocyanines…… 27
2.3 Conclusion and Future Work ……...……...38
2.4 Experimental…….39
2.4.1 General Experimental Information……39
2.4.2 Experimental Procedures……..39
2.5 References……52

3 Solid-Phase Synthesis of Asymmetrically Substituted "AB_3-Type" Phthalocyanines…..55
3.1 Introduction……..55
3.2 Results and Discussion……57
3.2.1 Solid-Phase Synthesis of "AB_3" Type Oligoethyleneglycol Substituted Phthalocyanines…….57
3.2.3 Activation of Hydroxy Functionalized Phthalocyanines Towards Conjugation to Biomolecules…….69
3.2.4 FRET-RET Pairing……...72
3.3 Conclusion and Future Work……...81
3.4 Experimental……82
3.4.1 General Experimental Information……...82
3.4.2 Experimental Procedures……..84
3.5 References……90

4 Microwave-Assisted Solid-Phase Synthesis of AB_3 Type Asymmetrically Substituted Mono-Amine Functionalized Phthalocyanines and Oligonucleotide Labeling Techniques……94
4.1 Introduction……..94
4.2 Results and Discussion……96
4.2.1 Effects of the Loading of the Resin and the Reaction Time on the Outcome of the Cyclotetramerization Reaction……96
4.2.2 Effects of Solvent and Incoming Reagent Concentration on the Outcome of the Cyclotetramerization Reaction……...102
4.2.3 Effects of Linker Length and Incoming Reagent's Concentration on the Outcome of the Cyclotetramerization Reaction……...110
4.2.4 Covalent Labeling of Oligonucleotides with Amine Functionalized Phthalocyanines……...116
4.2.5 Solid-Phase Synthesis of Phthalocyanine-Peptide Conjugate……122
4.3 Conclusion and Future Work……124
4.4 Experimental……..125
4.4.1 General Experimental Information……125
4.4.2 Experimental Procedures……127
4.5 References……134

5 In vitro Biological Evaluation of Oligoethyleneglycol Substituted Phthalocyanines for Photodynamic Therapy……137
5.1 Introduction……..……..137
5.2 Results and Discussion……..……140
5.2.1 Time-Dependent Cellular Uptake……...…141
5.2.2 Dark Cytotoxicity……142
5.2.3 Phototoxicity……...143
5.2.4 Intracellular Localization……145
5.3 Conclusion……..……150
5.4 Experimenta……...……150
5.5 References……..……152

Appendix
A- X-ray Diffraction Data……...……..155

B- Letter of Permission……...……..206

Vita……...208

List of Abbreviation and Symbols

δ	chemical shift
Boc	tert-butyloxycarbonyl
BuOH	butanol
CCA	α-cyano-4-hydroxycinnamic acid
^{13}C-NMR	carbon 13 nuclear magnetic resonance
DBU	1,8-diazabicyclo[5.4.0]-undec-7-ene
DIEA	diisopropylethyl amine
DMEM	Dulbecco's modified eagle medium
DMF	N,N-dimethylformamide
EDC	1-ethyl-3-(3-dimethylaminopropyl) carbodiimide
EtOAc	ethyl acetate
EtOH	ethanol
FBS	fetal bovine serum
FIB	focused ion beam
Fmoc	9-fluorenylmethoxycarbonyl
FRET	fluorescence resonance energy transfer
FTIR	fourier transform infrared spectroscopy
h	hour(s)
HBTU	O-(1-benzotriazol-1-yl)-1,1,3,3-tetramethyluronium Hexafluorophosphate
HEPES	4-(2-Hydroxyethyl)-1-piperazineethanesulfonic acid
HMDS	hexamethyldisilazane
^{1}H NMR	proton nuclear magnetic resonance
HOBt	1-hydroxybenzotriazole

HPLC	high performance liquid chromatography
HRMS	high resolution mass spectrometry
IR	infrared
Lys	lysine
M	molar
mM	milimolar
μM	micromolar
MALDI	matrix assisted laser desorption/ionization
MEM	minimum essential medium
min	minute(s)
mL	milliliter
MS	mass spectrometry
mmol	millimol
Mtt	4-methyltrityl
m/z	mass to charge ratio
NHS	N-hydroxysuccinimide
nm	nanometer
Pc	phthalocyanine
PDT	photodynamic therapy
PEG	polyethylene glycol
ppm	parts per million
PS	polystyrene
RET	resonance energy transfer
TEAA	triethylammonium acetate

rt	room temperature
THF	tetrahydrofuran
TFA	trifluoroacetic acid
TIPS	triisopropylsilane
TLC	thin layer chromatography
Tyr	tyrosine

Abstract

Phthalocyanines (Pcs) are excellent candidates for use as fluorophores for near-infrared (near-IR) fluorescent tagging of biomolecules and as photodynamic therapy (PDT) agents. Synthesis of Pcs with asymmetrical substitution on the periphery is often difficult due to the problems during the purification of the Pc mixtures obtained.

The objective of this project is to design and synthesize chemically robust near-IR fluorophores for bioanalytical applications and to develop new synthetic methods for rapid synthesis of the target compounds. A novel synthetic route was developed utilizing a hydrophilic, polyethylene glycol-based (PEG) support with different types of linkers. The Pcs were functionalized with either hydroxyl or amine groups for covalent conjugation purposes and were decorated with solubilizing groups such as carboxylic acids and short PEG chains. Mono-hydroxyl and mono-amine functionalized oligoethylene glycol substituted Pcs were synthesized via a solid-phase phthalonitrile tetramerization reaction. In order to alter the photophysical properties of the desired compounds different metals were inserted in the cavity of the macrocycle.

The potential of several of the compounds for PDT has been evaluated in vitro. Generally, these compounds are readily taken up in cells, have very low dark toxicity, exhibit rapid toxicity in near-infrared light, and are broadly dispersed in the cell including in lysosomes and in the endoplasmic reticulum.

Chapter 1
Introduction

1.1 Phthalocyanines

Phthalocyanines (Pcs), known systematically as tetraazatetrabenzporphyrins, are a member of porphyrinoid derivative aromatic compounds (Figure 1.1). Pcs are 18 π electron aromatic, planar macrocycles comprising four isoindole units linked together through their 1, 3 positions by aza bridges (Figure 1.1). Pcs have a number of characteristic properties such as high thermal stability, unique photophysical properties, intense color, non-toxicity and high phototoxicity upon irradiation with light, contributing to their effectiveness in different research areas.[1-4]

Photophysical properties of phthalocyanines are key to many of their industrial and research uses. Due to the four isoindole units linked via aza bridges, Pcs have a well-defined Q band (650-800 nm) lying well to the red relative to porphyrins.[5] On the other hand, B band (300-400 nm) of Pcs is less well-defined and broader than the one of porphyrins.[5] Pcs have moderate fluorescence quantum yields (Φ ~ 0.1-0.5) and high extinction coefficients (~10^5). Upon irradiation with red light, Pcs become very toxic to the surrounding environment by producing

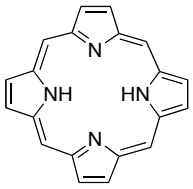

Porphyrin

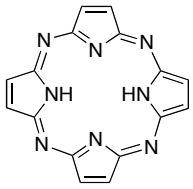

Tetraazaporphyrin

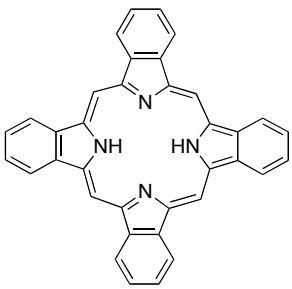

Tetrabenzoporphyrin

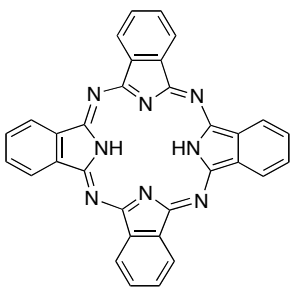

Phthalocyanine (Pc)

Figure 1.1 Porphyrinoid derivatives.

highly reactive oxygen species,[3,6] which makes them promising candidates as the next generation photosensitizers for photodynamic therapy (PDT) as discussed in the Chapter 5.

Chemical and photophysical properties of the Pcs can be tuned by replacing the two hydrogen atoms of the central cavity with over 70 different metals and/or altering the substituent pattern and/or the type of the substituent on the exterior of the ring system. For instance, solubility of the Pcs can be improved by decorating the macrocycle with carboxylic acids,[7] amine[7] or short polyethylene glycol (PEG) chains.[8] While strong emission can be obtained by having Zn, Al, or Si in the Pc core, Cu, as a metal guest, can turn off the fluorescence of the aromatic system.[9] All these properties of the Pcs make them excellent candidates for a wide variety of applications as discussed in detail in the Chapters 3 and 4.

Aggregation, a well-known phenomenon for Pcs and other macrocycles, is the main disadvantage of the Pcs. Due to the strong π-π interactions between the two aromatic cores of neighboring molecules, Pcs form dimers and higher order aggregates both in organic solvents and aqeous media, which causes problems in synthesis, purification and characterization of the target compounds. Concentration, solvent, pH, ionic strength and temperature influence the aggregation of the Pcs.[10] For instance, Seiters et. al., clearly demonstrated the effect of temperature on dimerization of the CoPc. As the temperature increased from 20 °C to 85 °C, the momomer predominated as judged by the red-shifted Q band of the CoPc.[11] Aggregation can be identified by a broadened and blue-shifted absorption band and/or splitting of the Q band and can be overcome by employing long alkyl chains or bulky groups as peripheral substitutions and/or having axially substituted metals such as Si or Al in the center of the ring.[12,13] Pcs, with six coordinate metals in the center, have a low tendency to aggregate since the axial ligands of the metal keep Pc molecules apart from each other due to the steric hindrance.

1.1.2 Synthesis of Phthalocyanines

After the first accidental synthesis of symmetrically-substituted Pc in 1907 by Braun,[14] different synthetic approaches have been described in the literature.[15] Due to the challenges faced during the isolation of the asymmetrically-substituted Pcs, various synthetic methods, including statistical condensation, subphthalocyanine route and solid-phase synthesis, employed to synthesize asymmetrically-substituted Pcs. Statistical condensation is utilized for preparation of AB_3 type phthalocyanines by employing appropriate stoichiometric ratios of the two different reactants (A and B).[16,17] Typically, $\geq$ 3:1 molar ratios are employed to give desired compound in yields ranging from 10 to 20%. A detailed discussion about the statistical condensation method is presented in the Chapter 2.

Kobayashi developed a new method, ring expansion of subphthalocyanines for selective synthesis of AB_3 type Pcs.[18] The reaction proceeds through a partial or total fragmentation of subphthalocyanine ring followed by ring closure of fragments which may result in formation of all possible Pc congeners via scrambling process.[18,19] It has been shown that the outcome of this reaction depends on the substituents on the starting materials.[20-23] The best yields and selectivity are achieved in the reaction between electron poor subphthalocyanine, having no substituents or electron withdrawing ones, and diiminoisoindoline derivatives bearing electron donating groups.

Solid-phase synthesis, mainly developed by Leznoff,[24-26] involves the immobilization of a phthalonitrile to a polymer support and condensation of the phthalonitrile-bound polymer support with a different type of phthalonitrile in solution. The main advantage of this route is that purification of the desired compound is relatively easy. Solid-phase synthesis of asymmetrically-substituted AB_3 type Pcs is discussed in detail in the Chapters 3 and 4.

Regardless of the chosen synthetic method, synthesis of tetra-substituted Pcs (Figure 1.2) from mono-substituted phthalonitriles or their derivatives yields a mixture of four different types

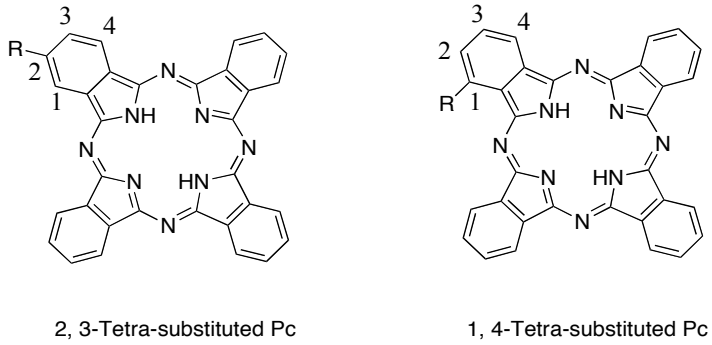

Figure 1.2 Tetra-substituted Pcs.

of isomers. [27] Figure 1.3 shows the structural isomers of 1,4-tetra-substituted Pcs. While the 2,3-tetra-substituted Pcs generally give constant isomer ratios, percentage of the each isomer highly depends on the bulkiness of the substitutent in the case of 1,4-tetra-substituted Pcs. It is also

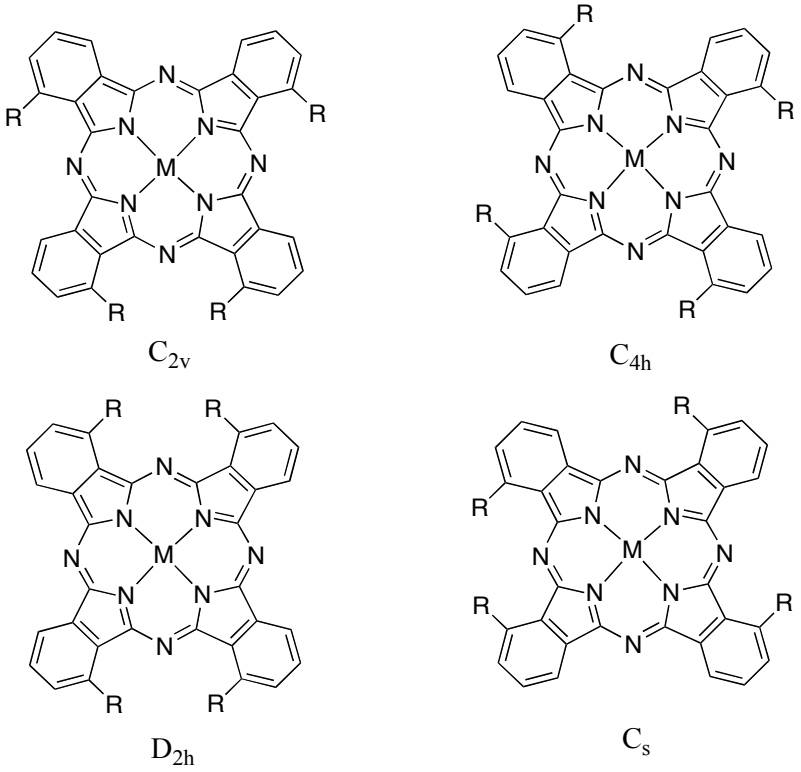

Figure 1.3 Structural isomers of 1,4-tetra-substituted Pcs.

possible to enrich one of the isomers by employing bulky substitutent bearing phthalonitrile precursors. If desired, each isomer of the 1,4-tetra-substituted Pc can be isolated by HPLC.[28]

Complete separation of the structural isomers of the 2,3-tetra-substituted Pcs was shown to be more difficult using chromatographic methods.[27]

1.1.3 Polymer Supports

Type of the polymer support, selected to be used for solid-phase synthesis of asymmetrically-substituted Pcs, has a great impact on the outcome of the cyclotetramerization reaction. Hydrophobic polystyrene (PS)-based polymer supports[29] (Figure 1.4) increase the non-covalent interactions between the resin and the Pc in solution. Consequently, isolation of the symmetrically-substituted Pc requires extensive extraction process.[24-26]

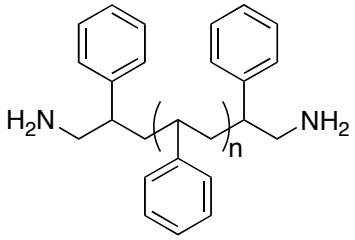

Figure 1.4 Simplified structure of aminomethyl PS-based resin.

Amphiphilic polyethyleneglycol (PEG)-based resins (Figure 1.5)[30] offer great advantages over PS-based resins: 1) Since the non-covalent interactions are greatly reduced, the product, asymmetrically- substituted Pc, is recovered without extensive purification process; 2) the PEG-based resin, made from primary ether bonds, is highly stable under the cyclotetramerization reaction and cleavage conditions; 3) amphiphilic resin is compatible with a wide variety of organic solvents as well as water which is utilized during the isolation of the symmetrically-

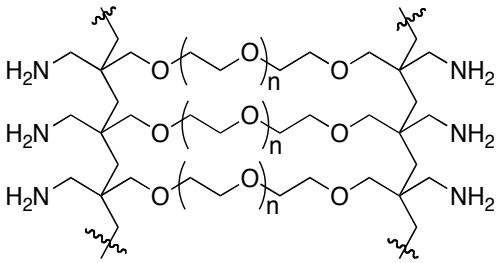

Figure 1.5 Simplified structure of aminomethyl PEG-based ChemMatrix resin.

substituted Pc. Due to the number of advantages, solid-phase synthesis of asymmetrically substituted Pcs was performed on PEG-based ChemMatrix resins. Extarnal surface and section of the ChemMatrix resin bead, obtained by focused ion beam (FIB), are shown in Figure 1.6.[30]

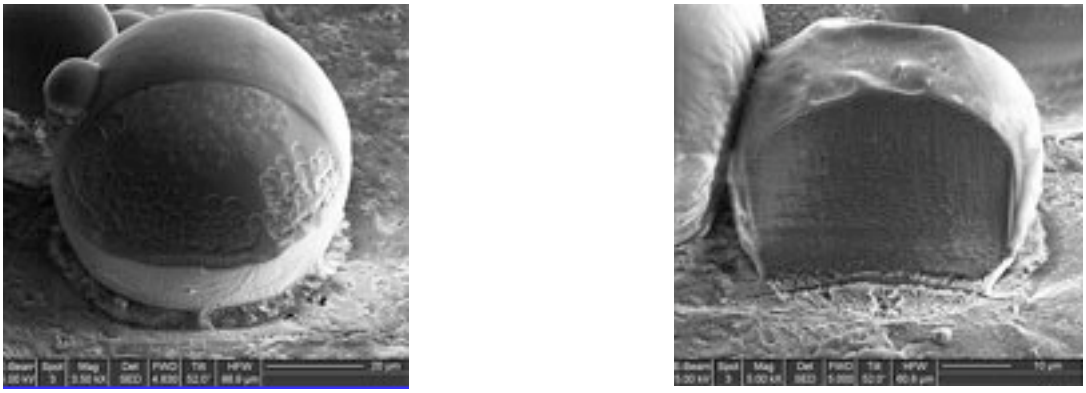

Figure 1.6 External surface of a ChemMatrix bead (left) and section of a ChemMatrix bead (right) by Focused Ion Beam (FIB).

1.1.4 Applications of Phthalocyanines

Since the discovery of Pcs in the early 1900's, they have drawn considerable attention in different research areas due to their exceptional chemical and electronic properties. Their ability to form a variety of condensed phases including monocrystals, polycrystalline films, liquid crystals and Langmuir-Blodgett films improved Pcs' incorporation into molecular devices.[1,31] The conducting properties of Pcs have been explored and devices like field-effect transistors have been prepared using LiPc.[32] Conductivity of the Pcs was further investigated by combining Pcs with macromolecules such as polymers and dendrimers.[33] A wide variety of polymer-Pc-based semiconductors have been developed using different types of metallo Pcs.[34-36] Utilizing Pcs π-π stacking abilities, outstanding Pc-based supramolecular wires were obtained, which utilize the Pc-Pc fast energy transfer.[37,38] Due to the Pcs' excellent stabilities and high extinction coefficients in the near-IR region of the electromagnetic spectrum, they are used for photovoltaic

systems for clean energy conversion. Using CuPc, efficient power conversion was obtained.[39] Recently, Pcs have also been used for organic light emitting devices.[40] Pcs' ability to generate highly reactive singlet oxygen is utilized not only for PDT but also catalytic oxidation of toxic compounds such as phenols, chlorinated phenols and sulfur containing compounds.[41]

1.2 Objective of the Project

The overall goal of this project was to design and synthesize chemically robust near-IR fluorophores for bioanalytical applications and to develop new synthetic methods for rapid synthesis of the target compounds. Pcs were selected as the potential fluorophores to develop the desired systems due to the their outstanding chemical and photophysical properties.

With the aim of conjugation of the Pc to biomolecules such as oligonucleotide and peptide, the asymmetrically-substituted target Pc was designed such that it has only one functional group for covalent conjugation and has multiple water solubilizing groups to improve the solubility of the hydrophobic core as shown in Figure 1.7. In order to tune the photophysical properties of the

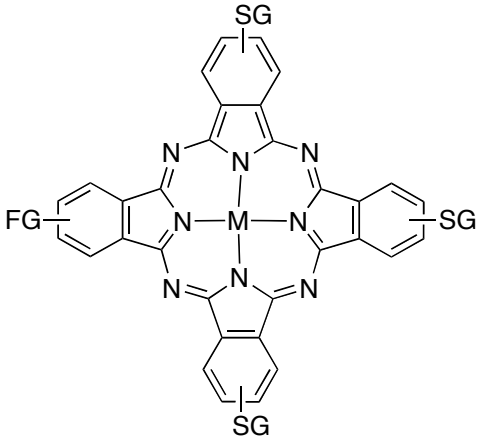

Solubilizing Group = COOH, $O(CH_2CH_2O)_xCH_3$
Functional Group = NH_2, OH, COOH
Metal = Zn(II), Cu(II), Ni(II), H_2

Figure 1.7 Design of asymmetrically-substituted AB_3 type of Pc.

desired compounds, different metals were inserted in the cavity of the macrocycle. The Pcs were functionalized with either hydroxyl or amine groups for covalent conjugation purposes and were decorated with solubilizing groups such as carboxylic acids and short PEG chains. With the

purpose of a rapid synthesis of the asymmetrically substituted Pcs a new synthetic method was developed.

1.3 References

(1) Dini, D.; Hanack, M. Phthalocyanines as materials for advanced technologies: some examples *J. Porphyr. Phthalocyanines* **2004**, *8*, 915-933.

(2) Giepmans, B. N. G.; Adams, S. R.; Ellisman, M. H.; Tsien, R. Y. Review The fluorescent toolbox for assessing protein location and function *Science* **2006**, *312*, 217-224.

(3) Rosenthal, I. In *Phthalocyanines Properties and Applications*; Leznoff, C. C. L., A.B.P., Ed.; VCH Publishers: New York, 1996; Vol. 4, p 485-514.

(4) Saji, T. In *Phthalocyanines Properties and Applications*; Leznoff, C. C. L., A.B.P., Ed.; VCH Publishers: New York, 1993; Vol. 2, p 167-195.

(5) Stuzhin, P. A.; Khelevina, O. G. Azaporphyrins: Structure of the reaction centre and reactions of complex formation *Coord. Chem. Rev.* **1996**, *147*, 41-86.

(6) Taquet, J. P.; Frochot, C.; Manneville, V.; Barberi-Heyob, M. Phthalocyanines covalently bound to biomolecules for a targeted photodynamic therapy *Curr. Med. Chem.* **2007**, *14*, 1673-1687.

(7) Kliesch, H.; Weitemeyer, A.; Muller, S.; Wohrle, D. Synthesis of Phthalocyanines with One Sulfonic-Acid, Carboxylic-Acid, or Amino Group *Liebigs Ann.* **1995**, 1269-1273.

(8) Erdem, S. S.; Nesterova, I. V.; Soper, S. A.; Hammer, R. P. Solid-phase synthesis of asymmetrically substituted "AB_3-type" phthalocyanines *J. Org. Chem.* **2008**, *73*, 5003-5007.

(9) Verdree, V. T.; Pakhomov, S.; Su, G.; Allen, M. W.; Countryman, A. C.; Hammer, R. P.; Soper, S. A. Water soluble metallo-phthalocyanines: The role of the functional groups on the spectral and photophysical properties *J. Fluoresc.* **2007**, *17*, 547-563.

(10) Stillman, M. J. N., T. In *Phthalocyanines Properties and Applications*; Leznoff, C. C. L., A.B.P., Ed.; VCH Publishers: New York, 1989; Vol. 1, p 139-247.

(11) Seiders, R. P.; Ward, J. R. Effect of Visible-Light on the Dimerization of Cobalt (II) Tetrasulfonated Phthalocyanine in Water *Anal. Lett. Pt A* **1984**, *17*, 1763-1769.

(12) Ford, W. E.; Rodgers, M. A. J.; Schechtman, L. A.; Sounik, J. R.; Rihter, B. D.; Kenney, M. E. Synthesis and Photochemical Properties of Aluminum, Gallium, Silicon, and Tin Naphthalocyanines *Inorg. Chem.* **1992**, *31*, 3371-3377.

(13) Li, H. R.; Jensen, T. J.; Fronczek, F. R.; Vicente, M. G. H. Syntheses and properties of a series of cationic water-soluble phthalocyanines *J. Med. Chem.* **2008**, *51*, 502-511.

(14) Braun, A.; Tcherniac, J. The products of the action of acet-anhydride on phthalamide *Ber. Der Dtsch. Chem. Ges.* **1907**, *40*, 2709-2714.

(15) Montfortz, F. P. In *The Porphyrin Handbook*; Kadish, K. M., Smith,K. M., Guilard, G., Ed.; Academic Press: New York, 1999; Vol. 19, p 105-149

(16) Vacus, J.; Memetzidis, G.; Doppelt, P.; Simon, J. The Synthesis of Unsymmetrically Functionalized Platinum and Zinc Phthalocyanine Complexes *J. Chem. Soc.-Chem. Commun.* **1994**, 697-698.

(17) Aoudia, M.; Cheng, G. Z.; Kennedy, V. O.; Kenney, M. E.; Rodgers, M. A. J. Synthesis of a series of octabutoxy- and octabutoxybenzophthalocyanines and photophysical properties of two members of the series *J. Am. Chem. Soc.* **1997**, *119*, 6029-6039.

(18) Kobayashi, N.; Kondo, R.; Nakajima, S.; Osa, T. New Route to Unsymmetrical Phthalocyanine Analogs by the Use of Structurally Distorted Subphthalocyanines *J. Am. Chem. Soc.* **1990**, *112*, 9640-9641.

(19) Sastre, A.; Torres, T.; Hanack, M. Synthesis of Novel Unsymmetrical Monoaminated Phthalocyanines *Tetrahedron Lett.* **1995**, *36*, 8501-8504.

(20) Kasuga, K.; Idehara, T.; Handa, M.; Isa, K. Preparation of Unsymmetrical Phthalocyanine by Means of a Ring Expansion of Subphthalocyanine *Inorg. Chim. Acta* **1992**, *196*, 127-128.

(21) Weitemeyer, A.; Kliesch, H.; Wohrle, D. Unsymmetrically Substituted Phthalocyanine Derivatives Via a Modified Ring Enlargement Reaction of Unsubstituted Subphthalocyanine *J. Org. Chem.* **1995**, *60*, 4900-4904.

(22) Sastre, A.; delRey, B.; Torres, T. Synthesis of novel unsymmetrically substituted push-pull phthalocyanines *J. Org. Chem.* **1996**, *61*, 8591-8597.

(23) Kobayashi, N.; Ishizaki, T.; Ishii, K.; Konami, H. Synthesis, spectroscopy, and molecular orbital calculations of subazaporphyrins, subphthalocyanines, subnaphthalocyanines, and compounds derived therefrom by ring expansion *J. Am. Chem. Soc.* **1999**, *121*, 9096-9110.

(24) Leznoff, C. C.; Hall, T. W. The Synthesis of a Soluble, Unsymmetrical Phthalocyanine on a Polymer Support *Tetrahedron Lett.* **1982**, *23*, 3023-3026.

(25) Hall, T. W.; Greenberg, S.; McArthur, C. R.; Khouw, B.; Leznoff, C. C. The Solid-Phase Synthesis of Unsymmetrical Phthalocyanines *New J. Chem.* **1982**, *6*, 653-658.

(26) Leznoff, C. C.; Svirskaya, P. I.; Khouw, B.; Cerny, R. L.; Seymour, P.; Lever, A. B. P. Syntheses of Monometallated and Unsymmetrically Substituted Binuclear Phthalocyanines and a Pentanuclear Phthalocyanine by Solution and Polymer Support Methods *J. Org. Chem.* **1991**, *56*, 82-90.

(27) Schmid, G. S., M.; Geyer, M.; Hanack, M. In *Phthalocyanines Properties and Applications*; Leznoff, C. C. L., A.B.P., Ed.; VCH Publishers: New York, 1996; Vol. 4, p 5-16.

(28) Hanack, M.; Schmid, G.; Sommerauer, M. Chromatographic-Separation of the 4 Possible Structural Isomers of a Tetrasubstituted Phthalocyanine - Tekrakis(2-Ethylhexyloxy)Phthalocyaninatonickel(II) *Angew. Chem.-Int. Edit. Engl.* **1993**, *32*, 1422-1424.

(29) Zikos, C. C.; Ferderigos, N. G. Preparation of High-Capacity Aminomethyl-Polystyrene Resin *Tetrahedron Lett.* **1995**, *36*, 3741-3744.

(30) Matrix-innovation ChemMatrix-100% PEG Matix **2008**, http://www.matrix-innovation.com/notes.asp.

(31) Bourgoin, J. P.; Doublet, F.; Palacin, S.; Vandevyver, M. High in-plane anisotropy in phthalocyanine LB films *Langmuir* **1996**, *12*, 6473-6479.

(32) Guillaud, G.; Simon, J.; Germain, J. P. Metallophthalocyanines - Gas sensors, resistors and field effect transistors *Coord. Chem. Rev.* **1998**, *180*, 1433-1484.

(33) Ali-Adib, Z.; Budd, P. M.; McKeown, N. B.; Thanapprapasr, K. Ordered Langmuir-Blodgett films derived from a mesogenic polymer amphiphile *J. Mater. Chem.* **2000**, *10*, 2270-2273.

(34) Nohr, R. S.; Kuznesof, P. M.; Wynne, K. J.; Kenney, M. E.; Siebenman, P. G. Highly Conducting Linear Stacked Polymers - Iodine-Doped Fluoroaluminum and Fluorogallium Phthalocyanines *J. Am. Chem. Soc.* **1981**, *103*, 4371-4377.

(35) Toscano, P. J.; Marks, T. J. Electrically Conductive Metallomacrocyclic Assemblies - High-Resolution Solid-State Nmr-Spectroscopy as a Probe of Local Architecture and Electronic-Structure in Phthalocyanine Molecular and Macromolecular Metals *J. Am. Chem. Soc.* **1986**, *108*, 437-444.

(36) Schouten, P. G.; Warman, J. M.; Dehaas, M. P.; Vannostrum, C. F.; Gelinck, G. H.; Nolte, R. J. M.; Copyn, M. J.; Zwikker, J. W.; Engel, M. K.; Hanack, M.; Chang, Y. H.; Ford, W. T. The Effect of Structural Modifications on Charge Migration in Mesomorphic Phthalocyanines *J. Am. Chem. Soc.* **1994**, *116*, 6880-6894.

(37) Engelkamp, H.; Middelbeek, S.; Nolte, R. J. M. Self-assembly of disk-shaped molecules to coiled-coil aggregates with tunable helicity *Science* **1999**, *284*, 785-788.

(38) Kobayashi, N. Dimers, trimers and oligomers of phthalocyanines and related compounds *Coord. Chem. Rev.* **2002**, *227*, 129-152.

(39) Xue, J. G.; Uchida, S.; Rand, B. P.; Forrest, S. R. Asymmetric tandem organic photovoltaic cells with hybrid planar-mixed molecular heterojunctions *Appl. Phys. Lett.* **2004**, *85*, 5757-5759.

(40) Hohnholz, D.; Steinbrecher, S.; Hanack, M. Applications of phthalocyanines in organic light emitting devices *J. Mol. Struct.* **2000**, *521*, 231-237.

(41) de la Torre, G.; Claessens, C. G.; Torres, T. Phthalocyanines: old dyes, new materials. Putting color in nanotechnology *Chem. Commun.* **2007**, 2000-2015.

Chapter 2
Solution Phase Synthesis of Phthalonitrile Precursors and Phthalocyanines

2.1 Introduction

One of the disadvantages of the phthalocyanines (Pcs) limiting their use in bioanalytical and medical applications is their hydrophobic structure. Hydrophilicity of dyes is crucial for different reasons as in many bioanalytical applications are performed in aqueous media such as labeling of the biomolecules,[1] in vivo imaging,[2] and photodynamic therapy (PDT), which requires injection of the photosensitizer into the blood stream or a biological medium.[3] Thus, for both applications, it is highly desired to have a readily water soluble Pc. Solubility of the Pc also plays a role during the preparation of the compound as it increase the variety of organic solvents and/or buffer solutions that can be used for purification and characterization. There is a lot of prior work on the synthesis of water-soluble Pcs utilizing different type of phthalonitriles bearing hydrophilic groups including carboxylate,[4] sulfonate,[5] phosphonate,[6] amine,[7] and polyethylene glycol (PEG).[8]

Herein are reported syntheses of new phthalonitriles, building blocks of the Pcs, decorated with water solubilizing groups, and asymmetrically- and symmetrically-substituted Pcs. Phthalonitriles, bearing carboxylic acid, polyethyleneglycol (PEG) or amine as water solubilizing group, were synthesized starting from commercially available nitro- or chloro-substituted phthalonitriles following the published methods in the literature. Pcs were synthesized employing the most commonly used method, statistical condensation. The Pcs containing carboxylic acid as a peripheral substituent have desired water solubility due to the capability to form multiple intra-and inter-molecular hydrogen bonds. Challenges faced during the solution-phase synthesis of the Pcs and attempts to modification of the peripheral substituents on the Pcs are discussed.

2.2 Results and Discussion

2.2.1 Synthesis of Phthalonitriles Bearing Carboxylate, Amine and Nitro Groups

Pcs having carboxylic acids as solubilizing group on the Pc core have been reported in the literature several times.[9] The interest in the carboxylic acid bearing Pcs is due to the their improved solubility in aqueous solutions as well as in organic solvents. With the aim of the synthesis of the readily water-soluble Pcs, corresponding phthalonitrile precursors were designed and synthesized as building blocks for the target Pcs.

Synthesis of the isophthalic butyl ester functionalized phthalonitrile **2.2** started with commercially available 5-hydroxyisophthalic acid. According to well established procedure,[10] 5-hydroxyisophthalic acid was refluxed in n-BuOH with catalytic amount of sulfuric acid. Following extractive workup, the ester was obtained in 88% yield (Scheme 2.1). Protection of the carboxylic acid is necessary to prevent possible side reactions such as esterification and amidation, which would occur during the cyclotetramerization of the phthalonitriles. Since the

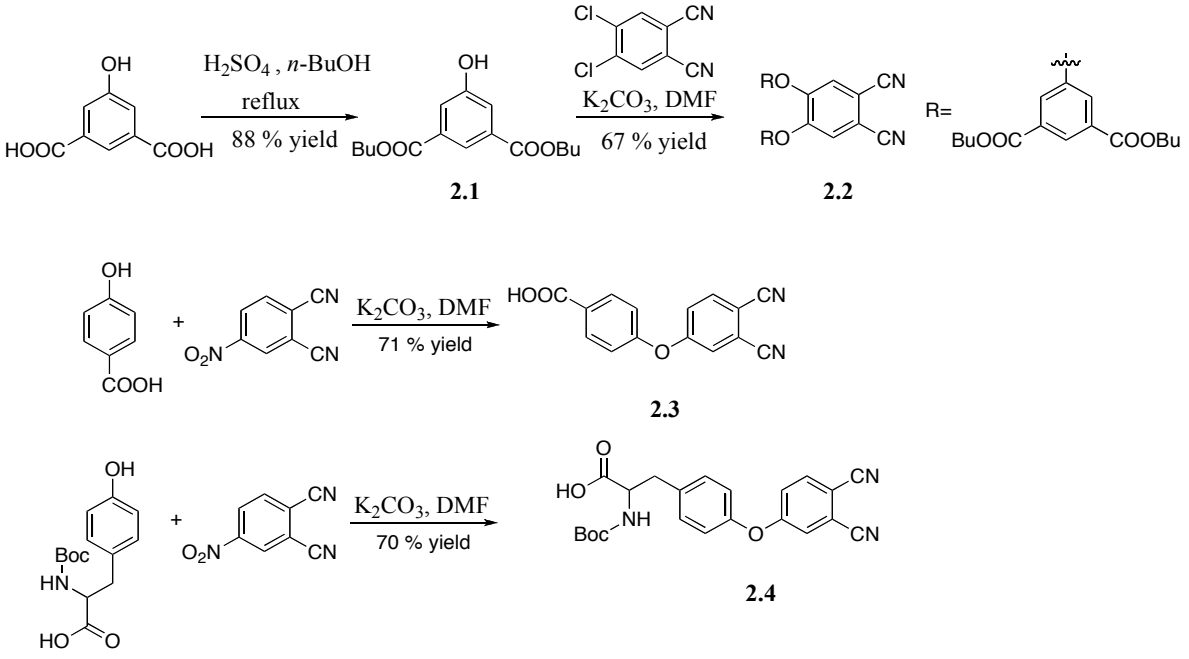

Scheme 2.1

cyclotetramerization reaction is typically performed in high boiling point alcohols such as *n*-BuOH or *n*-pentanol,[11] it is crucial to protect the carboxylic acid with the ester version of the

solvent to prevent side product formation as a result of transesterification reaction. Nucleophilic aromatic substitution of dibutyl 5-hydroxyisophthalate **2.1** with the chlorines on 4,5-dicholoro phthalonitrile was performed in DMF and ester functionalized phthalonitrile **2.2** was obtained in 67% yield (Scheme 2.1). Later experiments showed that increasing the amount of hydroxyisophthalate **2.1** from 2.1 equivalents to 3 or more equivalents relative to equivalency of 4, 5 dichloro phthalonitrile improves the yield to over 80%.

Synthesis of 4-(3,4-dicyanophenoxy)benzoic acid (**2.3**) (Scheme 2.1) was done following the very commonly used reaction for phthalonitrile synthesis, adopted from the literature.[11] Substitution of nitro group on commercially available 4-nitrophthalonitrile by 4-hydroxybenzoic acid proceeded via $S_{RN}1$ mechanism in which substitution occurs via a radical intermediate.[12] Substitution of aliphatic and aromatic nitro groups by a wide variety of nucleophiles has been studied by different research groups.[13-16] $S_{RN}1$ type of reactions proceed in three steps: Initiation, propagation and termination as shown in Scheme 2.2.[17] At the initiation step, a radical anion is formed by a single electron transfer to the substrate (nitro compound) and disassociation of the radical anion generates a radical and an anion. The propagation step, in where the chain reaction starts, involves the formation of a radical anion via reaction of the radical and the nucleophile.

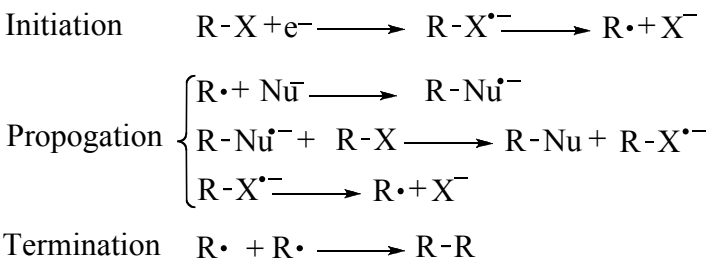

Scheme 2.2

(e.g., deprotonated form of 4-hydroxybenzoic acid). A single electron transfer from the newly formed radical anion to substrate generates the product (R-Nu) and a radical anion. In the last step, the chain reactions are quenched by termination of all radicals via coupling to each other

In the case of the synthesis of carboxylate phthalonitrile **2.3**, the suspension of 4-nitro phthalonitrile, 4-hydroxybenzoic acid and K_2CO_3 in anhydrous DMF was stirred at room temperature. The target compound was obtained by precipitation from acidic CH_3OH solution and further purified by column chromatography.

The last carboxylate-bearing phthalonitrile **2.4** (Scheme 2.1), 2-(*tert*-butoxycarbonylamino)-3-(4-(3,4-dicyanophenoxy)phenyl)propanoic acid, was synthesized employing the same synthetic strategy as used in the synthesis of carboxylic acid functionalized **2.3**. Commercially available Boc-Tyr-OH (Boc-protected α amine) was added to the suspension of 4-nitro phthalonitrile and K_2CO_3 in anhydrous DMF. The reaction was carried until the 4-nitrophthalonitrile was completely consumed. Following the aqueous work up, the product was purified by column chromatography and obtained in 70% yield. The last two phthalonitriles, discussed above (**2.3** and **2.4**), were synthesized to immobilize to a solid support via C-terminal amidation, which requires free carboxylic acid (discussed in the Chapter 4). Thus, the carboxylic acids were left unprotected.

After the successful synthesis of carboxylate-substituted phthalonitriles, syntheses of precursors were continued with amine and nitro functionalized phthalonitriles. These compounds were synthesized as starting materials for the solution-phase synthesis of AB_3 type Pcs having three or more carboxylic acid units and one amine group, which could be utilized for covalent conjugation of the biomolecules to the Pcs.[1] The nitro group on the 4-nitrophthalonitrile was reduced to amine by refluxing in CH_3OH with Fe and concentrated HCl.[18]

Following the work up, simple recrystalization from benzene gave the 4-amino phthalonitrile **2.5** in 70% yield (Scheme 2.3).

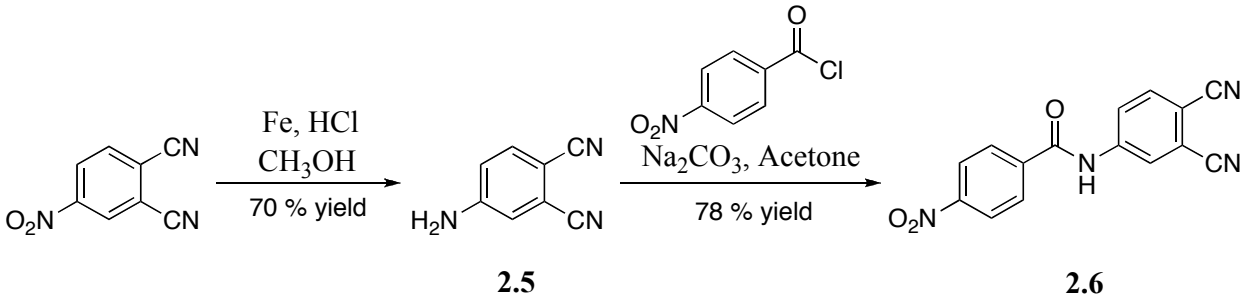

2.5 **2.6**

Scheme 2.3

N-(3,4-Dicyanophenyl)-4-nitrobenzamide (**2.6**) was synthesized via nucleophilic acyl substitution between 4-amino phthalonitrile **2.5** and commercially available 4-nitrobenzoylchloride (Scheme 2.3). In order to neutralize in situ generated HCl, the reaction was performed in the presence of a weak base, Na_2CO_3. The product was purified by column chromatography, recrystallized from acetone and obtained in 78% yield. The structure of the product was confirmed by X-ray crystallography (Figure 2.1).

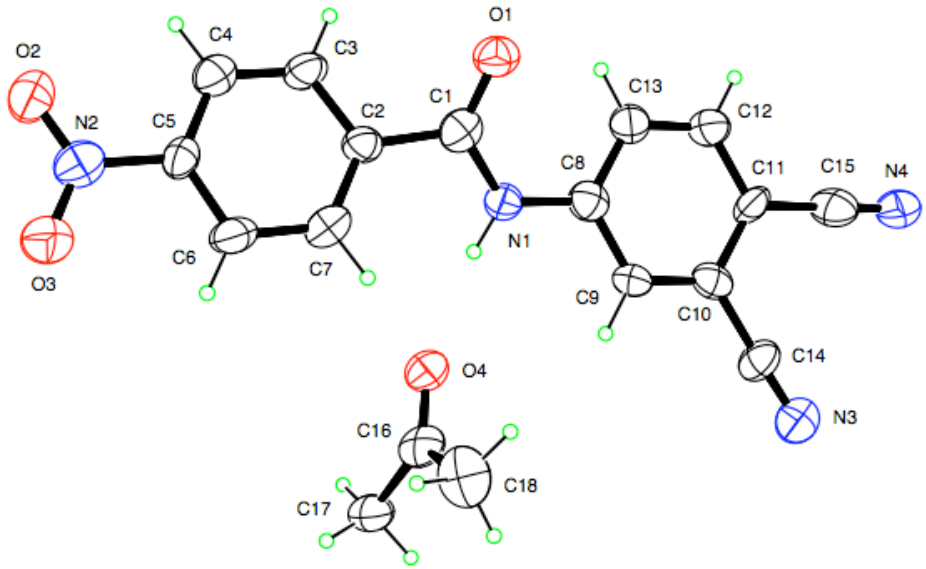

Figure 2.1 ORTEP representation of the molecular structure of **2.6** with 50% ellipsoids.

2.2.2 Synthesis of Polyethyleneglycol Substituted Phthalonitriles

Carboxylate-substituted phthalonitriles are great precursors for water-soluble Pcs. However, there are several disadvantages of carboxylic acid functionalized Pcs regarding to nature of the substituents. One of the biggest challenges is that they still have a tendency to aggregate,[19] which causes series of problems for any applications as well as purification processes. To improve the water solubility and to break the aggregates, high pH values may be necessary which may not be compatible with the desired application. We have hypothesized that the Pcs decorated with short ethylene glycol chains would have improved solubility in water and organic solvents and less tendency to aggregate. Thus, di- and triethyleneglycol-substituted phthalonitriles were synthesized starting from commercially available starting materials.

In order to convert hydroxyl group to a better living group, triethyleneglycol monomethyl ether was tosylated with 4-methyl-benzenesulfonyl chloride to give sulfonic acid ester[20] **2.7** (Scheme 2.4). High water solubility of triethyleneglycol monomethyl ether was utilized during the purification process. The product was simply purified by extraction and the clear oil was obtained in 94 % yield.

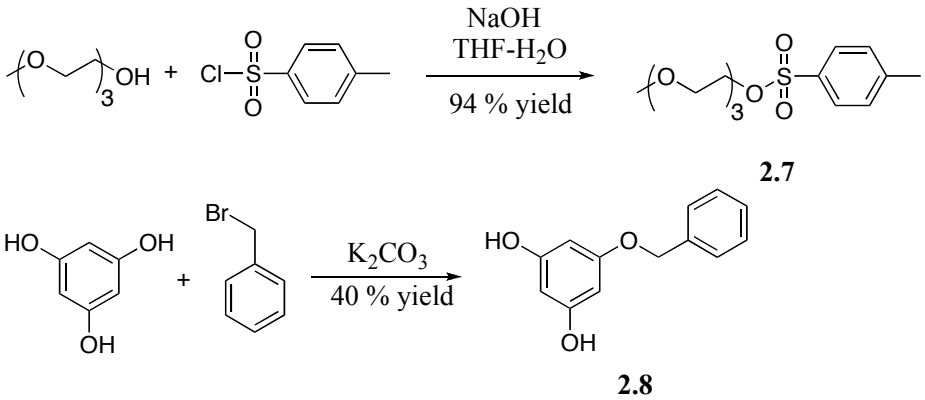

Scheme 2.4

Stepwise synthesis of oligoethyleneglycol-substituted phthalonitrile **2.11** was continued with the protection of one the hydroxyl groups on the phloroglucinol. The benzyl group was chosen

as a protecting group for two reasons: 1) The benzyl group can easily be cleaved under mild conditions by hydrogenation; 2) since the side product formation would be unavoidable, the separation of the product (**2.8**) from di- and tri-protected pholoroglucinol would be easier due to the expected difference of the R_f values of the each compound. For instance, initially a methyl group was employed as a protecting group and the reaction yield all three, mono-, di- and tri-protected, compounds as well as unreacted pholoroglucinol, which was used in large excess. Attempts to purify the target compound from the sea of the variously methylated phloroglucinols were unsuccessful due to the very close R_f values of the compounds. Benzylation of phloroglucinol was carried out by slow addition of benzyl bromide to the suspension of phloroglucinol and K_2CO_3 at room temperature.[21] While using a large excess of phloroglucinol prevented the formation of tri-protected compound, it was not enough to preclude the formation of di-protected phloroglucinol. The product was purified by column chromatography to give monobenzyl ether **2.8** in 40% yield. (Scheme 2.4)

The next nucleophilic substitution reaction involved formation of an ether bond. 3-fold molar excess of PEG-tosylated **2.7** was refluxed with monobenzyl ether **2.8** in freshly distilled 2-butanone in the presence of K_2CO_3 and catalytic amount of KI [22] (Scheme 2.5). Following the

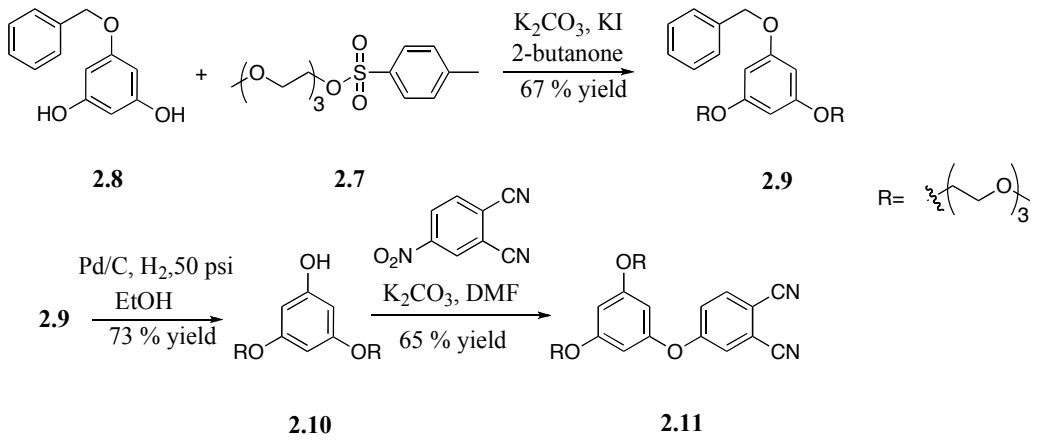

Scheme 2.5

aqueous work up procedure, pegylated monobenzyl ether **2.9** was purified by column chromatography and obtained as an oil in 67% yield. The benzyl group of **2.9** was cleaved by hydrogenation in the presence of a palladium on carbon in EtOH under 50 psi H_2.[21] (Scheme 2.5). Following the removal of the metal, the crude mixture was run through a silica gel column to give bis-triethyleneglycol phenol **2.10** in 73% yield.

A previously published procedure was followed to synthesize pegylated phthalonitrile **2.11** via an $S_{RN}1$ type of mechanism.[11] 4-Nitrophthalonitrile, an excess of bis-triethyleneglycol phenol **2.10**, and K_2CO_3 were stirred in DMF at room temperature until the 4-nitrophthalonitrile was consumed. It was noted that longer reaction times results in a large amount of green colored side product, the corresponding metal free Pc formed by self-cyclotetramerization of 4-nitrophthalonitrile. In general, this can be explained by an increased reactivity of the phthalonitrile towards nucleophilic attack. The strong electron-withdrawing nitro group activates the phthalonitrile to cyclotetramerization by increasing the positive charge density on the nitrile carbon. Nucleophilic attack to nitrile carbon starts the cyclotetramerization process. It is nearly impossible to prevent the Pc formation. However, using one of the reagents in excess reduces the quantity of the side product. Triethyleneglycol-decorated phthalonitrile **2.11** was purified by column chromatography and obtained in 65% yield (Scheme 2.5).

Two other phthalonitriles, having similar structures to pegylated phthalonitrile **2.11**, were designed hypothesizing that the Pcs synthesized from these phthalonitriles would have not only the desired water solubility but also different photophysical properties due to the altered substitution patterns. Retrosynthetic analysis of the two desired phthalonitriles revealed that the same starting material (**2.12**), could be used to synthesize two different phthalonitriles. The first step of the syntheses was the ether bond formation via S_N2 type mechanism (Scheme 2.6). Commercially available 1-bromo-2-(2-methoxyethoxy)ethane was added to the suspension of

hydroquionone and K_2CO_3 in acetonitrile at 50 °C and the mixture was brought to reflux.[23] In order to prevent formation of di-substituted product, hydroquinone was used in 3.3-fold molar excess. Following the filtration of excess of inorganic salts, the product was purified by column chromatography. Due to the formation of the large amount of di-substituted product, the yield of the reaction was only 35%.

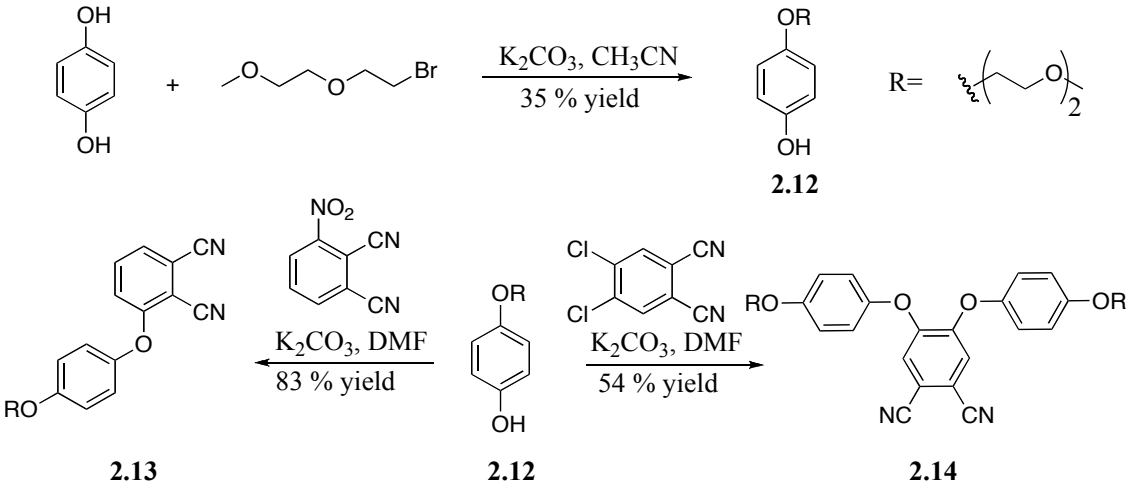

Scheme 2.6

Mono- and di-subtituted phthalonitriles **2.13** and **2.14** were synthesized employing the same synthetic strategy[11] discussed above, with either commercially available 3-nitrophthalonitrile or 4,5-dichlorophthalonitrile, respectively (Scheme 2.6). Nucleophilic substitution via radical intermediate ($S_{RN}1$) between diethyleneglycol-bearing phenol **2.12** and 3-nitrophthalonitrile gave the product in 83% yield after column chromatography. Nucleophilic aromatic substitution of the two chlorines on 4,5-dicholorophthalnitrile with phenol **2.12** yielded di-substituted phthalonitrile **2.14** and the mono-substituted side product as well. The product was purified by column chromatography and the target compound was obtained in 54% yield. Nucleophilic aromatic substitution with 4,5-dichlorophthalonitrile has usually low yields due to the mono substituted side product formation. Yet, it is possible to suppress the quantity of the side product

by using the nucleophile in large excess. The molecular structures of the diethyleneglycol-bearing phthalonitriles are presented in Figure 2. 2 and Figure 2.3.

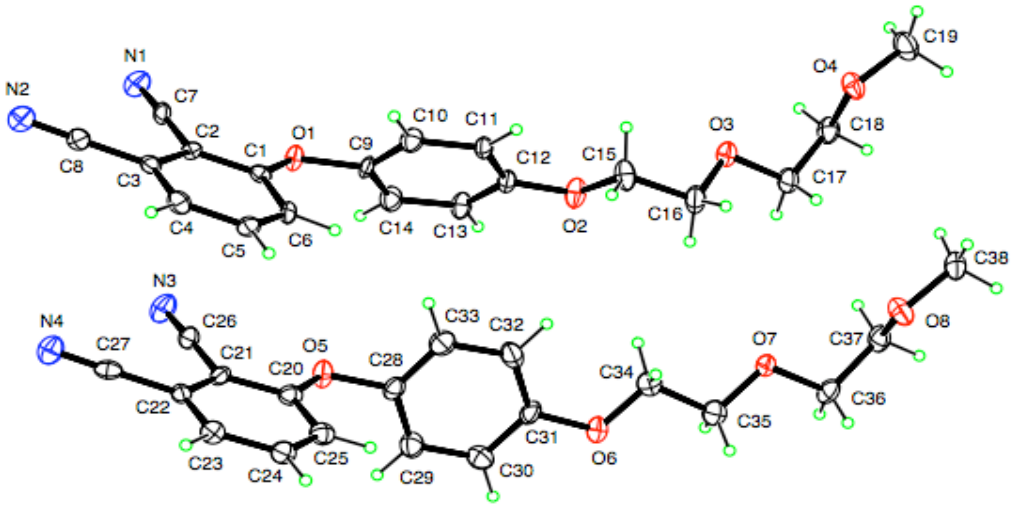

Figure 2.2 ORTEP representation of the molecular structure of **2.13** with 50% ellipsoids.

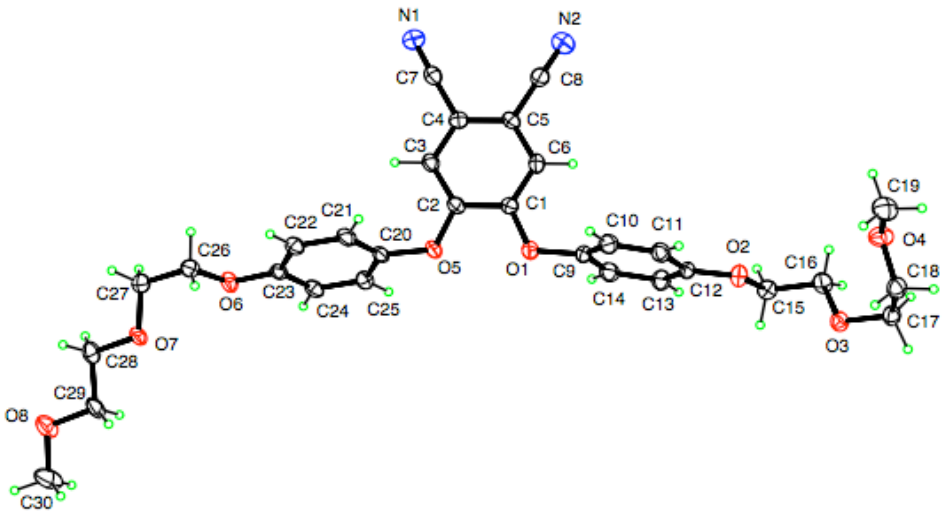

Figure 2.3 ORTEP representation of the molecular structure of **2.14** with 50% ellipsoids.

Oligoethyleneglycol-bearing phthalonitriles **2.11**, **2.13** and **2.14** have similar structural features. In all of them, ethylene glycol chains are connected to the phthalonitrile with an ether linkage via a benzene ring. Aggregation may be the main disadvantage of the Pcs synthesized from these phthalonitriles. We expected a high degree of aggregation due to the strong π-π

interactions between benzene rings. In order to overcome this expected problem, new series of phthalonitriles bearing ethylene glycol chains directly connected to phthalonitrile without a benzene ring were designed. The position of the substituents were altered to be able tune the photophysical properties of the Pcs. The same synthetic methods, discussed above, were employed to synthesize the target phthalonitriles. (Scheme 2.6)

Tri-or diethylene glycol-substituted phthalonitriles **2.15** and **2.16** were synthesized via $S_{RN}1$ type reaction.[11] 4-nitrophthalonitrile was stirred with either triethyleneglycol monomethylether (**2.15**) or diethylene glycol (**2.16**)[8] in the presence of K_2CO_3 in DMF (Scheme 2.7). In the case of triethyleneglycol-substituted phthalonitrile **2.15**, the reaction was quenched by pouring the suspension to ice-water and left overnight. The resulting precipitate was further purified by column chromatography to give 4-(2-(2-(2-methoxyethoxy)ethoxy)ethoxy)phthalonitrile **2.15** in 74% yield. During the purification of **2.16**, the precipitation step was skipped due to the high solubility of the product in water. 4-(2-(2-hydroxyethoxy)ethoxy)phthalonitrile **2.16** was purified by column chromatography and obtained in 58% yield. The molecular structures of the phthalonitriles are shown in Figure 2.4 and Figure 2.5.

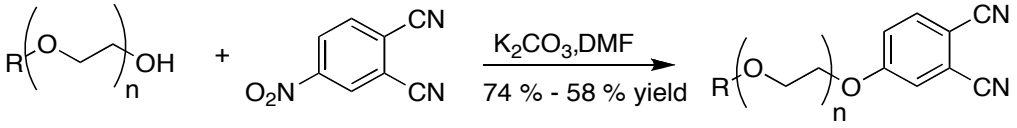

2.15 n=3, R=CH_3
2.16 n=2, R=H

Scheme 2.7

There are many examples in the literature regarding the red-shifted absorption spectrum of the Pcs synthesized from 3,6-disubstituted phthalonitriles.[24,25] 3,6-Dihydroxyphthalonitrile was selected as a common starting material for both of the target compounds. Commercially

available 3,6-dihydroxyphthalononitrile was stirred with a 2.2-fold molar excess of either tosylated triethyleneglycol monomethyl ether **2.7** or a primary halide, 1-bromo-2-(2-methoxyethoxy)ethane with K_2CO_3 in DMF (Scheme 2.8). Both of the reactions, preceded via

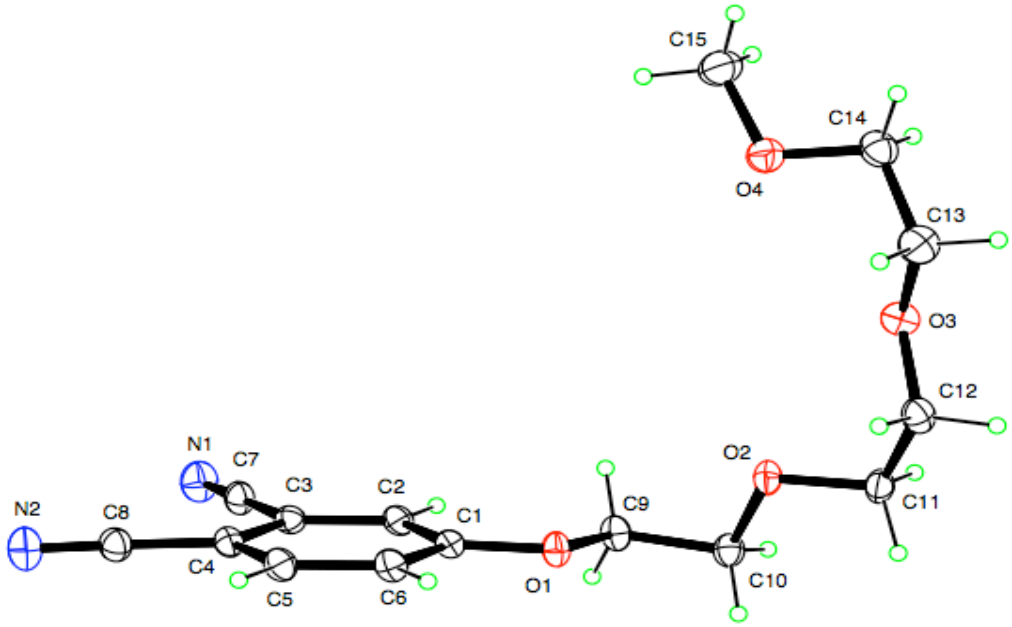

Figure 2.4 ORTEP representation of the molecular structure of **2.15** with 50% ellipsoids.

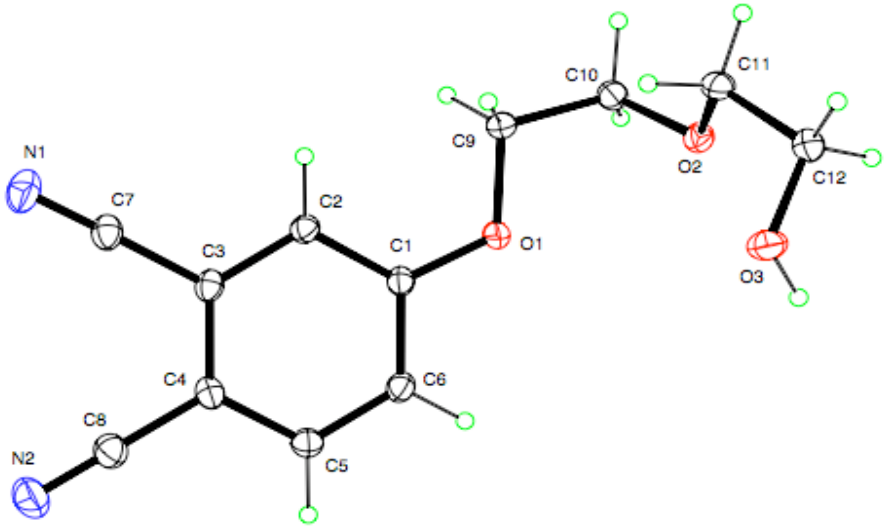

Figure 2.5 ORTEP representation of the molecular structure of **2.16** with 50% ellipsoids.

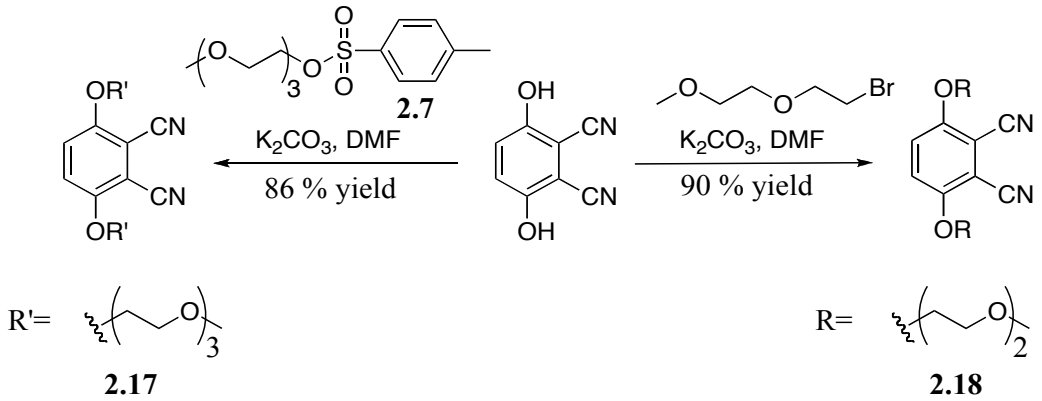

Scheme 2.8

S_N2 type mechanism, were followed by TLC. A very small amount of mono-substituted products were formed during the reactions. Following the work up, while triethyleneglycol-substituted phthalonitrile **2.17** was purified by column chromatography in 86% yield, diethyleneglycol-bearing phthalonitrile **2.18** was purified by recrsytallization from THF-hexane mixture and obtained in 90% yield. The molecular structures of short oligoethyleneglycol-substituted phthalonitriles **2.17** and **2.18** are shown in Figure 2.6 and Figure 2.7, respectively.

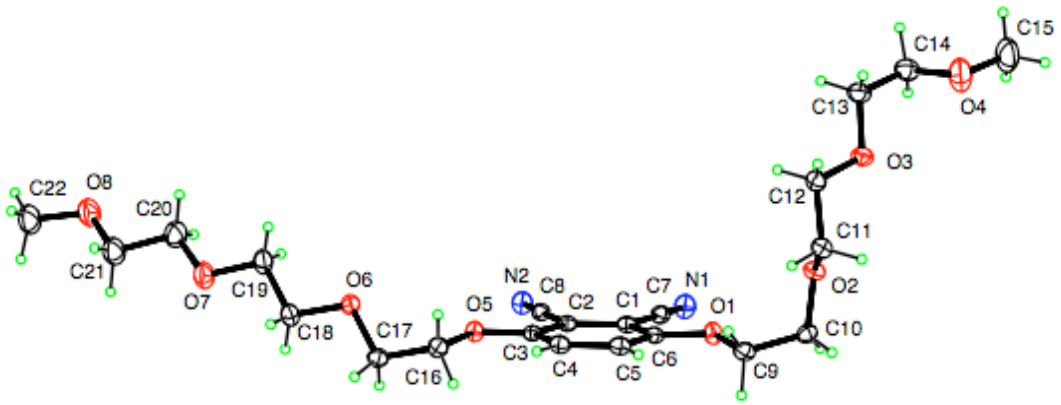

Figure 2.6 ORTEP representation of the molecular structure of **2.17** with 50% ellipsoids.

Preparation of ethyleneglycol-substituted phthalonitriles was continued with a small change in the linker type. Triethyleneglycol mono methyl ether was attached to the commercially available phthalonitriles via a thioether linkage at different positions. Synthesis of the three

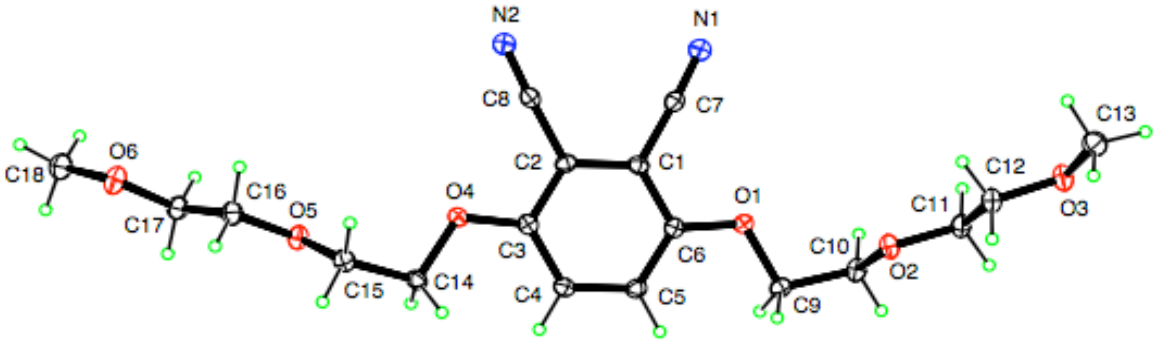

Figure 2.7 ORTEP representation of the molecular structure of **2.18** with 50% ellipsoids.

different phthalonitriles started with conversion of an alcohol to thiol via tosylate intermediate **2.7**.[26] Tosylated tirethyleneglycol **2.7** and thiourea were dissolved in EtOH-water mixture and brought to reflux. Following the workup procedure, the product was distilled under high vacuum and obtained as malodorous oil in 54 % yield (Scheme 2.9).

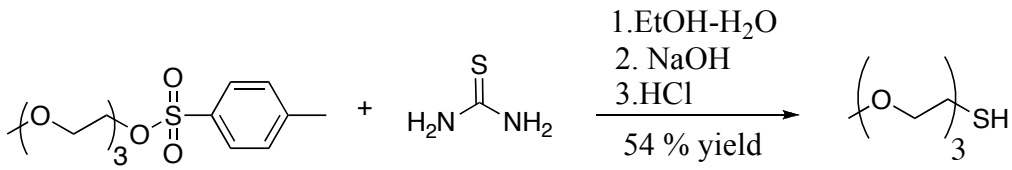

2.7 **2.19**

Scheme 2.9

The prepared thiol **2.19** was utilized in three different phthalonitrile syntheses. The procedure, employed in the synthesis of triethyleneglycol-substituted phthalonitrile **2.15**,[11] was used as a reference for the synthesis of thioethylene glycol-bearing phthalonitriles **2.20** and **2.21**. Excess of thiol **2.19** was stirred with either 3-nitrophthalonitrile (**2.20**) or 4-nitrophthalonitrile (**2.21**) in the presence of K_2CO_3 in DMF (Scheme 2.10). After completion of the reaction, 3-thioethylene glycol-substituted phthalonitrile **2.20** was simply purified by precipitation. The suspension was poured into ice-water mixture and left overnight at room temperature. The product was collected by filtration and obtained in 91% yield (Scheme 2.10). The same

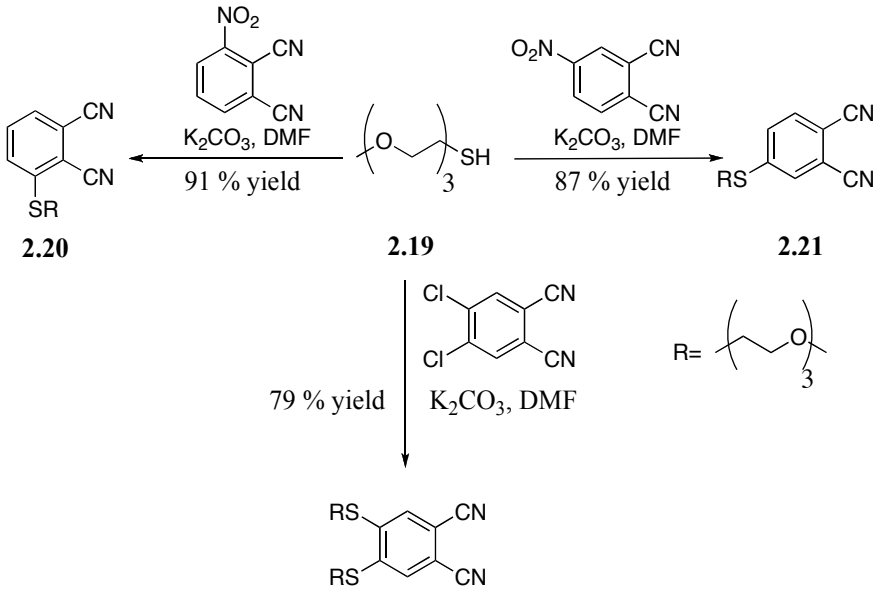

Scheme 2.10

purification method was also used to purify 4-thioethyleneglycol-substituted phthalonitrile **2.21**. However, the product was obtained in an oil form rather than solid. The molecular structure of the thio-pegylated phthalonitrile **2.20** is shown in Figure 2.8.

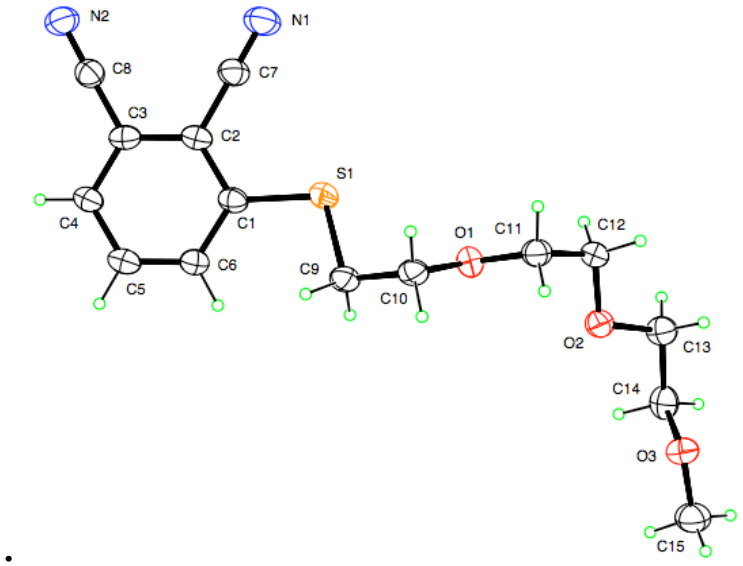

Figure 2.8 ORTEP representation of the molecular structure of **2.20** with 50% ellipsoids.

The last, di-substituted phthalonitrile, was synthesized via nucleophilic aromatic substitution between the thiol **2.19** and chlorine on the 4,5-dichlorophthalonitrile as previously discussed. The product was purified by column chromatography and obtained in 79% yield (Scheme 2.10).

2.2.3 Solution-Phase Synthesis of Phthalocyanines

After the successful syntheses of phthalonitrile precursors, bearing different types of water solubilizing groups, we attempted to synthesize asymmetrically- (AB_3) and symmetrically- (B_4 or A_4) substituted Pcs in solution via base-promoted cyclotetramerization of phthalonitriles. Two precedented methods were employed to synthesize both kinds of Pcs. The difference between the two methods is the reagents used during the synthesis. While the most commonly used cyclotetramerization method requires refluxing in high boiling point alcohol in the presence of a base, generally DBU,[11] the other method necessitates refluxing in DMF and utilizes HMDS as a base.[27] In both cases, the reaction proceeds through the similar mechanism: (Scheme 2.11)[28] Herein discussed is the mechanism of the first method which was predominantly used in the synthesis of the Pcs. Following the formation of an alkoxide in situ, the reaction starts with the nucleophilic attack to the one of the nitrile carbon on phthalonitrile (**2.23**) to generate isoindoline derivative (**2.24**). In the next step, isoindoline derivative behaves as a nucleophile and attacks the other phthalonitrile in solution to form dimeric species (**2.25**). In the presence of a metal salt, this step is facilitated due to the chelation of the metal with the nitrile group (**2.23**), which makes the nitrile carbon more electron deficient as a consequence more likely to be attacked by a nucleophile. This step is repeated one more time to generate another dimeric (half Pc) species. The ring closure occurs in two steps: Nucleophilic attack of the imide on the aryl ether followed by the loss of alkoxide leads the formation of an aza bridge (**2.26**). The repeat of this step generates anti-aromatic macrocycle **2.27**. By the loss of two electrons, the conjugated system

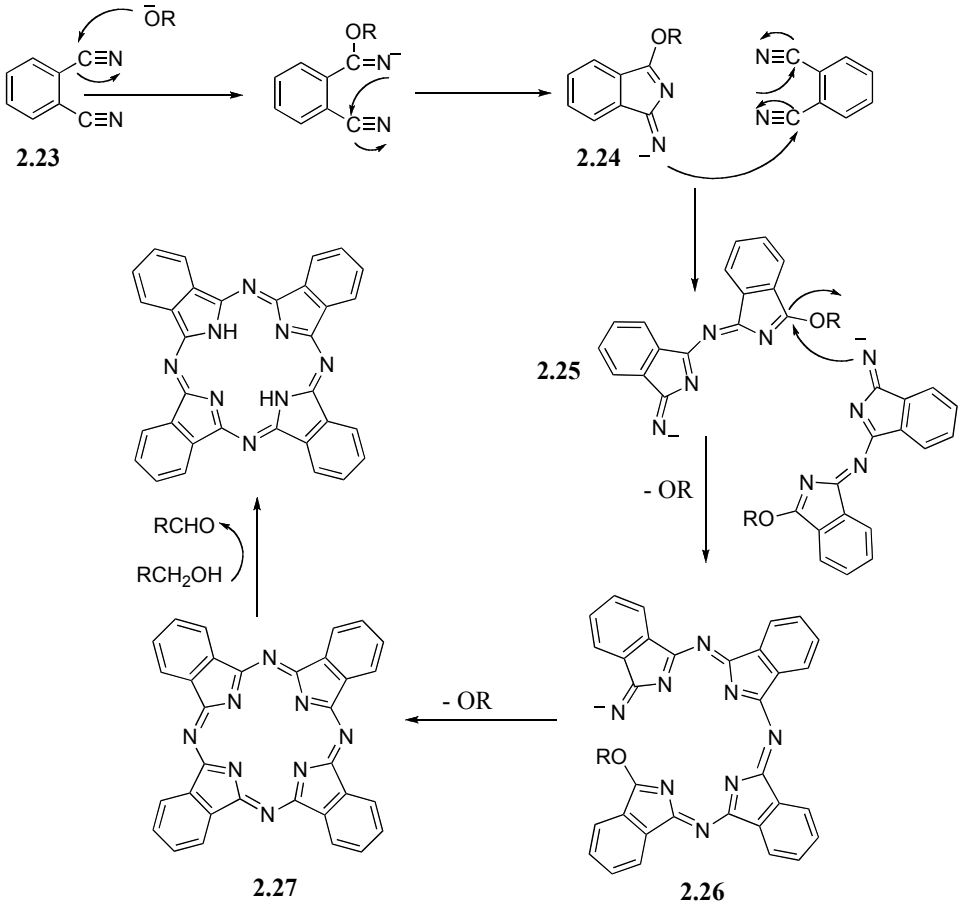

Scheme 2.11 The mechanism of cyclotetramerization in the presence of alkoxide

gains aromaticity, which is the driving force for the reaction, and the Pc is generated. The balanced equation of an unsubstituted-metal free Pc formation in BuOH is shown below in Equation 2.1.

Unsubstituted phthalonitrile ⟶ Unsubstituted-metal free Pc

$$4\ C_8H_4N_2 + C_4H_9OH \longrightarrow C_{32}H_{18}N_8 + C_4H_8O \qquad \text{(Eq. 2.1)}$$

The first target Pc **2.29** was designed to have dodeca-carboxylic acid units to improve the solubility of the hydrophobic Pc core and one amine group to utilize for covalent conjugation to biomolecules. As shown in Scheme 2.12, retrosynthetic analysis of amine functional Pc **2.30** revealed that the synthesis would start with condensation of two different phthalonitrile

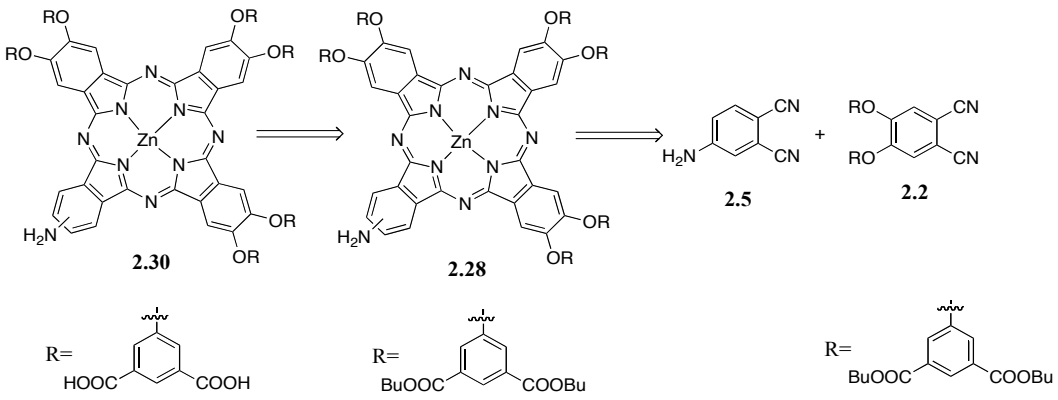

Scheme 2.12

precursors in 3:1 molar ratio, 4-amino phthalonitrile **2.2** and ester functionalized phthalonitrile **2.5** respectively. Following the isolation of dodeca-ester-bearing Pc **2.28**, hydrolysis of the ester groups would yield the target amino, carboxylic acid bearing Pc **2.30**. Amine and ester substituted phthalonitriles, **2.2** and **2.5** respectively, with $Zn(OAc)_2$, as a metal source, were dissolved in anhydrous BuOH in the presence of DBU. The reaction mixture was refluxed for 24h under Ar (Scheme 2.13). As a result of random chemoseletive process, cyclotetramerization

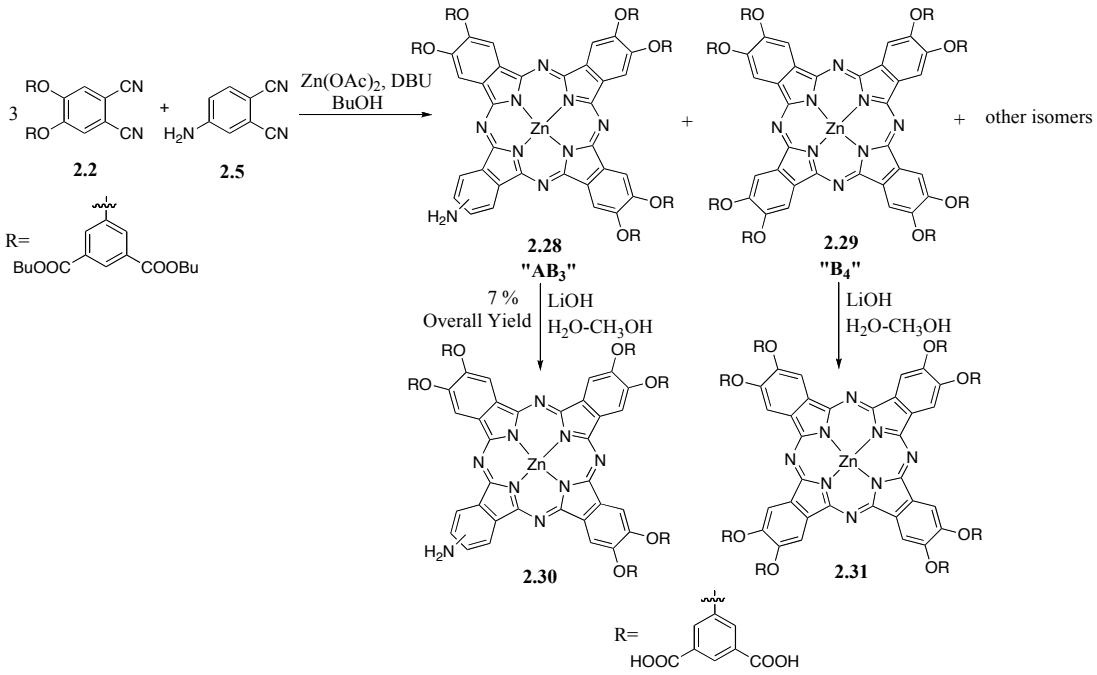

Scheme 2.13

of two different phthalonitriles produced a mixture of congeners, which required an extensive purification process to separate one congener from another. Figure 2.9 shows the mass spectrum (MALDI-MS) of the crude mixture as an indication of the random cyclotetramerization of the phthalonitriles during the reaction. The blue colored crude mixture contained the target AB_3 type Pc (**2.28)** along with symmetrically-substituted hexadeca-carboxylic acid-bearing B_4 type Pc (**2.29**), which was formed via self condensation of ester substituted Pc **2.2**, another symmetrically-substituted tetra amine units containing A_4 type Pc, as well as A_2B_2 and/or AB_2 type Pc having di-amines and octa-carboxylic acid units. The mass spectrum also showed

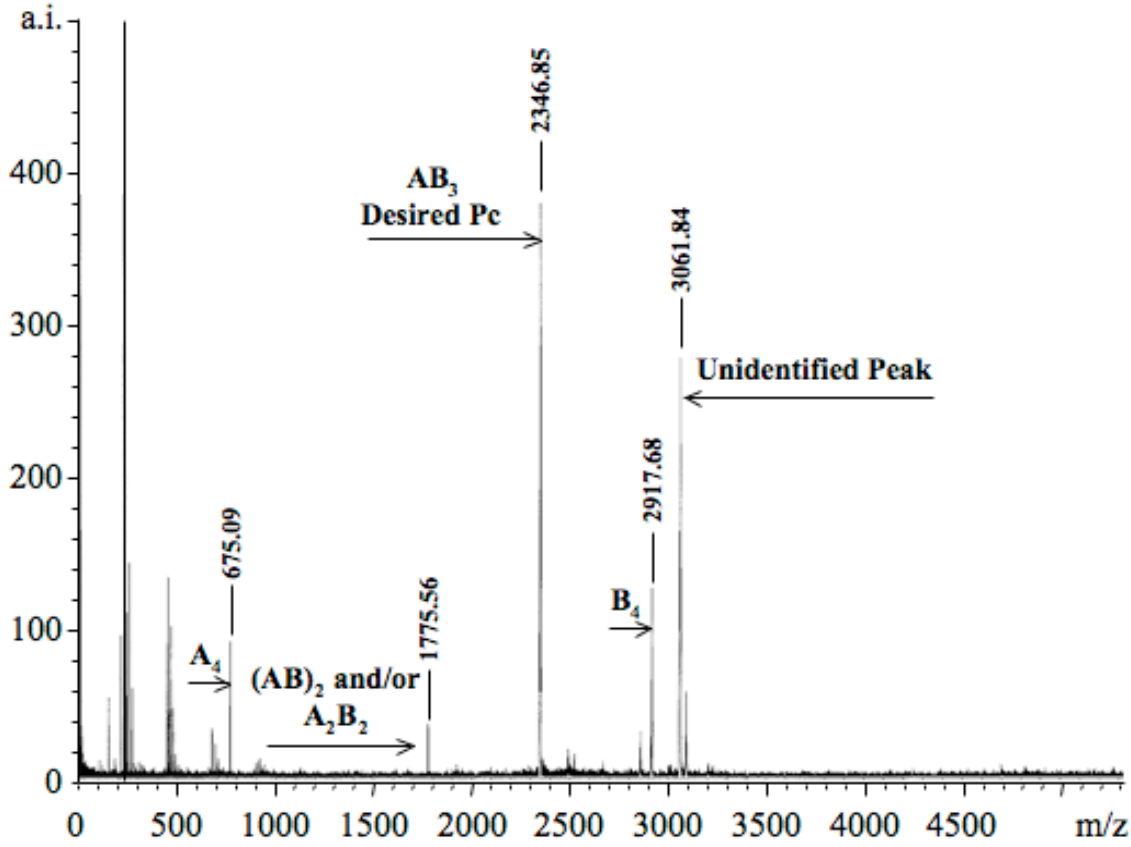

Figure 2.9 MALDI-MS spectrum of the crude mixture of ZnPc **2.28**.

another major peak with m/z value 3061, which could not be identified. Several attempts were made to purify the product by chromatographic methods. Series of column chromatography on

silica gel were performed to isolate the target Pc from the sea of Pcs. Purification of Pc mixtures is a laborious process due to their tendency to aggregate via non-covalent interactions. A wide variety of solvent systems and chromatographic methods must be employed to break down the aggregates in order to obtain pure Pcs. While symmetrically-substituted Pc **2.29** was isolated in 93% purity (by MALDI-MS), the desired Pc could not be entirely isolated from the mixture after running silica gel and ion exchange columns. The crude mixture of mono-amine functional Pc **2.28** and the purified symmetrically-substituted ester Pc **2.29** was individually submitted to hydrolysis reaction. Butyl ester groups were hydrolyzed to the parent carboxylic acid and alcohol using large excess of LiOH in CH_3OH-H_2O mixture at 60 °C.[29] The complete hydrolysis was achieved by repeating the reaction. Following the work up, symmetrically-substituted hexadeca-carboxylic acid-bearing Pc **2.31** was purified on silica gel column (Figure 2.10 shows the mass spectrum of **2.31**). In contrast, the mixture, containing the mono-amine functional desired Pc **2.30** and symmetrically-substituted Pc **2.31**, were submitted to series of column chromatography in order to isolate the dodeca-carboxylic acid-bearing Pc **2.30**. Initially, ion exchange column was run using MP-TsOH column. The target compound was expected to be "caught" by the sorbent bed, while the impurities, lacking an amine group, would pass through the column. Elution of the desired compound with an appropriate solvent system would yield pure mono-amine functional Pc **2.30**. Following the procedure, provided by the producer of the MP-TsOH column, two different fractions were collected. However, both fractions were a mixture of the two Pc congeners. Further purification of the mono-amine functionalized Pc **2.30** was performed by column chromatography on silica gel column. Four different silica gel columns, using different eluting systems, were followed by a reverse phase C^{18} column to isolate mono-amine functional dodeca-carboxylic acid bearing Pc **2.30** in 7% overall yield. Figure 2.11 shows the mass spectrum of desired AB_3 type asymmetrically-substituted Pc **2.30**.

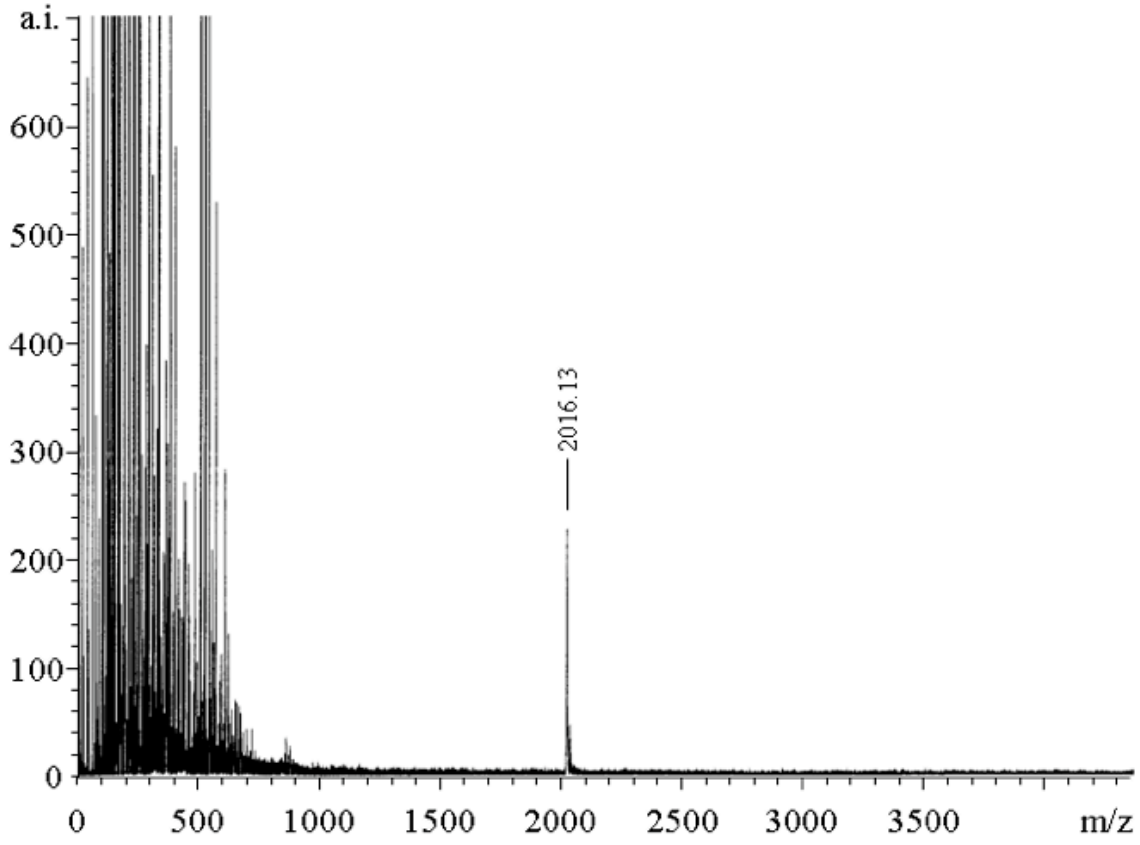

Figure 2.10 MALDI-MS spectrum of ZnPc **2.31**.

Uv-vis spectra of the isolated Pcs, before and after hydrolysis, had close absorption maxima along with similar Q band shapes. The absorption spectra in Figure 2.12 belong to the crude mixture of symmetrically-substituted ester Pc **2.28** (after attempted purification) and AB_3 type asymmetrically-substituted mono-amine contaning Pc **2.29**. Both of the spectra were taken in CH_2Cl_2. While hexadeca-ester-bearing Pc **2.28** had absorption maxima at 686 nm, dodeca-ester containing **2.29** had a split Q band with absorption maxima at 642 and 676 nm. Broadness and the splitting of the Q band indicated the aggregation of the Pcs in the selected solvent. After hydrolysis, while asymmetrically-substituted mono-amine functionalized Pc **2.30** had a sharp Q band at 677 nm in DMSO, hexadeca-carboxylic acid-bearing Pc **2.31** showed signs of aggregation in THF with a split Q band with absorption maxima at 676 and 649 nm (Figure 2.13)

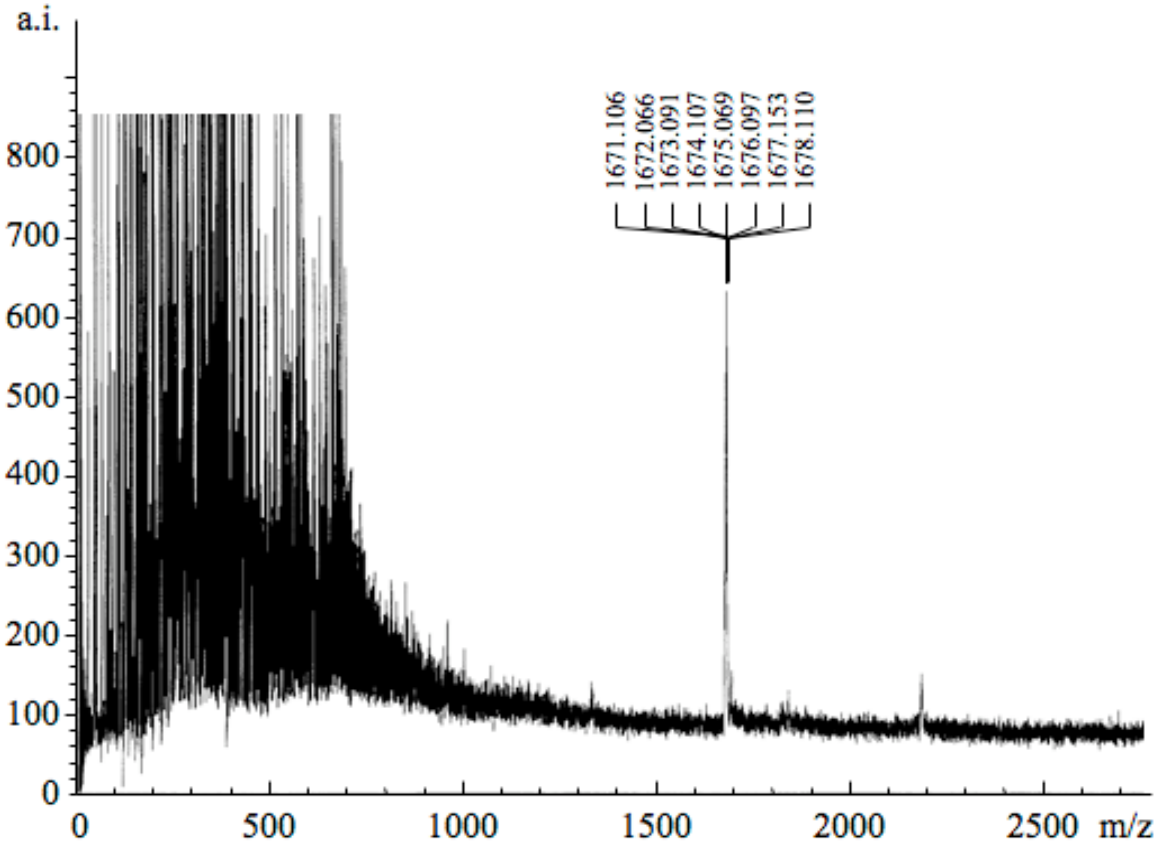

Figure 2.11 MALDI-TOF spectrum of ZnPc **2.30**.

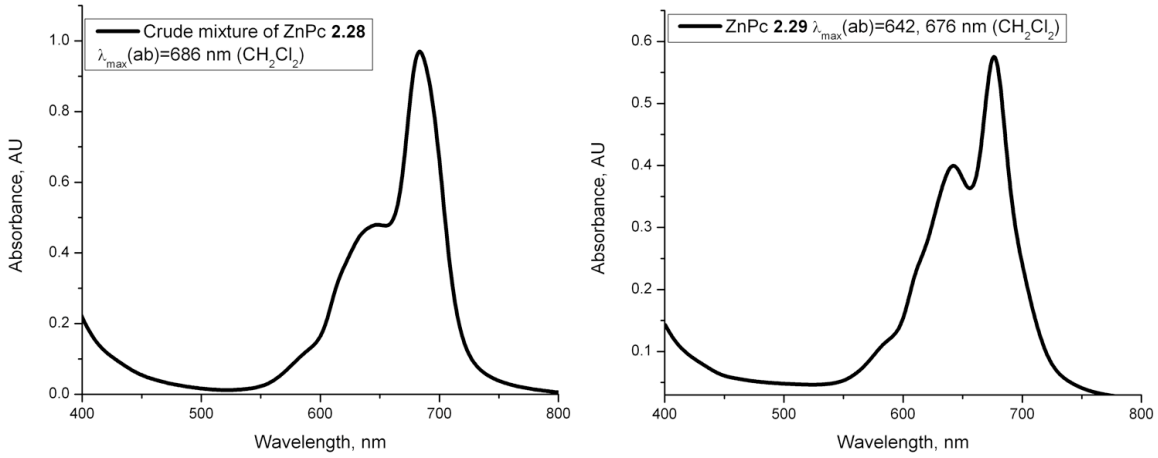

Figure 2.12 Absorption spectra of ZnPc **2.28** (left) and ZnPc **2.29** (right).

In contrast to asymmetrically-substituted Pcs, purification of the symmetrically-substituted Pcs, synthesized from single phthalonitrile precursors, is relatively easy process since the crude mixture contains the target compound without contamination of any other Pc congeners.

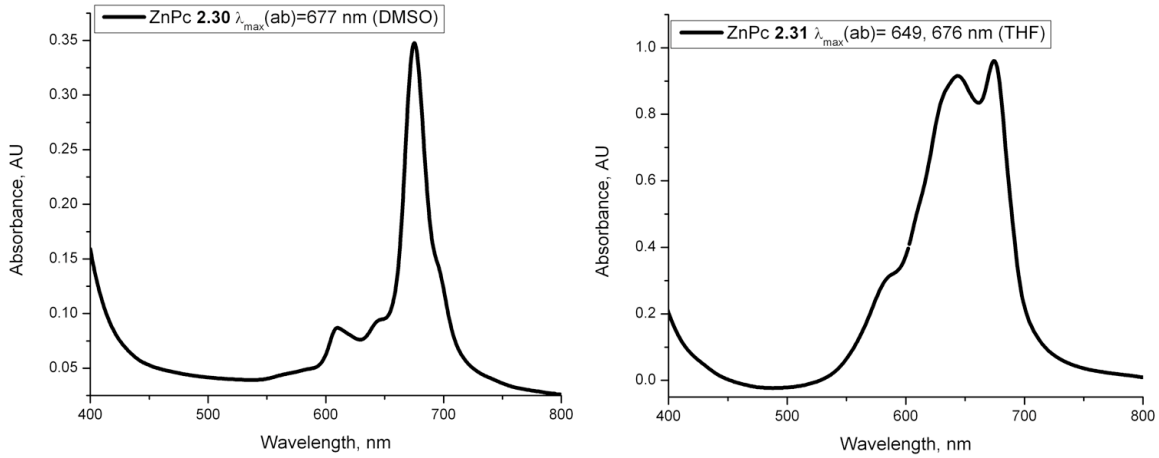

Figure 2.13 Absorption spectra of ZnPc **2.30** (left) and ZnPc **2.31** (right).

Symmetrically-substituted target Pc **2.32** was designed to have octa-ethylene glycol chains as water solubilizing groups. Triethyleneglycol-substituted phthalonitrile **2.11** and $Zn(OAc)_2$ with DBU was refluxed in BuOH for 24h. (Scheme 2.14) Oligoethyleneglycol-substituted Pc **2.32**

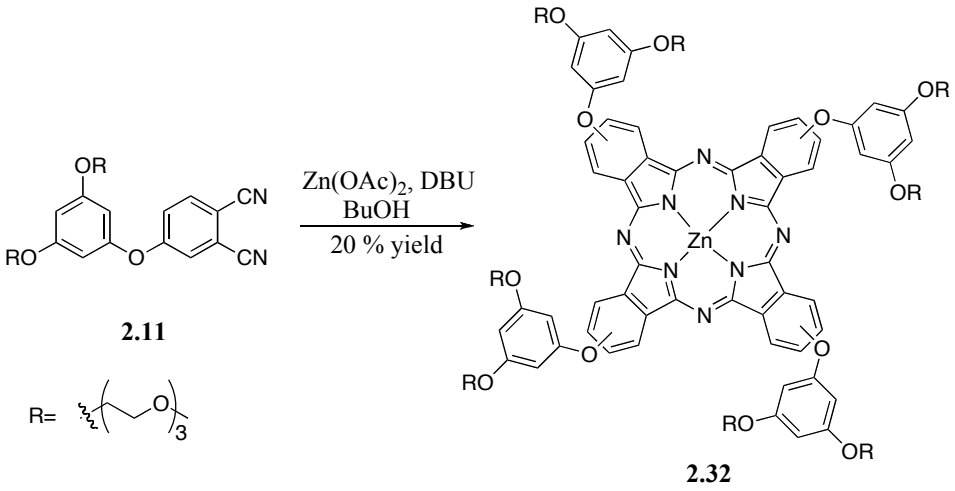

Scheme 2.14

was purified on silica gel column and obtained in 20% yield. As a result of randomregioselective cyclotetramerization, the product was obtained as a mixture of isomers. However, any attempt to isolate a single isomer has not made.

Unlike mono-amine functional asymmetrically-substituted Pc **2.30**, octa-triethyleneglycol-bearing symmetrically-substituted Pc **2.32** was obtained in moderate yield due to the two factors: 1) Cyclotetramerization of a single type phthalonitrile yields only one of the six congeners of the Pc. The crude mixture contains high percentage of the desired Pc contaminated with some low molecular weight impurities; 2) limited column chromatography on silica gel reduces loss as nonspecific adsorption of Pcs to the silica gel results in poor recovery of the Pcs. Consequently, as the number of chromatography steps on silica gel increase, the yield of the product decreases.

Symmetrically-substituted Pc **2.32,** decorated with triethyleneglycol chains, has a distinctive Q band with absorption maxima at 680 nm in DMSO (Figure 2.14) and a well-defined emission band at 688 nm upon excitation at 610 nm (Figure 2.15). A broad, split and blue shifted Q band of oligoethyleneglycol-substituted Pc **2.32** in CH_3OH, water and CH_3OH-H_2O mixtures

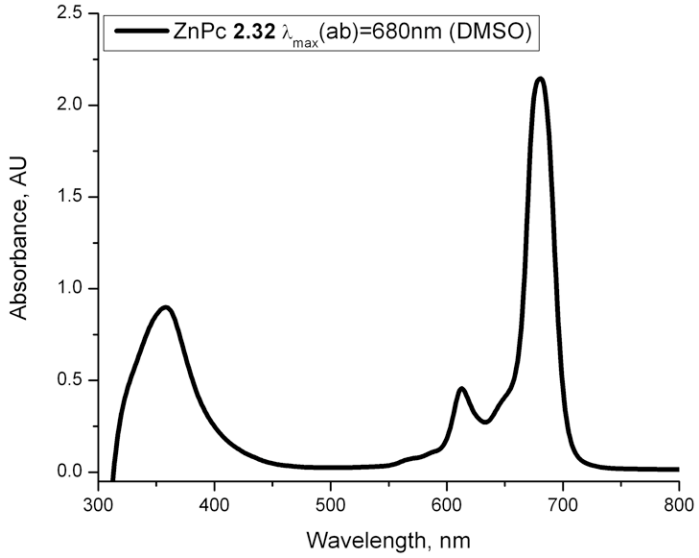

Figure 2.14 Absorption spectrum of **2.32** in DMSO systems (Figure 2.16).

at different ratios at 10^{-5} M concentration was an indication of aggregation of the Pc in the selected solvent. Consequently, symmetrically substituted Pc **2.32** has very low fluorescence intensity and blue shifted emission band in CH_3OH upon excitation at 610 nm. Absorption

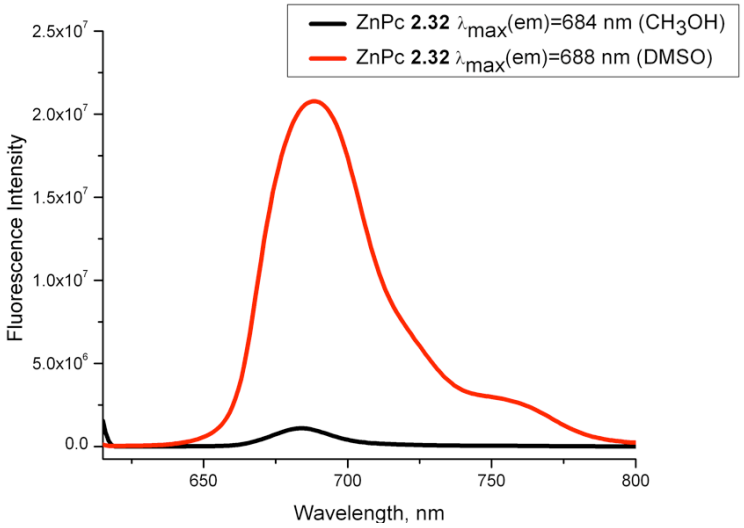

Figure 2.15 Emission spectra of **2.32** in DMSO (red) and CH_3OH (black).

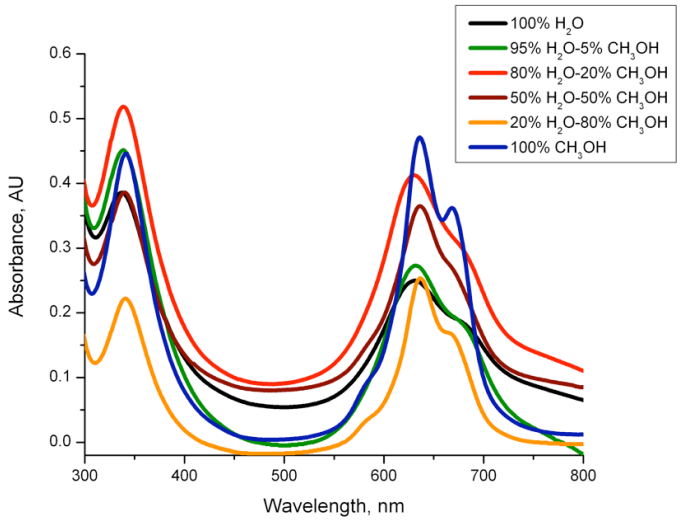

Figure 2.16 Absorption spectra of **2.32** in different ratios of CH_3OH-H_2O mixtures.

profiles of the target Pc in different ratios of CH_3OH-water mixture are shown in Figure 2.16.

Syntheses of symmetrically substituted Pcs were continued with the nitro substituted Pc **2.33**. The target Pc was designed to have tetra-nitro groups as a functional group, which could be reduced to amine to increase the solubility after the cyclotetramerization reaction. To prevent any premature reactions during the cyclotetramerization of the phthalonitrile, reduction of the nitro group was planned as the final step in the syntheses. Self condensation of 4-nitro

benzamide phthalonitrile **2.6** with $Zn(OAc)_2$ and HMDS in DMF for 12h.[27] gave a dark green colored crude mixture of symmetrically substituted tetra-nitro bearing Pc **2.33** (Scheme 2.15).

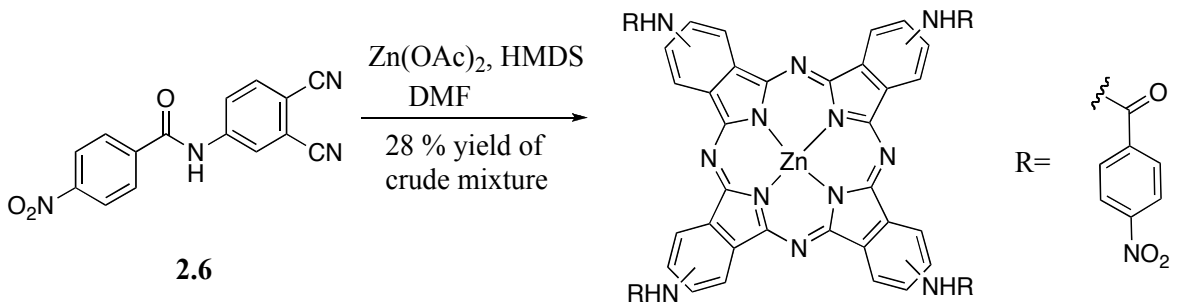

2.6 **2.33**

Scheme 2.15

The crude mixture of the target compound was only soluble in DMF and DMSO and partially soluble in ether and acetone. Due to the poor solubility of the Pc, it was nearly impossible to purify the desired compound by chromatographic techniques. Attempted purification of the nitro functional Pc **2.33** by simply washing the crude mixture with CH_3OH and H_2O, and boiling the crude product in different organic solvents for 2 h. was partially successful at removing the low molecular weight impurities. While the mass spectrum of the symmetrically substituted Pc confirmed the identity of the product, the purity of the product was questionable. Without any further purification, the crude mixture was submitted to next reaction.

Reduction of the nitro groups of the crude mixture of **2.33** was performed via catalytic hydrogenation. (Scheme 2.16) Treatment of tetra-nitro containing Pc **2.33** with Raney-nickel under 50 psi H_2[30] resulted in cleavage of the amide bond at several positions, which was not expected. With the assumption of high pressure would initiate the amide bond cleavage, catalytic hydrogenation was performed at atmospheric pressure in the presence of Pd/C as a metal catalyst (Scheme 2.16). Surprisingly, this method resulted in decomposition of the Pc. The product of the reaction, brown colored solid, could not be identified. The last method, employed

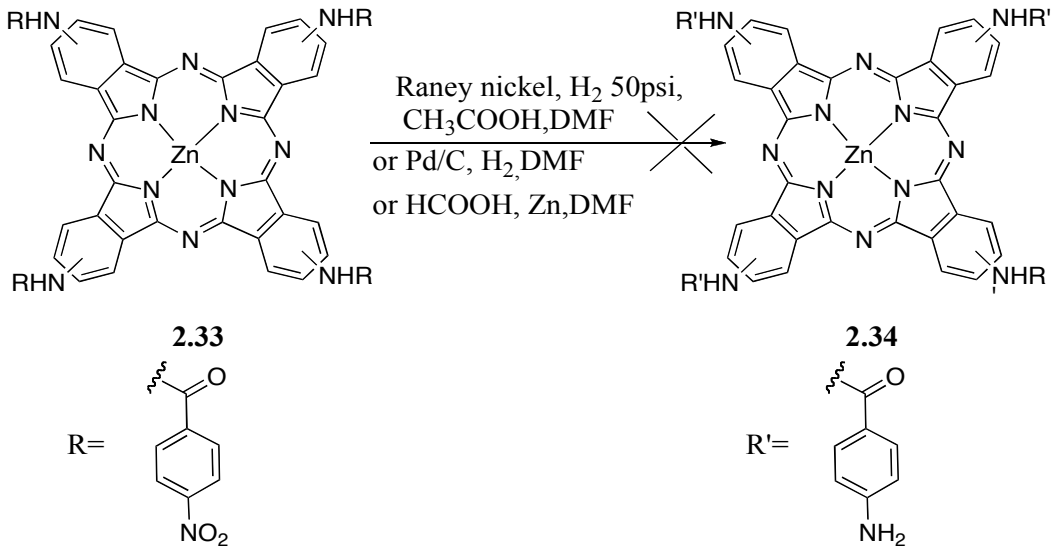

Scheme 2.16

to reduce the nitro groups, was Zn catalyzed reduction in the presence of acetic acid.[31] Mass spectrum of the green colored solid, did not show any evidence to support the formation of amine containing Pc **2.34**. Any other route to synthesize the Pc **2.34** was not attempted.

2.3 Conclusion and Future Work

In this chapter synthesis of phthalonitrile precursors, bearing a variety of water solubilizing groups, and water-soluble symmetrically- and asymmetrically-substituted Pcs via solution phase cyclotetramerization are reported. Synthesis of phthalonitrile precursors starting from commercially available phthalonitriles was a success. While the purification of the symmetrically substituted Pcs can be accomplished in relatively short amount of time, modification of the products was an unexpected problematic situation. As a result of congener formation, purification of the asymmetrically-substituted Pcs using chromatographic techniques is a laborious and extremely difficult process. Great amount of time needs to be invested to isolate the desired compound. For a general, reproducible synthesis of asymmetrically-substituted Pcs, an improved method needs to be developed.

2.4 Experimental

2.4.1 General Experimental Information

Unless otherwise indicated, all commercially available starting materials were used directly without any further purification. Reactions under anhydrous conditions were performed in dried solvents under argon atmosphere. Commercially available starting compounds were used without further purification. Reactions were monitored by TLC using Sorbent Technologies silica gel plates 250 μm with UV activator. Silica gel Sorbent Technologies 40-63 μm was used for column chromatography. ^{1}H NMR and ^{13}C NMR were obtained on DPX-250 Bruker spectrometer. Chemical shifts (δ) are given in ppm relative to methylene chloride (5.32 ppm ^{1}H; 54 ppm, ^{13}C NMR) or DMSO (2.49 ppm ^{1}H NMR; 39.51 ppm ^{13}C NMR). Low-resolution mass spectra (MS) were obtained on a Bruker Proflex III MALDI-TOF massspectrometer. Unless otherwise indicated, all MALDI-MS spectra were obtained using CCA as a matrix. FT-IR spectra were obtained on Bruker Tensor 27 spectrometer. Electronic absorption spectra were measured on a Perkin-Elmer Lambda 35 UV-vis spectrophotometer. Emission spectra were obtained using a FLUOROLOG-3 spectrofluorometer (Horiba Jobin Yvon, Edison, NJ) equipped with a 450-W xenon lamp and a cooled Hamamatsu R928 photomultiplier operated at 900V in the photon-counting mode. A quartz cuvette with a 10 mm path length was utilized throughout these experiments. All measurements were performed under ambient room conditions within 3h. of solutions preparation. Stock solution and dilutions were prepared in anhydrous DMSO, CH_3OH, THF or CH_2Cl_2.

2.4.2 Experimental Procedures

5-Hydroxy isophthalic acid dibutyl ester (2.1)

To a solution of 5-hydroxyisophthalic acid (5 g, 27.4 mmol) in C_4H_9OH, (30 mL), a catalytic amount of concentrated H_2SO_4 was added and the clear solution was refluxed for 5 h. The

mixture was concentrated by evaporating of C_4H_9OH and the residue was dissolved in EtOAc. The organic layer was washed with saturated $NaHCO_3$ solution (3x50 mL), H_2O (3x50 mL), brine (2x50 mL) and then dired over $MgSO_4$. (White crystals, 88%) ^1H NMR (250 MHz, DMSO-d_6) δ10(1H), 7.9(1H), 7.5(2H), 4.3(4H), 1.6(4H), 1.4(4H), 0.9(6H)

4-(3,5-Bis(2-(2-(2-methoxyethoxy)ethoxy)ethoxy)phenoxy)phthalonitrile (2.2)

5-Hydroxyisophthalic acid dibutyl ester (**1**) (2.5 g, 8.5 mmol) and K_2CO_3 (1.2 g, 9 mmol) were stirred in anhydrous DMF (10 mL) at 70 ^oC for 30 minutes. The solution of 4,5-dichloro-phthalonitrile (0.79 g, 4 mmol) in DMF (4 mL) was added to the suspension dropwise. After seven h, (yellow suspension), the solvent was evaporated and the crude mixture was dissolved in CH_2Cl_2 and washed with saturated $NaHCO_3$ (3x50 mL), H_2O (3x50 mL) and brine (2x50 mL). The crude mixture was purified by column chromatography on silica gel with CH_2Cl_2-hexane (3:2) as eluting solvent to give a white solid in 67% yield. ^1H NMR (250 MHz, DMSO-d_6) δ 8.2(1H), 8.1(1H), 7.7(2H), 4.3(4H), 1.7(4H), 1.4(4H), 0.94(6H).

4-(3,4-Dicyanophenoxy)benzoic acid (2.3)

Into a solution of 4-hydroxybenzoic acid (2.4 g, 17.3 mmol) in anhydrous DMF (10 mL), 4-nitrophthalonitrile (2.0 g, 11.6 mmol) and finely ground K_2CO_3 (4.8 g, 34.7 mmol) were added. The mixture was stirred at room temperature for 24 h. As the reaction proceeded, a light yellow precipitate formed. **Purification method 1:** The crude mixture was evaporated to dryness and the resultant mixture was dissolved in CH_3OH (~10 mL) and neutralized by 1N HCl solution. The light yellow colored precipitate was collected by filtration and was further purified by column chromatography on silica gel with EtOAc-hexanes (1:1) as eluting solvent to give a white solid 71% yield. **Purification method 2:** Following the removal of the inorganic salts, the reaction mixture was diluted with CH_2Cl_2 (~ 20 mL) and it was neutralized with 1N HCl solution with continuous stirring at room temperature. The product was extracted with CH_2Cl_2

and the solvent was evaporated. The resultant oil was solidified by pouring into the 400 mL ice-water and the precipitate was collected by filtration to give the product as a white solid in 67% yield. ^{1}H NMR (250 MHz, DMSO-d_6) δ 8.1(1H), 8.0(2H), 7.9(1H), 7.5(1H), 7.2(2H) ^{13}C NMR (250MHz,CH_2Cl_2-d_2)δ 169.40, 160.14, 135.54, 132.77, 126.37, 122.50, 119.83, 117.70, 115.18, 114.78, 110. 00. FT-IR (KBr, cm^{-1}) 3087, 3039, 2846, 2553, 2231, 1672, 1608, 1589, 1570, 1504, 1489, 1427, 1309, 1296, 1278, 1252, 1211, 1165, 1127, 1112, 1088, 1014, 951, 934, 905, 869, 848, 776, 734, 710.

2-(Tert-butoxycarbonylamino)-3-(4-(3,4-dicyanophenoxy)phenyl)propanoic acid (2.4)

Into a solution of 4-nitrophthalonitrile (1.35 g, 7.8 mmol) in anhydrous DMF (10 mL), Boc-Tyr-OH (2 g, 7.1 mmol) and finely ground K_2CO_3 (1.95 g, 14.2 mmol) were added. The mixture was stirred at room temperature for 24 h. The color of the solution turned from yellow to clear overnight. The reaction was followed by TLC. After running the TLC (EtOAc), the plate was placed in concentrated HCl chamber for a minute to remove the Boc protecting group and then was stained with ninhydrin solution. The clear TLC plate was heated with a heat gun until the purple spot with higher R_f value relative to Boc-Tyr-OH was appeared, corresponding to free amine containing compound. Following the removal of inorganic salts, the solution was neutralized with 1N HCl solution. The product was extracted with EtOAc and purified by column chromatography on silica gel. The column was first washed with EtOAc-hexane (99.5:0.5) mixture and the excess of 4-nitrophthalonitrile was collected. EtOAc concentration was gradually increased up to 100% to collect the product. Following the evaporation of the solvent, the product was obtained as a yellow solid in 70% yield. ^{1}H NMR (250 MHz, CH_2Cl_2-d_2) δ 7.8 (1H), 7.3 (5H), 7.1(2H), 4.7(1H), 3.3(1H), 3.0(1H)

4-Aminophthalonitrile (2.5)

4-Nitrophthalonitrile (0.77 g, 4.45 mmol) was added to mixture of CH_3OH (16 mL) and concentrated HCl (3.5 mL). Suspension was brought to boil and Fe dust (0.8 g, 14.5 mmol) was added portionwise over 45 minutes. Heating continued briefly and CH_3OH was evaporated. The mixture was poured into the 200 mL of H_2O and filtered. Recrystallization of crude mixture from benzene gave a pale yellow product in 70% yield. ^{1}H NMR(250 MHz, DMSO-d_6) δ 7.7(1H), 7.0(1H), 6.9(1H), 6.7(2H); ^{13}C NMR (250 MHz, DMSO-d_6) δ150.02, 132.14, 121.24, 120.14, 117.12, 115.24, 116.45, 104.20. GC-MS Cald $C_8H_5N_3^+$: 143.0; found: 143.0

N-(3,4-Dicyanophenyl)-4-nitrobenzamide (2.6)

To a stirring solution of 4-nitrobenzoylchloride (2.72 g, 14.7 mmol) in anhydrous acetone (40 mL), 4-aminophthalonitrile (1.43 g, 10 mmol) and Na_2CO_3 (5.3 g, 50 mmol) were added and the mixture was refluxed for 4 h. Dark yellow suspension was filtered when it was hot. Filtrate was left in -20 ^{o}C overnight. Crystals were collected and dissolved in CH_2Cl_2 and purified by column chromatography on silica gel with CH_3OH-CH_2Cl_2 (3:97) as eluting solvent. The product was recrystallized from EtOH to give a pale yellow solid in 70% yield. mp: 259-261^{o}C; ESI Calcd $C_{15}H_8N_4O_3$-H: 291.0; found 291.1. ^{1}H NMR (250 MHz, DMSO-d_6) δ11.3(2H), 8.4(3H), 8.2(4H) ^{13}C NMR (250 MHz, DMSO-d_6) δ 193.76, 165.69, 150.45, 144.45, 140.20, 140.14, 135.90, 130.36, 125.08, 125.00, 124.58, 116.69, 116.23, 109.23, 109.5

Toluene-4-sulfonic acid 2-[2-(2-methoxyethoxy)-ethoxy]-ethyl ester (2.7)

NaOH (1.6 g, 40 mmol) was dissolved in H_2O (10 mL) and added to solution of 2-[2-(2-methoxyethoxy)-ethoxy]-ethanol (4.6 g, 20 mmol) in THF (10 mL). The mixture was cooled down to 0-5 ^{o}C and the solution of p-toluene sulfonyl chloride (5 g, 20 mmol) in THF (10 mL) was added to reaction mixture over 1 hour. The mixture was poured into the ice-water (50 mL) and extracted with CH_2Cl_2 (2x75 mL). The combined organic layers were washed with H_2O

(2x75 mL) and brine (2x75 mL). The organic layer was dried over $MgSO_4$ and CH_2Cl_2 was evaporated to give a clear oil in 94% yield. ^{1}H NMR (250 MHz, CH_2Cl_2-d_4) δ 7.8(2H), 7.7(2H), 4.1(2H), 3.6(10H), 2.4(3H); ^{13}C NMR (250 MHz, DMSO-d_6) δ 145.75, 133.51, 131.23, 130.81, 128.80, 128.70, 127.87, 73.30, 72.16, 71.81, 70.58, 7.84, 61.20, 58.90, 25.94, 21.74.

5-Benzyloxybenzene-1,3-diol (2.8)

Phloroglucinol, (3 g, 23 mmol) was dissolved in anhydrous DMF (10 mL) and added to suspension of K_2CO_3 (1.44 g, 10 mmol) in DMF (10 mL). The mixture was stirred for 10 minutes. Benzyl bromide (1.76 g, 1 mmol) in DMF (5 mL) was added to mixture dropwise over 40 minutes. The brown colored mixture was stirred 1 more hour and inorganic salts were removed by filteration. DMF was evaporated and the crude mixture was dissolved in EtOAc and washed with 1N HCl solution (3x20 mL). Organic layers was combined and purified by column chromatography on silica gel with THF- CH_2Cl_2 (7:93) to give a light brown oil in 40% yield. ^{1}H NMR (250 MHz, DMSO-d_6) δ 9.1(2H), 7.3(5H), 5.8(3H), 4.9 (2H). GC-MS Cald $C_{13}H_{12}O_3^+$: 216.0; found: 216.2

1-Benzyloxy-3,5-bis-{2-[2-(2-methoxyethoxy)-ethoxy]-ethoxy}-benzene (2.9)

5-Benzyloxy-benzene-1,3-diol (**2.8**) (0.6 g, 2.7 mmol) and toluene-4-sulfonic acid 2-[2-(2-methoxyethoxy)-ethoxy]-ethyl ester (**2.7**) (2.65 g, 8.3 mmol) were dissolved in freshly distilled 2-butanone (20 mL). After addition of K_2CO_3 (4 g, 28.9 mmol) and a spatula tip quantity of KI, the yellow suspension was refluxed under Ar for 20 h. The solvent was evaporated to dryness and the crude mixture was redissolved inCH_2Cl_2. The organic layer was washed with 1N HCl (2x50 mL), H_2O (2x50 mL), brine (2x50 mL) and dried over $MgSO_4$. The crude mixture was purified by column chromatography on silica gel by washing the column with hexane-EtOAc (1:1), EtOAc, and EtOAc-CH_3OH (9:1) to give a light brown oil in 67% yield. ^{1}H NMR (250 MHz, DMSO-d_6) δ 7.4(5H), 6.1(3H), 5.05(2H), 4.04(5H), 3.7(5H), 3.5(18H),3.24(8H)

3,5-Bis-{2-[2-(2-methoxyethoxy)-ethoxy]-ethoxy}-phenol (2.10)

Into a solution of benzyl ether **2.9** (0.3 g, 0.59 mmol) was dissolved in EtOH (8 mL) and Pd/C (30 mg, 10% by weight) was added. Reaction was run under 50 psi H_2 (g) for 20 h. The resultant suspension was passed through a plug of celite and EtOH was evaporated. The crude mixture was loaded onto a 10 g silica column. First, column was washed with EtOAc-CH_2Cl_2 (9:1) and then with CH_3OH-EtOAc-CH_2Cl_2 mixture by increasing gradually CH_3OH percentage by 1% in until the percentage of CH_3OH reaches 10% in the mixture. The light brown oil was obtained in 73% yield. ^{1}H NMR (250 MHz, DMSO-d_6) δ 9.59(1H), 5.9(3H), 3.99(4H), 3.7(4H), 3.4(16H), 3.3(6H). GC-MS Cald $C_{20}H_{34}O_9^+$: 418.2; found: 418.3.

4-(3,5-Bis-{2-[2-(2-methoxyethoxy)-ethoxy]-ethoxy}-phenoxy)-phthalonitrile (2.11)

Into a solution of 4-nitrophthalonitrile (0.17 g, 0.97mmol) in anhydrous DMF (5 mL), 3,5-bis-{2-[2-(2-methoxyethoxy)-ethoxy]-ethoxy}-phenol (**2.10**) (0.45 g, 1.07 mmol) and finely ground K_2CO_3 (0.3g, 1.94 mmol) was added. As soon as K_2CO_3 was added, the color of the solution turned from yellow to dark brown. The mixture was stirred at room temperature for 48 h. After removal of the inorganic salts by filtration, DMF was evaporated and the crude mixture was purified by column chromatography on silica gel with CH_3OH-EtOAc (1:199) as eluting solvent to give a brown oil in 65% yield. ^{1}H NMR (250 MHz, $CDCl_3$-d_6) δ 7.7(1H), 7.3(2H), 7.2(1H), 6.4(1H), 6.2(2H), 4.1(4H), 3.8(4H), 3.7(16H), 3.5(4H)

4-(2-(2-Methoxyethoxy)ethoxy)phenol (2.12)

Hydroquinone (10 g, 90.9 mmol) was dissolved in CH_3CN with K_2CO_3 (12.5 g, 90.9 mmol) and stirred at 50 °C for 20 minutes. 1-Bromo-2-(2-methoxyethoxy)ethane (3.7 mL, 27.3 mmol) was dropwise added to mixture. The color of the suspension changed from yellow to pale yellow over the time. After 24 h, salts were removed by filtration and the filtrate evaporated to dryness. The crude mixture was dissolved in CH_2Cl_2 and resulting precipitate, excess of hydroquinone, was

removed by filtration. The filtrate was concentrated and purified by column chromatography with CH_3OH-CH_2Cl_2 (9:91) mixture as eluting solvent. The product was obtained in 35% yield. ^{1}H NMR (250MHz,DMSO-d_6) δ 8.9(1H), 6.8(2H), 6.6(2H), 3.9(2H), 3.7(2H), 3.6(2H), 3.4(2H), 3.2(3H); ^{13}CNMR (250MHz, DMSO-d_6) δ 152.09, 116.55, 116.21, 72.14, 70.54, 69.94, 68.37, 58.92, 54.83

3-(4-(2-(2-Methoxyethoxy)ethoxy)phenoxy)phthalonitrile (2.13)

Into a solution of 3-nitrophthalonitrile (1.1 g, 6.45 mmol) in anhydrous DMF (10 mL), 4-(2-(2-methoxyethoxy)ethoxy)phenol (**2.12**) (1.1 g, 5.3 mmol) and K_2CO_3 (1.48 g, 10.74 mmol) were added. The mixture was stirred at room temperature under Ar for 24 h. Following the filtration of the salts, DMF was evaporated to dryness. The product was purified by column chromatography on silica gel. The silica gel column was initially washed with CH_2Cl_2, then with CH_3OH-CH_2Cl_2 (5:95) mixture as eluting solvent. The product was obtained in 83% yield. The compound was recyrstallized from n-BuOH. M.p. 58 °C; GCMS Calcd $C_{19}H_{18}N_2O_4^+$: 338.1; found: 338.0. ^{1}H NMR (250MHz, DMSO-d_6) δ7.8(2H), 7.2(3H), 7.1(2H), 4.1(2H), 3.7(2H), 3.6(2H), 3.5(2H), 3.2(3H); ^{13}CNMR (250MHz, DMSO-d_6) δ161.70, 157.21, 147.86, 136.81, 128.48, 122.54, 121.75, 116.61, 114.36, 105.09, 72.16, 70.58, 69.74, 68.49, 58.95.

4,5-Bis(4-(2-(2-methoxyethoxy)ethoxy)phenoxy)phthalonitrile (2.14)

Into a solution of 4-(2-(2-methoxyethoxy)ethoxy)phenol (**2.12**) (1.75 g, 8.25 mmol) in anhydrous DMF (2 mL), K_2CO_3 (1.13 g, 8.25 mmol) was added and the mixture stirred for 0.5 h at 70 ^{o}C. 4,5-Dichlorophthalonitrile (0.77 g, 3.9 mmol) in DMF (2 mL) was added to reaction mixture dropwise. The yellow colored mixture was stirred for 5.5 h at 90 °C. After removal of K_2CO_3 by filtration, DMF was evaporated and the crude mixture was purified by column chromatography on silica gel with EtOAc:hexanes (2:1) mixture as eluting solvent to give a brown solid in 54% yield. The compound was recrystallized from n-BuOH. ^{1}H NMR

(250MHz,DMSO-d_6) δ 7.5(2H), 7.1(2H),7.0(4H),4.1(4H), 3.7(4H), 3.6(4H), 3.4(4H), 3.2(6H); ^{13}CNMR (250MHz, DMSO-d_6) δ 156.64, 152.58, 148.62, 123.75, 121.43, 116.83, 116.30, 110.67, 72.15, 70.57, 69.77, 68.44, 58.95 GC-MS Cald $C_{30}H_{32}N_2O_8^+$: 548.2; found: 548.1

4-(2-(2-(2-Methoxyethoxy)ethoxy)ethoxy)phthalonitrile (2.15)

Into a solution of 4-nitrophthalonitrile (2.0 g, 11.6 mmol) in anhydrous DMF (10 mL), trietyhleneglycol monomethylether (3.8 g, 23.1 mmol) and finely ground K_2CO_3 (6.38 g, 46.2 mmol) were added. As soon as K_2CO_3 was added, the color of the solution turned from yellow to dark brown. The mixture was stirred at room temperature for 24 h. The crude mixture was poured into the 450 mL of ice-water and left overnight. The resulting yellow precipitate was isolated by filtration and purified by column chromatography on silica gel with EtOAc-hexane (1:1) as an eluting solvent to give yellow solid in 74% yield. The compound was recrystallized from n-BuOH. m.p. 63 °C; ^{1}H NMR (250 MHz, DMSO.d_6) δ 8.0(1H), 7.7(1H), 7.4(1H), 4.2(2H), 3.7(2H), 3.5(6H), 3.4(2H), 3.2(3H); ^{13}C NMR (250 MHz, DMSO-d_6) δ 162.7, 136.6, 121.2, 121, 117.11, 116.6, 106.8, 72.1, 70.8, 70.6, 70.4, 69.4, 69.3, 58.9

4-(2-(2-Hydroxyethoxy)ethoxy)phthalonitrile (2.16)

To diethyleneglycol (22.5 mmol, 2.14 mL) under Argon, a solution of 4-nitrophthalonitrile (15 mmol, 2.59 g) in anhydrous DMF (6 mL) and K_2CO_3 (30 mmol, 4.14 g) were added. The suspension was stirred at room temperature for 12 h. The color of the reaction turned from colorless to yellow-green over 12 h. Following the filtration to remove the salts, the DMF was evaporated and crude mixture was purified by column chromatography on silica gel with EtOAc as an eluting solvent. The yellow solid was obtained in 58% yield. The compound was recrystallized from n-BuOH. m.p. 58-60 °C. ^{1}H NMR (250 MHz, DMSO-d_6) δ 7.7(1H), 7.3(1H), 7.2(1H), 4.2(2H), 3.8(2H), 3.8(2H), 3.6(2H), 1.8(1H). ^{13}C NMR (300 MHz, DMSO-d_6) δ 162.5, 135.8, 120.4, 120.1, 117.4, 116.4, 116, 107.3, 73.2, 72.7, 69.3, 61.7

3,6-Bis(2-(2-(2-methoxyethoxy)ethoxy)ethoxy)phthalonitrile (2.17)

2,3-Dicyanohydroquinone (2.5 g, 15.6 mmol) and K_2CO_3 (5 g, 36.2 mmol) was stirred in anhydrous DMF (7 mL) for 30 min. at 50 °C. Toluene-4-sulfonic acid 2-[2-(2-methoxyethoxy)-ethoxy]-ethyl ester (**2.7**) (10.9 g, 34.3 mmol) in anhydrous DMF (10 mL) was added to reaction mixture dropwise over 40 min. The suspension was heated up to 90°C and vigorously stirred for 24h. The color of the suspension turned from yellow to brown over the time. Following the removal of salts, DMF was evaporated and the crude mixture was dissolved in EtOAc. The organic layer was washed with $NaHCO_3$ (3x50 mL), H_2O (3x50 mL) and brine (2x50 mL). The combined organic layers were evaporated and the crude mixture was purified by column chromatography on silica gel with EtOAc-CH_3OH (8:92) mixture as an eluting solvent. A yellow solid was obtained in 85% yield. The compound was recrystallized from n-BuOH. m.p. 46-48 °C; ^{1}H NMR (250 MHz, DMSO-d_6) δ 7.6(2H), 4.3(4H), 3.7(4H), 3.6(4H), 3.5(8H), 3.4(4H), 3.(6H); ^{13}C NMR (300 MHz, DMSO-d_6) δ 155.86, 121.70, 114.44, 103.84, 72.12, 70.94, 70.63, 70.45, 69.52, 58.9

3,6-Bis(2-(2-methoxyethoxy)ethoxy)phthalonitrile (2.18)

2,3-Dicyanohydroquinone (2.5 g, 15.6 mmol) and K_2CO_3 (5 g, 36.2 mmol) was stirred in anhydrous DMF (7 mL) for 30 min. at 50 °C. 1-Bromo-2-(2-methoxyethoxy)ethane (4.6 mL, 34.3 mmol) in anhydrous DMF (4 mL) was added to reaction mixture dropwise in 40min. The suspension was heated up to 60°C and vigorously stirred for 24h. Following the removal of salts, DMF was evaporated and the crude mixture was dissolved in EtOAc. The organic layer was washed with $NaHCO_3$ (3x50 mL), H_2O (3x50 mL) and brine (2x50 mL). The combined organic layers were evaporated and the crude mixture was purified by recrystallization from THF-hexanes mixture. The crude mixture was dissolved in a minimum amount of THF at room temperature. Hexanes was added to the solution until it got cloudy and retained the cloudiness

for 30 seconds. The solution was kept at -5 °C overnight. Following the filtration, the product was obtained in 90% yield as a yellow solid. m.p. 75-76 °C; ^{1}H NMR (250 MHz, DMSO-d_6) δ 7.6(2H), 4.3(2H), 3.7(2H), 3.6(2H), 3.4(2H), 3.2(6H); ^{13}C NMR (300 MHz, DMSO-d_6) δ 155.87, 121.72, 114.44, 103.87, 72.12, 70.27, 70.53, 69.51, 58.94

2-(2-(2-Methoxyethoxy)ethoxy)ethanethiol (2.19)

Toluene-4-sulfonic acid 2-[2-(2-methoxyethoxy)-ethoxy]-ethyl ester (**2.7**) (10.8 g, 34 mmol) and thiourea (2.6 g, 34 mmol) were dissolved in a mixture of absolute EtOH (20 mL) and H_2O (14 mL) and the mixture was refluxed for 3h. 4N NaOH solution (10 mL) was added to mixture and the reaction mixture refluxed 2 more h. The reaction mixture was concentrated under reduced pressure to ~ 10 mL, diluted with distilled H_2O (10 mL) and neutralized with concentrated HCl. The solution was extracted with CH_2Cl_2 (3x10mL) and the solvent was evaporated under reduced pressure. The pink-yellow liquid was distilled at 0.45 torr pressure. The product was collected as a clear liquid and obtained in 54% yield. B.p. 55-57 °C at 0.45 torr. GC-MS Calcd. $C_7H_{16}O_3S^+$: 180.0; found: 179.9. ^{1}H NMR (250 MHz, $CDCl_3$) δ 3.6(6H), 3.5(4H), 3.4(3H), 2.7(2H), 1.6(1H); ^{13}C NMR (300 MHz, $CDCl_3$) δ 76.92, 73.30, 72.34, 70.98, 70.63, 59.46, 24.66

3-(2-(2-(2-Ethoxyethoxy)ethoxy)ethylthio)phthalonitrile (2.20)

Into a solution of 3-nitrophthalonitrile (2.5 g, 13.9 mmol) in anhydrous DMF (5 mL), 2-(2-(2-methoxyethoxy)ethoxy)ethanethiol (**2.19**) (2 g, 11.6 mmol) and finely ground K_2CO_3 (1.9 g, 13.9 mmol) were added. The yellow colored mixture was stirred at room temperature for 5.5 h. The crude mixture was poured into the 600 mL of ice-water and left at room temperature overnight. The resulting yellow precipitate was isolated by filtration to give a yellow solid in 91% yield. The compound was recrystallized from n-BuOH. m.p. 58-59 °C; GCMS Calcd $C_{15}H_{18}N_2O_3S^+$: 306.1; found: 306.8. ^{1}H NMR (250 MHz, DMSO-d_6) δ 7.8(3H), 3.6(3H), 3.4(12H), 3.2(3H); ^{13}C

NMR (300 MHz, DMSO- d_6) δ 145.46, 134.55, 132.93, 131.17, 116.71, 115.13, 113.73, 72.12, 70.62, 70.46, 69.50,32.92

4-(2-(2-(2-Ethoxyethoxy)ethoxy)ethylthio)phthalonitrile (2.21)

Into a solution of 4-nitrophthalonitrile (1.6 g, 9.24 mmol) in anhydrous DMF (5 mL), 2-(2-(2-methoxyethoxy)ethoxy)ethanethiol (**2.19**) (1.9 g, 10 mmol) and finely ground K_2CO_3 (2.55 g, 18.4 mmol) were added. The yellow suspension was stirred at room temperature for 24 h. The crude mixture was poured into the 500 mL of ice-water and left overnight at room temperature. The resulting oil was extracted with CH_2Cl_2 and dried over $MgSO_4$. The solvent was evaporated under reduced pressure to give a yellow solid in 87% yield. m.p. 35-36 °C; GCMS Calcd $C_{15}H_{18}N_2O_3S^+$: 306.1; found: 306.1. ^{1}H NMR (250 MHz, DMSO-d_6) δ 8.1(1H), 7.9(1H), 7.7(1H), 3.6(2H), 3.5(6H), 3.4(4H), 3.2(3H); ^{13}C NMR (300 MHz, DMSO- d_6) δ 169.07, 157.70, 147.50, 134.45, 131.49, 131.38, 117.00, 116.55, 115.87, 110.51, 72.11, 70.63, 70.45, 69.47, 58.90, 31.65

4,5-Bis(2-(2-(2-ethoxyethoxy)ethoxy)ethylthio)phthalonitrile (2.22)

2-(2-(2-Methoxyethoxy)ethoxy)ethanethiol (**2.19**) (2 g, 10.15 mmol) in anhydrous DMF (5 mL) and finely ground K_2CO_3 (2.8 g, 20.3 mmol) were heated up to 70 °C and the mixture stirred at that temperature for 0.5 h. 4,5 Dichlorophthalonitrile (3.65 g, 20.3 mmol) in anhydrous DMF (6 mL) was added to reaction mixture dropwise. The mixture was stirred for 6 h at 70 °C. The color of the solution was turned from yellow to orange over the time. After removal of K_2CO_3 by filtration, DMF was evaporated and the crude mixture was purified by column chromatography on silica gel with EtOAc-hexanes (3:1) mixture as eluting solvent to give a yellow oil in 79% yield. ^{1}H NMR (250 MHz, DMSO-d_6) δ7.9(2H), 3.7(4H), 3.5(12H), 3.4(8H), 3.2(6H); ^{13}C NMR (300 MHz, DMSO- d_6) δ143.82, 129.76, 116.93, 110.92, 72.70, 70.64, 70.47, 69.32, 58.91, 32.50

23-Amino, 2,3,9,10,16,17 hexa-(3,5 dibutoxycarbonyl) phthalocyanato zinc (2.28).

4,5-Bis isophthalic acid dibutyl ester phthalonitrile (**2.2**) (0.71 g, 1 mmol), 4-aminophthalonitrile (**2.5**) (0.047 g, 0.3 mmol) and $Zn(OAc)_2$ (0.12 g, 0.65 mmol) was added to anhydrous C_4H_9OH (5 mL) under argon and heated up to 90 ^oC. DBU (0.1 mL, 0.6 mmol) was added to mixture and the mixture was refluxed for 36 hours. The color of the solution was turned from yellow to dark blue. The solvent was evaporated and the crude mixture was partially purified by column chromatography on silica gel first with EtOAc-CH_2Cl_2 (1:199) and then starting from 1:199 EtOAc-CH_2Cl_2, gradually EtOAc percentage was increased up to 2%. Pc **2.29** was isolated from the crude mixture. The remaining of the crude mixture was dissolved in CH_2Cl_2 and loaded to MP-TsOH ion exchange column. By washing column with EtOAc, CH_2Cl_2 and CH_3OH first fraction was collected.. Column was washed with 1M NH_3 in CH_3OH solution to collect second fraction. Pc **2.28** could not be isolated and the crude mixture was submitted to the next reaction. MALDI-MS Calcd. $C_{160}H_{176}N_8O_{40}Zn^+$: 2916.46; found 2916.39

23-Amino, 2, 3, 9, 10, 16, 17 hexa-(3,5 dicarboxylic acid) phthalocyanato zinc (2.30-2.31)

Solution of the crude mixture of **2.28** and **2.29** (0.2 g, 0.085 mmol) was individually dissolved in 3 mL THF and were added dropwise to a solution of LiOH (0.43 g, 17.9 mmol) in CH_3OH-H_2O (7:3) .Blue colored solutions were stirred at 60 ^oC for 16 hours. The organic layers were removed in under high pressure and aqueous layer was washed with $CHCl_3$ (3x20 mL) and acidified with 4N HCl to pH 2. The resultant precipitates were filtered, washed with $CHCl_3$ (3x20 mL) and H_2O. The crude mixture of **2.30** was dissolved in CH_3OH and run through MP-TsOH ion exchange column. Column was washed with 1M NH_3 in CH_3OH solution and finally with H_2O to collect two different fractions. Collected fractions were further purified by column chromatography on silica gel. EtOAc-CH_2Cl_2 (1:199), CH_3OH-CH_2Cl_2 (3:97;2 times), EtOAc-CH_2Cl_2-THF (94:4:2). Finally, C^{18} column was run starting from 100% H_2O and gradually

increasing CH_3OH percentage up to 100%. Asymmetrically-substituted, desired Pc was obtained in 7%yield. **2.30**: MALDI-MS Calcd. $C_{80}H_{41}N_9O_{30}Zn^+$:1671.13; found: 1671.10; **2.31**: MALDI-MS Calcd. $C_{96}H_{48}N_8O_{40}Zn^+$: 2016.13; found 2016.70

Octa-triethyleneglycol monomethyl ether substituted ZnPc (2.32)

Oligoethyleneglycol-substituted phthalonitrile **2.11** (0.22 g, 0.4 mmol), and $Zn(OAc)_2$ (0.036 g, 0.2 mmol) was added to anhydrous C_4H_9OH (4 mL) under argon and heated up to 90 ^oC. DBU (0.03 mL, 0.2 mmol) was added to mixture and the mixture was refluxed for 36 hours. Color of the solution was turned from yellow to dark green overnight. The solvent was evaporated and the crude mixture was purified by column chromatography on silica gel starting from 1% CH_3OH in CH_2Cl_2, the percentage of the CH_3OH was gradually increased up to 5%. MALDI-MS Calcd. $C_{112}H_{144}N_8O_{36}Zn^+$: 2240.90, found 2240.16

2,9,16,23 Tetra-(4-nitrobenzamide) phthalocyanato zinc (2.33)

N-(3,4-Dicyano-phenyl)-4-nitrobenzamide (**2.6**) (0.06g, 0.2 mmol) and $Zn(OAc)_2$ (0.09g, 0.05mmol) were added to 10 mL round bottom flask and argon flushed through 2-3 minutes. Anhydrous DMF (3 mL) and HMDS (0.086 mL, 0.4 mmol) were added to flask. The mixture was heated at 100 ^oC for 10 hours. DMF was evaporated and the crude mixture was washed with H_2O (30 mL) and CH_3OH (30 mL). The crude mixture was boiled in acetone, CH_3OH, EtOAc, EtOH mixture for 2 hours and filtered after cooled down to room temperature to give a dark green solid in 28% yield. MALDI-MS Calcd. $C_{60}H_{32}N_{16}O_{12}Zn^+$: 1232.16; found: 1232.65

2,9,16,23 Tetra-(4-aminobenzamide) phthalocyanato zinc (2.34)

A) Tetra-nitro Pc **2.33**(100 mg, 0.08 mmol) was dissolved in DMF (2 mL) and 3 mL of CH_3COOH with 1 mL of Raney-Nickel catalyst were added to solution. The reaction was run under 50 psi H_2 (g) for 5 hours. The mixture was run through celite and the solvent was evaporated under reduced pressure. The green solid was washed with saturated Na_2CO_3 solution

and H_2O. MALDI-MS results showed a peak corresponding to cleavage of the amide bond. MALDI-MS Calcd $C_{60}H_{40}N_{16}O_4Zn^+$:1112.30 found; 879.47, 861.05,825.36, 650.75

B) Tetra-nitro Pc **2.33** (100 mg, 0.08 mmol) was dissolved in DMF (2 mL) and flask was flushed with N_2 (g) for 5 minutes. Pd/C (10 mg, 10% by weight) was added to green solution and all the N_2 (g) was vacuumed. H_2 (g) was flushed and vacuumed back for 3 times. Flask was flushed with H_2 (g) the last time and the reaction stirred at room temperature over night. Decomposition of phthalocyanine was observed.

C) Tetra-nitro Pc **2.33** (150 mg, 0.12 mmol) was dissolved in 3 mL DMF containing Zn powder (48.5 g, 0.75 mmol). To the stirring mixture, 88% HCOOH (2.5 mL) was added in one portion. Reaction mixture was stirred at room temperature for 4 hours. After removal of the remaining Zn dust by filtration, DMF was removed in under reduced pressure to provide the green solid. The solid was washed with saturated Na_2CO_3 and brine solution several times.

2.5 References

(1) Nesterova, I. V.; Verdree, V. T.; Pakhomov, S.; Strickler, K. L.; Allen, M. W.; Hammer, R. P.; Soper, S. A. Metallo-phthalocyanine near-IR fluorophores: Oligonucleotide conjugates and their applications in PCR assays *Bioconjugate Chem.* **2007**, *18*, 2159-2168.

(2) Nilsson, F. Y.; Tolmachev, V. Affibody (R) molecules: New protein domains for molecular imaging and targeted tumor therapy *Curr. Opin. Drug Discov. Dev.* **2007**, *10*, 167-175.

(3) Palumbo, G. Photodynamic therapy and cancer: a brief sightseeing tour *Expert Opin. Drug Deliv.* **2007**, *4*, 131-148.

(4) Zimcik, P.; Miletin, M.; Musil, Z.; Kopecky, K.; Slajsova, D. The synthesis and characterization of novel unsymmetrical azaphthalocyanines containing one carboxylic group *Dyes Pigment.* **2008**, *77*, 281-287.

(5) Cauchon, N.; Tian, H. J.; Langlois, J.; La Madeleine, C.; Martin, S.; All, H.; Hunting, D.; van Lier, J. E. Structure-photodynamic activity relationships of substituted zinc trisulfophthalocyanines *Bioconjugate Chem.* **2005**, *16*, 80-89.

(6) Sharman, W. M.; Kudrevich, S. V.; vanLier, J. E. Novel water-soluble phthalocyanines substituted with phosphonate moieties on the benzo rings *Tetrahedron Lett.* **1996**, *37*, 5831-5834.

(7) Sesalan, B. S.; Koca, A.; Gul, A. Water soluble novel phthalocyanines containing dodeca-amino groups *Dyes Pigment.* **2008**, *79*, 259-264.

(8) Erdem, S. S.; Nesterova, I. V.; Soper, S. A.; Hammer, R. P. Solid-phase synthesis of asymmetrically substituted "AB_3-type" phthalocyanines *J. Org. Chem.* **2008**, *73*, 5003-5007.

(9) Akkurt, B.; Hamuryudan, E. Enhancement of solubility via esterification: Synthesis and characterization of octakis (ester)-substituted phthalocyanines *Dyes Pigment.* **2008**, *79*, 153-158.

(10) Cole, A. C.; Jensen, J. L.; Ntai, I.; Tran, K. L. T.; Weaver, K. J.; Forbes, D. C.; Davis, J. H. Novel bronsted acidic ionic liquids and their use as dual solvent-catalysts *J. Am. Chem. Soc.* **2002**, *124*, 5962-5963.

(11) Ng, A. C. H.; Li, X. Y.; Ng, D. K. P. Synthesis and photophysical properties of nonaggregated phthalocyanines bearing dendritic substituents *Macromolecules* **1999**, *32*, 5292-5298.

(12) Galli, C.; Bunnett, J. F. Evidence Further Substantiating the Srn1 Mechanism of Aromatic-Substitution *J. Am. Chem. Soc.* **1979**, *101*, 6137-6139.

(13) Bunnett, J. F. Aromatic-Substitution by Srn1 Mechanism *Accounts Chem. Res.* **1978**, *11*, 413-420.

(14) Rossi, R. A.; Rossi, R. H. D.; Lopez, A. F. Molecular-Orbital Approach to Srn1 Mechanism of Aromatic-Substitution *J. Org. Chem.* **1976**, *41*, 3367-3371.

(15) Rossi, R. A.; Rossi, R. H. D.; Lopez, A. F. Photostimulated Arylation of Cyanomethyl Anion by Srn1 Mechanism of Aromatic-Substitution *J. Org. Chem.* **1976**, *41*, 3371-3373.

(16) Kim, J. K.; Bunnett, J. F. Evidence for a Radical Mechanism of Aromatic Nucleophilic Substitution *J. Am. Chem. Soc.* **1970**, *92*, 7463-7365.

(17) F. A. Carey, R. J. S. In *Advanced Organic Chemistry Part A: Structure and Mechanisms*; 4th ed.; Kluwer Academic / Plenum Pubslihers: New York, Boston, dordrecht, London, Moscow, 2000; Vol. 1, p 727-734.

(18) Griffiths, J.; Roozpeikar, B. Synthesis and Electronic Absorption-Spectra of Dicyano-Derivatives of 4-Diethylaminoazobenzene *J. Chem. Soc.-Perkin Trans. 1* **1976**, 42-45.

(19) Ogunsipe, A.; Nyokong, T. Photophysical and photochemical studies of sulphonated non-transition metal phthalocyanines in aqueous and non-aqueous media *J. Photochem. Photobiol. A-Chem.* **2005**, *173*, 211-220.

(20) Ouchi, M.; Inoue, Y.; Liu, Y.; Nagamune, S.; Nakamura, S.; Wada, K.; Hakushi, T. Convenient and Efficient Tosylation of Oligoethylene Glycols and the Related Alcohols in

Tetrahydrofuran Water in the Presence of Sodium-Hydroxide *Bull. Chem. Soc. Jpn.* **1990**, *63*, 1260-1262.

(21) Huang, F. H.; Gibson, H. W.; Bryant, W. S.; Nagvekar, D. S.; Fronczek, F. R. First pseudorotaxane-like [3]complexes based on cryptands and paraquat: Self-assembly and crystal structures *J. Am. Chem. Soc.* **2003**, *125*, 9367-9371.

(22) Wosnick, J. H.; Mello, C. M.; Swager, T. M. Synthesis and application of poly(phenylene ethynylene)s for bioconjugation: A conjugated polymer-based fluorogenic probe for proteases *J. Am. Chem. Soc.* **2005**, *127*, 3400-3405.

(23) Messmore, B. W.; Hulvat, J. F.; Sone, E. D.; Stupp, S. I. Synthesis, self-assembly, and characterization of supramolecular polymers from electroactive dendron rodcoil molecules *J. Am. Chem. Soc.* **2004**, *126*, 14452-14458.

(24) Wu, Y. Z.; Tian, H.; Chen, K. C.; Liu, Y. Q.; Zhu, D. B. Synthesis and properties of soluble metal-free phthalocyanines containing tetra- or octa-alkyloxy substituents *Dyes Pigment.* **1998**, *37*, 317-325.

(25) Nyokong, T.; Isago, H. The renaissance in optical spectroscopy of phthalocyanines and other tetraazaporphyrins *J. Porphyr. Phthalocyanines* **2004**, *8*, 1083-1090.

(26) Snow, A. W.; Foos, E. E. Conversion of alcohols to thiols via tosylate intermediates *Synthesis* **2003**, 509-512.

(27) Uchida, H.; Reddy, P. Y.; Nakamura, S.; Toru, T. Novel efficient preparative method for phthalocyanines from phthalimides and phthalic anhydride with HMDS *J. Org. Chem.* **2003**, *68*, 8736-8738.

(28) Montfortz, F. P. In *The Porphyrin Handbook*; Kadish, K. M., Smith,K. M., Guilard, G., Ed.; Academic Press: New York, 1999; Vol. 19, p 105-149.

(29) Dayal, B.; Salen, G.; Toome, B.; Tint, G. S.; Shefer, S.; Padia, J. Lithium Hydroxide Aqueous Methanol - Mild Reagent for the Hydrolysis of Bile-Acid Methyl-Esters *Steroids* **1990**, *55*, 233-237.

(30) Henrie, S.; Majerle, R. S. K. An efficient, self-protecting route to dimethyl 4-amino-4-[2-(methoxycarbonyl)ethyl]-heptanedioate HCl *Molecules* **1999**, *4*, 13-15.

(31) Gowda, D. C.; Mahesh, B.; Gowda, S. Zinc-catalyzed ammonium formate reductions: Rapid and selective reduction of aliphatic and aromatic nitro compounds *Indian J. Chem. Sect B-Org. Chem. Incl. Med. Chem.* **2001**, *40*, 75-77.

Chapter 3
Solid-Phase Synthesis of Asymmetrically Substituted "AB_3-Type" Phthalocyanines[1]

3.1 Introduction

As discussed in the previous chapter, synthesis of Phthalocyanines (Pcs) with asymmetrical substitution on the periphery is most commonly performed by a statistical condensation of two different phthalonitriles or related derivatives, which yields a mixture of six Pc congeners.[1] While it is beneficial to isolate multiple products to assess the relative importance of each Pc in different applications, isolation of the desired AB_3 (or A_3B) Pc is often laborious due to difficulty in separating chemically similar species out of the Pc mixtures obtained.

To date, several chemoselective techniques for asymmetric Pc synthesis have been described in the literature including the subphthalocyanine (subPc) route[2] and solid-phase synthesis.[3-5] The subPc route is a well-known method for the synthesis of AB_3 type of Pcs, though it is only applicable to certain phthalonitrile precursors. For example, the condensation of a diiminoisoindoline having electron-donating groups and an unsubstituted subPc or one with electron-withdrawing groups promotes the selective synthesis of AB_3 type Pcs. Contrastingly, in the presence of electron-donating substitutents on the subPc leads to a mixture of Pcs through a scrambling process that results from disassembly of the subPc under the reaction conditions to form the Pc.[6-8] Solid-phase synthesis of AB_3 type asymmetric Pcs is as yet an underutilized method. Leznoff and co-workers' solid-phase synthesis of AB_3 type asymmetrically-substituted Pcs using a polystyrene resin support is touted as the first synthesis of pure asymmetric Pcs.[3,4] Solid-phase synthesis of Pcs starts with one of the

[1] Reproduced with permission from S. Sibel Erdem, Irina V. Nesterova, Steven A. Soper and Robert P. Hammer, The Journal of Organic Chemistry, 73 (13), pp 5003–5007, 2008, American Chemical Society.

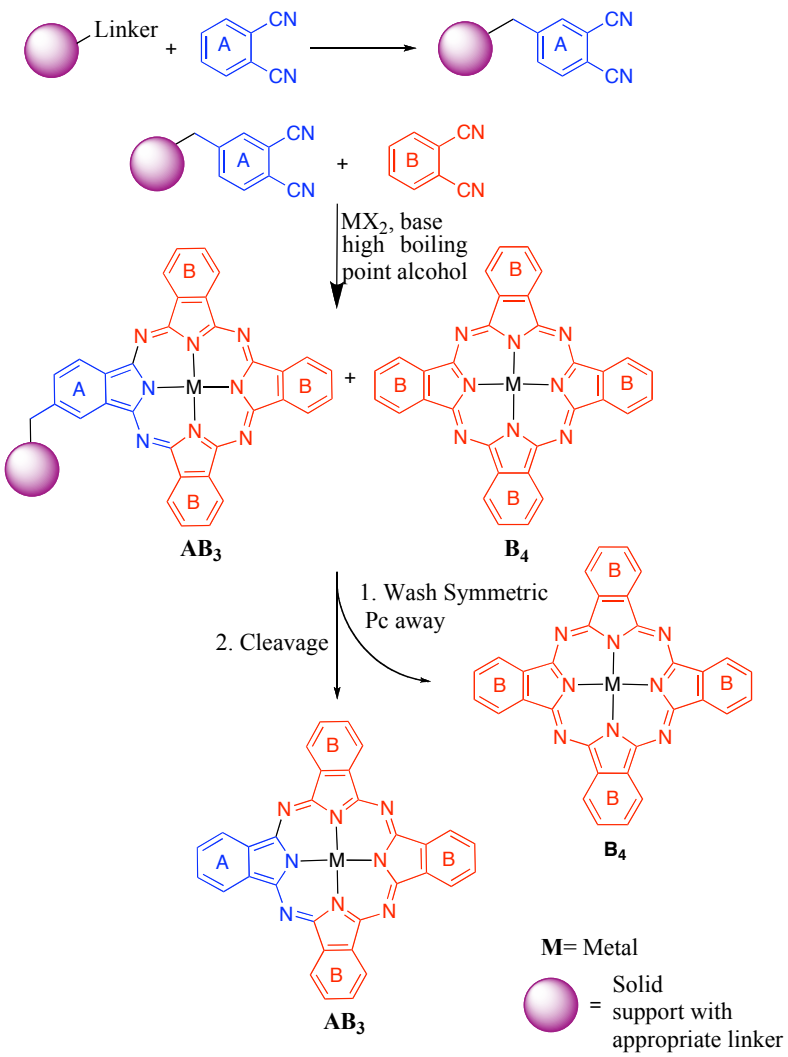

Scheme 3.1 Solid-Phase Synthesis of Pcs

phthalonitrile precursors (Scheme 3.1) attached to the support via a cleavable linker. Reaction of the solid supported phthalonitrile with an excess of phthalonitrile B in solution produces the AB_3 type asymmetrically-substituted Pc on the solid support while the B_4 type symmetrical Pc forms in solution. Symmetrical Pc is removed by washing and subsequent cleavage of the linkage of "A" from the resin yields the pure AB_3 type Pc (Scheme 3.1). Such a strategy has also been utilized in the polymer-supported synthesis of monofunctionalized mesotetraarylporphyrins as developed by Borhan and co-workers.[9] One of the challenges of the method of Leznoff is the requirement for extensive washing via Soxhlet extraction to

remove symmetrical B_4 Pc from the hydrophobic polystyrene resin. Additionally, Soxhlet extraction is required to fully remove the cleaved asymmetrical AB_3 Pc from the polymer support. For example, Leznoff reports[4] that 4-5 days of Soxhlet extraction are required to isolate pure asymmetrical Pc. The challenge of removing the symmetrical Pc product was demonstrated in a later paper by Leznoff[5] that reported the failure of even extensive Soxhlet extraction to completely remove the symmetrical Pc from the resin. This resulted in a contaminated "AB_3" product after cleavage from the support that required additional chromatographic purification to obtain pure asymmetrically- substituted Pc.

It is clear that a new chemoselective synthetic methodology needs to be developed, which yields a single Pc congener without need of extensive chromatographic purification techniques. Herein this chapter described the solid-phase synthesis of AB_3 type asymmetrically-substituted Pcs utilizing a polyethylene glycol (PEG)-based support. In a desire to provide a scalable and rapid synthesis of asymmetrically-substituted Pcs, we hypothesized that a more hydrophilic resin would reduce nonspecific adsorption of Pc products on the solid support. Thus, we utilized a hydrophilic, poly(ethylene glycol) (PEG) resin in place of the more traditional polystyrene support. Using a Wang-type linker, we have developed the synthesis of monohydroxylated, oligoethylene glycol- substituted Pcs utilizing an amidine-base promoted, solid-supported phthalonitrile tetramerization reaction. The use of the hydrophilic support allows symmetrical Pc product formed in solution to be readily and completely removed by washing, while retaining the AB_3 product on the support.

3.2 Results and Discussion

3.2.1 Solid-Phase Synthesis of "AB_3" Type Oligoethyleneglycol Substituted Phthalocyanines

Wang-ChemMatrix resin was chosen as the point of attachment for a hydroxy-functionalized phthalonitrile to the solid support since the benzyl ether linkage would be

stable to the basic reaction conditions for Pc formation. Initially, we chose this system of almost symmetrical oligoethylene glycol-substituted Pcs as a demonstration of the method as it would be nearly impossible to separate mixtures of congeners of such similar Pcs by chromatographic or other methods. The Wang linker was activated by tricholoroacetonitrile, and the resulting trichloroacetimidate resin[10] **3.1** was treated with an excess of hydroxyfunctionalized phthalonitrile **2.16**, to give resin-bound phthalonitrile **3.2** in high yield with a loading capacity of 0.54 mmol/g (90% yield based on starting loading capacity of the Wang resin, 0.6 mmol/g) (Scheme 3.2). As further evidence for

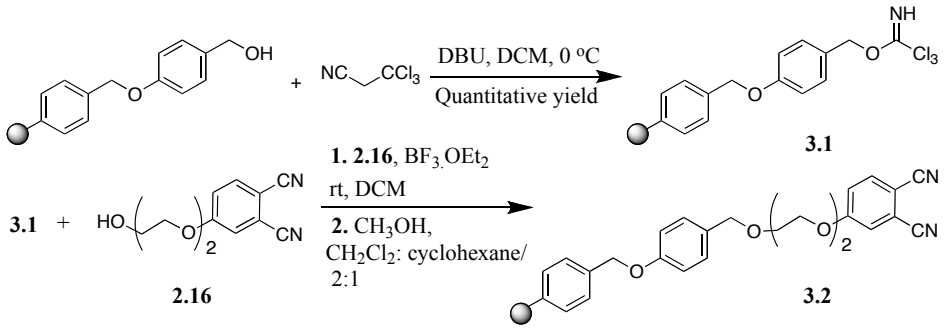

Scheme 3.2

the integrity of the reaction, FT-IR shows the disappearance of the acetimidate NH band at 3055 cm-1 of resin **3.1** and the appearance of a CN band at 2229 cm^{-1} of polymer-bound phthalonitrile **3.2**.

Condensation of resin-bound phthalonitrile **3.2** with phthalonitrile **2.15** in solution in the presence of $Zn(OAc)_2$ and DBU in refluxing BuOH for 24 h produced a mixture of resin-bound AB_3 Pc and the corresponding symmetrically-substituted Pc **3.3** in solution (Scheme 3.3). The resin was washed with hot BuOH and CH_2Cl_2 until a colorless filtrate was collected. The absorbance spectrum of each successive wash solution showed decreasing absorbance. Dramatic decrease of the absorbance was observed after the first two washes indicating the most of the symmetrically-substituted Pc **3.3** was washed away by the first

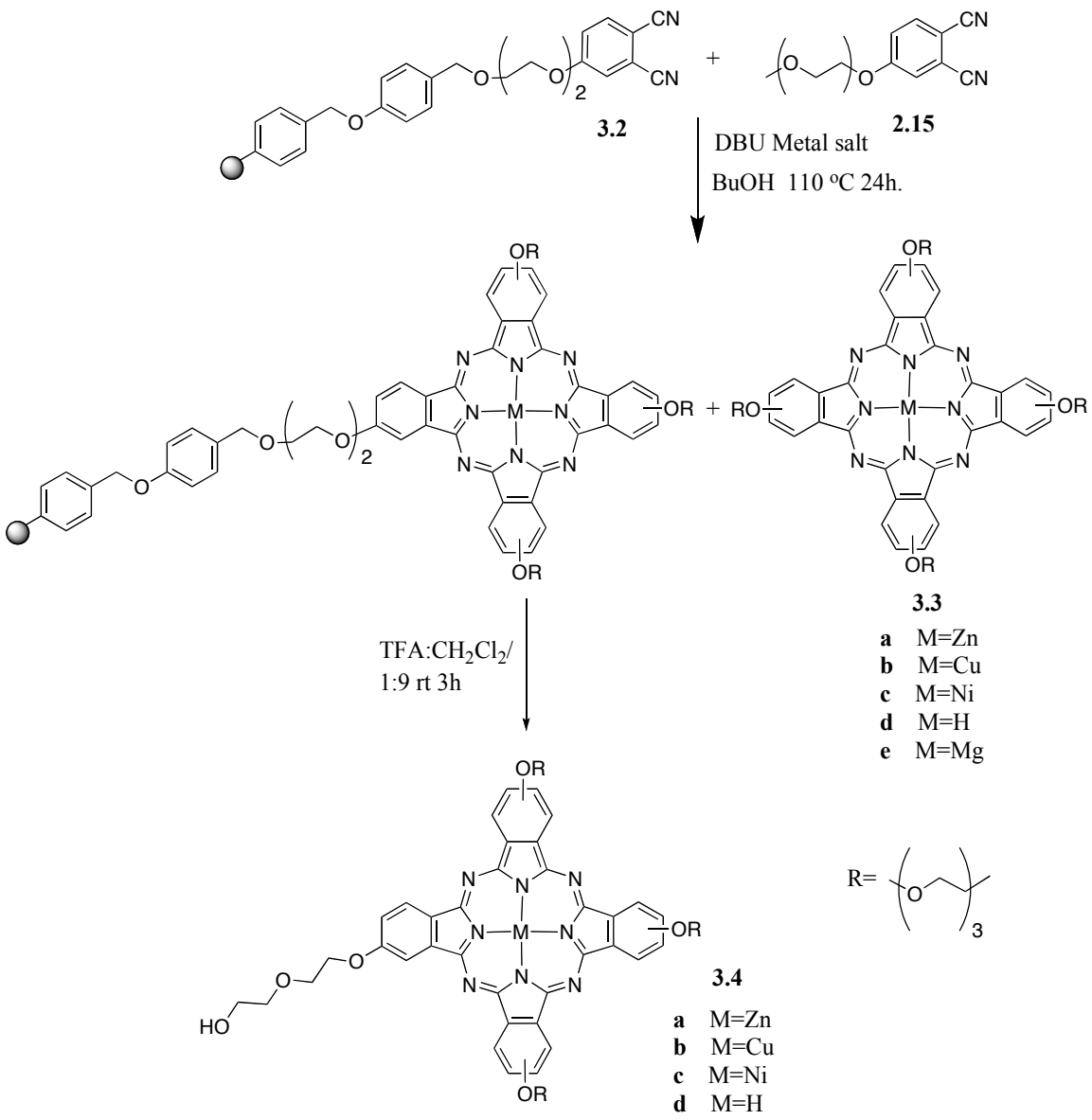

Scheme 3.3

BuOH and CH_2Cl_2 washes (typical washing times, 3-5 h). Polymer-bound *p*-alkoxybenzyl ethers can be cleaved in 1-10% TFA in CH_2Cl_2 solution.[10] High concentrations of TFA (>70%) resulted in decomposition of Pc as well as removal of the metal from the Pc core. Cleavage conditions were optimized by monitoring the absorbance of the cleavage cocktail at 1%, 5%, and 10% TFA in CH_2Cl_2. 10% TFA in CH_2Cl_2 resulted in the highest

cleavage yield (as judged by absorbance of the washes) without loss of the metal from the Pc core and thus was selected as the standard cleavage cocktail. (Later experiments showed that addition of scavengers such as triisopropylsilane to the cleavage cocktail or increased TFA concentrations as high as 20% do not degrade the Pc product purity.) Analysis of the crude cleavage solution showed that none of the symmetrical B_4 product was present, but that the desired AB_3 Pc was accompanied by a significant amount (~20% MALDI-MS) of the A_2B_2 (or AB_2) Pc. This may have been due to increased rate of intra resin reactions[11,12] due to the relatively high loading of the resin (0.54 mmol/g). That is, reactions between phthalonitrile active sites on the resin **3.2** are similar in rate to reactions between activated phthalonitrile species in solution and resin-bound phthalonitriles, thus producing the undesired A_2B_2 Pc. In order to overcome this problem, we reduced the loading of the resin (Scheme 3.2) by reaction of trichloroacetimidate resin **3.1** with only 1.2 equiv of hydroxyphthalonitrile **2.16** followed by capping of the remaining amidate sites with an excess of CH_3OH to give a phthalonitrile resin **3.2** at a loading of 0.28 mmol/g. Resin-bound phthalonitrile **3.2** was reacted as before with an excess of oligoethylene glycol-substituted phthalonitrile **2.15** in the presence of $Zn(OAc)_2$. Following the removal of symmetrical **3.3a** by washing, the desired Pc was cleaved from the polymer support. The crude mixture was filtered through a silica gel column to remove low molecular weight impurities to give Zn-Pc **3.4a** in 12% yield (based on 0.28 mmol/g loading capacity) without contamination from the A_2B_2 Pc product (Scheme 3.3). Reducing the loading capacity resulted in the pure AB_3 type Pc, but the overall yield, based on the initial loading of the phthalonitrile, was not reduced. All the symmetrically-substituted Pc products **3.3** were recovered and purified by precipitation of a MeOH solution into ether. Asymmetrical Pcs **3.4** were purified by filtration through silica gel column, except for CuPc **3.4b** and H_2Pc **3.4d,** which were purified by Sephadex LH-20

chromatography. We have found that LH-20 is the preferred method of purification as there is less nonspecific adsorption of Pcs to the LH-20 matrix and results in improved Pc recovery. All Pcs prepared in this work were characterized by absorbance and fluorescence spectroscopy, HPLC, and mass spectrometry. Figure 3.1 shows the mass spectrum of the desired ZnPc **3.4a**. The HPLC chromatogram with absorption and emission spectra of the ZnPc **3.4a** are presented in Figure 3.2**.** The target compound had a characteristic Q-band at 680 nm and emission maxima at 690 nm in DMSO. Fluorescence quantum yield of **3.4a** was calculated as 0.15, which is in the range of the reported quantum yields of tetra-substituted ZnPcs.[13]

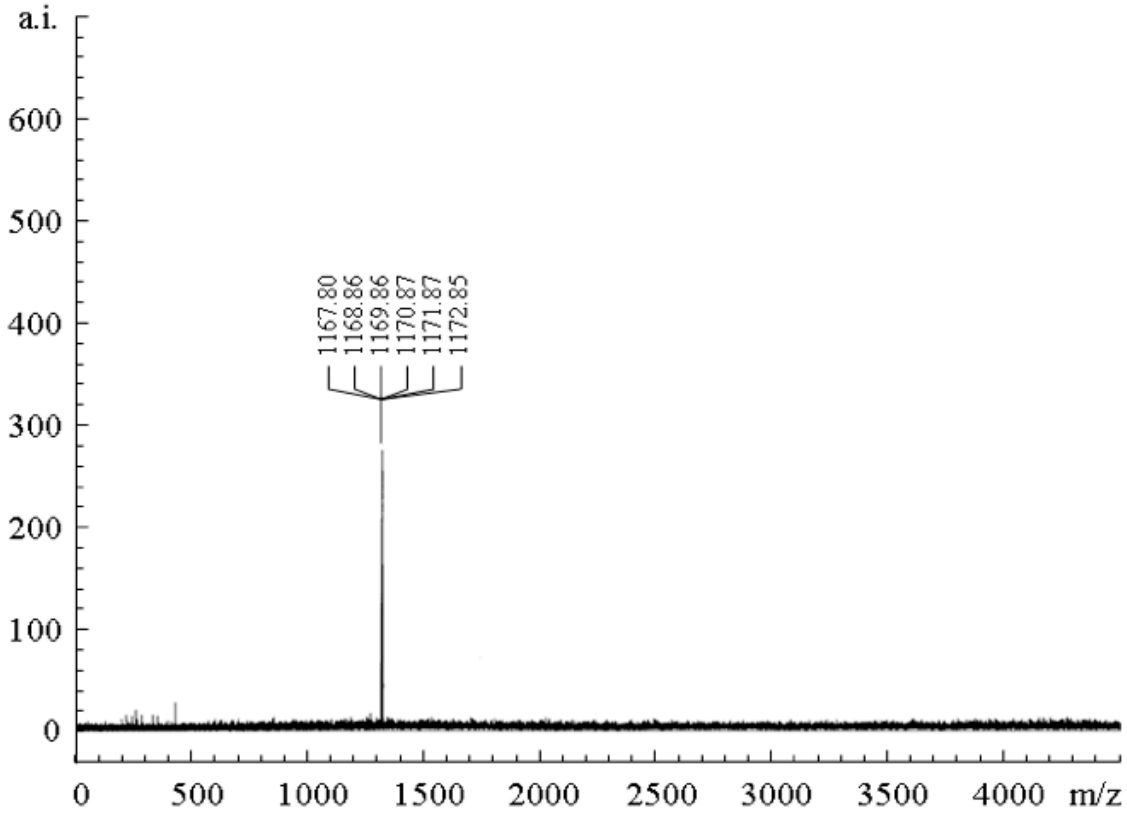

Figure 3.1 MALDI-MS spectrum of Pc ZnPc **3.4a**.

The same synthetic route to ZnPc **3.4a** was applied to synthesize Cu, Ni, and metal-free Pcs. Condensation of ethyleneglycol-substituted phthalonitrile **2.15** with resin-bound

phthalonitrile **3.2** in the presence of $CuBr_2$ and DBU in refluxing BuOH for 24 h gave a dark blue solution and resin (Scheme 3.3).Following purification, mono-hydroxy functionalized phthalonitrile **3.2** in the presence of $CuBr_2$ and DBU in refluxing BuOH for 24 h gave a dark

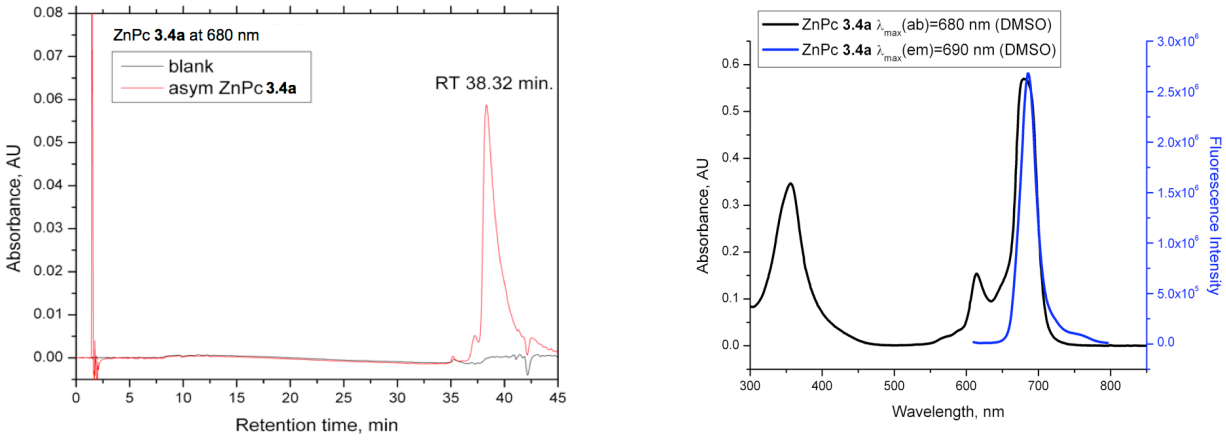

Figure 3.2 HPLC chromatogram of **3.4a** (left), absorption-emision spectra of **3.4a** (right).

CuPc **3.4b** was obtained in 13% yield (Table 3.1). In the case of NiPcs (**3.3c**, **3.4c**) $NiCl_2$ was employed as a metal source. Due to the low solubility of $NiCl_2$ in BuOH, the reaction was carried out at higher temperature and NiPc **3.4c** was purified by filtration through a silica gel column in 11% yield (Table 1). To synthesize the metal-free Pc (**3.3d**, **3.4d**), the same strategy was employed except without any metal ion. But in this case, cleavage of metal-free Pc resin yielded two products, the AB_3 metal-free Pc **3.4d** and an A_2B_2 H_2Pc in 3:2 molar ratio (MALDI-MS). As an alterative route to the asymmetrical H_2Pc, Mg^{2+} ion was utilized to template the tetramerization, as it is known that the acidity of the cleavage cocktail is sufficient for the removal of Mg from the Pc core to yield metal free Pc. Thus, condensation of polymer –bound phthalonitrile **3.2** with oligoethylene glycol-substituted phthalonitrile **2.15** in the presence of $MgCl_2$ (Scheme 3.3) gave, following the cleavage, AB_3 H_2Pc **3.4d** without any contamination by the A_2B_2 product in 17% yield. From the results of the synthesis of the metal-free Pc **3.4d**, it is clear that the metal ion plays a crucial role in the

tetramerization process. Adding divalent metal ion improves the effective site isolation of the reactive groups in the resin matrix. As argued by Jayalekshmy and Mazur, this improved

Table 3.1 Oligoethyleneglycol Substituted Pcs

	Compound Number[2] / Pc	Metal Salt	Yield (%)[3]	λ_{max} (abs) (nm)	log ε ($cm^{-1}M^{-1}$)	λ_{max} (em) (nm)[4]	ϕ_f[c]
AB_3 Type Pcs	**3.4a** / ZnPc	$Zn(OAc)_2$	12	680	4.9	690	0.15
	3.4b / CuPc	$CuBr_2$	13	681	4.8	n.d	n.d
	3.4c / NiPc	$NiCl_2$	11	671	4.3	678	0.0003
	3.4d / H_2Pc	$MgCl_2$	16	646, 676, 706	3.4, 3.5, 3.4	709	0.08
B_4 Type Pcs	**3.3a** / ZnPc	$Zn(OAc)_2$	21	681	5.5	691	0.15
	3.3b / CuPc	$CuBr_2$	15	681	5.1	n.d	n.d
	3.3c / NiPc	$NiCl_2$	17	671	5.1	678	0.0038
	3.3d / H_2Pc	-	18	676, 706	3.5, 3.5	709	0.06
	3.3e / MgPc	$MgCl_2$	20	682	5.5	691	0.31
	3.6a / ZnPc	$Zn(OAc)_2$	13	740	4.4	751	0.12

"pseudodilution"[12] of sites is a kinetic phenomena since we know that phthalonitrile cyclotetramerization is faster in the presence of metal ion. We propose a pathway that accounts for this pseudodilution in the presence of metal ion, which follows from the proposed mechanism of DBU-promoted phthalonitrile tetramerization in alcohol.[14] That is,

[2] Asymmetrically-substituted Pcs, **3.4**, were purified by filtration through silica gel, except for **3.4b** and **3.4d,** which were purified by Sephadex LH-20 chromatography.

[3] Yields of asymmetrically-substituted Pcs were calculated based on the loading of the phthalonitrile on the support.

[4] Fluorescence spectra and quantum yield determinations were done using 605 nm excitation wavelength for **3.4a**, **3.4c**, **3.4d**, **3.3a**, 607 nm for **3.3c** and **3.3e**, and 615 nm for **3.3d,** 664 nm for **3.6a**. CuPcs **3.3b** and **3.4b** did not show any detectable fluorescence, which is noted in the table as "n.d.". All Spectra were taken in DMSO except for **3.3c** and **3.3d**, which were taken in THF. Fluorescence quantum yield measurements for all Pcs were done using methylene blue as a standard at absorbance 0.04 - 0.05 for both Pc and standard solutions to avoid any error due to inner-filter effect.[42]

metal chelated isoindolines (or other similar phthalonitrile derived precursors) present in solution react faster with resin-bound phthalonitriles than the resin-bound phthalonitriles can react with themselves, resulting in only AB_3 products. In the absence of metal, the reaction of resin-bound phthalonitriles with solution intermediates is slowed so that resin-bound intermediates have a longer time to find a proximate resin-bound phthalonitrile with which to react, thus giving rise to a significant fraction of A_2B_2 H_2Pc products (Scheme 3.4). Similar results were also obtained during the synthesis of non-peripherally substituted ZnPc **3.6b** (1, 4 substitution pattern, Figure 3.3). Since nonperipherally substituted phthalonitriles have low reactivity in cyclotetramerization reaction, it is usually necessary to convert one of the phthalonitriles to more reactive and advanced precursor, diiminoisoindoline.[15] Thus, prior the

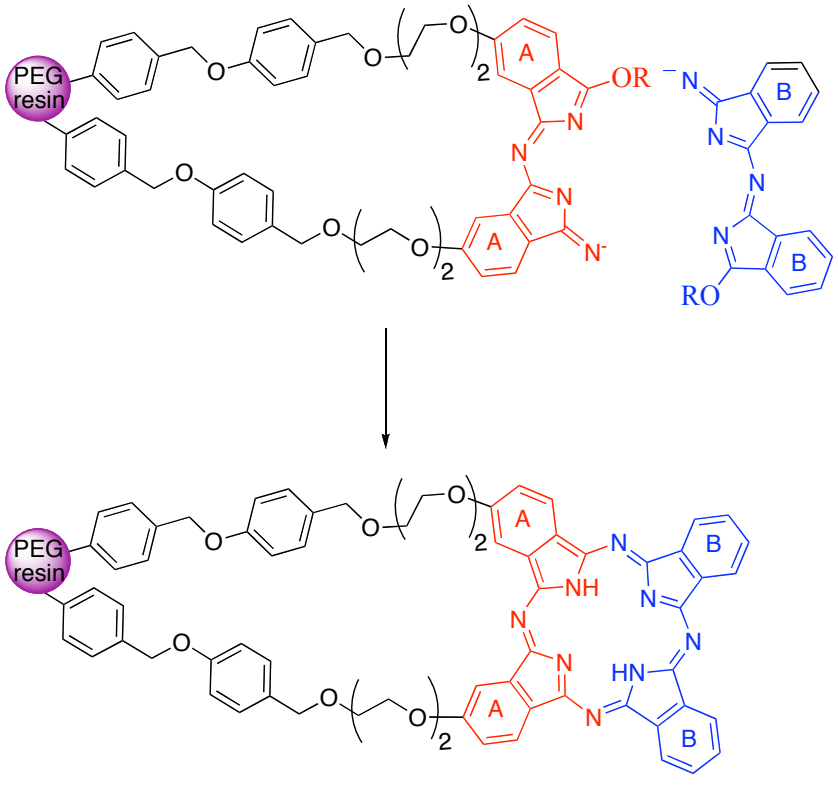

A_2B_2

Scheme 3.4

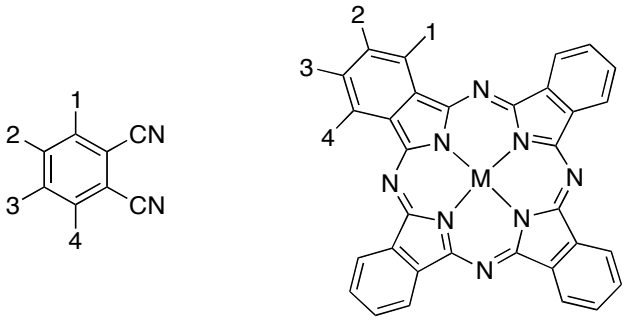

Figure 3.3 Substitution pattern of peripherally and non-peripherally substituted phthalonitriles and Pcs.

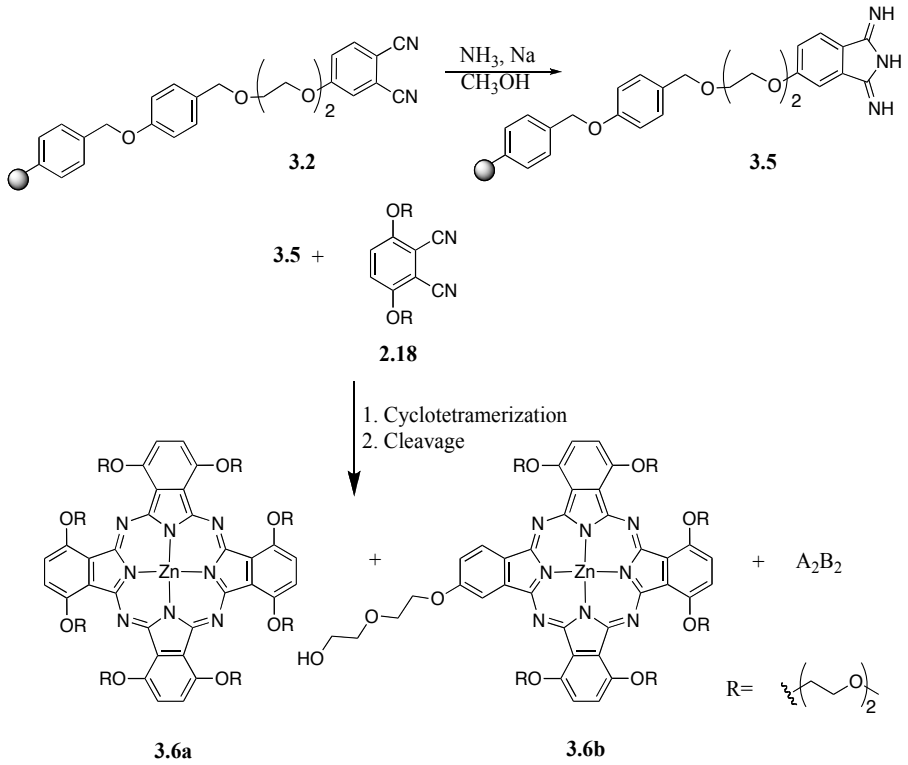

Scheme 3.5

cyclotetramerization, polymer bound phthalonitrile was converted to corresponding diiminoisoindoline unit (Scheme 3.5). While cyclotetramerization gave the corresponding symmetrically-substituted ZnPc **3.6a**, mass spectrometry of the cleaved crude product showed that the desired non-peripherally substituted ZnPc **3.6b** was contaminated with A_2B_2 side product (13%). In a similar mechanism to metal free Pc synthesis, the

cyclotetramerization in solution proceeds slower than the one on the solid-support due to the low reactivity and/or the steric hindrance of the employed phthalonitrile, resulting in formation of A_2B_2 type Pcs on the polymer support.

In order to explore the applicability of the method to different systems, variety of symmetrically- and asymmetrically-substituted Pcs were synthesized. In each case, different phthalonitrile precursor was condensed with resin-bound phthalonitrile **3.2** in BuOH in the presence of $Zn(OAc)_2$ and DBU. Pcs synthesized by solid-phase method and the corresponding phthalonitrile precursors are shown in Schemes 3.6 and 3.7. All asymmetrically-substituted Pcs were purified by filtering the crude mixture through LH-20 column to remove low molecular weight impurities. Table 3.2 summarizes the spectroscopic properties of all the Pcs. It was noted that the type and the position of the substitution,

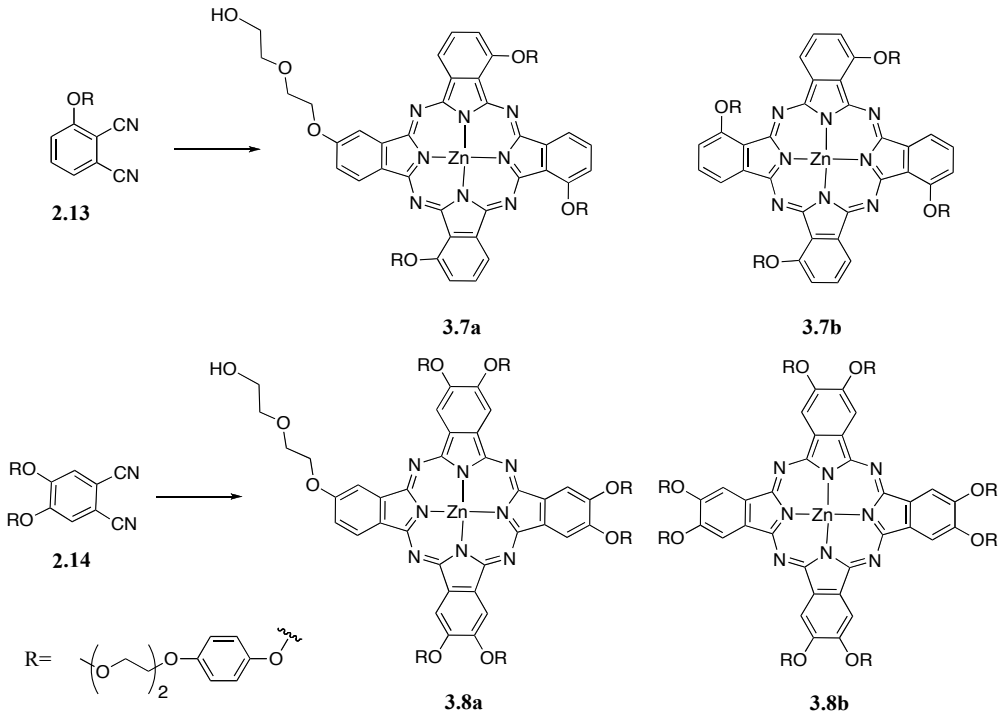

Scheme 3.6

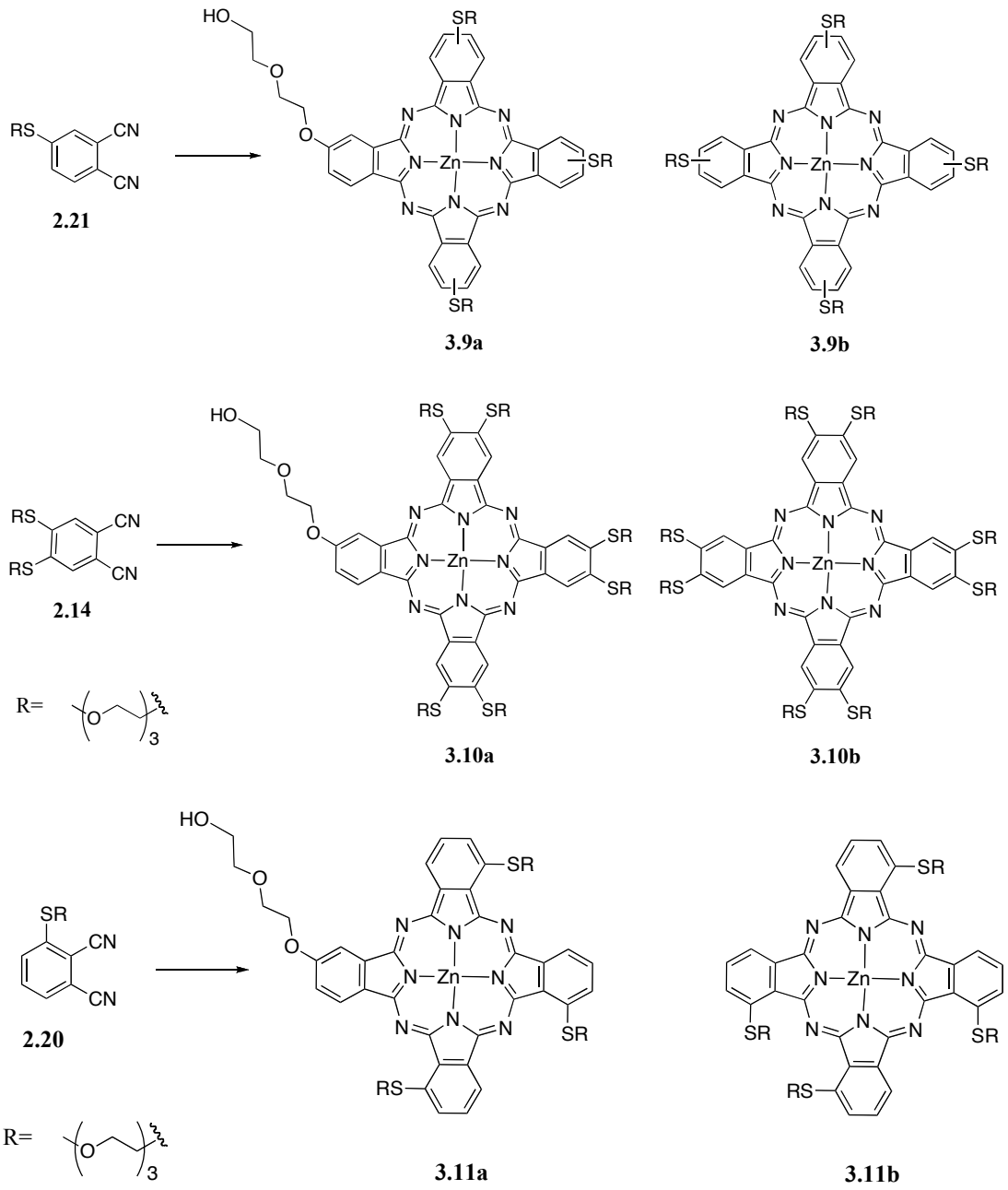

Scheme 3.7

peripheral vs. non-peripheral, was very effective in tuning the spectral properties of the Pcs. For instance, while Pc ZnPc **3.11b,** bearing oligoethylene glycol chains via thio linkage as non-peripheral substituent, had a red shifted Q band at 713 nm, ZnPc **3.9b** bearing the same substitution at the peripheral position had a Q band at 692 nm. The similar effect was alsoobserved in the case of Pc non-peripherally substituted **3.7b** (Table 3.2). The red shift of

the Q band can be explained by two reasons: 1) Lone pair electrons of the O or S at the non-peripheral position are in conjugation with the 18 π electron system, which results in longer wavelength absorption.[16] This effect is more significant with electron donating substituents linked to the Pc via thio linkage due to the interaction of the 3p orbital of the sulfur with the

Table 3.2 Peripherally and non-Peripherally Oligoethyleneglycol Substituted Pcs

	Compound Number / Pc	Yield (%)[5]	λ_{max} (abs) (nm)	Excitation Wavelength (nm)	log ε ($cm^{-1}M^{-1}$)	λ_{max} (em) (nm)[6]	ϕ_f^c
AB_3 Type Pcs	**3.7a** / ZnPc	8	695	625	4.9	702	0.17
	3.8a / ZnPc	15	681	615	5.1	687	0.13
	3.9a / ZnPc	13	690	610	5.5	698	0.06
	3.10a / ZnPc	10	705	610	5.5	712	0.10
	3.11a / ZnPc	8	691	610	5.0	699	0.10
B_4 Type Pcs	**3.7b** / ZnPc	19	698	630	5.4	705	0.04
	3.8b / ZnPc	17	681	615	5.2	685	0.08
	3.9b / ZnPc	27	692	610	5.3	695	0.13
	3.10b / ZnPc	19	709	610	5.5	716	0.13
	3.11b / ZnPc	16	713	610	5.2	718	0.07

2p orbital of the carbon at the non-peripheral position;[17] 2) while electron donating substituents at the non-peripheral position significantly destabilize the HOMO, they slightly destabilize the LUMO resulting in smaller HOMO-LUMO gap.[18] As a result, Q band, compiled mainly HOMO-LUMO interactions shifts to the longer wavelengths. Position of the substituent not only affects the absorption wavelength but also fluorescence quantum yields. Lower fluorescence quantum yield of non-peripherally substituted ZnPc **3.11b** relative to peripherally substituted ZnPc **3.9b** can be due to the destabilization of the π

[5] Yields of asymmetrically-substituted Pcs were calculated based on the loading of the phthalonitrile on the support.

[6] All Spectra were taken in DMSO. Fluorescence quantum yield measurements for all Pcs were done using methylene blue as a standard at absorbance 0.04 - 0.05 for both Pc and standard solutions to avoid any error due to inner-filter effect.[42]

orbitals as result of deviation from planarity of the Pc ZnPc **3.11b**. In order to have a better understanding of the relationship between the planarity and the fluorescence quantum yield, several attempts have been made to grow a single crystal of ZnPcs **3.11b** and **3.9b**. However, these attempts were unsuccessful. Effects of the deviated planarity on the spectral properties of the Pcs were discussed in the literature several times.[16,19-21] Kobayashi and coworkers showed that the perfectly flat Pc skeleton could be easily disordered by the substituent pattern. They reported highly disordered, with a maximum degree of deviation 1.03 Å, tetra substituted Pcs, bearing bulky phenyl groups at the non-peripheral poisition.[22] In another paper, Kobayashi discussed the effect of peripheral substitution on absorption and fluorescence spectra of Zn and metal free Pcs.[18] Authors reported fluorescence quantum yields as low as 0.038 for the Pcs decorated with electron donating groups at the non-peripheral position. The gap between HOMO and LUMO is the main factor determining the fluorescence quantum yield. As the energy difference between the two orbitals, HOMO and LUMO, decreases, non-radiative decay becomes easier than radiative decay, which yields a weak fluorescence.[18] Since the energy difference between HOMO-LUMO is smaller in non-peripherally substituted ZnPc **3.11b** than peripherally substituted ZnPc **3.9b**, judged by the absorption and emission spectra, non-peripherally substituted ZnPc **3.11b** more likely undergoes to non-radiative decay as it returns to the ground state. The similar effect was also seen for ZnPc **3.7b** having tetra- phenoxy groups at the non-peripheral positions. While the ZnPc **3.7b** had a red shifted Q band at 698 nm, as a result of extended conjugation, fluorescence quantum yield of the ZnPc **3.7b** was as low as 0.04.

3.2.3 Activation of Hydroxy Functionalized Phthalocyanines Towards Conjugation to Biomolecules

After the successful syntheses of mono hydroxy functionalized Pcs, the next goal was to activate the hydroxy group for covalent conjugation of the Pcs to bioorganic molecules. The

first attempt was the conversion of the hydroxy group of ZnPc **3.7a** to *p*-cyanoethyl phosphoramidite via nucleophilic substitution of the hydroxy with chlorine on commercially available N,N-diisopropylamino cyanoethyl phosphoramidyl chloride (Scheme 3.8).[23] Since the phosphitylating reagent is very prone to hydrolysis, the reaction was carried in anhydrous THF and was followed by ^{31}P NMR (Figure 3.4). After 24h. time period, ^{31}P NMR spectrum of the reaction mixture showed three peaks at 180, 140,

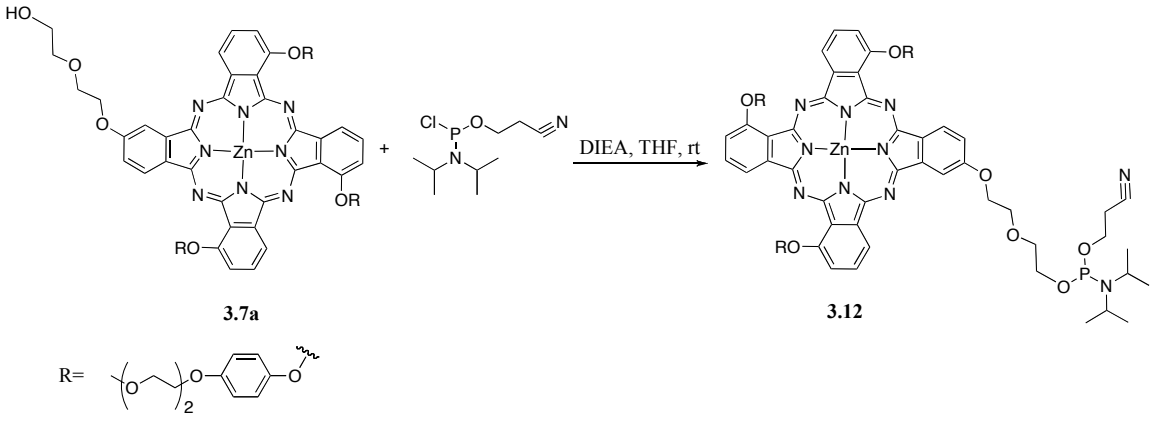

Scheme 3.8

15 ppm corresponding to unreacted N, N-diisopropylamino cyanoethyl phosphoramidyl chloride, the target compound and the side product formed by the hydrolysis of the phosphitylating reagent, respectively. The major peak at 15 ppm suggested that even under anhydrous conditions the hydrolysis of N, N-Diisopropylamino cyanoethyl phosphoramidic-Cl took place as a major reaction. This could be due to the hygroscopic nature of the ZnPc **3.7a** due to the oligoethylene glycol chains. Since longer reaction times did not improve the yield of the reaction, judged by ^{31}P NMR, the reaction was quenched with anhydrous CH_3OH. Following the extraction, ^{31}P NMR spectrum of the crude mixture revealed that while the peak at 180 ppm disappeared, another peak at 150 ppm emerged along with the other two peaks at 141 and 15 ppm. The peak at 150 ppm was assigned as the methyl ester form of phosphitylating reagent, formed after the addition of the CH_3OH. Nucleophilic

substitution of chlorine with methoxy group and hydrolysis of the starting material was further confirmed by performing a control experiment employing triethyleneglycol monomethyl ether as an alcohol source. Attempt to purify **3.12** by filtration through LH-20column was unsuccessful. Thus, precipitation of CH_3OH solution into ether was selected

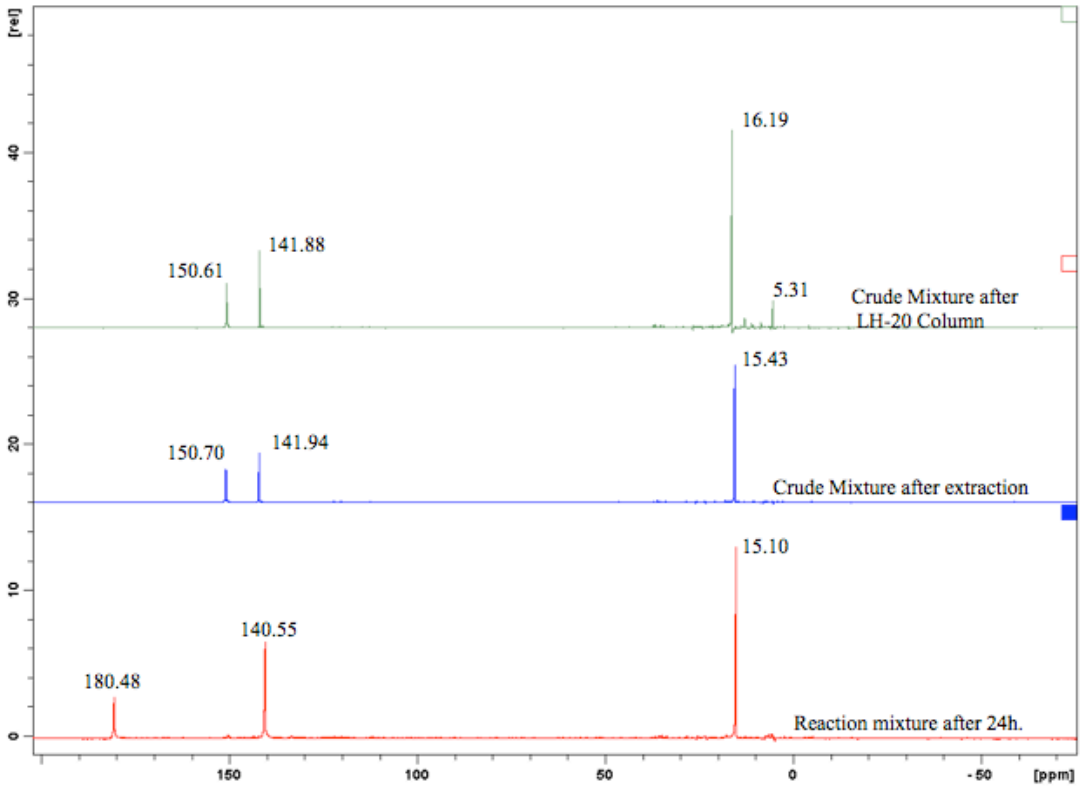

Figure 3.4 ^{31}P NMR of the reaction mixture and purification progress of the phosphitylation of ZnPc **3.12**.

as an appropriate purification method. Collected blue color precipitate and supernatant was submitted to ^{31}P NMR. In both cases, only one peak was observed at 15 ppm confirming the decomposition of the desired compound during the purification process.

Due to the inconveniences during the synthesis and the purification of ZnPc **3.10,** another approach was taken to convert to hydroxy group to more reactive functional group, ester. Synthesis of succinimide ester of Pc ZnPc **3.11a** started with alkylation of mono-

hydroxy functioanalized **3.11a** with iodoacetic acid to provide carboxylic acid **3.13** (Scheme 3.9).[24] Due to the incomplete reaction, this step was repeated twice using 10-fold molar excess of NaH as a base and 5-fold molar excess of iodoacetic acid (Scheme 3.9). The analysis of the crude mixture by mass spectrometry showed that the mixture

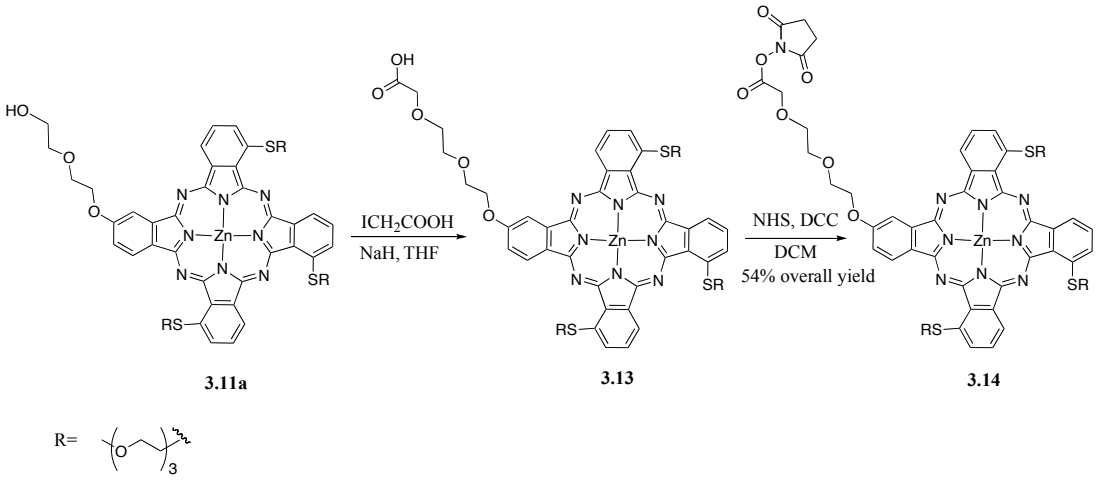

Scheme 3.9

contained ~ 7% of the starting material, mono-hydroxy functionalized ZnPc **3.11a**. Without any purification, the crude mixture was submitted to the next reaction. Active ester of **3.13** was prepared employing a standard protocol for esterification with DCC and N-hydroxysuccinimide in anhydrous CH_2Cl_2.[25] Succinimide ester functionalized ZnPc **3.14** was purified by precipitation from CH_2Cl_2 followed by LH-20 column and obtained in 54% overall yield.

3.2.4 FRET-RET Pairing

Pcs, having absorption and emission profiles in the far-red and near-infrared region of the electromagnetic spectrum with easily tunable photophysical properties, are excellent candidates for various bioanalytical applications using fluorescence as the read out mode for the detection such as analysis of PCR products,[26] single gene mutation detection[27] and numerous fluorescence resonance energy transfer (FRET) based assays.[28] To date, the most

commonly used dyes for the desired applications are tricarbocyanines having absorption and emission profiles in the visible range of the electromagnetic spectrum.[29] While these dyes have extinction coefficients as high as 10^5 $M^{-1}cm^{-1}$ with favorable water solubility, their poor chemical and photochemical stability disfavor their use in the bioanalytical applications.[30] The biggest advantage of Pcs over other dyes is their moderate fluorescence quantum yields, coupled with low photobleaching quantum yields,[13] high molar absorptivities (>10^5 $M^{-1}cm^{-1}$)[13,31] and excellent chemical and photochemical stabilities. All these properties of the Pcs bring numerous advantages to these applications. Besides taking advantage of using cheap diode lasers, background interferences are significantly reduced since very limited number of molecules fluoresce in the Near-IR region of the electromagnetic spectrum. Narrow emission band of the Pcs is utilized to diminish the spectral leakage, which increases the possibility for ultra sensitive applications. In spite of the fact that their attractive properties, Pcs have limited usage in the bioanalytical applications for a number of reasons. From the synthetic perspective, one of the main challenges of the Pcs is the difficulty faced in the purification process a fluorophore possessing favorable properties discussed above.

The desired applications are established based on resonance energy transfer between two fluorophores utilizing from molecular beacons, synthetic DNA molecules having "stem-loop" structure with two fluorophores at the 5'and 3'ends (Figure 3.5).[32] The

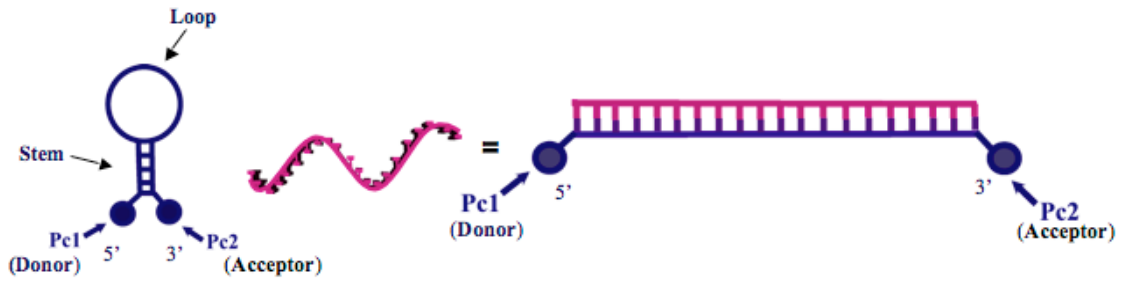

Figure 3.5 Pc based molecular beacon.

stem, complimentary to itself, remains closed and energy transfer between donor and acceptor takes place until the addition of complimentary DNA. The stem is reversibly disassociated by the hybridization of the loop with the complimentary DNA and energy transfer is ended due to the large distance in between the donor and the acceptor molecules. Molecular beacons are widely used in variety of applications including real-time nucleic acid detection,[33,34] quantitative real-time PCR detection,[35] single gene mutation detection[36] and mRNA detection in living cells.[37]

Dr. Irina V. Nesterova performed FRET-RET experiments of symmetrically- substituted Pcs in solution to determine the best FRET-RET pair among the oligoethylene glycol-substituted Pcs. Based on the spectral overlap of absorption with emission spectra, ZnPc **3.3a** was chosen as a potential donor to be paired with ZnPcs **3.10b** or **3.11b** as an acceptor (Scheme 3.10). Absorption and emission spectra of the selected Pcs are presented in Figure

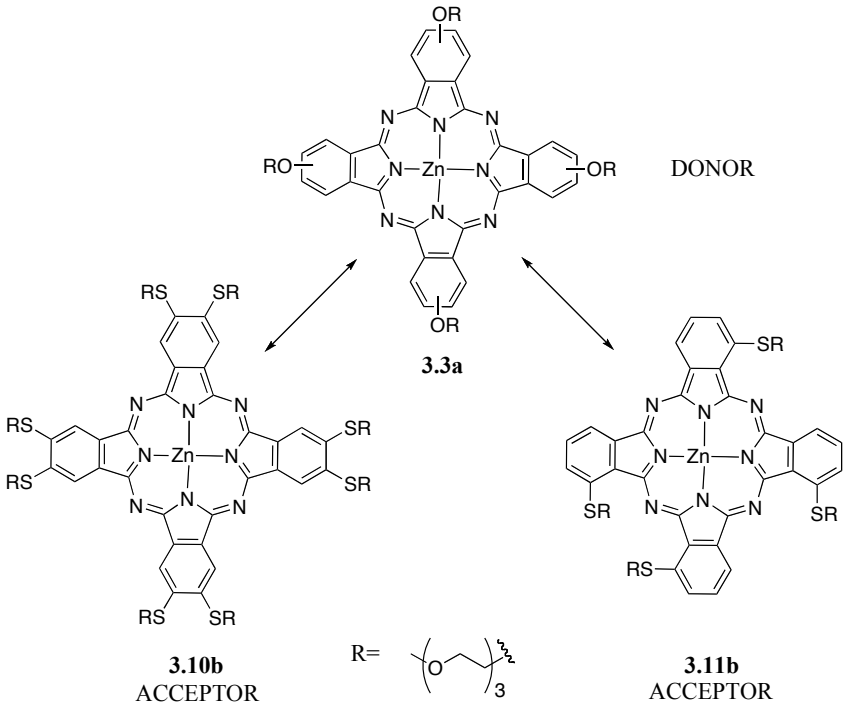

Scheme 3.10

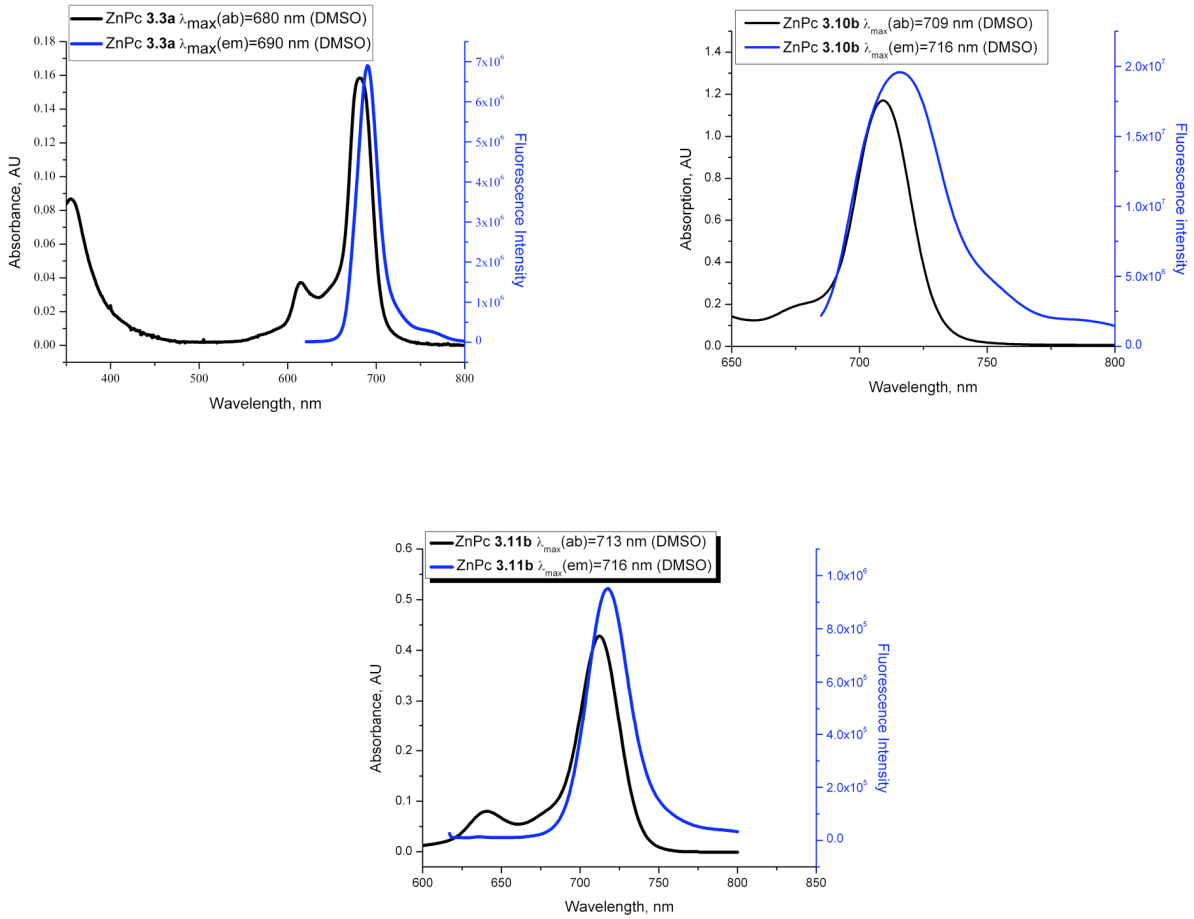

Figure 3.6 Absorption and emission spectra of ZnPcs **3.3a** (up left), **3.10b** (up right) and **3.11b** (bottom).

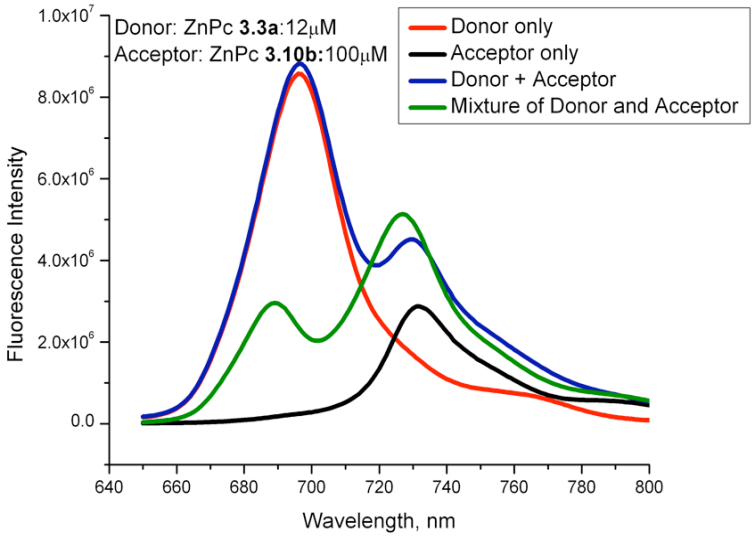

Figure 3.7 Emission spectra of donor (blue), acceptor (black), mixture of donor and acceptor (green) and theoretical emission of the mixture of the donor and acceptor (blue).

3.6. Figure 3.7 shows the overlayed emission profiles of Pcs as well as the mixture of donor and acceptor solutions. The red and black lines are the emission profiles of the donor and acceptor, respectively. The blue line is the theoretical emission profile of the mixture of the donor and the acceptor, obtained by linear addition of individualemission spectrum of the corresponding Pcs together. The green line is the emission of the mixture of the ZnPcs **3.3a** and **3.10b** at known concentration. As it is clearly seen, while the intensity of the donor emission significantly decreased, the acceptor's emission intensity increased, indicating the occurrence of FRET between the **3.3a-3.10b** pair. The area of the spectral overlaps of the donor emission and the acceptor absorption, proportionally related to energy transfer rate, were calculated from the absorption and emission spectra of the fluorophores. Besides the spectral overlap, FRET highly depends on the distance between the donor and the acceptor molecules. If the distance between the molecules is greater than the Förster distance R_0, the distance at which 50% energy transfer occur, the energy transfer efficiency immediately drops to zero.[28] Reported R_0 distances of the commonly used donor-acceptor pairs are in a range from 20 to 90 Å.[28] From the absorption and emission spectra of the fluorophores, the R_0 value of the selected ZnPc pair, **3.3a-3.10b,** was calculated as 63 Å. Based on the results, it was concluded that the more efficient energy transfer is expected between the selected donor and acceptor pair than the commonly used TMR-Cy5 FRET pair (Table 3.3).[38]

The same experiment and the calculations were also performed for the next ZnPc pair, **3.3a-3.11b**. The emission spectra of the mixture of the fluorophores are presented in Figure

Table 3.3 Calculated Spectral Overlap and Förster Distances for FRET Pairs

Donor	Acceptor	Overlap integral ($J(\lambda)$, $M^{-1}cm^{-1}nm^4$)	Förster Distance (R_0, Å)
3.3a	**3.10b**	3.44×10^{16}	63
	3.11b	1.06×10^{16}	56
TMR	Cy5	$5.5x10^{15}$	46

3.8. In comparison with the **3.3a-3.10b** pair, slightly shorter distance is required, for 50% efficient energy transfer between the two fluorophores. However, the distance is still

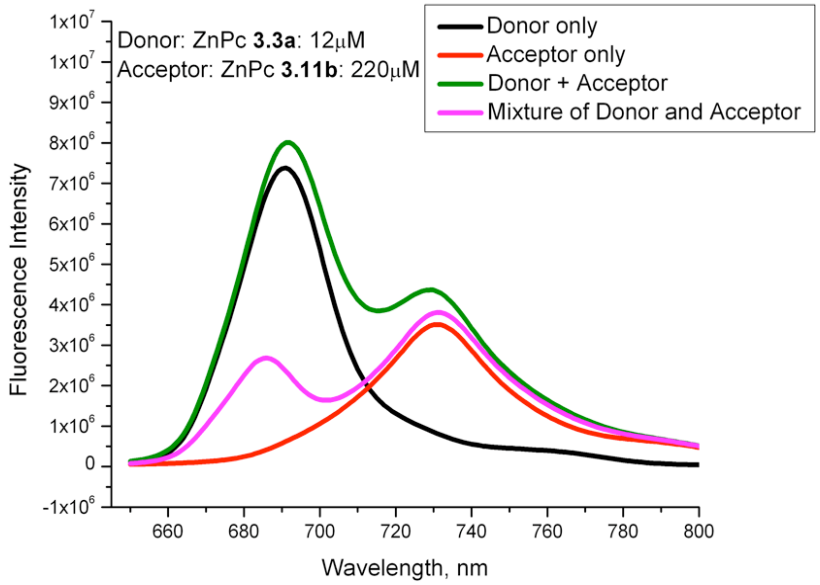

Figure 3.8 Emission spectra of donor (red), acceptor (black), mixture of donor and acceptor (green) and theoretically obtained emission of the donor and acceptor (blue).

convenient to study various biological molecules. Between two FRET pairs, the **3.3a-3.11b** displays slightly better spectral overlap and longer Förster distance for efficient FRET, which could be beneficial for studies with larger biomolecules.

RET experiments were performed in a similar way using two different Pc pair. NiPc **3.3c** and CuPc **3.3b** were selected as potential quenchers (acceptor) and ZnPc **3.3a** was selected as the donor (Scheme 3.11). Figure 3.9 shows the absorption profiles of the selected acceptor Pcs. Figures 3.10 and 3.11 shows the emission spectra of the donor and acceptor mixtures at different concentrations. Excitation wavelength of 605 nm, providing excitation of donor molecule, was used throughout the experiments. As the quencher concentration was increased, the intensity of the emission decreased, indicating the energy transfer from the donor to the acceptor. While in the case of ZnPc-CuPc (**3.3a-3.3b**) pair,

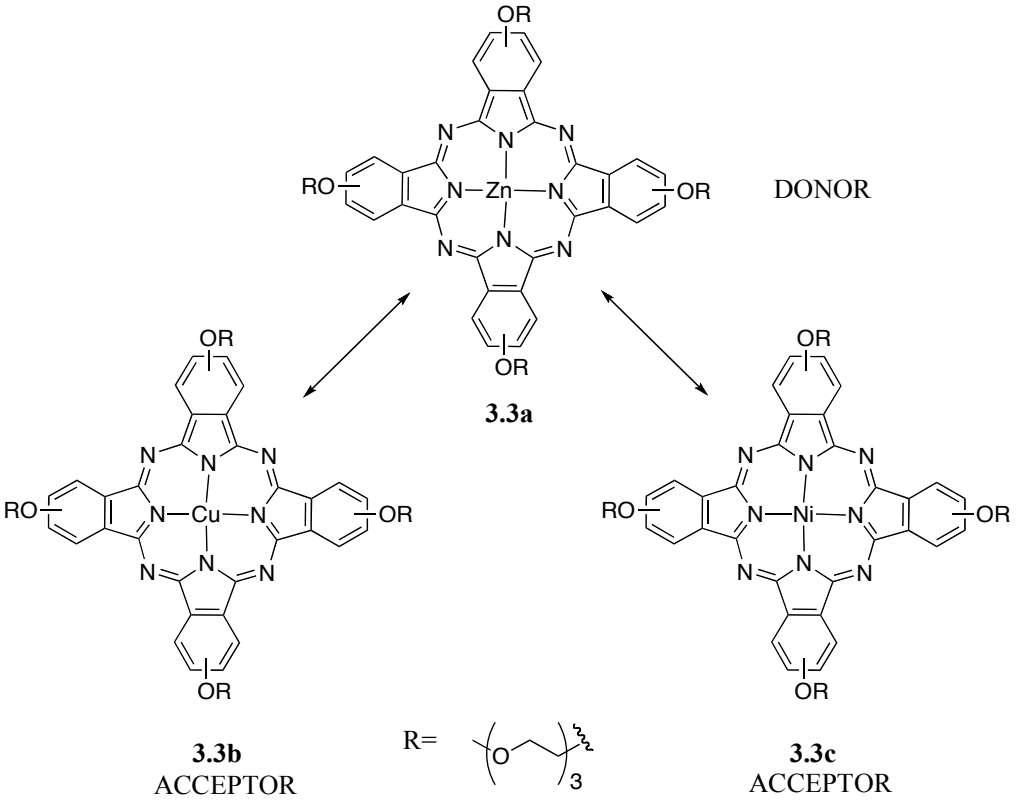

Scheme 3.11

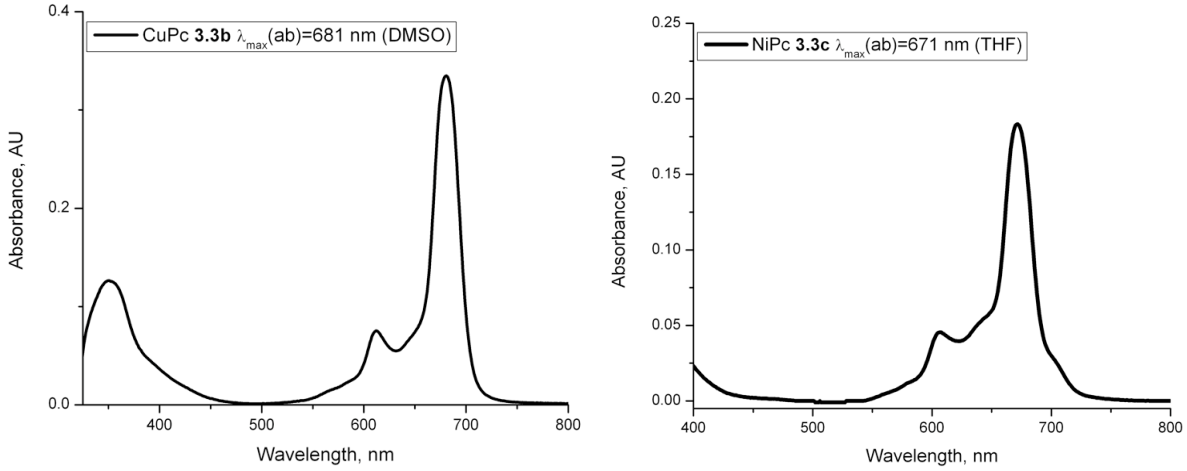

Figure 3.9 Absorption profiles of the potential acceptor Pcs: CuPc **3.3b** (left) and NiPc **3.3c** (right).

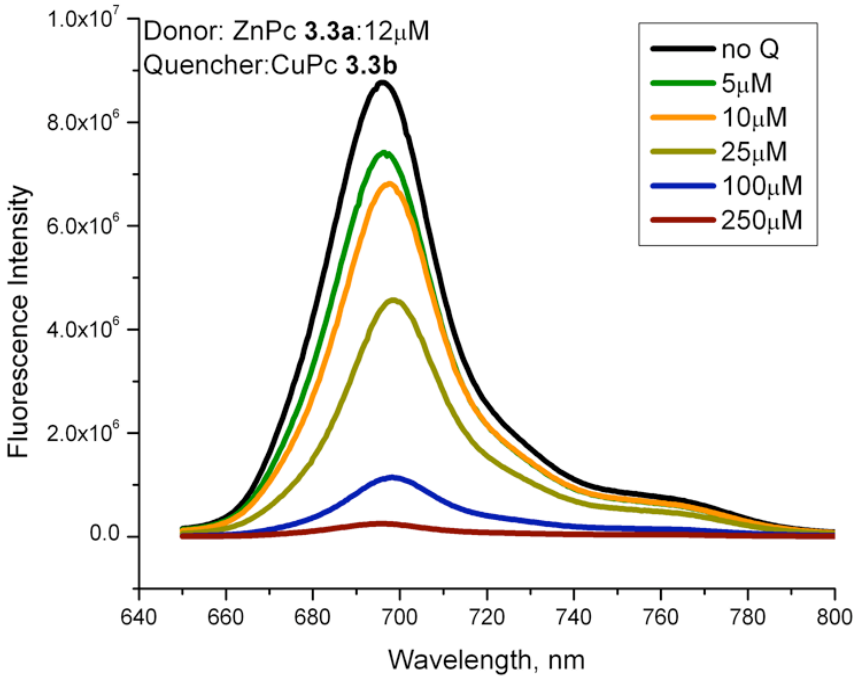

Figure 3.10 Emission spectra of fluorescence quenching.

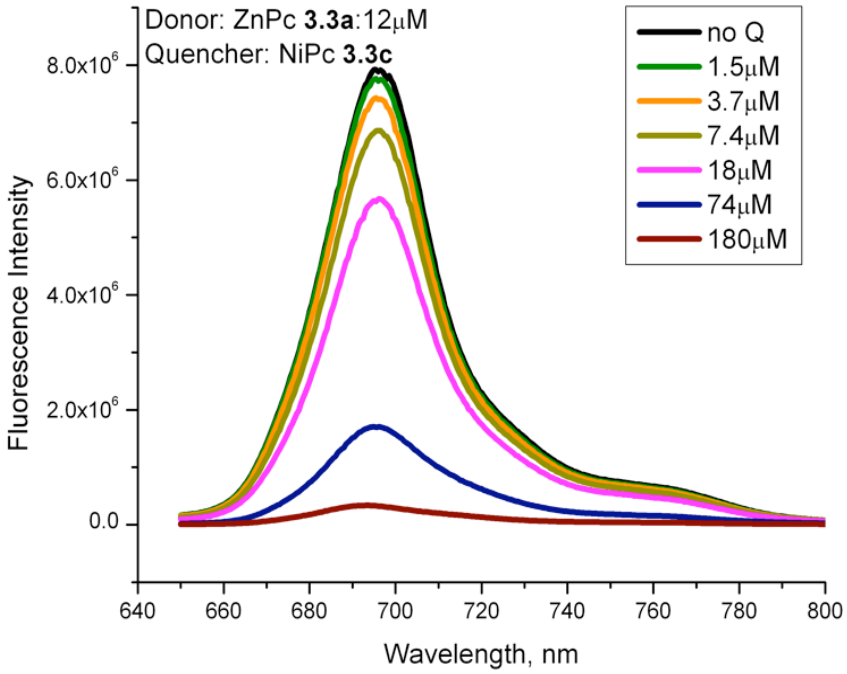

Figure 3.11 Emission spectra of fluorescence quenching.

250 μM concentration of the quencher was required to diminish the emission of the donor 97 % (Figure 3.10), for ZnPc-NiPc (**3.3a-3.3c**) pair this value was 180 μM (Figure 3.11)

Spectral overlaps and Förster distances were calculated from the absorption and emission spectra. Preliminary results indicated that ZnPc-CuPc (**3.3a-3.3b)** is a promising candidate for the desired applications due to the better spectral overlap in larger Förster distance (Table 3.4). Thus, better energy transfer efficiency is expected for ZnPc-CuPc (**3.3a-3.3b**) pair than ZnPc-NiPc (**3.3a-3.3c**). SternVolmer plots were evaluated for both of the systems (Figure 3.12). As predicted from the previous results, CuPc **3.3b** provided better quenching efficiencies with K_{SV}=35569 M^{-1} than NiPc **3.3c**, K_{SV}=21292 M^{-1}.

Table 3.4 Calculated Spectral Overlap and Förster distances for RET Pairs

Donor	Acceptor (Quencher)	Overlap integral ($J(\lambda)$, $M^{-1}cm^{-1}nm^4$)	Förster Distance (R_0, Å)
3.3a	**3.3b**	1.22×10^{16}	53
	3.3c	2.45×10^{15}	41

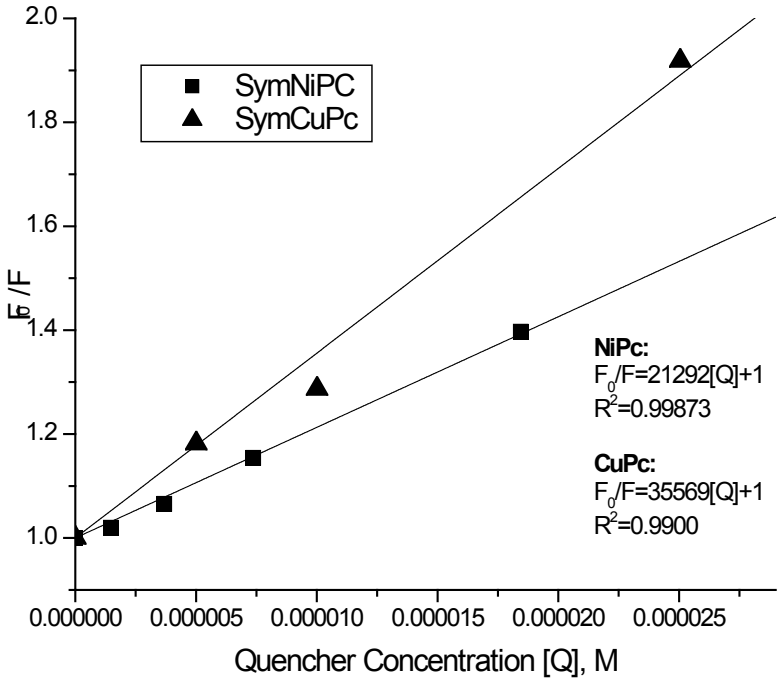

Figure 3.12 Stern-Volmer plot of **3.3a-3.3b** and **3.3a-3.3c** quenching systems.

3.3 Conclusion and Future Work

Solid-phase synthesis is a fundamental methodology in organic synthesis, and it has been utilized for preparation of myriad different molecular classes and cyclization reaction types. Since the development of solid-phase synthesis[39] related phenomena such as intrasite interaction and site isolation have been extensively studied. It has been shown that the outcome of a reaction on solid support is significantly influenced from intrasite reactions, which can be diminished by altering the loading or the cross-linked density of the polymer, changing the structure of the linker, increasing the concentration of incoming reagent, or changing the solvent and reaction temperature.[40] While intrasite interaction generally leads to undesired products, it can be utilized for selective synthesis of dimeric cross-linked molecules. Schreiber et al. showed the synthesis of homodimeric molecules via intrasite olefin crossmetathesis on solid support using highly loaded (1-2 mmol/g) and lightly cross-linked (1% DVB) polystryene resin with the goal of split-pool synthesis of homodimer libraries.[41] Thus, it may be possible through optimization of resin, solvent, and other reaction conditions to prepare "2 + 2" (A_2B_2) Pc products as the predominant or only product, which may have unique applications as well.

The advantage of the solid-phase method described here is the ability to synthesize a variety of asymmetrical phthalocyanines quickly and easily without the need for extensive purification steps to get homogeneous Pc products. The method is a significant advancement of previous solid-phase synthesis of Pcs and applicable to Pcs with wide variety of substituents. The use of hydrophilic PEG-based resin is key for the success of this method to allow easy removal of symmetrical Pc coproducts by washing of the resin as well as to prevent noncovalent adsorption of the desired AB_3 Pc to the support. Site-isolation on the PEG-based resin can be accomplished using slightly lower loadings and by inclusion of a

divalent metal ion in alkoxide-promoted phthalonitrile tetramerization. The method described here provides *pure* asymmetrically-substituted Pcs is very efficient, taking <3 days to complete including loading, Pc formation, washings, cleavage, and simple chromatography.

Using solid-phase synthesis method, vide variety of AB_3 type substituted, mono hydroxy functionalized fairly water-soluble Pcs were synthesized and evaluated for possible FRET-RET applications. Attempts to convert the hydroxy group to more reactive functional groups were somehow successful. Since the conversion requires extra steps and is not applicable to different functional groups, it is necessary to synthesize Pcs having more reactive functional groups using alternative solid-support linking strategies to be able to conjugate the Pcs to biomolecules without the need of extra step.

3.4 Experimental

3.4.1 General Experimental Information

Unless otherwise indicated, all commercially available starting materials were used directly without any further purification. Reactions under anhydrous conditions were performed in dried solvents under argon atmosphere. Reactions were monitored by TLC using Sorbent Technologies silica gel plates 250 μm with UV activator. Silica gel Sorbent Technologies 40-63 μm was used for column chromatography. PEG-based Wang Resin was obtained from Matrix-Innovation. Sephadex^{TM} LH-20, in 18-111 μm particle size, was used for purification of the asymmetrically-substituted Pcs. Unless otherwise indicated, MALDI-MS spectra of the compounds were obtained using CCA as a matrix. FT-IR spectra were obtained on Bruker Tensor 27 spectrometer. Electronic absorption spectra were measured on a Perkin-Elmer Lambda 35 UV-vis spectrophotometer. The HPLC chromatograms were obtained using a JASCO (Easton, MD) 2000-series HPLC equipped with a quaternary gradient pump, autosampler, and fluorescence and diode-array detectors.

HPLC was performed using Zorbax, C_{18} 5µm, 150 × 4.6 mm column with a 1 mL/min flow rate. Three different solvent gradient conditions were used: Condition A: HPLC was performed with 0.05 M TEAA in a H_2O and CH_3OH as the eluents. Column was initially held at 95% 0.1 M TEAA-5% CH_3OH for 5 min and then concentration of CH_3OH was ramped to the 95% in 30 min. and was held at that concentration for 5 min. Column was washed with 100% CH_3OH for 15 min. The column was allowed to equilibrate at the initial mobile phase conditions for 20 min before the next injection. Condition B: 0.05M TEAA in a H_2O and CH_3OH-THF (80:20) was used as an eluting solvent. Column was initially held at 50% 0.1 M TEAA-50% CH_3OH for 5 min and than it was ramped to the 5% 0.05 M TEAA-95% CH_3OH in 15 min and held at that concentration for 15 min. The column was allowed to equilibrate at the initial mobile phase conditions for 20 min before the next injection. Condition C: CH_3OH was used as an eluting solvent. Column was held at 100% CH_3OH for 30 min. The column was allowed to equilibrate at the initial mobile phase conditions for 20 min before the next injection.

Emission spectra were obtained using a FLUOROLOG-3 spectrofluorometer (Horiba Jobin Yvon, Edison, NJ) equipped with a 450-W xenon lamp and a cooled Hamamatsu R928 photomultiplier operated at 900V in the photon-counting mode. A quartz cuvette with a 10 mm path length was utilized throughout these experiments. All measurements were performed under ambient room conditions within 3 h of solutions preparation. Stock solution and dilutions were prepared in anhydrous DMSO or THF. The quantum yields were calculated using a secondary standard method.[42] Methylene blue, a dye with excitation/emission wavelengths similar to Pcs and an established quantum yield was used as a secondary standard. According to the approach, the integrated fluorescence intensity of the analyte (I) and standard (I_R), the optical density of the analyte (OD) and the standard (OD_R),

and the refractive index of analyte solvent (n) and standard solvent (n_R) are related to the quantum yield of the analyte (Q) as:

$$Q = Q_R \frac{I}{I_R} \frac{OD_R}{OD} \frac{n^2}{n_R^2}$$

where Q_R is a quantum yield of the reference standard (0.03 for Methylene Blue). To account for incomplete spectra, the bands were extrapolated using appropriate fitting models whenever necessary.

3.4.2 Experimental Procedures

Trichloroacetimidate resin (3.1)

Chem-Matrix™ Wang resin (0.6g, 0.6 mmol/g loading) was swelled in an anhydrous CH_2Cl_2 (20 mL) for an hour. Tricholoracetonitrile (5.4 mmol, 0.54 mL) was added to resin and the mixture was cooled to 0 °C. A catalytic amount of DBU was added to the suspension over 5 min and the reaction continued at 0 °C for an additional 45 min. The color of the solution changed from clear to light brown. The resin was washed with CH_2Cl_2 (4 x 20 mL), DMSO (2 x 20 mL), THF (3 x 20 mL) and CH_2Cl_2 (3 x 20 mL). FTIR (KBr, cm^{-1}) 3055, 2872, 1665, 1512, 1452, 1348, 1265, 1093, 951, 836, 798, 730, 700, 648.

Polymer-supported 4-(2-(2-hydroxyethoxy)ethoxy)phthalonitrile (3.2)

Trichloroacetimidate resin **3.1** (0.6 g) was suspended into the anhydrous CH_2Cl_2-cyclohexane (2:1; 20 mL) under argon for 40 min. Hydroxyphthalonitrile **2.16** (100 mg, 0.43 mmol) was dissolved in anhydrous CH_2Cl_2 (2 mL) and added to the suspension over 5 min at room temperature. $BF_3.OEt_2$ (5 μL) was added to the suspension and reaction was monitored by FT-IR. After 3 hrs, anhydrous CH_3OH (2.5 mL) in anhydrous CH_2Cl_2 (1.5 mL) was added to suspension and the reaction continued for an additional 3 hrs. The resin was washed with

CH_2Cl_2 (5 x 20 mL), THF (3 x 20 mL) and CH_2Cl_2 (6 x 20 mL). FTIR (KBr, cm^{-1}) 2868, 2229, 1764, 1659, 1597, 1510, 1453, 1349, 1295, 1248, 1088, 946, 841, 730, 699.

Diiminoisoindoline Resin (3.5)

Resin **3.2** (0.6 g) was swelled in anhydrous CH_3OH (15 mL) for 30 min. Na metal (0.04 g) was dissolved in anhydrous CH_3OH (5mL) and the solution was added to the well -swelled resin. Anhydrous NH_3 was bubbled through the reaction mixture and the mixture refluxed for 4h. The reaction was followed by FT-IR and run until the CN stretching peak was disappeared. The resin was washed with CH_3OH (5 x 30 mL), CH_2Cl_2 (5 x 30 mL), CH_2Cl_2–THF (1:1; 2 x 15 mL) and finally with CH_2Cl_2 (5 x 15 mL). FTIR (KBr, cm^{-1}) 3055, 2870, 1665, 1510, 1453, 1348, 1268, 1093, 950, 836, 798, 730, 700, 648.

General Procedure for Synthesis of Pc (3.3-3.11)

Resin **3.2** (0.6 g) was swelled in 15 mL of anhydrous BuOH overnight. A 9 fold molar excess of corresponding phthalonitrile (3.24 mmol) and metal salt (0.9 mmol) were dissolved in anhydrous BuOH (7 mL) and added to well swelled resin under Ar. Concentration of phthalonitrile in the reaction mixture was kept around 0.16 M. The mixture was heated up to 90 °C and DBU (1.8 mmol, 0.27 mL) was added to mixture. The reaction was carried out at 110 °C for 24 hrs. The resin was washed until a colorless filtrate was obtained, first with hot BuOH (15 x 25 mL), CH_2Cl_2 (5 x 25 mL), and then BuOH-CH_2Cl_2 (1:1; 3 x 25 mL) and CH_2Cl_2 (2 x 25 mL).

General Procedure for Purification of Symmetrical Pcs (3.3-3.11)

Filtrate solutions were combined and evaporated to dryness. A portion (100 mg) of the crude mixture was dissolved in ~3 mL of CH_3OH and 50 mL of diethyl ether was added to solution. Solution was left in the fridge overnight and the suspension was centrifuged to give Pcs **3.3-3.11** as a blue / green solid.

General Procedure for Cleavage of the AB_3 type Pc (3.3-3.11)

The resin was suspended into a solution of TFA-CH_2Cl_2 (1:9; 50 mL) and left in the shaker for 3h. at room temperature. Filtrate was evaporated to dryness and the crude mixture was purified by filtration through a silica gel or LH-20 column using CH_3OH as an eluting solvent.

Determination of the Loading Capacity of Resin 3.2

The loading capacity of **3** was determined by cleavage of the ether bond as described in general procedure for cleavage of the AB_3 type Pc. From 0.5 g of **3.2**, 0.033g, (0.14 mmol) of 4-(2-(2-hydroxyethoxy)ethoxy)phthalonitrile (**2.16**) was obtained. The loading capacity of **3.2** was determined as 0.28 mmol/g. The yields of the AB_3 type Pcs were calculated based on 0.28 mmol/g.

Diisopropylphosphoramidite ZnPc(3.12)

ZnPc **3.7a** (115 mg, 8.7μmol) was dissolved in anhydrous pyridine (4 mL) and the solvent was evaporated under Ar. This step was repeated three times. **3.7a** was redissolved in THF (5 mL) and N, N-Diisopropylamino cyanoethyl phosphoramidyl chloride (8 μL, 35μmol) with DIEA (7.6μL, 43μmol) were added to the solution under Ar. The reaction was stirred at room temperature for 24h. Anhydrous CH_3OH (10mL) was added to mixture and the solvent was evaporated to dryness. The crude mixture was dissolved in EtOAc (8 mL) and washed with water (3 x 8 mL). Combined organic layers were evaporated to dryness and the crude mixture was filtrated through LH-20 column using DMF as eluting solvent. ^{31}P NMR (250 MHz, CD_2Cl_2) δ 150.88, 141.68, 16.19, 5.31 Attempt for further purification of the crude mixture was resulted in decomposition of the product: The crude mixture was dissolved in CH_2Cl_2 (1 mL) and ether (10 mL) was added to solution. The solution was kept at -20 °C overnight and the suspension was centrifuged.

Carboxylated ZnPc (3.13)

To a mixture of anhydrous THF (1 mL) and NaH (7.5 mg, 156 μmol) ZnPc **3.11a** (38 mg, 31.2 μmol) in anhydrous THF (3 mL) was added and the mixture was stirred at 0 °C for an h. Iodoacetic acid (57.4 mg, 312 μmol) was dissolved in anhydrous THF (3 mL) and added to the mixture drop wise. The reaction was stirred at room temperature overnight. The mixture was diluted with water and water layer was saturated with NaCl. The pH was adjusted to 4 with concentrated HCl. The crude mixture was extracted with EtOAc (3 x 15 mL) and purified by filtration through LH-20 column using CH_3OH as eluent. MALDI-MS: Cald $C_{59}H_{68}N_8O_{14}S_3Zn$ $+H^+$: 1273.33; found 1273.35, 1214.35

Succinimide Ester ZnPc (3.14)

Pc **3.13** (57.5 mg, 45 μmol), DCC (93 mg, 45 μmol) and N-Hydroxy succinimide ester (52 mg, 45 μmol) were dissolved in anhydrous CH_2Cl_2 and stirred under Ar for 24h. After 3h. white precipitate was formed. The suspension was cooled down to 0 °C and precipitate was filtered off. The crude mixture was initially filtered through LH-20 column and collected blue band was evaporated to dryness. The crude mixture was further purified by precipitation of the impurities from CH_2Cl_2. Pc **3.14** was obtained in 54% overall yield. MALDI-MS: Cald $C_{63}H_{71}N_9O_{16}S_3Zn+Na^+$: 1394.33; found 1394.56

ZnPc (3.3a): 21% yield as a blue solid. Condition A was employed to perform HPLC. t_R=39.71 min. MALDI-MS: Calcd $C_{60}H_{72}N_8O_{16}Zn+H^+$: 1225.44; found 1225.40. λ_{max} (DMSO): 681 nm (logε=5.5). λ_{max} (em) (DMSO): 691 nm. ϕ_f : 0.15

CuPc (3.3b): 15% yield by centrifuging the suspension. Condition B was employed to perform HPLC. t_R=22.65 min. MALDI-MS: Calcd $C_{60}H_{72}CuN_8O_{16}+H^+$: 1124.44; found: 1124.45. λ_{max} (DMSO): 681 nm (logε=5.1). λ_{max} (em): n.d. ϕ_f : n.d.

NiPc (3.3c): 17% yield as a blue solid. Condition B was employed to perform HPLC. t_R=23.32 min. MALDI-MS: Calcd. $C_{60}H_{72}N_8NiO_{16}^+H$: 1219.44; found: 1219.43. λ_{max} (THF): 671 nm (logε=4.3). λ_{max} (em) (THF): 678 nm. ϕ_f: 0.0003

H_2Pc (3.3d): 18% yield as a blue solid. Condition C was employed to perform HPLC. t_R=6.56 min. MALDI-MS: Calcd $C_{60}H_{74}N_8O_{16}^+$: 1162.52; found: 1162.51. λ_{max} (DMSO): 676 nm (logε=3.5), 706 nm (logε=3.5). λ_{max} (em) (DMSO): 709 nm. ϕ_f: 0.06

MgPc (3.3e): 20% yield as a blue solid. Condition A was employed to perform HPLC. t_R=38.15 min. MALDI-MS: Calcd $C_{60}H_{72}MgN_8O_{16}+H^+$: 1185.49; found: 1185.50. λ_{max} (DMSO): 682 nm (logε=5.5). λ_{max} (em) (DMSO): 691 nm. ϕ_f: 0.31

ZnPc (3.4a): The crude mixture was purified by column chromatography on silica gel with a mixture of CH_3OH-CH_2Cl_2 starting from 1:99 and gradually increasing the CH_3OH percentage up to 5% in CH_2Cl_2 to give **ZnPc** in 12% yield. Condition A was employed to perform HPLC. t_R=38.32 min. MALDI-MS: Calcd $C_{57}H_{66}N_8O_{15}Zn+H^+$: 1167.39; found: 1167.80. λ_{max} (DMSO): 680 nm (logε=4.9). λ_{max} (em) (THF): 690 nm. ϕ_f: 0.15

CuPc (3.4b): The crude mixture was purified by running it through a LH-20 column with CH_3OH as an eluting solvent to give **CuPc** in 13% yield. Condition B was chosen as the eluent to perform HPLC. t_R=20.31 min. MALDI-MS:Calcd $C_{57}H_{66}CuN_8O_{15}+H^+$: 1166.39; found: 1166.38. λ_{max} (DMSO): 671 nm (logε=4.8). λ_{max} (em): n.d. ϕ_f: n.d.

NiPc (3.4c): The crude mixture was purified by column chromatography on silica gel with CH_3OH-CH_2Cl_2 (1:19) as the eluent to give **NiPc** in 11% yield. HPLC was performed under the B condition. t_R=37.27 min. MALDI-MS: Calcd $C_{57}H_{66}N_8NiO_{15}+H^+$: 1161.40; found: 1161.39. λ_{max} (THF): 671 nm (logε=5.1). λ_{max} (em) (THF): 678 nm. ϕ_f: 0.0038

H_2Pc (3.4d): The crude mixture was purified by running it through a LH-20 column with CH_3OH as an eluting solvent to give **H_2Pc** in 16% yield. Condition C was employed to perform

HPLC. t_R=5.39 min. Calcd $C_{57}H_{68}N_8O_{15}+H^+$: 1105.48; found: 1105.47. λ_{max} (DMSO): 646 nm (logε=3.4), 676 nm (logε=3.5), 706 nm (logε=3.4). λ_{max} (em) (DMSO): 709 nm. ϕ_f: 0.08

ZnPc (3.6a): 13% yield as a blue solid. Condition A was employed to perform HPLC. ESI: Calcd $C_{72}H_{96}N_8O_{24}Zn+2H$: 761.30; found: 761.30. λ_{max} (DMSO): 740 nm (logε=4.4). λ_{max} (em) (DMSO): 751 nm. ϕ_f: 0.12

ZnPc (3.7a): 8% yield as a blue solid. Condition A was employed to perform HPLC. t_R=34.17 min. MALDI-MS Calcd $C_{69}H_{66}N_8O_{15}Zn^+$: 1310.39; found: 1310.03. λ_{max} (DMSO): 695 nm (logε=4.9). λ_{max} (em) (DMSO): 702 nm. ϕ_f: 0.17

ZnPc (3.7b): 19% yield as a blue solid. Condition A was employed to perform HPLC. t_R=32.66, 33.54, 34.88, 37.31 min. MALDI-MS Calcd $C_{76}H_{72}N_8O_{16}Zn^+$: 1416.44; found: 1416.33. λ_{max} (DMSO): 698 nm (logε=5.4). λ_{max} (em) (DMSO): 705 nm. ϕ_f: 0.04

ZnPc (3.8a): 15% yield as a blue solid. Condition A was employed to perform HPLC. t_R=38.57 min. MALDI-MS Calcd $C_{102}H_{108}N_8O_{27}Zn^+$: 1943.41; found: 1943.40 λ_{max} (DMSO): 681 nm (logε=5.1). λ_{max} (em) (DMSO): 687 nm. ϕ_f: 0.13

ZnPc (3.8b): 17% yield as a blue solid. Condition A was employed to perform HPLC. t_R=44.35 min. MALDI-MS Calcd $C_{120}H_{128}N_8O_{32}Zn^+$: 2256.79; found: 2256.98. λ_{max} (DMSO): 681 nm (logε=5.2). λ_{max} (em) (DMSO): 685 nm. ϕ_f: 0.08

ZnPc (3.9a): 13% yield as a blue solid. Condition A was employed to perform HPLC. t_R=34.72 min. MALDI-MS Calcd $C_{57}H_{66}N_8O_{12}S_3Zn^+$: 1214.33; found: 1214.94. λ_{max} (DMSO): 690 nm (logε=5.5). λ_{max} (em) (DMSO): 698 nm. ϕ_f: 0.06

ZnPc (3.9b): 27% yield as a blue solid. Condition A was employed to perform HPLC. t_R=36.65 min. ESI Calcd $C_{60}H_{72}N_8O_{12}S_4Zn+H$: 1289.35; found: 1289.36. λ_{max} (DMSO): 692 nm (logε=5.3). λ_{max} (em) (DMSO): 695 nm. ϕ_f: 0.13

ZnPc (3.10a): 10% yield as a green solid. Condition A was employed to perform HPLC. t_R=33.85 min. ESI Calcd $C_{78}H_{108}N_8O_{21}S_6Zn^+$: 1751.53; found: 1751.01. λ_{max} (DMSO): 705 nm (logε=5.5). λ_{max} (em) (DMSO): 712 nm. ϕ_f: 0.10

ZnPc (3.10b): 10% yield as a green solid. Condition A was employed to perform HPLC. t_R=37.90 min. ESI Calcd $C_{88}H_{128}N_8O_{24}S_8Zn^+$: 2003.93; found: 2003.59 λ_{max} (DMSO): 709 nm (logε=5.5). λ_{max} (em) (DMSO): 716 nm. ϕ_f: 0.13

ZnPc (3.11a): 8% yield as a green solid. Condition A was employed to perform HPLC. MALDI-MS Calcd $C_{57}H_{66}N_8O_{12}S_3Zn^+$: 1214.33; found: 1214.73. λ_{max} (DMSO): 691 nm t_R=19.80 min., 22.83 min., 27.98min. (logε=5.0). λ_{max} (em) (DMSO): 699 nm. ϕ_f: 0.10

ZnPc (3.11b): 16% yield as a green solid. Condition A was employed to perform HPLC. t_R=33.53, 36.70 min. MALDI-MS Calcd $C_{60}H_{72}N_8O_{12}S_4Zn^+$: 1288.34; found: 1288.57. λ_{max} (DMSO): 713 nm (logε=5.2). λ_{max} (em) (DMSO): 718 nm. ϕ_f: 0.07

3.5 References

(1) Ng, A. C. H.; Li, X. Y.; Ng, D. K. P. Synthesis and photophysical properties of nonaggregated phthalocyanines bearing dendritic substituents *Macromolecules* **1999**, *32*, 5292-5298.

(2) Kobayashi, N.; Kondo, R.; Nakajima, S.; Osa, T. New Route to Unsymmetrical Phthalocyanine Analogs by the Use of Structurally Distorted Subphthalocyanines *J. Am. Chem. Soc.* **1990**, *112*, 9640-9641.

(3) Leznoff, C. C.; Hall, T. W. The Synthesis of a Soluble, Unsymmetrical Phthalocyanine on a Polymer Support *Tetrahedron Lett.* **1982**, *23*, 3023-3026.

(4) Hall, T. W.; Greenberg, S.; McArthur, C. R.; Khouw, B.; Leznoff, C. C. The Solid-Phase Synthesis of Unsymmetrical Phthalocyanines *New J. Chem.* **1982**, *6*, 653-658.

(5) Leznoff, C. C.; Svirskaya, P. I.; Khouw, B.; Cerny, R. L.; Seymour, P.; Lever, A. B. P. Syntheses of Monometallated and Unsymmetrically Substituted Binuclear Phthalocyanines and a Pentanuclear Phthalocyanine by Solution and Polymer Support Methods *J. Org. Chem.* **1991**, *56*, 82-90.

(6) Sastre, A.; delRey, B.; Torres, T. Synthesis of novel unsymmetrically substituted push-pull phthalocyanines *J. Org. Chem.* **1996**, *61*, 8591-8597.

(7) Sastre, A.; Torres, T.; Hanack, M. Synthesis of Novel Unsymmetrical Monoaminated Phthalocyanines *Tetrahedron Lett.* **1995**, *36*, 8501-8504.

(8) Weitemeyer, A.; Kliesch, H.; Wohrle, D. Unsymmetrically Substituted Phthalocyanine Derivatives Via a Modified Ring Enlargement Reaction of Unsubstituted Subphthalocyanine *J. Org. Chem.* **1995**, *60*, 4900-4904.

(9) Yang, Q. F.; Streb, K. K.; Borhan, B. Polymer-supported synthesis of mono-substituted porphyrins *Tetrahedron Lett.* **2005**, *46*, 6737-6740.

(10) Hanessian, S.; Xie, F. Polymer-bound p-alkoxybenzyl trichloracetimidates: Reagents for the protection of alcohols as benzyl ethers on solid-phase *Tetrahedron Lett.* **1998**, *39*, 733-736.

(11) Regen, S. L.; Lee, D. P. Influence of Solvent on Site Isolation in Polystyrene Resins *Macromolecules* **1977**, *10*, 1418-1419.

(12) Jayalekshmy, P.; Mazur, S. Pseudodilution, Solid-Phase Immobilization of Benzyne *J. Am. Chem. Soc.* **1976**, *98*, 6710-6711.

(13) Ogunsipe, A.; Chen, J. Y.; Nyokong, T. Photophysical and photochemical studies of zinc(II) phthalocyanine derivatives - effects of substituents and solvents *New J. Chem.* **2004**, *28*, 822-827.

(14) Montfortz, F. P. In The Porphyrin Handbook; Academic Press: New York, 1999; Vol. 19, Chapter 119, p.105-149.

(15) Lee, S. W.; White, A. J. P.; Williams, D. J.; Barrett, A. G. M.; Hoffman, B. M. Synthesis of near-IR absorbing/emitting porphyrazine derivatives with tunable solubility *J. Org. Chem.* **2001**, *66*, 461-465.

(16) Nyokong, T.; Isago, H. The renaissance in optical spectroscopy of phthalocyanines and other tetraazaporphyrins *J. Porphyr. Phthalocyanines* **2004**, *8*, 1083-1090.

(17) Guo, L. Q.; Ellis, D. E.; Hoffman, B. M.; Ishikawa, Y. Ligand substitution effect on electronic structure and optical properties of nickel porphyrazines *Inorg. Chem.* **1996**, *35*, 5304-5312.

(18) Kobayashi, N.; Ogata, H.; Nonaka, N.; Luk'yanets, E. A. Effect of peripheral substitution on the electronic absorption and fluorescence spectra of metal-free and zinc phthalocyanines *Chem.-Eur. J.* **2003**, *9*, 5123-5134.

(19) N. Kobayashi, H. K. In Phthalocyanines Properties and Applications; VCH: New York, 1996; Vol. 4, Chapter 9, p. 343-404.

(20) Kobayashi, N.; Konami, H. Molecular orbitals and electronic spectra of benzo-fused and related porphyrin analogues *J. Porphyr. Phthalocyanines* **2001**, *5*, 233-255.

(21) Kobayashi, N.; Sasaki, N.; Higashi, Y.; Osa, T. Regiospecific and Nonlinear Substituent Effects on the Electronic and Fluorescence-Spectra of Phthalocyanines *Inorg. Chem.* **1995**, *34*, 1636-&.

(22) Kobayashi, N.; Fukuda, T.; Ueno, K.; Ogino, H. Extremely non-planar phthalocyanines with saddle or helical conformation: Synthesis and structural characterizations *J. Am. Chem. Soc.* **2001**, *123*, 10740-10741.

(23) Nielsen, M.; Thomsen, A. H.; Clo, E.; Kirpekar, F.; Gothelf, K. V. Synthesis of linear and tripoidal oligo(phenylene ethynylene)-based building blocks for application in modular DNA-programmed assembly *J. Org. Chem.* **2004**, *69*, 2240-2250.

(24) Carrillo, R.; Martin, V. S.; Lopez, M.; Martin, T. Synthesis and cation complexation properties of new macrolides *Tetrahedron* **2005**, *61*, 8177-8191.

(25) Murakami, T.; Hirono, R.; Furusawa, K. Efficient stereocontrolled synthesis of sphingadienine derivatives *Tetrahedron* **2005**, *61*, 9233-9241.

(26) Nesterova, I. V.; Verdree, V. T.; Pakhomov, S.; Strickler, K. L.; Allen, M. W.; Hammer, R. P.; Soper, S. A. Metallo-phthalocyanine near-IR fluorophores: Oligonucleotide conjugates and their applications in PCR assays *Bioconjugate Chem.* **2007**, *18*, 2159-2168.

(27) Balashov, S. V.; Gardiner, R.; Park, S.; Perlin, D. S. Rapid, high-throughput, multiplex, real-time PCR for identification of mutations in the cyp51A gene of Aspergillus fumigatus that confer resistance to itraconazole *J. Clin. Microbiol.* **2005**, *43*, 214-222.

(28) J.R.Lakowicz In *Principles of Fluorescence Spectroscopy*; Kluwer Academic/Plenum Publisher: New York, Boston, Dordecht, London, Moscow, 1999, p 368-391.

(29) Strekowski, L.; Lipowska, M.; Gorecki, T.; Mason, J. C.; Patonay, G. Functionalization of near-infrared cyanine dyes *J. Heterocycl. Chem.* **1996**, *33*, 1685-1688.

(30) Soper, S. A.; Mattingly, Q. L.; Vegunta, P. Photon Burst Detection of Single near-Infrared Fluorescent Molecules *Anal. Chem.* **1993**, *65*, 740-747.

(31) Erdem, S. S.; Nesterova, I. V.; Soper, S. A.; Hammer, R. P. Solid-phase synthesis of asymmetrically substituted "AB_3-type" phthalocyanines *J. Org. Chem.* **2008**, *73*, 5003-5007.

(32) Drake, T. J.; Tan, W. H. Molecular beacon DNA probes and their bioanalytical applications *Appl. Spectrosc.* **2004**, *58*, 269A-280A.

(33) Dubertret, B.; Calame, M.; Libchaber, A. J. Single-mismatch detection using gold-quenched fluorescent oligonucleotides (vol 19, pg 365, 2001) *Nat. Biotechnol.* **2001**, *19*, 680-681.

(34) Sandhya, S.; Chen, W.; Mulchandani, A. Molecular beacons: A real-time polymerase chain reaction assay for detecting Escherichia coli from fresh produce and water *Anal. Chim. Acta* **2008**, *614*, 208-212.

(35) Papaparaskevas, J.; Houhoula, D. P.; Siatelis, A.; Tsakris, A. Molecular-beacon-based real-time PCR for detection and quantification of Mycobacterium tuberculosis DNA in clinical samples *J. Clin. Microbiol.* **2008**, *46*, 3177-3178.

(36) Wabuyele, M. B.; Farquar, H.; Stryjewski, W.; Hammer, R. P.; Soper, S. A.; Cheng, Y. W.; Barany, F. Approaching real-time molecular diagnostics: Single-pair fluorescence resonance energy transfer (spFRET) detection for the analysis of low abundant point mutations in K-ras oncogenes *J. Am. Chem. Soc.* **2003**, *125*, 6937-6945.

(37) Santangelo, P. J.; Nix, B.; Tsourkas, A.; Bao, G. Dual FRET molecular beacons for mRNA detection in living cells *Nucleic Acids Res.* **2004**, *32*.

(38) Massey, M.; Algar, W. R.; Krull, U. J. Fluorescence resonance energy transfer (FRET) for DNA biosensors: FRET pairs and Forster distances for various dye-DNA conjugates *Anal. Chim. Acta* **2006**, *568*, 181-189.

(39) Merrifield, R. B. Solid Phase Peptide Synthesis .1. Synthesis of a Tetrapeptide *J. Am. Chem. Soc.* **1963**, *85*, 2149-2154.

(40) Shi, R. R.; Wang, F.; Yan, B. Site-site isolation and site-site interaction - Two sides of the same coin *Int. J. Pept. Res. Ther.* **2007**, *13*, 213-219.

(41) Blackwell, H. E.; Clemons, P. A.; Schreiber, S. L. Exploiting site-site interactions on solid support to generate dimeric molecules *Org. Lett.* **2001**, *3*, 1185-1188.

(42) Fery-Forgues, S.; Lavabre, D. Are fluorescence quantum yields so tricky to measure? A demonstration using familiar stationery products *J. Chem. Educ.* **1999**, *76*, 1260-1264.

Chapter 4
Microwave-Assisted Solid-Phase Synthesis of AB_3 Type Asymmetrically Substituted Mono-Amine Functionalized Phthalocyanines and Oligonucleotide Labeling Techniques

4.1 Introduction

Solid-phase synthesis is a paramount method to obtain AB_3 type asymmetrically-substituted phthalocyanines (Pcs) in a short period of time with comparable yields to the statistical condensation method.[1] Covalent conjugation of mono-hydroxy functionalized Pcs to the biomolecules of interest typically requires additional steps to activate the hydroxy group. In addition, the modification of the Pcs can be problematic depending on the selected method as discussed in Chapter 3. In order to overcome this problem, we explored the alternative linkage strategies to synthesize amine functionalized Pcs.

Conventional synthesis of Pcs requires long reaction times (10-48 h) at elevated temperatures (100-150 °C) depending on the nature of the phthalonitrile derivatives and the metal template used.[2] As a result of harsh reaction conditions, increased number of side reactions cause low Pc yields. It is well-known that microwave irradiation can accelerate organic reactions and can greatly promote the reactions proceeding through a dipolar transition state via neutral reagents.[3] Microwave assisted synthesis of symmetrically-substituted metal free or metallo Pcs and related macrocycles in a variety of solvents and as well as under solvent free conditions have been reported in the literature.[4-6] Herein, microwave-assisted solid-phase synthesis of AB_3 type asymmetrically-substituted Pcs and conjugation strategies to biomolecules are presented.

With the aim of oligonucleotide labeling, designing of the Pcs are based on the following criteria: 1) In order to prevent formation of the side products in the latter step, conjugation of the Pcs to biomolecules, Pc should bear *only* one functional group; 2) to improve the solubility of the hydrophobic macrocycle, the Pc should be decorated with solubilizing peripheral or non-peripheral substituents; 3) to have an efficient energy transfer between the donor and the

acceptor molecules for FRET-RET based assays, maximum overlap between the absorption spectrum of the acceptor with emission spectrum of the donor is desired.

Retrosynthetic analysis of the mono functionalized Pc revealed that the synthesis would start with immobilization of the amine functionality and the phthalonitrile to the polymer support via a cleavable linker (Scheme 4.1). Cyclo-tetramerization of polymer bound phthalonitrile with the

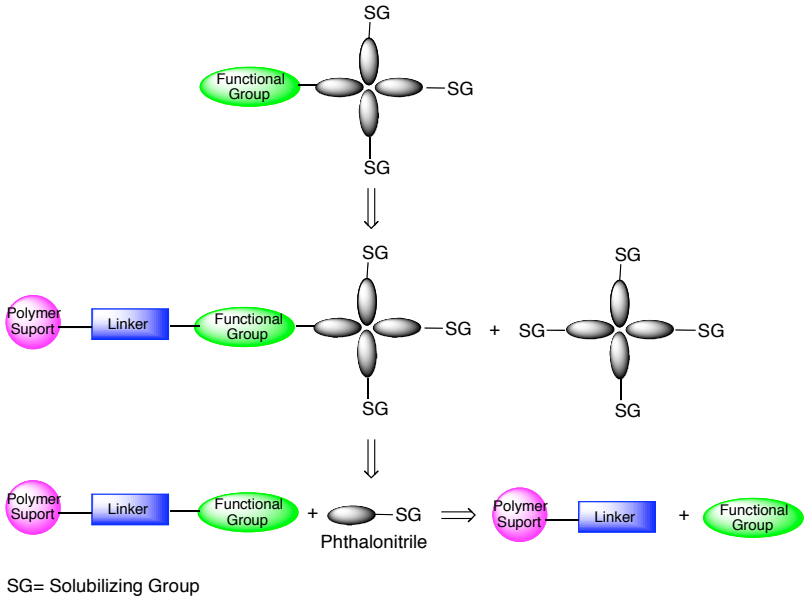

Scheme 4.1

second type of phthalonitrile in solution having solubilizing group would yield the target Pc on the polymer support and the symmetrically-substituted Pc in solution. Cleavage of the Pc from the polymer support would give the desired compound.

Due to the dynamic nature of the polymer, outcome of the solid-phase reactions are affected by many factors such as reaction time and the temperature, loading of the resin, linker length, availability of the nearby groups, reactivity of the functional groups, solvent and the concentration of the incoming reagent.[7] In order to obtain AB_3 type Pcs in high purity with improved yields, the cyclo-tetramerization reaction was optimized by tuning the solid-phase reaction parameters and evaluating the outcome of the each reaction in all cases.

4.2. Results and Discussion

4.2.1 Effects of the Loading of the Resin and the Reaction Time on the Outcome of the Cyclotetramerization Reaction

Polyethyleneglycol (PEG)-based Rink Amide ChemMatrix^{TM} resin with initial loading of 0.52 mmol/g was chosen as the starting point. Amine functionality could be obtained by either incorporation of the natural amino acids having an amine functional group on the side chain such as lysine or with modified amino acids bearing more than one functional group like tyrosine. Fmoc solid-phase peptide synthesis method[8] was utilized to immobilize the selected amino acids and the phthalonitrile to the polymer support (Scheme 4.2).

Solid-phase peptide synthesis is a practical method to synthesize different length of peptides in a short period of time without extensive purification process. In general, solid-phase peptide synthesis starts with deprotection of the temporary protecting group on the linker to obtain free amine where the peptide starts to grow. This step can be skipped depending on the selected linker type. The first amino acid, having temporary protecting group on the α amine and the permanent protecting group on the side chain amine, is anchored to the linker via amidation. Following the removal of the temporary protecting group, the next amino acid is coupled to amino terminus of the polymer bound amino acid. This cycle can be repeated until the desired sequence is built on the polymer support. Generally, acidic cleavage gives the desired peptide and removes all permanent acid labile protecting groups on the side chains of the residues. We modified the last step of the solid-phase peptide synthesis by anchoring the carboxylic acid functionalized phthalonitrile to the amino terminus of the amino acid on the polymer support. Phthalonitrile loaded resin is submitted to cyclotetramerization to give polymer bound Pc. Acidic cleavage of the product from the linker yields peptide-Pc conjugate.

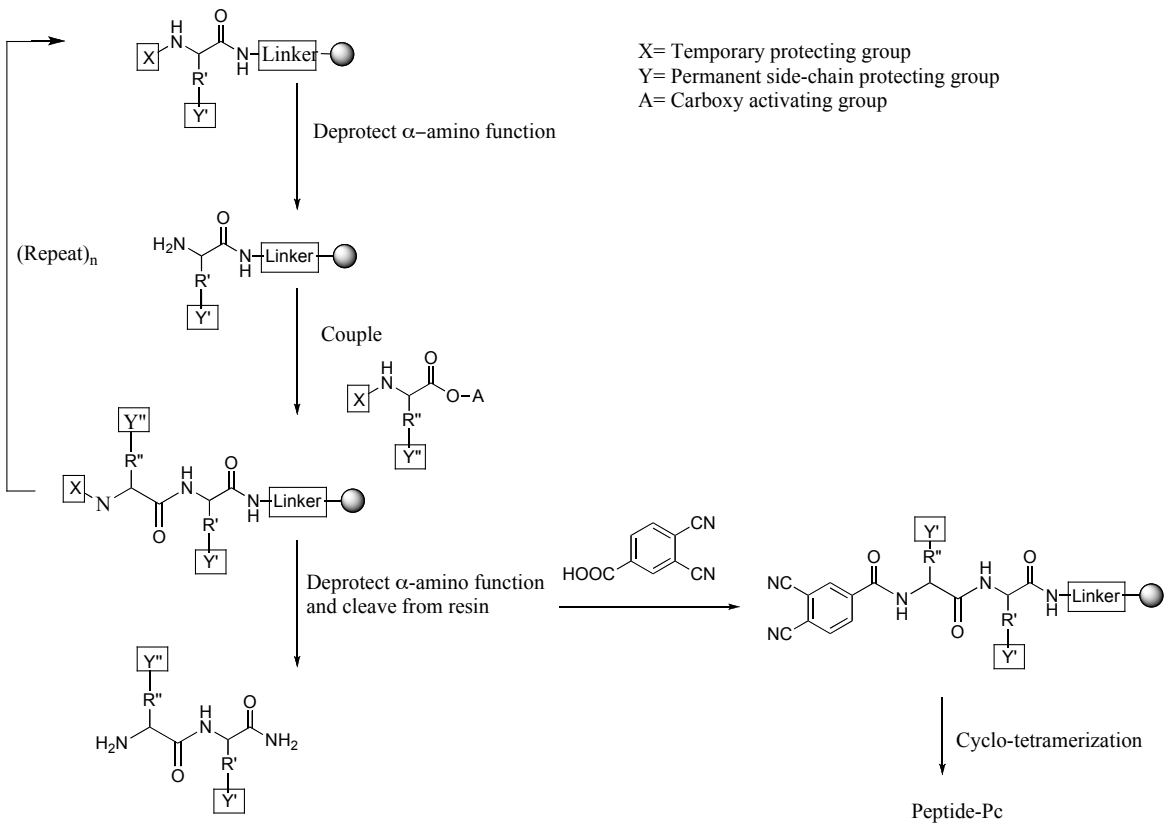

Scheme 4.2

Synthesis of the amine functional Pcs **4.4, 4.5** and **4.6** started with coupling of commercially available Fmoc-Lys-(Boc)-OH, having the base labile Fmoc protecting group on the α amine and the acid labile Boc protecting group on the ε–amine, which gives the Pc an amine functionality after the cleavage of the product from the polymer support (Scheme 4.3). Coupling efficiency of the Fmoc-Lys-(Boc)-OH was qualitatively followed by bromophenol blue test[8,9] and following the removal of the Fmoc group, commercially available Fmoc-8-amino-3,6-dioxaoctanoic acid (mini-PEG) was anchored to the α amine of the polymer bound Lys via amidation. Mini peg would not only serve as a spacer between the amine group and the Pc but also improve the solubility of the target compound. In order to examine the dependence of site-site interactions on the loading of the resin, which gives a rise to formation of the other Pc congeners on the polymer

support, immobilization of the carboxylate phthalonitrile **2.3** to the polymer support was performed at three different phthalonitrile concentrations. Consequently, the phthalonitrile loading of the each resin significantly differ from each other. Loading capacities of the polymer supports **4.3** were determined as 0.46, 0.23 and 0.1 mmol/g using quantitative Fmoc test[8] (Table 4.1). In each case, phthalonitrile coupling was confirmed by FT-IR spectrum showing CN

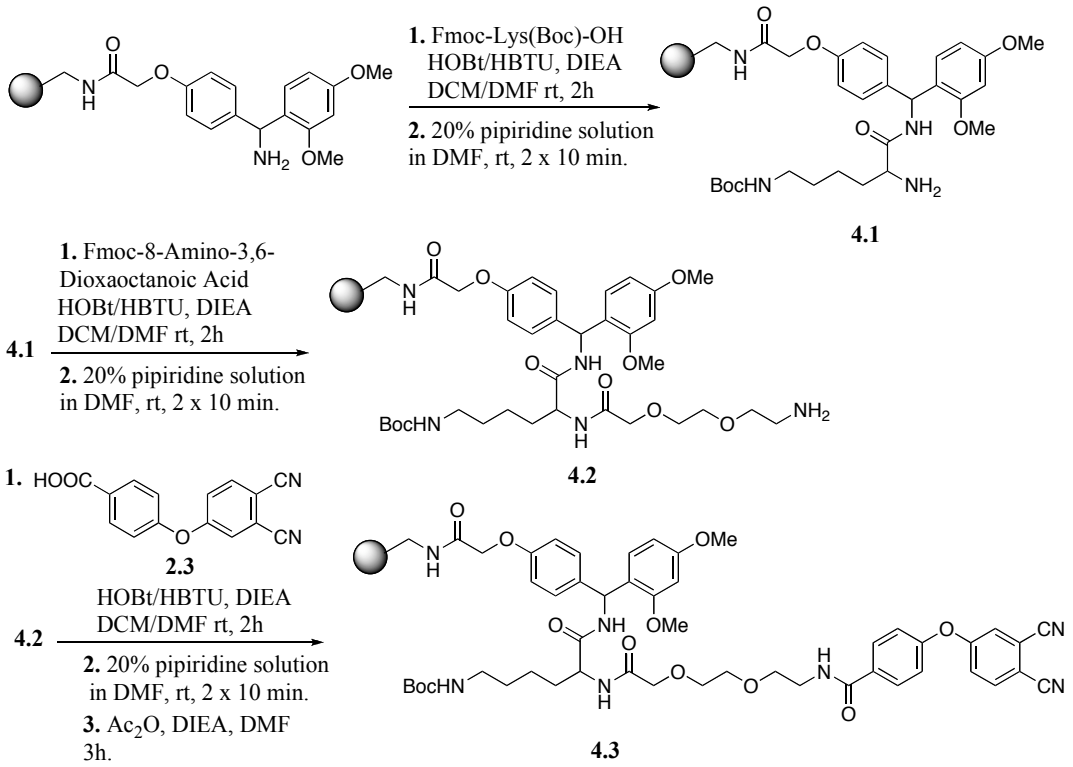

Scheme 4.3

stretching at 2232 cm^{-1}.The rest of the active sites on the polymer support were acetylated with excess amount of acetic anhydride to prevent premature reactions during the cyclotetramerization process.

Cyclotetramerization reactions were performed at the constant reaction concentration (0.16 M) employing one of the oligoethyleneglycol-substituted phthalonitrile precursors (**2.15**, **2.20** or **2.22)** at different reaction times under microwave irradiation as well as using conventional heating (Scheme 4.4) (Table 4.1). Following the condensation, the symmetrically-substituted

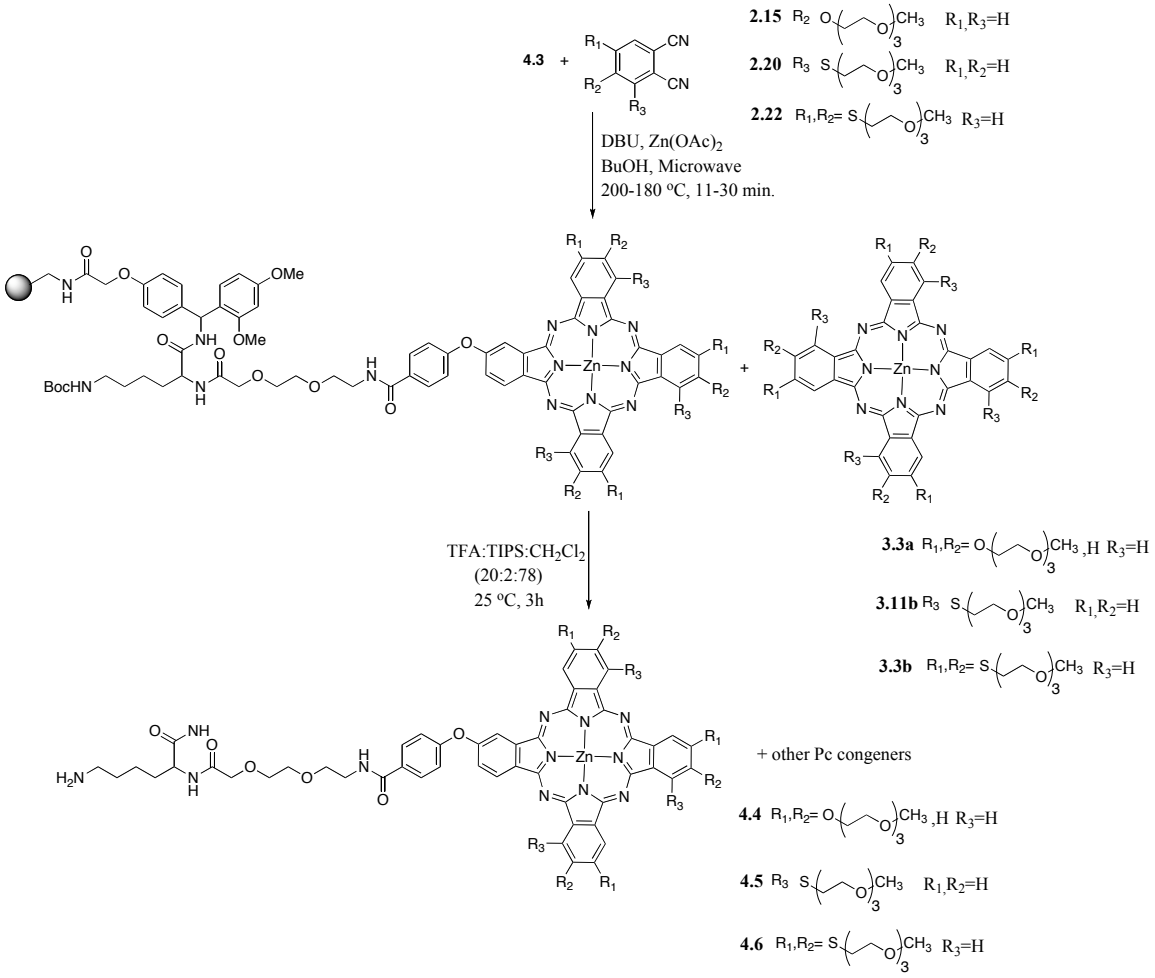

Scheme 4.4

Pcs were removed by washing the resin with hot BuOH until a colorless filtrate was collected. Polymer bound amides are typically cleaved in 88% TFA solution in CH_2Cl_2.[8] Since high acid concentration of TFA (>70%) results in decomposition of the Pc and removal of the metal from the Pc core, optimized standard cleavage solution, 20% TFA in CH_2Cl_2 in the presence of Triisopropylsilane as a scavenger, was used to cleave the asymmetrically-substituted Pcs from the polymer support. Following the filtration of the each crude product through LH-20 column to remove low molecular weight impurities, MALDI-MS analysis of the asymmetrically-oligoethyleneglycol-substituted Pcs revealed that the Pc **4.6** was contaminated with other Pc

congeners as result of high loading of the resin, 0.46 mmol/g (Table 4.1, entries 1-3). As the phthalonitrile loading decreased from 0.46 mmol/g to 0.23 mmol/g, A_3B type Pc was eliminated (Table 4.1, entries 4-7). However, complete site isolation could not be achieved even at the loadings as low as 0.1 mmol/g. Thus, formation of A_2B_2 type Pc could not be prevented (Table 4.1, entries 8-9).

Occurrence of site interactions as a result of high loading was published in the literature several times since the invention of the solid phase synthesis.[10-13] Yan and Sun clearly demonstrated the occurrence of site-site interactions via hydrogen bonding by using three different 1% DVB polystyrene resins, *p*-alkoxy benzyl (Wang resin), Hydroxymethyl and Trityl alcohol.[7] They also discussed the effects of steric hindrance on interactions of alcohols. In another paper, Grubbs and co-workers tested the activity of the titanocene catalyst in hydrogenation of organic compounds.[14] Authors reported that as the loading of the titanocene increased, the reaction rate was decreased indicating the reduced activity of the catalyst as a result of the interactions of the nearby sites. The rate of the reaction reached a maximum with lower loadings of the catalyst.

While neither the reaction time nor the temperature affected the outcome of the cyclotetramerization reaction, the yield of the recovered product was improved as the reaction time increased (Table 4.1, entries 1-3). At elevated reaction temperatures (>180 °C) we saw the decomposition of the PEG resin. Thus, later experiments were performed at 150 °C. Changing the amino acid sequence on the resin, Lys-mini-PEG-phthalonitrile vs. mini-PEG-Lys-phthalonitrile, did not affect the outcome of the reaction at or above 0.23 mmol/g of loading. Interestingly, MALDI-MS mass spectrometry analysis of the cleaved products showed another major ion at m/z M+100, corresponding to displacement of t-butyl group of the Boc protecting group with n-butyl (Table 4.1, entry 4). Further proof for this transition was obtained by

performing the reaction in different solvents such as n-pentanol and 2-butanol. In both cases, MALDI-MS mass spectrometry showed the corresponding peaks at m/z M+114 and M+99, respectively (Table 4.1, entries 5 and 6). Unlike Boc protecting group, the newly formed n-butyl,

Table 4.1 Effects of the Phthalonitrile Loading and the Reaction Time on Cyclotetramerization Reaction

	Squence on the Resin	Loading of the Resin (mmol/g)	Reaction Concentration (M) / Phthalonitrile Precursor Used	Reaction Condition	Solvent	Outcome of the Reaction / Crude Mixture Yield (%)
1	Lys(Boc)-mini-PEG-phthalonitrile	0.46	0.16 / **2.22**	Microwave, 11 min. 200 °C	BuOH	Mixture of all Pc congeners / 6 %
2	Lys(Boc)-mini-PEG-phthalonitrile	0.46	0.16 / **2.22**	Microwave, 18 min. 200 °C	BuOH	Mixture of all Pc congeners / 9 %
3	Lys(Boc)-mini-PEG-phthalonitrile	0.46	0.16 / **2.22**	Microwave, 30 min. 200 °C	BuOH	Mixture of all Pc congeners / 19 %
4	mini-PEG-Lys(Boc)-phthalonitrile	0.23	0.16 / **2.20**	Microwave, 30 min. 180 °C	BuOH	Mixture of AB_3, A_2B_2 and (M+100) / 20 %
5	mini-PEG-Lys(Boc)-phthalonitrile	0.23	0.16 / **2.20**	Microwave, 30 min. 180 °C	n-Pentanol	Mixture of AB_3, A_2B_2 and (M+114) / 20%
6	mini-PEG-Lys(Boc)-phthalonitrile	0.23	0.16 / **2.20**	Microwave, 30 min. 180 °C	2-Butanol	Mixture of AB_3, A_2B_2 and (M+99) / 8 %
7	mini-PEG-Lys(Boc)-phthalonitrile	0.23	0.16 / **2.15**	Microwave, 30 min. 180 °C	BuOH	Mixture of AB_3, A_2B_2 and (M+100) / 21 %

Table 4.1 Contd.

8	mini-PEG-Lys(Mtt)-phthalonitrile	0.10	0.16 / **2.20**	Microwave, 30 min. 150 °C	BuOH	Mixture of AB_3 and A_2B_2 / 18 %
9	Lys(Boc)-mini-PEG-phthalonitrile	0.10	0.16 / **2.20**	Conventional heating, 24h. 120°C	BuOH	Mixture of AB_3, A_2B_2 and (M+100) / 7 %

n-pentyl or 2-butyl carbamates could not be cleaved under acidic conditions due to the unstable carbocation formation. Mechanism of the transition has not been studied. However, we speculate that it is either transesterification taking place between the alcohol and the Boc group, or the amide nitrogen is deprotonated to give isocyanate derivative which is attacked by the nucleophile, solvent, to give the corresponding carbamates. Due to the inseparable mixtures obtained with Boc protected amine, we switched to another acid labile protecting group, Mtt (Table 4.1, entry 8). Mtt protecting group is easily cleaved under very mild acidic conditions (1-3% TFA).[15] Since the cleavage of the Pc from the polymer support requires more acidic condition (20% TFA), during the cleavage of the product, Mtt group is also removed. In view of the fact that it was nearly impossible to obtain pure AB_3 type Pcs by only altering the loading capacity of the resin, we explored other variables to achieve our goal.

4.2.2 Effects of Solvent and Incoming Reagent Concentration on the Outcome of the Cyclotetramerization Reaction

In order to evaluate the effect of the solvent and the incoming reagent concentration on the outcome of the cyclotetramerization reaction on solid support, resin **4.7** was prepared with three different phthalonitrile loadings. The cyclotetramerization reaction was carried at variable incoming reagent concentrations employing two different solvents under microwave irradiation.

Synthesis of phthalonitrile loaded resin **4.7** started with anchoring of mini-PEG to the Rink Amide resin, as the first amino acid, utilizing Fmoc solid phase synthesis as discussed above (Scheme 4.5). Following the removal of the Fmoc protecting group, commercially available Fmoc-Lys-(Mtt)-OH was coupled to the amino terminus of the mini-PEG residue. After removal of the temporary α amine protecting group, carboxylate phthalonitrile **2.3** was coupled to the amino terminus of the polymer bound Lys. The last step was carried at different phthalonitrile concentrations to give resin **4.7** with three different phthalonitrile loadings. Loading capacities of the polymer supports **4.7** were determined as 0.20, 0.14 and 0.10 mmol/g using quantitative Fmoc test[8] (Table 4.2). The rest of the active sites on the resin **4.7** were capped with excess amount of acetic anhydride.

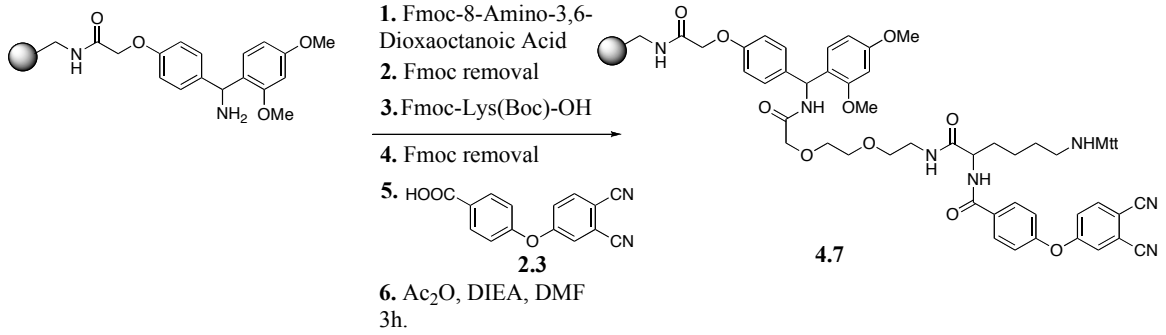

Scheme 4.5

Synthesis of oligoethyleneglycol-substituted Pcs **4.8** - **4.12** were performed under microwave irradiation employing resin bound phthalonitrile **4.7** and one of the oligoethylene glycol-substituted phthalonitriles **2.15**, **2.20** or **2.22** with DBU in the presence of metal salt as well as in metal free condition (Scheme 4.6). Initially, the effect of the incoming reagent concentration on the outcome of the cyclotetramerization reaction was evaluated. At high incoming reagent concentration, molecules in solution occupy most of the active sites and the remaining sites have difficulty to find the nearby reactive groups to react. As a result of this,

site-site interactions in solid support decrease. Cyclotetramerization reaction was performed at three different concentrations. Modified resin **4.7** with 0.20 mmol/g phthalonitrile loading was

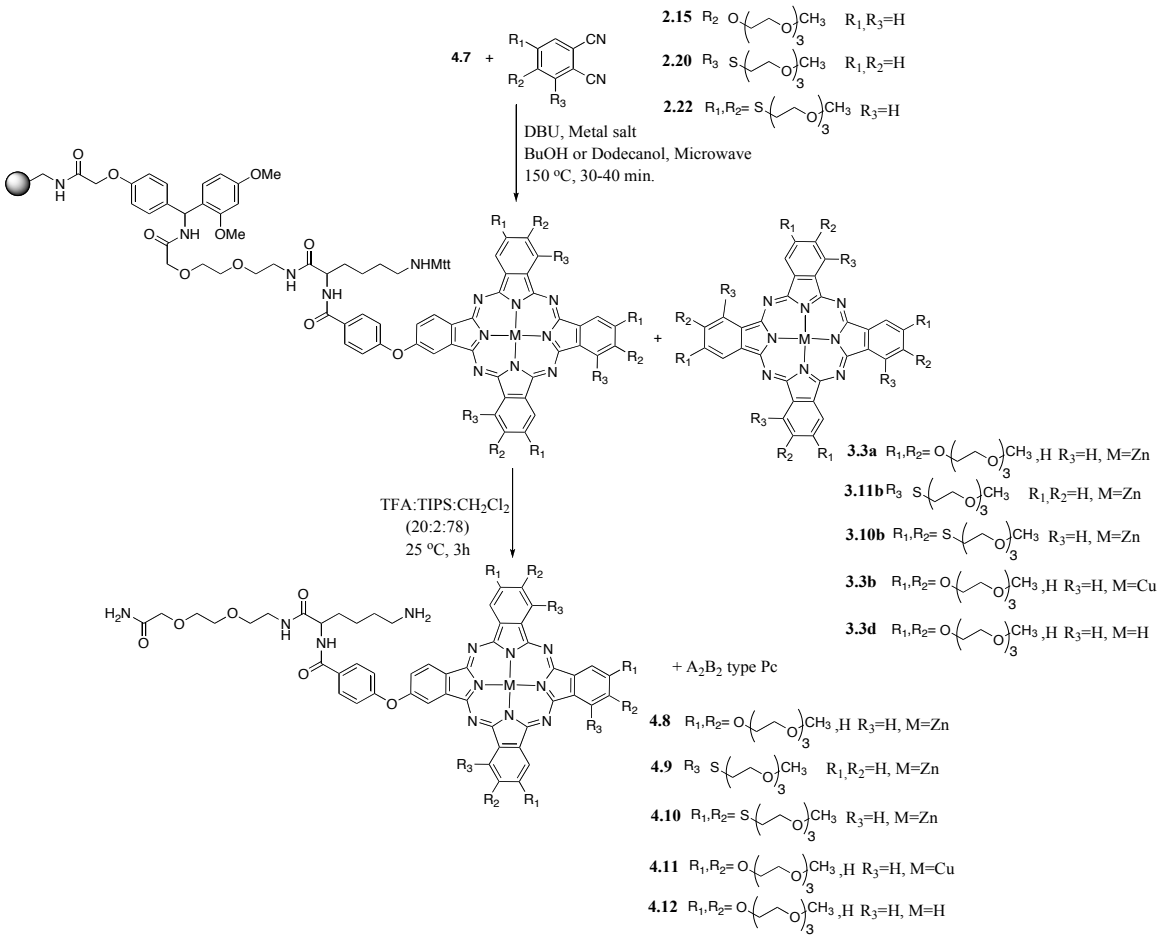

Scheme 4.6

condensed with ethyleneglycol-substituted thio-ether phthalonitrile **2.20** in BuOH at 0.16, 0.20 and 0.27 M concentrations under microwave irradiation for 30 min (Table 4.2, entries 1-3). Symmetrically substituted Pcs were washed away using hot BuOH until a colorless filtrate was collected and the desired products were cleaved from the resin under acidic condition. All asymmetrically-substituted desired Pcs were purified by filtering through LH-20 column. Mass spectrometry analysis of the recovered Pcs revealed that in all cases the desired Pc **4.9** was contaminated with up to 33% of A_2B_2 type congener (Table 4.2, entry 2). As the reaction

concentration increased from 0.16 M to 0.27 M, the percentage of the A_2B_2 type congener in the mixture slightly decreased (MALDI-MS) (Table 4.2, entry 3). However, complete site isolation could not be achieved under the applied conditions.

Solvent effect is another factor regulating site interactions in polymer support.[16] While "bad" solvents that do not swell the resin maximally decrease the site-site interactions by

Table 4.2 Effects of Incoming Reagent Concentration and Solvent on the Outcome of the Cyclotetramerization Reaction

	Squence on the Resin	Loading of the Resin (mmol/g)	Reaction Concentration (M) / Phthalonitrile Precursor Used	Reaction Condition	Solvent	Outcome of the Reaction / Crude Mixture Yield (%)
1	mini-PEG-Lys(Mtt)-phthalonitrile	0.20	0.16 / **2.20**	Microwave, 30 min. 150 °C	BuOH	AB_3:A_2B_2 (67:33) / 18 %
2	mini-PEG-Lys(Mtt)-phthalonitrile	0.20	0.20 / **2.20**	Microwave, 30 min. 150 °C	BuOH	AB_3:A_2B_2 (74:26) / 18 %
3	mini-PEG-Lys(Mtt)-phthalonitrile	0.20	0.27 / **2.20**	Microwave, 30 min. 150 °C	BuOH	AB_3:A_2B_2 (80:20) / 19 %
4	mini-PEG-Lys(Mtt)-phthalonitrile	0.20	0.20 / **2.20**	Microwave, 30 min. 150 °C	Dodecanol	AB_3:A_2B_2 (>95:<5) / 16 %

limiting the mobility of the active sites on the resin, "good" solvents, in which the resin is swelled maximally raise the chance for site-site interactions due to the increased mobility of the nearby sites on the polymer support. Dodecanol, having a high boiling point in which the resin swelling is minimum, was selected as the "bad" solvent to perform the cyclotetramerization reaction. The major disadvantage of dodecanol is that phthalonitrile precursors are not soluble in the solvent at room temperature. This problem was solved by heating the suspension up to 80 °C in water bath and transferring the solution into a microwave vessel.

Condensation of resin **4.7** with oligoethyleneglycol-substituted phthalonitrile **2.20** in dodecanol at 0.27M concentration gave the desired Pc **4.9,** accompanied with small amount (<5%) of A_2B_2 type Pc, in 16% yield (Table 4.2, entry 4). It was possible to decrease the amount of the side product (A_2B_2 type Pc) by only changing the solvent. However, it was not enough to completely overcome the site-site interactions at 0.20 mmol/g of phthalonitrile loading. It was also noted that changing the solvent from BuOH to dodecanol slightly decreased the yield. This can be explained by poor swelling of the resin in dodecanol. As the polymer support swells in a solvent, active sites on the resin expands and have a higher chance to react. In poor swelling solvents, most of the active sites are buried in the channels and polymer backbone's dynamic fluctuation is limited, consequently the limited number of them get involve in the reaction causing low yields.

Influence of the solvent on site isolation has been previously published in the literature starting from as early as 1970's. Regen and Lee studied the solvent effect by detecting the complex formation between poly(styry1-diphenylphosphine) and $Co(NO)(CO)_3$ through FT-IR analysis with highly (20%) and lightly (2%) cross-linked polystyrene resins.[17] They showed that in the presence of "good" solvent, CH_2Cl_2, only 35% of 1:1 cobalt complex formed. On the other hand, in the absence of solvent or by addition of "bad" solvent, n-hexadecane, 2:1 complex of cobalt was not detected indicating the achievement of complete site isolation. Regardless of the cross-linking degree of the polymer, they obtained similar results. Another example of the solvent effect was clearly demonstrated in Wulff and Schulze's paper.[18] The polymer support, having mercapto groups in random distribution, was prepared from p-vinylbenzyl thioacetate. Due to the increased mobility of the active sites in good swelling solvent, toluene, formation of disulfide bridges increased via oxidation of the nearby mercapto groups.

Employed phthalonitriles and metal salt also play an important role on the outcome of the cyclotetramerization reaction due to the difference of their reactivity. In order to have a better understanding about the solid-phase cyclotetramerization reaction, oligoethyleneglycol-substituted phthalonitriles with different substitution pattern, **2.15** and **2.22**, were employed in condensation reaction under the condition described in Table 4.2, entry 4. Unfortunately, in both

Table 4.3 Effect of Reactivity of Phthalonitrile on the Outcome of the Cyclotetramerization Reaction

	Squence on the Resin	Loading of the Resin (mmol/g)	Reaction Concentration (M) / Phthalonitrile Precursor Used	Reaction Condition	Solvent	Outcome of the Reaction / Crude Mixture Yield (%)
1	mini-PEG-Lys(Mtt)-phthalonitrile	0.20	0.20 / **2.15**	Microwave, 30 min. 150 °C	Dodecanol	AB_3:A_2B_2 (3:1) / 19 %
2	mini-PEG-Lys(Mtt)-phthalonitrile	0.20	0.20 / **2.22**	Microwave, 30 min. 150 °C	Dodecanol	AB_3:A_2B_2 (1:1) / 16 %

cases the desired Pcs, **4.8** and **4.10** were contaminated with the corresponding A_2B_2 type congeners up to 50% (Scheme 4.6) (Table 4.3, entries 1-2). Increased amount of the side product formation can be explained by low reactivity of the phthalonitrile used. Since 4,5 disubstituted phthalonitrile, **2.22**, has low reactivity, relative to 4-oligoethyleneglycol-substituted phthalonitrile (**2.15**), polymer bound phthalonitriles have longer time to find a proximate resin-bound phthalonitrile with which to react. Consequently, A_2B_2 type Pc forms on solid support.

Similar results were also obtained in the case of CuPc (**4.11**) and metal free Pcs (**4.12**). CuPc (**4.11**) were synthesized employing $CuBr_2$ as a metal source (Scheme 4.6). Due to the low solubility of $CuBr_2$ in dodecanol, the reaction was carried in a mixture of BuOH-dodecanol (2:8). Following the cyclotetramerization, blue colored symmetrically-substituted CuPc **3.3b** was washed away using wide variety of solvents. Unlike other metallo Pcs, due to the high adsorption of the

CuPc on solid support, isolation of the symmetrically-substituted CuPc required extensive wash with hot BuOH, CH_2Cl_2, CH_3OH and 1:1 mixture of CH_3OH-BuOH. Following the cleavage of the polymer bound Pc and filtration through LH-20 column; MALDI-MS mass spectrometry analysis of the CuPc revealed that the desired compound was contaminated with A_2B_2 type congener (Table 4.4, entry 1). In the case of metal free Pc (**4.12**), cyclotetramerization reaction was performed employing the same oligoethyleneglycol-substituted phthalonitrile **2.15** and DBU in the absence of a metal salt. Interestingly, after cyclotetramerization reaction, very light green-brown color solution and lime color beads were obtained indicating the extremely slow reaction. As a result of that, trace amount of symmetrically-substituted metal free Pc **3.3d** was recovered. Following the quick wash of the beads with hot BuOH, the acidic cleavage gave trace amount of the metal free Pc, **4.12**. Mass spectrometry analysis of the crude mixture showed that the metal free Pc **4.12** was contaminated with a significant amount of A_2B_2 type congener (Table 4.4, entry 2). The low yields and the contamination of the desired product not only related the loading capacity of the resin but also the particularly slow reaction in the absence of a metal template. Since the desired results could not be obtained by only changing the swelling property of the resin and/or employing different types of phthalonitrile precursor, loading capacity of the polymer support was lowered from 0.20 mmol/g to 0.14 mmol/g.

Condensation of polymer support **4.7**, with 0.14 mmol/g phthalonitrile loading, with **2.15** in the presence of $Zn(OAc)_2$ and DBU in dodecanol under microwave irradiation gave the symmetrically-

Table 4.4 Effect of the Metal Template on the Outcome of the Cyclotetramerization Reaction

	Squence on the Resin	Loading of the resin (mmol/g) / Pc	Reaction Concentration (M) / Phthalonitrile Precursor Used	Reaction Condition	Solvent	Outcome of the Reaction / Crude Mixture Yield (%)
1	mini-PEG-Lys(Mtt)-phthalonitrile	0.20 / CuPc	0.20 / **2.15**	Microwave, 30 min. 150 °C	Dodecanol	AB_3:A_2B_2 (2:1) / 25 %
2	mini-PEG-Lys(Mtt)-phthalonitrile	0.20 / H_2Pc	0.20 / **2.15**	Microwave, 40 min. 150 °C	Dodecanol	AB_3:A_2B_2 (2:1) / <1 %

substituted Pc **3.3a** in solution and the corresponding asymmetrically-substituted Pc on solid support (Scheme 4.6). After standard purification and cleavage processes, mono-amine functionalized Pc **4.8** was obtained as a mixture with A_2B_2 type congener (Table 4.5, entry 1). Since dropping the phthalonitrile loading on the resin from 0.2 mmol/g to 0.14 mmol/g did not make a significant difference on the outcome of the reaction, further experiments with the 0.15 mmol/g phthalonitrile loaded resin was skipped.

The exploration of the solid-phase synthesis of asymmetrically-substituted Pcs continued with the condensation of polymer support, having 0.10 mmol/g phthalonitrile loading, with oligoethylene glycol-substituted **2.15** in the presence of $Zn(OAc)_2$ as a metal source under microwave irradiation for 40 min (Scheme 4.6). The target ZnPc **4.8** was cleaved from the resin and purified by filtration through LH-20 column. Desired compound was obtained in 27% yield without contamination of any other Pc congeners (Table 4.5, entry 2). It was noted that 10 min. increase of the reaction time significantly improved the yield of the reaction. The same synthetic strategy was employed to synthesize the ZnPc **4.10**. However, the mass spectrometry analysis of the cleaved product showed that the ZnPc **4.10** was contaminated with significant amount of A_2B_2 type Pc (Table 4.5, entry 3).

Table 4.5 Effect of Loading, Reaction Time and Reactivity of the Phthalonitrile on the Outcome of the Cyclotetramerization Reaction

	Squence on the Resin	Loading of the Resin (mmol/g)	Reaction Concentration (M) / Phthalonitrile Precursor Used	Reaction Condition	Solvent	Outcome of the Reaction / Crude Mixture Yield (%)
1	mini-PEG-Lys(Mtt)-phthalonitrile	0.14	0.20 / **2.15**	Microwave, 30 min. 150 °C	Dodecanol	AB_3:A_2B_2 (3:1) / 17 %
2	mini-PEG-Lys(Mtt)-phthalonitrile	0.10	0.20 / **2.15**	Microwave, 40 min. 150 °C	Dodecanol	AB_3 / 27 %
3	mini-PEG-Lys(Mtt)-phthalonitrile	0.10	0.20 / **2.22**	Microwave, 40 min. 150 °C	Dodecanol	AB_3:A_2B_2 (2:1) / 22 %

From the results above, it can be concluded that at or above 0.1 mmol/g phthalonitrile loading outcome of the reaction subjected to change depending on the reactivity of the employed phthalonitrile precursor. Swelling property of the resin plays an irrelevant role due to the minor difference of the swelling of the resin in the selected solvents. Increase of the reaction time, from 30 min. to 40 min., remarkably improves the yield of the recovered Pcs. Since the results were not satisfying, optimization of the solid-phase cyclotetramerization reaction continued with the altering the linker length and the concentration of the incoming reagent.

4.2.3 Effects of Linker Length and Incoming Reagent's Concentration on the Outcome of the Cyclotetramerization Reaction

With aim of the synthesis of *pure* asymmetrically-substituted mono amine functionalized Pcs, the linker length was altered by excluding the mini-PEG from the sequence. Resin **4.14** was prepared employing the Fmoc solid-phase peptide synthesis method[8] as discussed before. Fmoc-Lys(Mtt)-OH was anchored as the first amino acid to the PEG based Rink Amide Resin (Scheme 4.7). Coupling efficiency of the Fmoc-Lys-(Mtt)-OH was qualitatively followed by Bromophenol blue test.[9] Fmoc protecting group was cleaved from the α amine of the Lys using 20% 4-methyl piperidine solution in DMF. In order to alter the phthalonitrile loading of the polymer support, coupling of carboxylate phthalonitrile **2.3** was performed using different amounts of the selected phthalonitrile. Polymer support **4.13** was split in two halves and the carboxylate phthalonitrile was coupled to each batch individually. Following the immobilization of the phthalonitrile to the resin, the remaining active sites were acetylated with acetic anhydride. Loading of the resin **4.14** was determined as 0.3 and 0.1 mmol/g using quantitative Fmoc analysis test.[8] The modified polymer supports were individually submitted to cyclotetramerization reaction.

Initially, polymer support **4.14** with 0.30 mmol/g phthalonitrile loading was employed for the synthesis of ZnPc **4.15**. Condensation of polymer bound phthalonitrile **4.14** with

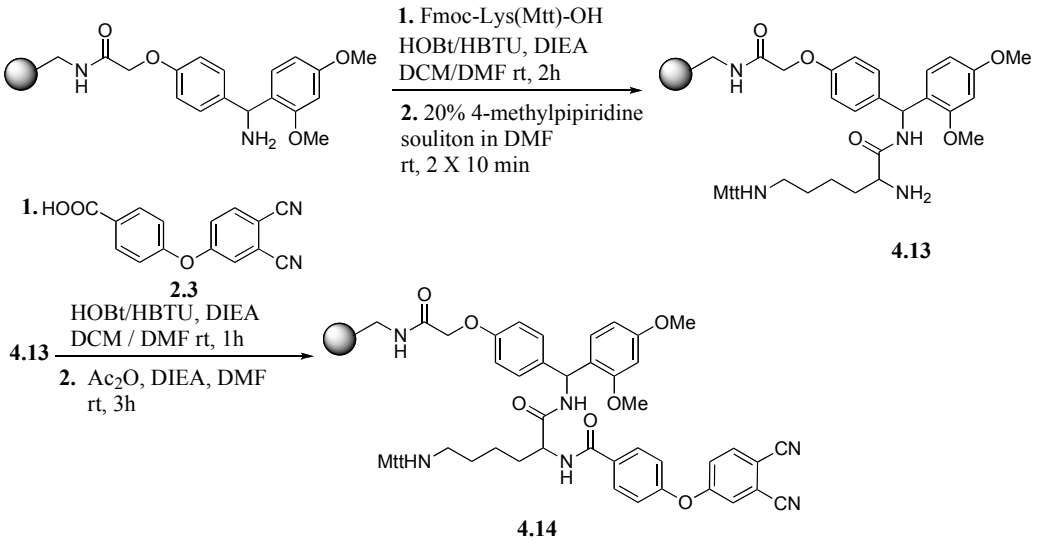

Scheme 4.7

oligoethyleneglycol -substituted phthalonitrile **2.15** in the presence of $Zn(OAc)_2$ was carried under microwave irradiation at 0.20 M concentration for 40 min (Scheme 4.8). Following the standard washing procedure to isolate the symmetrically-substituted ZnPc **3.3a**, the target compound was cleaved from the polymer support under the acidic condition. Mass spectrometry analysis of the recovered ZnPc **4.15** showed that the desired compound was obtained as a 1:1 mixture with A_2B_2 type congener (Table 4.6, entry 1). From the results above it can be concluded that the loading of the resin is the key factor of the solid-phase synthesis of the Pcs. As the loading of the resin increase, regardless of the linker length, site-site interactions occur due to the highly dynamic nature of the polymer.

Yan and Sun demonstrated the influence of the solid-phase reactions on the linker length and incoming reagent concentration via diester formation using various linker length.[7] From the results obtained by interpretation of the FT-IR spectra of the polymer supports, they concluded that the linker length plays a marginal role on regulating the site-site interactions on the resin. Further more, they stated that the linker length effect can be diminished by using large excess of incoming reagent.

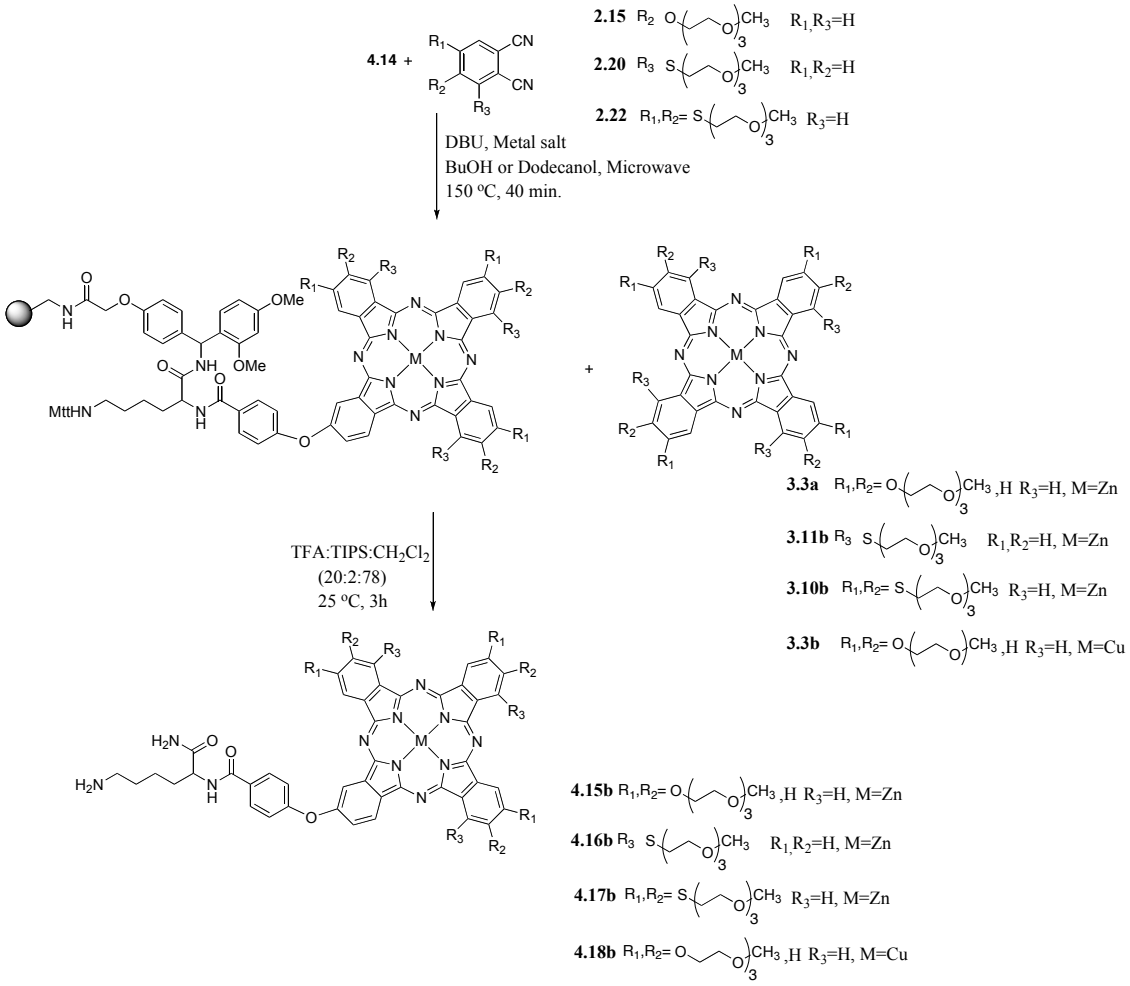

Scheme 4.8

In order to examine the effect of linker length at low loading of resin, synthesis of **4.15** was performed using the polymer support **4.14** with 0.10 mmol/g phthalonitrile loading. The reaction was performed at 0.30 M concentration in Dodecanol (Scheme 4.8). Mass spectrometry analysis of the cleaved product showed that the desired ZnPc was contaminated with a trace amount of A_2B_2 type congener (Table 4.6, entry 2).

The next reaction was performed using the same resin **4.14** (0.1 mmol/g) and the phthalonitrile precursor (**2.15**) at different concentration, 0.8M (Table 4.6, entry 3). Symmetrically-substituted Pc was washed away with hot BuOH until a colorless filtrate was

Table 4.6 Effect of Linker Length and Incoming Reagent Concentration on the Outcome of the Cyclotetramerization Reaction

	Squence on the Resin	Loading of the Resin (mmol/g)	Reaction Concentration (M) / Phthalonitrile Precursor Used	Reaction Condition	Solvent	Outcome of the Reaction / Crude Mixture Yield (%)
1	Lys(Mtt)-phthalonitrile	0.30	0.20 / **2.15**	Microwave, 40 min. 150 °C	Dodecanol	AB_3:A_2B_2 (1:1) / 18 %
2	Lys(Mtt)-phthalonitrile	0.10	0.30 / **2.15**	Microwave, 40 min. 150 °C	Dodecanol	AB_3:A_2B_2 (97:3)/ 22 %
3	Lys(Mtt)-phthalonitrile	0.10	0.80 / **2.15**	Microwave, 40 min. 150 °C	Dodecanol	AB_3[7] / 24 %
4	**Lys(Mtt)-phthalonitrile**	**0.10**	**0.80 / 2.15**	**Microwave, 40 min. 150 °C**	**BuOH**	**AB_3[7] / 28 %**

collected and the polymer bound ZnPc was cleaved from the resin. The crude mixture was filtered through a LH-20 column and the collected blue band was submitted to mass spectrometry analysis. MALDI-MS analysis showed a major ion peak corresponding to the desired Pc. ZnPc **4.15** was obtained in 24% yield without contamination of the other Pc congeners (Table 4.6, entry 3). With the purpose of examining the solvent effect under the selected conditions, the same reaction was performed in another solvent, BuOH. The desired compound was obtained as a single congener. As expected, the yield of the reaction was improved to 28% by only changing the solvent (Table 4.6, entry 4). Thus, later experiments were performed in BuOH by employing the conditions showed in Table 4, entry 4. Increase of the yield is due to the slightly better swelling property of the resin in BuOH. Figure 4.1 shows

[7] A_2B_2 type congener was not detected

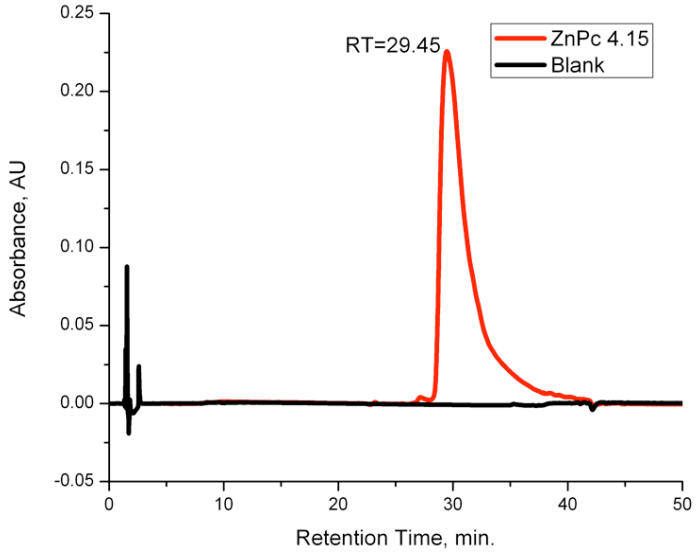

Figure 4.1 HPLC chromatogram of ZnPc **4.15**.

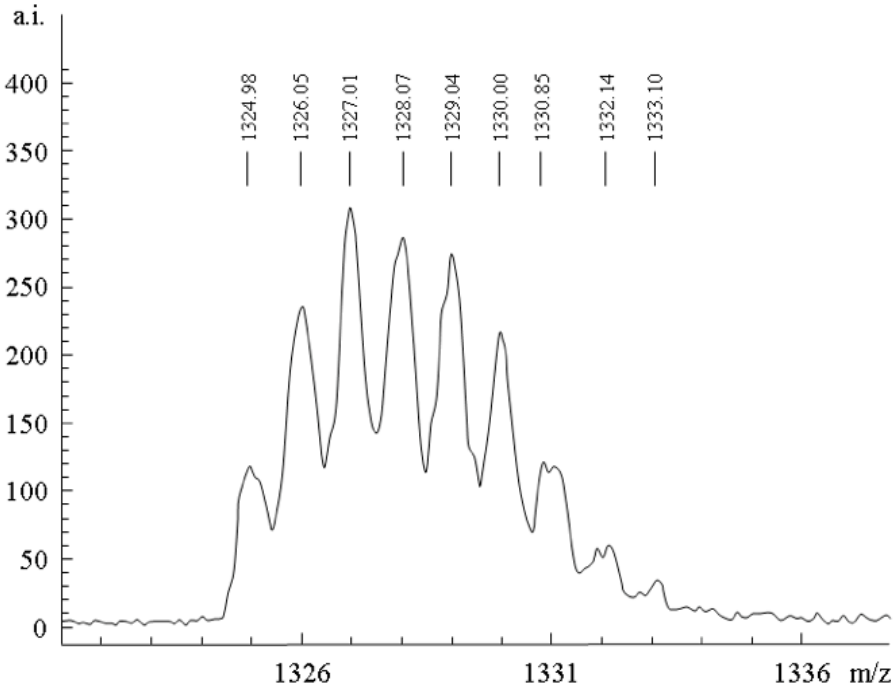

Figure 4.2 MALDI-MS Spectrum of ZnPc **4.15**

HPLC chromatogram and Figure 4.2 shows the MALDI-MS spectrum of the ZnPc **4.15** with expected isotopic pattern. ZnPc **4.15** showed sharp Q band at 681 nm and emission band at 691 nm upon excitation at 615 nm (Table 4.7).

The same synthetic strategy was employed to synthesize mono amine functionalized Pcs **4.16**, **4.17** and **4.18**. In the case of **4.16**, phthalonitrile, substituted with oligoethyleneglycol via sulfur linkage, **2.20** was condensed with polymer bound phthalonitrile **4.14** in the presence of $Zn(OAc)_2$ and DBU in BuOH. Following the standard purification method, ZnPc **4.16b** was obtained in 19% yield (Table 4.7).

The last Zn hosting Pc **4.17b** was synthesized using 4,5 bis-Oligoethyleneglycol-substituted phthalonitrile **2.22**. Condensation of resin **4.14** with **2.22** gave the desired Pc in 15% (Table 4.7). The low yield of the desired Pc, relative to **4.15,** is associated with the low reactivity of the employed phthalonitrile in cyclotetramerization reaction.

In the case of CuPc **4.18**, $CuBr_2$ was used as a metal source in the condensation of the polymer support **4.14** with **2.15**. Due to the high adsorption of the symmetrically-substituted CuPc on solid support, it was necessary to wash the polymer support with wide variety of hot solvents until a colorless filtrate was collected. Following the cyclotetramerization reaction, the

Table 4.7 Mono-amine Functionalized Pcs

	Compound Number / Pc	Metal Salt	Yield (%)[8]	λ_{max} (abs) (nm)	log ε ($cm^{-1}M^{-1}$)	λ_{max} (em) (nm)	ϕ_f[9]
AB_3 Type Pcs	**4.8** / ZnPc	$Zn(OAc)_2$	27	680	5.1	690	0.10
	4.15 / ZnPc	$Zn(OAc)_2$	28	681	5.0	691	0.10
	4.16 / ZnPc	$Zn(OAc)_2$	19	701	5.1	708	0.09
	4.17 / ZnPc	$Zn(OAc)_2$	15	701	5.2	709	0.11
	4.18 / CuPc	$CuBr_2$	24	680	4.3	n.d	n.d

[8] Yields of asymmetrically-substituted Pcs (**4.15**-**4.18**) were calculated based on the loading of the phthalonitrile on the support, 0.1 mmol/g and **4.8** was calculated based on 0.3 mmol/g.

[9] Fluorescence spectra and quantum yield determinations were done using 613 nm excitation wavelength for **4.15** and **4.8**, 630 nm for **4.16** and **4.17**. CuPc **4.18b** did not show any detectable fluorescence, which is noted in the table as "n.d.". All spectra were taken in DMSO. Fluorescence quantum yield measurements for all Pcs were done using methylene blue as a standard at absorbance 0.04 - 0.05 for both Pc and standard solutions to avoid any error due to inner-filter effect.

polymer support was washed with hot solvents including BuOH, CH_3OH, CH_2Cl_2, CH_3OH-BuOH mixture to completely isolate the symmetrically-substituted Pc. Following the cleavage and simple purification process, CuPc **4.18** was obtained in 24% yield (Table 4.7).

4.2.4 Covalent Labeling of Oligonucleotides with Amine Functionalized Phthalocyanines

The successful syntheses of the amine functionalized oligoethyleneglycol-substituted AB_3 type Pcs was followed by the covalent labeling of oligonucleotides for FRET-RET based applications.

Oligonucleotide is a small fragment of DNA or RNA consisting of 10-100 nucleic acids (adenine, cytosine, guanine, thymine / uracil). Due to the weak fluorescence intensity of the oligonucleotides for bioanalytical applications, it is necessary to label them with fluorescent molecules for fluorescence-based applications. Labeling of the oligonucleotides is accomplished by non-covalent or covalent labeling techniques. Non-covalent labeling composed of hydrophobic and electrostatic interactions between the fluorescent molecule, intercalating dye, and the oligonucleotide.[19,20] Commonly used intercalating dyes are ethidium bromide, thiazole orange, oxazole yellow and their homodimers.[21]

Covalent labeling of the oligonucleotides is achieved by employing pre-synthetic or post synthetic methods. In pre-synthtetic method, the fluorescence dye is covalently conjugated to oligonucleotide's 3'or 5' ends and as well as any desired internal position utilizing phosphoramidite chemistry during the oligonucleotide synthesis. Several labeling techniques at different regions of the oligonucleotide including phosphate backbone,[22] sugar[23] and base residue[24] (purine or pyrimidine) labeling have been published in the literature. Post-synthetic labeling is the covalent attachment of the fluorescent dye to the oligonucleotide after the synthesis of the probe.[25-27] Thus, this technique requires modification of oligonucleotides with the desired functional groups at the 3' and/or 5' ends. The major disadvantage of the post labeling is that oligonucleotides can easily be hydrolyzed at low pH values or at elevated

temperatures. Also, their limited solubility in organic solvents restricts the post synthetic applications or requires extra steps for modification of the fluorescent labeling dyes.

Conjugation of amine functionalized Pcs to oligonucleotides was achieved by employing the post synthetic methods. 13mer oligonucleotide, modified with C_{10} carboxylic acid linker at the 5' end, was used for the labeling experiment. The sequence of the oligonucleotide is given below.

5'(Carboxylic acid C10)-GTA AAA CGA CGG CCA GT 3'

Prior the labeling, oligonucleotide was purified by ethanol precipitation to remove any amine containing compounds. Amine functional ZnPc **4.15** was covalently attached to the oligonucleotide via C_{10} carboxylic acid linker by amide formation (Scheme 4.9). The labeling was performed in microwave at 75 °C for 30 min. in the presence of large excess of coupling reagents, EDC and NHS, in pH 7.6 carbonate buffer. The conjugate was separated from large excess of the dye by ethanol precipitation and the labeled oligonucleotide (**4.19**) was isolated by

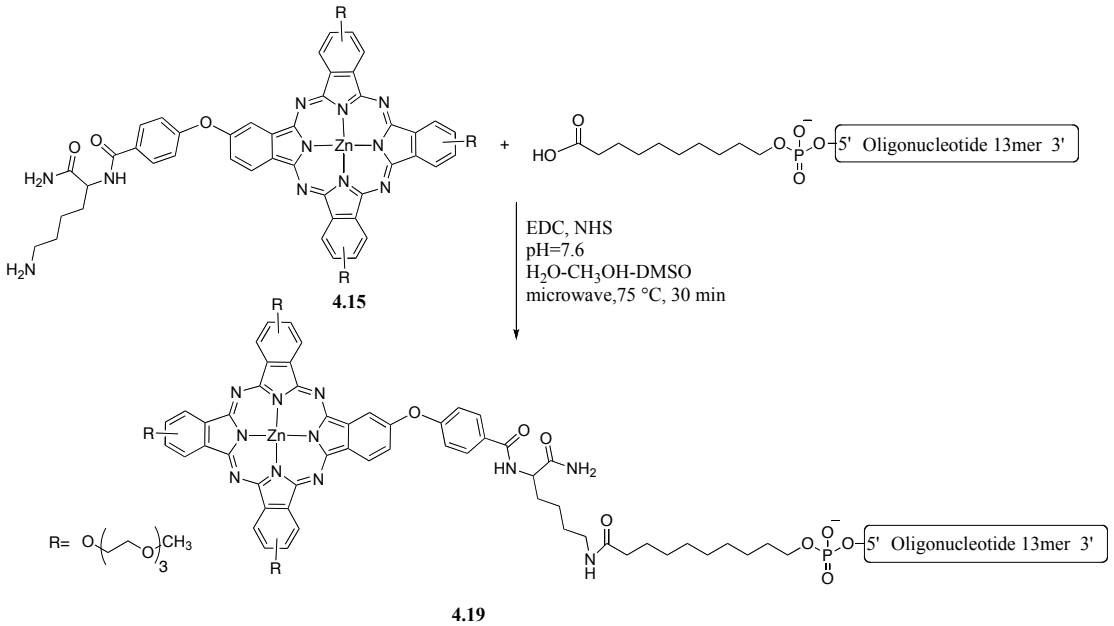

Scheme 4.9

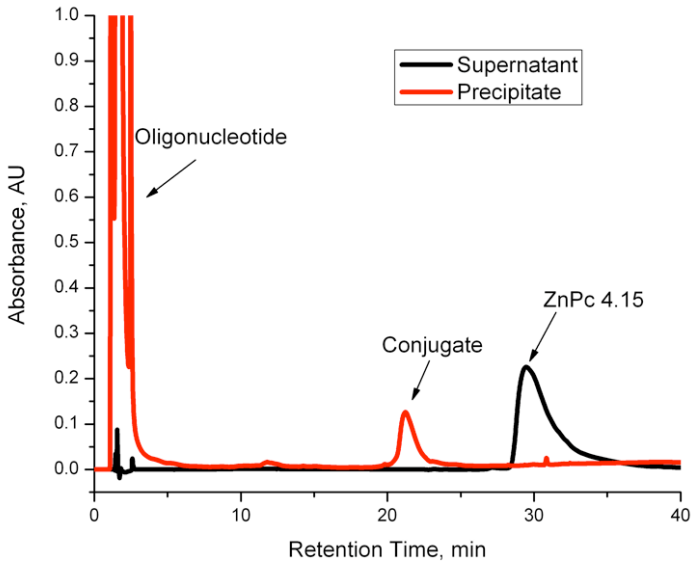

Figure 4.3 Supernatant's data was extracted at 680 nm and the precipitate's data was extracted at 260 nm wavelength.

reverse-phase HPLC. Figure 4.3 shows the HPLC chromatograms of the supernatant and the precipitate after the ethanol precipitation. In order to verify that non-covalent labeling does not occur between the oligonucleotide and the selected ZnPc and to confirm that the dye is stable

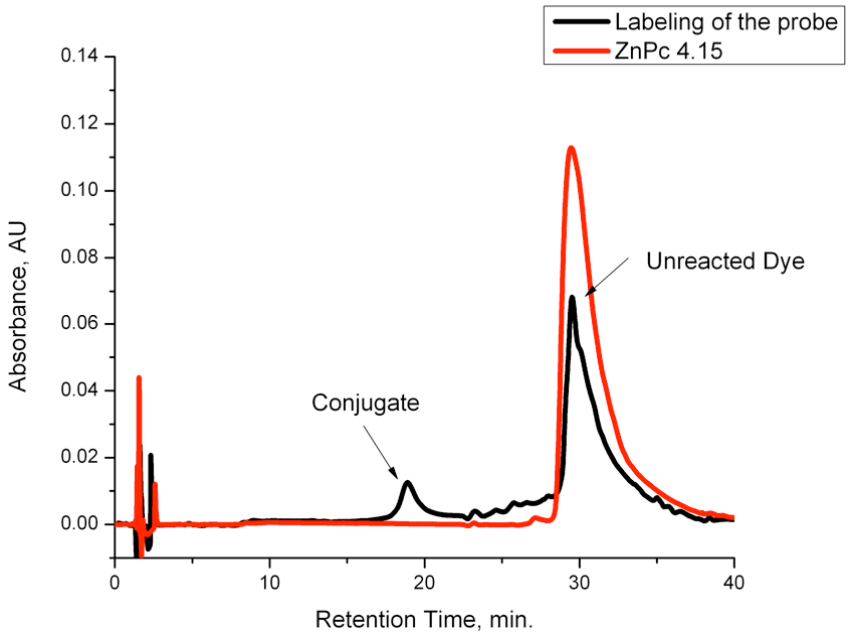

Figure 4.4 HPLC analysis of oligonucleotide labeling with ZnPc **4.15.** The data were extracted at 680 nm wavelength.

under the selected reaction conditions control experiments were also performed in the presence and absence of the oligonucleotide employing the same conditions. HPLC chromatograms of the labeling experiment were shown in Figure 4.4. The control experiments did not show any evidence neither for the non-covalent interaction between the dye and the oligonucleotide nor the decomposition of the dye under the reaction condition.

Labeling of the oligonucleotides was continued with a 13mer oligonucleotide modified with 4-formyl N-Hexylbenzamide via C6 linker at the 5' end. Sequence of the oligonucleotide is given below.

5'(Aldehyde C6)-GTA AAA CGA CGG CCA GT 3'

ZnPc **4.15** was conjugated to oligonucleotide via reductive amination[28,29] in the presence of large excess of $NaCNBH_3$ as reducing reagent in pH 5.5 NaOAc buffer (Scheme 4.10). The reaction

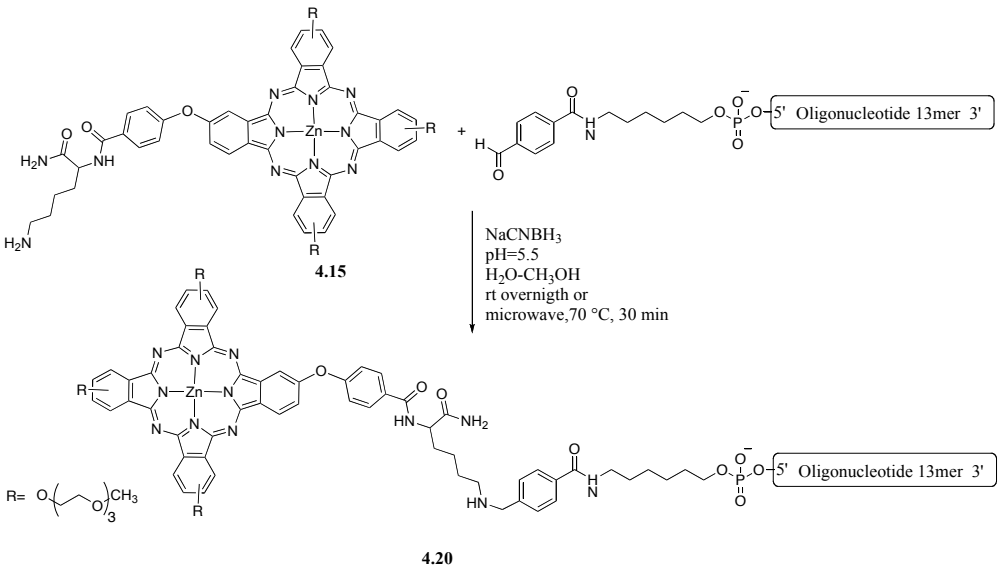

Scheme 4.10

was incubated in microwave at 70 °C as well as at room temperature overnight. After the labeling processes, the conjugates were precipitated in ethanol and further purified by reverse-phase HPLC (Figure 4.5). Control experiments were performed under the same condition as the

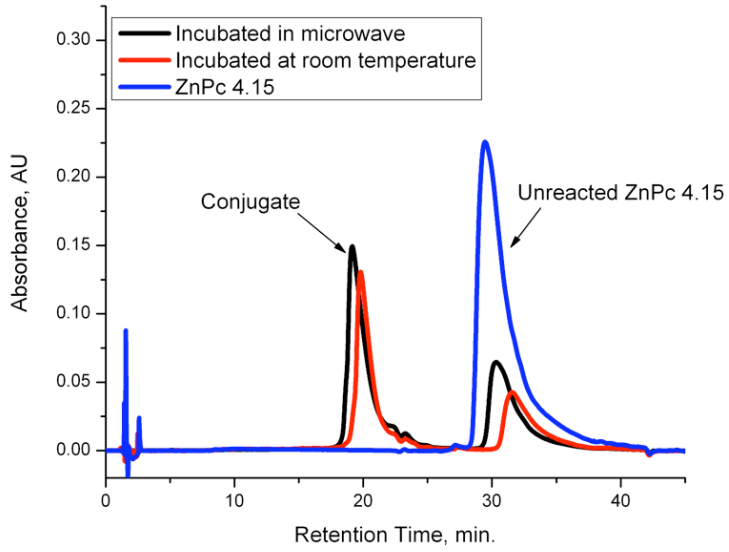

Figure 4.5 Labeling of the oligonucleotide via reductive amination. The data were extracted at 680 nm wavelength.

labeling reactions were done. Analysis of the HPLC chromatograms of the control experiments revealed that there was not any non-covalent interaction between the Pc and the oligonucleotide. Also, the ZnPc **4.15** was stable in the presence of a reducing reagent under the reaction conditions. While microwave irradiation did not significantly affect the labeling efficiency of the oligonucleotide, it reduced the reaction time from hours to minutes.

Conjugation of Pcs to biomolecules continued with a double labeling of a oligonucleotide on both the 3' and 5' ends. Since their report in 1996,[30] doubly-dye-labeled oligonucleotide ($(Pc)_2$-DNA), referred to as molecular beacons, are widely used in various bioanalytical applications including detection of interactions of nucleic acids with proteins,[31] PCR monitoring[32,33] and nucleic acid analysis.[34]

For this study, the designed $(Pc)_2$-DNA had a stem containing 5 bases, and the loop consisting of 19 nucleotide bases. Both the 5' and 3'ends of the probe were modified with 4-formyl N-hexylbenzamide via C6 linker (Figure 4.6). In order to utilize self-quenching ability of

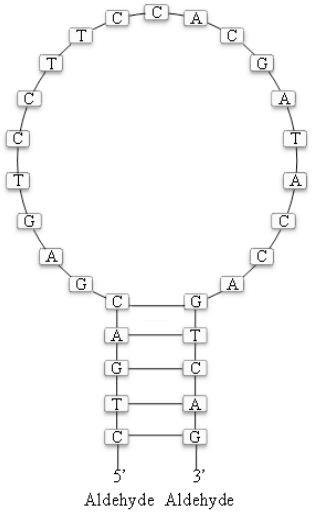

Figure 4.6 Squence of the doubly-labeled oligonucleotide used in the labeling experiment.

the Pcs due to the high degree of aggregation, both ends of the probe were labeled with the ZnPc **4.15** instead of two different dyes serving as a quencher and a donor. The ZnPc **4.15** was conjugated to both the 3' and 5' ends of the doubly-labeled oligonucleotide, using twice as much dye relative to labeling of **4.20**, via reductive amination in the presence of large excess of the dye and $NaCNBH_3$ in pH 5.5 NaOAc buffer (Scheme 4.11). The labeling and the control reactions

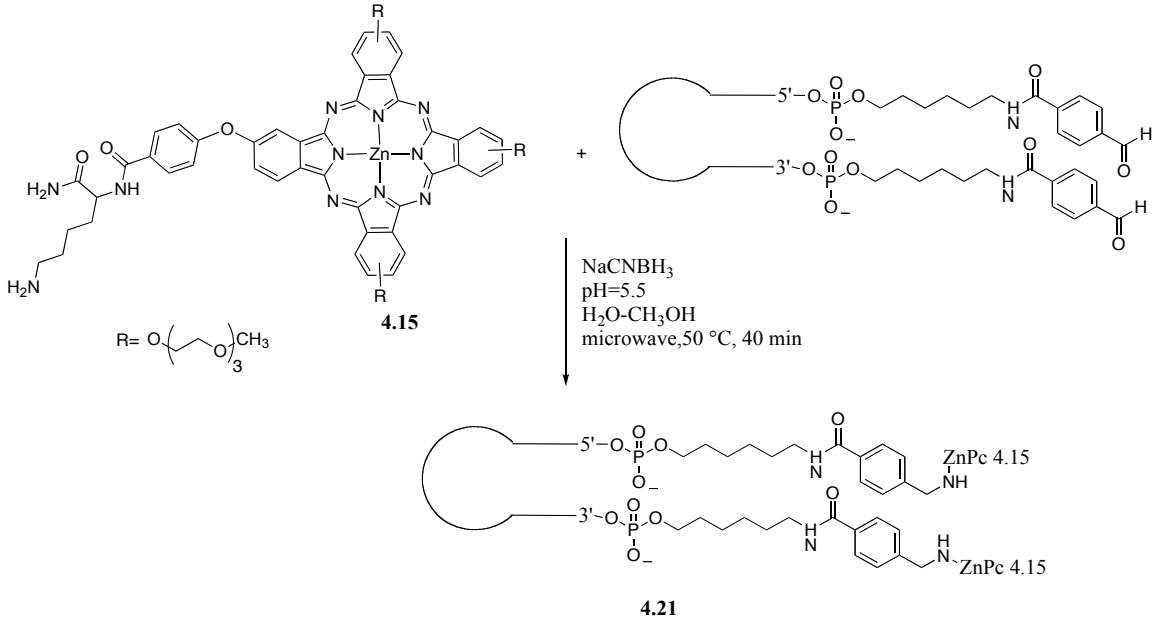

Scheme 4.11

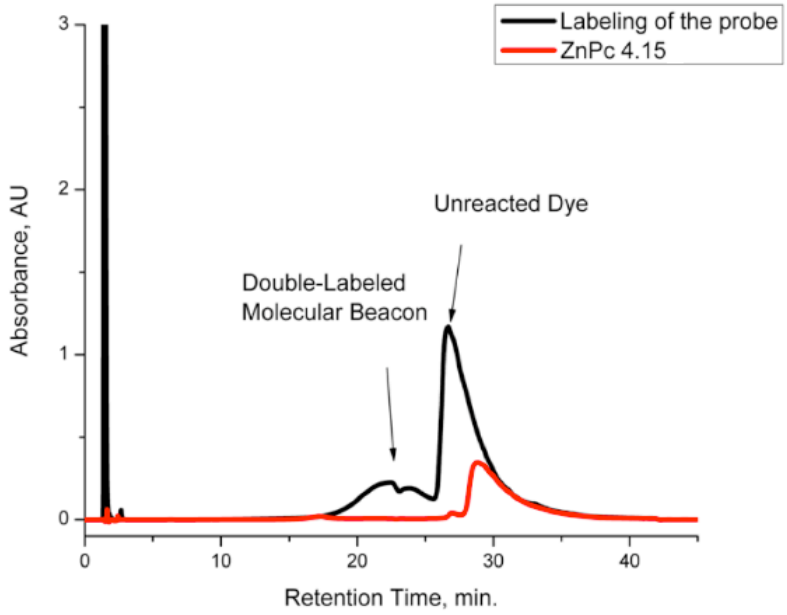

Figure 4.7 HPLC chromatograms of the ZnPc **4.15** and the doubly-labeled oligonucleotide. The data of the ZnPc **4.15** was extracted at 680 nm and the conjugation reaction's data was extracted at 260 nm.

were performed in microwave at 50 °C for 40 min (Scheme 4.11). Ethanol precipitation of the conjugate was followed by isolation of the labeled molecular beacon by reverse phase HPLC (Figure 4.7).

4.2.5 Solid-Phase Synthesis of Phthalocyanine-Peptide Conjugate

Further investigation of conjugation of the Pcs to biomolecules continued by preparing a Pc-peptide conjugate on the solid support. In collaboration with Margaret W. Ndinguri, the conjugate was prepared using solid-phase Pc and peptide syntheses. ZnPc **4.15** was synthesized in microwave with a minor change in the preparation of the polymer support **4.14**. Limited amount of Lys was coupled to the resin to give 0.1 mmol/g of loading. The rest of the active sites of the resin was acetylated before the phthalonitrile anchored to the α amine of the polymer bound Lys. Since the peptide starts to grow on the ε amine of the Lys, it is necessary not to have a free Lys to prevent the formation of the Lys-peptide side product. The prepared resin was

submitted to cyclotetramerization reaction. Following the washing of symmetrically-substituted Pc **3.3a**, Mtt protecting group on the ε-amine of the Lys was selectively removed by treating the resin with 2% TFA solution in CH_2Cl_2 without cleaving the Pc **4.15b** from the polymer support (Scheme 4.12). Cleavage of the Mtt group was observed by the collected yellow filtrate after

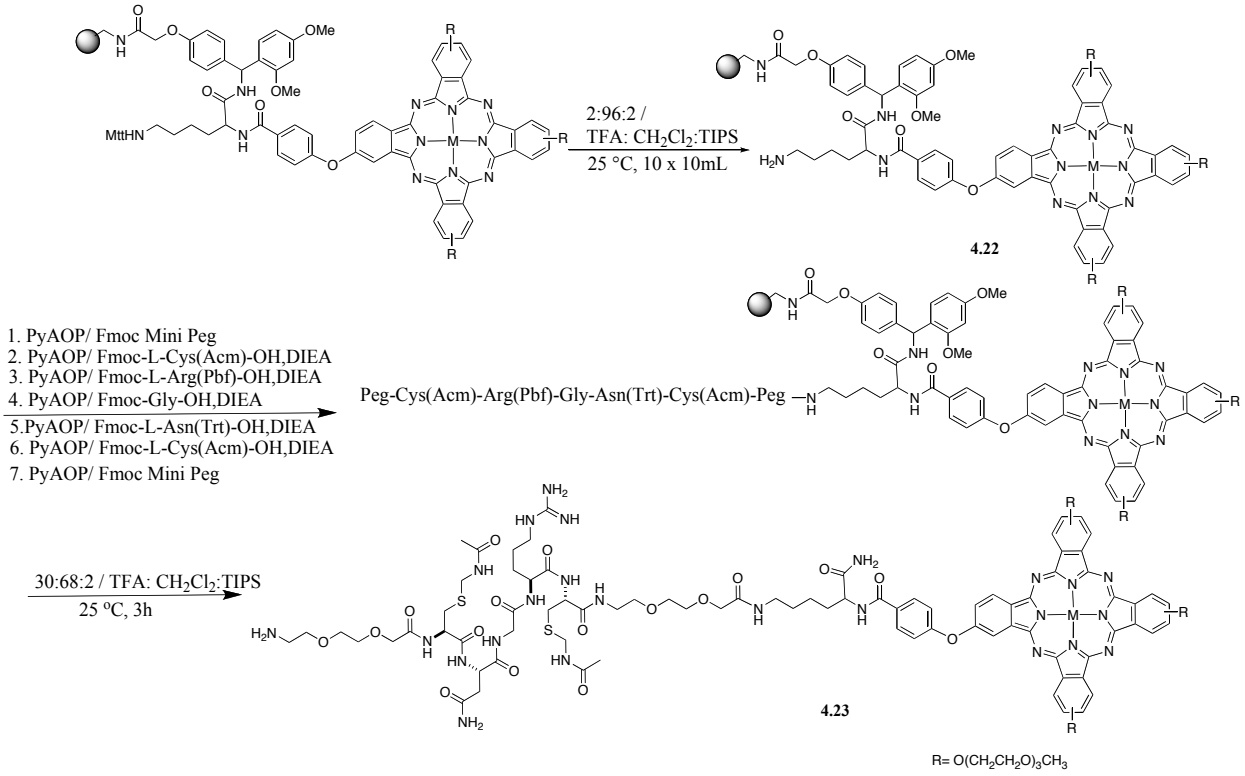

Scheme 4.12

each wash of the polymer support with the cleavage solution. The resin was washed with the acidic solution until a colorless filtrate was collected and the polymer support **4.22** was submitted to next step, anchoring of the amino acids to the free amine on the polymer support. Peptide synthesis on the solid support was done by Margaret W. Ndinguri using automated peptide synthesizer. The product was cleaved from the resin under acidic conditions to give Pc-peptide conjugate. Analysis of the crude mixture by mass spectrometry showed the

corresponding m/z ion peak. However, attempts to cyclisize the peptide before the cleavage step was not successful.

The successful synthesis of the Pc-peptide conjugate on solid support was a demonstration of the stability of the Pc on solid support under strong basic conditions under which the peptide synthesis is done. Using the same method, it is possible to synthesize wide variety of Pc-peptide conjugates in less then 3 days.

4.3 Conclusion and Future Work

Microwave assisted solid-phase synthesis of mono-amine functionalized Pcs was achieved in high yields and short amount of time relative mono-hydroxy functionalized Pcs as discussed in the Chapter 3. Microwave irradiation not only improved the yield of the cyclotetramerization reaction but also reduced the reaction time from hours to minutes.

From the results discussed through this chapter, we concluded that while outcome of the solid-phase cyclotetramerization reaction highly depends on the phthalonitrile loading of the resin, linker length and incoming reagent concentration, choice of solvent has a marginal effect on the purity of the product when a longer linker is used. It is possible to improve the yield of the reaction by choosing a solvent in which the resin moderately swells. Linker structure plays a crucial role during the reaction by regulating the site-site interactions. Comparison of two different types of linkers, Rink Amide and *p*-alkoxy benzyl, it is concluded that the every type of resin has a different phthalonitrile loading which needs to be determined during the optimization of the reaction in order to obtain pure AB_3 type asymmetrically-substituted Pcs. For instance, while with Rink Amide linker, complete site isolation was achieved at 0.1 mmol/g phthalonitrile loading at 0.8 M reaction concentration, the similar results were obtained at 0.28 mmol/g of phthalonitrile loading at 0.16 M concentration with *p*-alkoxy benzyl type linker.

Covalent conjugation of Pcs to biomolecules, oligonucleotide and peptide, was achieved employing well-established solid and solution phase synthetic methods. While microwave irradiation did not significantly improve the labeling efficiency of the oligonucleotide, it greatly reduced the reaction time giving an opportunity to synthesize and isolate the labeled oligonucleotide in the same day.

As a future work, using the same synthetic methods, it is possible to synthesize Pcs with a wide variety of substituent patterns to alter their chemical and photophysical properties for the need of biological and bioanalytical applications. Alternative linkers can be explored to synthesize AB_3 type asymmetrically-substituted Pcs with different functional groups such as carboxylic acid, hydroxylamine, or azide which gives a chance to use alternative conjugation strategies.

4.4 Experimental

4.4.1 General Experimental Information

Unless otherwise indicated, all commercially available starting materials were used directly without any further purification. PEG-based Rink Amide Resin was obtained from Matrix-Innovation. Sephadex^{TM} LH-20, 18-111 μm, was used for purification of the asymmetrically-substituted Pcs. FT-IR spectra were obtained on Bruker Tensor 27 spectrometer. Microwave reactions were performed in MARS Extraction system. Unless otherwise indicated, MALDI-MS mass spectra of the compounds were obtained using CCA as a matrix. Electronic absorption spectra were measured on a Perkin-Elmer Lambda 35 UV-vis spectrophotometer. The HPLC chromatograms were obtained using a JASCO (Easton, MD) 2000-series HPLC equipped with a quaternary gradient pump, autosampler, and fluorescence and diode-array detectors. HPLC was performed using Zorbax, C_{18} 5μm, 150 × 4.6 mm column with a 1 mL/min flow rate. Three different solvent gradient conditions were used: Condition A: HPLC was performed with 0.05

M TEAA in H_2O and CH_3OH as the eluants. Column was initially held at 95% 0.1 M TEAA-5% CH_3OH for 5 min and then concentration of CH_3OH was ramped to the 95% in 30 min. and was held at that concentration for 5 min. Column was washed with 100% CH_3OH for 15 min. The column was allowed to equilibrate at the initial mobile phase conditions for 20 min before the next injection. Condition B: 0.05M TEAA in a H_2O and CH_3OH-THF (80:20) was used as an eluting solvent. Column was initially held at 50% 0.1 M TEAA, 50% CH_3OH-THF (80:20) for 5 min and than it was ramped to the 5% 0.05 M TEAA, 95% CH_3OH-THF (80:20) in 30 min and held at that concentration for 5 min. The column was washed with 100% CH_3OH-THF (80:20) for 15 min. The column was allowed to equilibrate at the initial mobile phase conditions for 20 min before the next injection. Condition C: CH_3OH was used as an eluting solvent. Column was held at 100% CH_3OH for 30 min. The column was allowed to equilibrate at the initial mobile phase conditions for 20 min before the next injection. Emission spectra were obtained using a FLUOROLOG-3 spectrofluorometer (Horiba Jobin Yvon, Edison, NJ) equipped with a 450-W xenon lamp and a cooled Hamamatsu R928 photomultiplier operated at 900V in the photon-counting mode. A quartz cuvette with a 10 mm path length was utilized throughout these experiments. All measurements were performed under ambient room conditions within 3 h of solutions preparation. Stock solution and dilutions were prepared in anhydrous DMSO or THF. The quantum yields were calculated using a secondary standard method.[35] Methylene blue, a dye with excitation/emission wavelengths similar to Pcs and an established quantum yield was used as a secondary standard. According to the approach, the integrated fluorescence intensity of the analyte (I) and standard (I_R), the optical density of the analyte (OD) and the standard (OD_R), and the refractive index of analyte solvent (n) and standard solvent (n_R) are related to the quantum yield of the analyte (Q) as:

$$Q = Q_R \frac{I}{I_R} \frac{OD_R}{OD} \frac{n^2}{n_R^2}$$

where Q_R is a quantum yield of the reference standard (0.03 for methylene blue). To account for incomplete spectra, the bands were extrapolated using appropriate fitting models whenever necessary. In order to remove any amine containing compounds, all oligonucleotides were purified by ethanol precipitation before the conjugation reactions. Oligonucleotides were dissolved in nuclease free water and their concentrations were calculated based on the absorption at 260 nm in their electronic absorption spectra. Labeling buffers were prepared using corresponding salts in nuclease free water. The pH values were adjusted using HCl and/or NaOH. Labeling efficiencies of the conjugation reactions were calculated using the following equation.[25]

Extent of Labeling % = $((A_{\text{control 260 nm}} - A_{\text{sample 260 nm}}) / (A_{\text{control 260 nm}})) \times 100$

$A_{\text{control 260 nm}}$: peak area (absorption at 260nm) of the unlabeled oligonucleotide in the control reaction (no dye present)

$A_{\text{sample 260 nm}}$: peak area (absorption at 260nm) of the unlabeled oligonucleotide in the post-reaction

4.4.2 Experimental Procedures

General Procedure for Amino Acid Coupling to the Rink Amide Resin

Prior to the synthesis, the Rink Amide resin (0.4 g) with 0.52 mmol/g loading capacity was swelled in CH_2Cl_2 (20 mL) for 30 min. The solvent was filtered off and CH_2Cl_2 (3 mL) was added to the well-swelled resin. HOBt (0.83 mmol, 0.11 g), HBTU (0.83 mmol, 0.31 g) and the selected amino acid (0.83 mmol) were dissolved in DMF (1 mL) to have 0.2 M amino acid concentration in the reaction mixture. The solution and DIEA (1.66 mmol, 0.29 mL) were added to the resin and the reaction flask was placed in a shaker and kept at room temperature for 2h.

The reaction was followed by bromophenol blue test: A few resin beads were taken and placed in a small test tube. The beads were washed with CH_2Cl_2 several times to remove the residual amount of DMF. Couple of drops of 1% solution of bromophenol blue in acetonitrile was placed on the resin beads and the color change of the beads was observed. While yellow beads confirm the complete reaction, blue beads indicate the presence of free amine on the resin. Following the bromophenol blue test, the resin was washed with CH_2Cl_2 (4 x 15 mL), DMF (3 x 15 mL) and CH_2Cl_2 (3 x 15 mL).

General Procedure for Fmoc Cleavage

The resin was suspended in 20% solution of piperidine or 4-methyl piperidine in DMF (10 mL). The reaction was placed in a shaker and kept at room temperature for 10 min. Following the filtration of the solution, the fresh cleavage cocktail (10 mL) was added to the resin and the reaction was shaken 10 more min. at room temperature. The reaction was followed by bromophenol blue test. The resin was washed with DMF (5 x 15 mL), CH_2Cl_2 (3 x 15 mL) and the resin was submitted to next amino acid coupling.

General Procedure for Acetylation of the Polymer Support

The resin was suspended in 0.28 M solution of DIEA in DMF (25 mL). Ac_2O (8.4 mmol, 0.8 mL) was added to the suspension and the reaction was placed in a shaker and kept at room temperature for 3h. The reaction was followed by bromophenol blue test. Following the completion of the reaction, the resin was washed with DMF (5 x 15 mL) and CH_2Cl_2 (5 x 15 mL).

Polymer supported 4-(3,4-dicyanophenoxy)benzoic Acid (4.14)

4-(3, 4-Dicyanophenoxy)benzoic acid (0.05 mmol, 13 mg), HOBt (0.05 mmol, 6.7 mg) and HBTU (0.05 mmol, 19 mg) were dissolved in DMF (1 mL). The solution was added to the resin in CH_2Cl_2 (7 mL). DIEA (0.1 mmol, 17.4 μL) was added to the suspension and the reaction flask

was placed in a shaker and kept at room temperature for 1h to give the resin **4.14** with 0.1 mmol/g of loading. (0.15 mmol of 4-(3,4-Dicyanophenoxy)benzoic acid with proportional amount of coupling reagents and DIEA were used to prepare the resin **4.14** with 0.3 mmol/g of phthalonitrile loading) The resin was washed with CH_2Cl_2 (4 x 15 mL), DMF (2 x 15 mL) and CH_2Cl_2 (4 x 15 mL). FT-IR (KBr, cm^{-1}): 3513, 3305, 3055, 2865, 2233, 1953, 1738, 1651, 1611, 1589, 1536, 1507, 1487, 1454, 1348, 1324, 1293, 1248, 1209, 1176, 1093, 1035, 948, 840, 771

Determination of Loading Capacity of the Phthalonitrile Bound Resin

Before the acetylation step, ~ 50 mg of the resin was taken and placed in 5 mL syringe equipped with coarse frit and CH_2Cl_2 (0.5 mL) was added to the resin. Commercially available Fmoc-Gly-OH (0.1 mmol, 29.7 mg), HOBt (0.1 mmol, 13.5 mg) and HBTU (0.1 mmol, 38 mg) were dissolved in DMF (1 mL). The solution and DIEA (0.2 mmol, 35 μL) were added to the suspension and the reaction was placed in a shaker and kept at room temperature for 2h. The reaction was followed by bromophenol test. Following the completion of the coupling, the resin was washed with DMF (4 x 5 mL) and CH_2Cl_2 (4 x 5 mL) and dried in the desicator for 4-5 h. 6-7 mg of the dry resin was placed in the 3 mL syringe equipped with coarse frit and swelled in CH_2Cl_2 (1 mL) for 30 min. Following the filtration of the CH_2Cl_2, the resin was placed in 20% piperidine or 4-methyl piperidine solution in DMF (1 mL) and kept in the cleavage solution for 20 min. The solution was collected by filtration and the resin was washed with CH_3OH (3 x 2 mL). Combined filtrate solution (7 mL) was detected with electronic absorption spectrometry. The loading capacity of the resin was calculated using the following equation:

$0.52 - (UV_{300} \times 10^6 \times 0.007L) / (7800 \times \#\text{ of mg of the resin})$

General Procedure for Synthesis of AB_3 Type Pcs (4.15-4.18)

The resin **4.14** (0.4 g) was swelled in BuOH (2 mL) for 30 min in the microwave vessel. Corresponding phthalonitrile (5 mmol, xx g) and metal salt (1.4 mmol, xx g) were placed in a 20 mL glass vial in BuOH (4.5 mL) and heated up to 90 °C in water bath. DBU (2.8 mmol, 0.38

mL) was added to the suspension and the mixture was vigorously stirred until all the metal salt was dissolved. The solution was quickly transferred to the microwave vessel, having the resin **4.14** with BuOH (2 mL), and the screw-capped vessel was tightened. The microwave vessel was equipped with the pressure and temperature probes and the reaction irradiated in the microwave at 850 W. The temperature was ramped to 150 °C in 5 min. and held at the temperature for 40 min. The resin was washed, until a colorless filtrate was obtained, first with hot BuOH (12 x 25 mL), and then hot CH_2Cl_2 (3 x 25 mL). In the case of CuPc **4.18**, the resin was washed with hot BuOH (10 x 25 mL), CH_3OH (5 x 30 mL), CH_2Cl_2 (5 x 30 mL), CH_3OH-BuOH (1:1; 8 x 30 mL) and finally with BuOH (3 x 30 mL).

General Procedure for Cleavage of the AB_3 type Pc (4.4-4.18)

The resin was suspended into a solution of TFA-CH_2Cl_2-TIPS (20:78:2; 25 mL) and left in the shaker for 3h at room temperature. Filtrate was evaporated to dryness and the crude mixture was purified by filtration through a LH-20 column using CH_3OH as eluent. For the purification and the analysis of the symmetrically substituted Pcs, see the experimental section in Chapter 3.

ZnPc (4.8): 27% yield as a blue solid. Condition A was employed to perform HPLC. t_R=33.24 min. MALDI-MS: Calcd $C_{72}H_{86}N_{12}O_{18}Zn^+$: 1470.55; found: 1470.93 λ_{max} (DMSO): 680 nm (logε=5.3). λ_{max} (em) (DMSO): 690 nm. ϕ_f : 0.10

ZnPc (4.15): 28% yield as a blue solid. Condition A was employed to perform HPLC. t_R=29.45 min. MALDI-MS: Calcd $C_{66}H_{75}N_{11}O_{15}Zn^+$: 1325.47; found: 1324.98 λ_{max} (DMSO): 681 nm (logε=5.2). λ_{max} (em) (DMSO): 691 nm. ϕ_f : 0.10

ZnPc (4.16): 19% yield as a green solid. Condition A was employed to perform HPLC. t_R=34.77 min. MALDI-MS: Calcd $C_{66}H_{75}N_{11}O_{12}S_3Zn^+$: 1373.41; found: 1373.69 λ_{max} (DMSO): 701 nm (logε=5.1). λ_{max} (em) (DMSO): 708 nm. ϕ_f : 0.09

ZnPc (4.17): 15% yield as a green solid. Condition A was employed to perform HPLC. t_R=30.37 min. MALDI-MS: Calcd $C_{87}H_{117}N_{11}O_{21}S_6Zn^+$: 1907.60; found: 1907.77 λ_{max} (DMSO): 701 nm (logε=5.3). λ_{max} (em) (DMSO): 709 nm. ϕ_f : 0.11

CuPc (4.18): 24% yield as a blue solid. CuPc **4.18** could not be eluted from the column. MALDI-MS: Calcd $C_{66}H_{75}CuN_{11}O_{15}^+$: 1324.47; found: 1324.81 λ_{max} (DMSO): 680 nm (logε=4.3). λ_{max} (em) n.d. ϕ_f : n.d.

Preparation of Oligonucleotide-Pc Conjugate (4.19)

To a 3.6 mM oligonucleotide solution in water (4.4 μL) in an Eppendorf tube, $NaHCO_3$ buffer (pH=7.6; 60 μL), 10 mM ZnPc **4.15** solution in CH_3OH (30 μL), 150 mM EDC solution in DMSO (5 μL) and 350 mM NHS solution in DMSO (5 μL) were added in the given order. The Eppendorf tube was placed in a screw-capped microwave vessel containing enough water to surround the Eppendorf tube (~1.5 mL) and the vessel tightened. The microwave vessel was equipped with the temperature and pressure probes and the reaction was irradiated at 400 W. The temperature was ramped to 75 °C in 1 min. and held at the set temperature for 30 min. Following the completion of the reaction, cold ethanol (300 μL) and 3M NaCl solution in water (10 μL) were added to reaction mixture and the suspension was placed in -20 °C and kept for an hour. The suspension was centrifuged at 4 °C at 12,000 rpm for 30 min. The precipitate was reconstituted in 0.05 M TEAA solution in water and isolated by HPLC in 35% labeling efficiency. Condition B was employed to perform HPLC. t_R=19.17 min. Two of the control experiments were also performed employing the same method using the reagents in the following ratios:

Control Experiment 1. 3.6 mM oligonucleotide solution in water (4.4 μL) $NaHCO_3$ buffer (pH=7.6; 60 μL), 10 mM ZnPc **4.15** solution in CH_3OH (30 μL), and DMSO (10 μL)

Control Experiment 2. Water (4.4 μL) $NaHCO_3$ buffer (pH=7.6; 60 μL), 10 mM ZnPc **4.15** solution in CH_3OH (30 μL), 150 mM EDC solution in DMSO (5 μL) and 350 mM NHS solution in DMSO (5 μL).

Preparation of Oligonucleotide-Pc Conjugate (4.20)

To a 4.3 mM oligonucleotide solution in water (4.4 μL) in an Eppendorf tube, NaOAc buffer (pH=5.5; 50 μL), 10 mM ZnPc **4.15** solution in CH_3OH (51.6 μL) and 10 mM $NaCNBH_3$ solution in CH_3OH (10 μL) were added in the given order. The reaction was incubated either at room temperature for 16 h or in microwave for 30 min. The Eppendorf tube was placed in a screw-capped microwave vessel containing enough water to surround the Eppendorf tube (~1.5 mL) and the vessel tightened. The microwave vessel was equipped with temperature and pressure probes and the reaction was irradiated at 400 W. The temperature was ramped to 70 °C in 1 min. and held at the set temperature for 30 min. Following the completion of the reactions, cold ethanol (300 μL) and 3 M NaCl solution in water (10 μL) were added to reaction mixtures and the suspensions were placed in -20 °C and kept for an hour. The suspensions were centrifuged at 4 °C at 12,000 rpm for 30 min. The precipitates were reconstituted in 0.05 M TEAA solution in water and isolated by HPLC in 79% labeling efficiency. (76% labeling efficiency was obtained when the reaction was incubated at room temperature.) Condition B was employed to perform HPLC. t_R=18.95 min. ESI-TOF Calcd (M-3): 2255.14; found: 2255.14. Two of the control experiments were also performed employing the same methods using the reagents in the following ratios.

Control Experiment 1. 4.3 mM oligonucleotide solution in water (4.4 μL) NaOAc buffer (pH=5.5; 50 μL), 10 mM ZnPc **4.15** solution in CH_3OH (51.6 μL) and CH_3OH (10 μL)

Control Experiment 2. Water (4.4 μL), NaOAc buffer (pH=5.5; 50 μL), 10 mM ZnPc **4.15** solution in CH_3OH (51.6 μL) and 10 mM $NaCNBH_3$ solution in CH_3OH (10 μL).

Preparation of Oligonucleotide-Pc Conjugate (4.21)

To a 5 mM oligonucleotide solution in water (4 μL) in an Eppendorf tube, NaOAc buffer (pH=5.5; 50 μL), 20 mM ZnPc **4.15** solution in CH_3OH (50 μL) and 10 mM $NaCNBH_3$ solution in CH_3OH (10 μL) were added in the given order. The Eppendorf tube was placed in a screw-capped microwave vessel containing enough water to surround the Eppendorf tube (~1.5 mL) and the vessel tightened. The microwave vessel was equipped with temperature and pressure probes and the reaction was irradiated at 400 W. The temperature was ramped to 50 °C in 1 min. and held at the set temperature for 40 min. Following the completion of the reaction, cold ethanol (300 μL) and 3 M NaCl solution in water (10 μL) were added to reaction mixture and the suspension was placed in -20 °C and kept for an hour. The suspensions were centrifuged at 4 °C at 12,000 rpm for 30 min. The precipitate was reconstituted in 0.05 M TEAA solution in water and isolated by HPLC in 35 % labeling efficiency. Condition B was employed to perform HPLC. t_R=22.57 min. Two of the control experiments were also performed employing the same methods using the reagents in the following ratios.

Control Experiment 1. 5 mM oligonucleotide solution in water (4 μL) NaOAc buffer (pH=5.5; 50 μL), 20 mM ZnPc **4.15** solution in CH_3OH (50 μL) and CH_3OH (10 μL)

Control Experiment 2. Water (4μL), NaOAc buffer (pH=5.5; 50 μL), 10 mM ZnPc **4.15** solution in CH_3OH (50 μL) and 10 mM $NaCNBH_3$ solution in CH_3OH (10 μL).

Selective Cleavage of the Mtt protecting group (4.22)

The Pc bound polymer support was suspended into a solution of TFA-CH_2Cl_2-TIPS (2:96:2; 10 mL) and left in the shaker for 2 min. and the solution was filtered off. This step was repeated for 10 times using 10 mL f cleavage cocktail at a time. The resin was washed with CH_2Cl_2 (10 X 10 mL) and submitted to the next step.

Preparation of Pc-Peptide Conjugate (4.23)

ZnPc **4.15** was prepared as discussed above and the resin was placed in automated peptide synthesizer with the appropriate amino acids and the reagents. Following the conjugation, ~ 50 mg of the polymer-bound Pc-peptide conjugate was cleaved using TFA-CH_2Cl_2-TIPS (30:68:2; 2 mL) solution. The crude product was obtained in ~ 15% yield and analyzed by mass spectrometry. MALDI-MS: Calcd $C_{102}H_{138}N_{24}O_{29}S_2Zn^+$: 2290.88; found: 2290.37

4.5 References

(1) Erdem, S. S.; Nesterova, I. V.; Soper, S. A.; Hammer, R. P. Solid-phase synthesis of asymmetrically substituted "AB_3-type" phthalocyanines *J. Org. Chem.* **2008**, *73*, 5003-5007.

(2) Torres, T. Perspectives in the selective synthesis of phthalocyanines and related compounds *J. Porphyr. Phthalocyanines* **2000**, *4*, 325-330.

(3) Perreux, L.; Loupy, A. A tentative rationalization of microwave effects in organic synthesis according to the reaction medium, and mechanistic considerations *Tetrahedron* **2001**, *57*, 9199-9223.

(4) Tolbin, A. Y.; Ivanov, A. V.; Tomilova, L. G.; Zefirov, N. S. Synthesis of 1,2-bis(3,4-dicyanophenoxymethyl)benzene and binuclear zinc phthalocyanines of clamshell and ball types *J. Porphyr. Phthalocyanines* **2003**, *7*, 162-166.

(5) Samaroo, D.; Soll, C. E.; Todaro, L. J.; Drain, C. M. Efficient microwave-assisted synthesis of amine-substituted tetrakis (pentafluorophenyl) porphyrin *Org. Lett.* **2006**, *8*, 4985-4988.

(6) Shaabani, A.; Maleki-Moghaddam, R.; Maleki, A.; Rezayan, A. H. Microwave assisted synthesis of metal-free phthalocyanine and metallophthalocyanines *Dyes Pigment.* **2007**, *74*, 279-282.

(7) Yan, B.; Sun, Q. Crucial factors regulating site interactions in resin supports determined by single bead IR *J. Org. Chem.* **1998**, *63*, 55-58.

(8) Chan, W. C., White, P.D Fmoc solid Phase Peptide Synthesis A Practical Approach; Oxford University: New York, 2000.

(9) Sheridan, P.; Ambroziak, A.; Fryer, I.; Priest, A. The Thermodynamics and Kinetics of the Proton-Transfer Reactions between Bromophenol Blue and Some Aromatic-Amines in Aprotic Solution *Int. J. Chem. Kinet.* **1993**, *25*, 169-182.

(10) Crowley, J. I.; Harvey, T. B.; Rapoport, H. Solid-Phase Synthesis - Evidence for Quantification of Intraresin Reactions *J. Macromol. Sci. Chem.* **1973**, *A 7*, 1117-1126.

(11) Shi, R. R.; Wang, F.; Yan, B. Site-site isolation and site-site interaction - Two sides of the same coin *Int. J. Pept. Res. Ther.* **2007**, *13*, 213-219.

(12) Merrifield, R. B. Solid Phase Peptide Synthesis .1. Synthesis of a Tetrapeptide *J. Am. Chem. Soc.* **1963**, *85*, 2149-2154.

(13) Lindsley, C. W.; Chan, L. K.; Goess, B. C.; Joseph, R.; Shair, M. D. Solid-phase biomimetic synthesis of carpanone-like molecules *J. Am. Chem. Soc.* **2000**, *122*, 422-423.

(14) Grubbs, R.; Lau, C. P.; Cukier, R.; Brubaker, C. Polymer Attached Metallocenes - Evidence for Site Isolation *J. Am. Chem. Soc.* **1977**, *99*, 4517-4518.

(15) Li, D.; Elbert, D. L. The kinetics of the removal of the N-methyltrityl (Mtt) group during the synthesis of branched peptides *J. Pept. Res.* **2002**, *60*, 300-303.

(16) Blackwell, H. E.; Clemons, P. A.; Schreiber, S. L. Exploiting site-site interactions on solid support to generate dimeric molecules. *Org. Lett.* **2001**, *3*, 1592-1592.

(17) Regen, S. L.; Lee, D. P. Influence of Solvent on Site Isolation in Polystyrene Resins *Macromolecules* **1977**, *10*, 1418-1419.

(18) Wulff, G.; Schulze, I. Enzyme-Analogous Polymers .7. Directed Cooperativity and Site Separation of Mercapto Groups in Synthetic-Polymers *Angew. Chem.-Int. Edit. Engl.* **1978**, *17*, 537-538.

(19) Lepecq, J. B.; Paoletti, C. A Fluorescent Complex between Ethidium Bromide and Nucleic Acids - Physical-Chemical Characterization *J. Mol. Biol.* **1967**, *27*, 87-106.

(20) Rye, H. S.; Glazer, A. N. Interaction of Dimeric Intercalating Dyes with Single-Stranded-DNA *Nucleic Acids Res.* **1995**, *23*, 1215-1222.

(21) Benson, S. C.; Mathies, R. A.; Glazer, A. N. Heterodimeric DNA-Binding Dyes Designed for Energy-Transfer - Stability and Applications of the DNA Complexes *Nucleic Acids Res.* **1993**, *21*, 5720-5726.

(22) Lewis, F. D.; Zhang, Y. F.; Letsinger, R. L. Bispyrenyl excimer fluorescence: A sensitive oligonucleotide probe *J. Am. Chem. Soc.* **1997**, *119*, 5451-5452.

(23) Yamana, K.; Nunota, K.; Nakano, H.; Sangen, O. A New Method for Introduction of a Pyrene Group into a Terminal Position of an Oligonucleotide *Tetrahedron Lett.* **1994**, *35*, 2555-2558.

(24) Sigmund, H.; Maier, T.; Pfleiderer, W. A new type of fluorescence labeling of nucleosides, nucleotides and oligonucleotides *Nucleos. Nucleot.* **1997**, *16*, 685-696.

(25) Nesterova, I. V.; Verdree, V. T.; Pakhomov, S.; Strickler, K. L.; Allen, M. W.; Hammer, R. P.; Soper, S. A. Metallo-phthalocyanine near-IR fluorophores: Oligonucleotide conjugates and their applications in PCR assays *Bioconjugate Chem.* **2007**, *18*, 2159-2168.

(26) Hammer, R. P.; Owens, C. V.; Hwang, S. H.; Sayes, C. M.; Soper, S. A. Asymmetrical, water-soluble phthalocyanine dyes for covalent labeling of oligonucleotides *Bioconjugate Chem.* **2002**, *13*, 1244-1252.

(27) Chernonosov, A. A. Phthalocyanine conjugates of oligonucleotides as new reagents for sensitized and catalytic modification of DNA and DNA-binding proteins *FEBS J.* **2005**, *272*, 542-543.

(28) Borch, R. F.; Bernstei.Md; Durst, H. D. Cyanohydridoborate Anion as a Selective Reducing Agent *J. Am. Chem. Soc.* **1971**, *93*, 2897-2904.

(29) Kangasmetsa, J. J.; Johnson, T. Microwave-accelerated methodology for the direct reductive amination of aldehydes *Org. Lett.* **2005**, *7*, 5653-5655.

(30) Tyagi, S.; Kramer, F. R. Molecular beacons: Probes that fluoresce upon hybridization *Nat. Biotechnol.* **1996**, *14*, 303-308.

(31) Fang, X. H.; Li, J. J.; Tan, W. H. Using molecular beacons to probe molecular interactions between lactate dehydrogenase and single-stranded DNA *Anal. Chem.* **2000**, *72*, 3280-3285.

(32) Helps, C.; Reeves, N.; Tasker, S.; Harbour, D. Use of real-time quantitative PCR to detect Chlamydophila felis infection *J. Clin. Microbiol.* **2001**, *39*, 2675-2676.

(33) Fang, Y.; Wu, W. H.; Pepper, J. L.; Larsen, J. L.; Marras, S. A. E.; Nelson, E. A.; Epperson, W. B.; Christopher-Hennings, J. Comparison of real-time, quantitative PCR with molecular beacons to nested PCR and culture methods for detection of Mycobacterium avium subsp paratuberculosis in bovine fecal samples *J. Clin. Microbiol.* **2002**, *40*, 287-291.

(34) Yates, S.; Penning, M.; Goudsmit, J.; Frantzen, I.; van de Weijer, B.; van Strijp, D.; van Gemen, B. Quantitative detection of hepatitis B virus DNA by real-time nucleic acid sequence-based amplification with molecular beacon detection *J. Clin. Microbiol.* **2001**, *39*, 3656-3665.

(35) Fery-Forgues, S.; Lavabre, D. Are fluorescence quantum yields so tricky to measure? A demonstration using familiar stationery products *J. Chem. Educ.* **1999**, *76*, 1260-1264.

Chapter 5
In vitro Biological Evaluation of Oligoethyleneglycol Substituted Phthalocyanines for Photodynamic Therapy

5.1 Introduction

Long wavelength absorption in the electromagnetic spectrum (650-800 nm) coupled with high extinction coefficients and low photobleaching yields, make phthalocyanines (Pcs) promising drug, photosensitizer candidates for photodynamic therapy (PDT). PDT is a treatment in which the combination of dye, light, and oxygen causes photochemically induced cell death.[1,2] The PDT agent, which is injected to the blood stream or other biological fluid (eye)[3,4] selectively localizes in the neoplastic tissues in a mechanism that is not fully understood. Irradiation of the localized photosensitizer with a specific wavelength of light results in death of the malignant tissue via formation of the cytotoxic species such as singlet oxygen, super oxide and radical hydroxyl.[1,5]

Figure 5.1 shows the simplified Jablonski diagram for the PDT process.[6] Excitation of the photosensitizer from its singlet ground state (S_0) produces an excited state (S_1) (**1**) sensitizer. The sensitizer, existing in the lowest excited singlet state (S_1), can relax to the ground state (S_0) via different pathways including fluorescence (emission of light) (**2**), and non-radiative decay (dissipation of the energy as heat) (**3**). An alternative way to return to the ground state is that

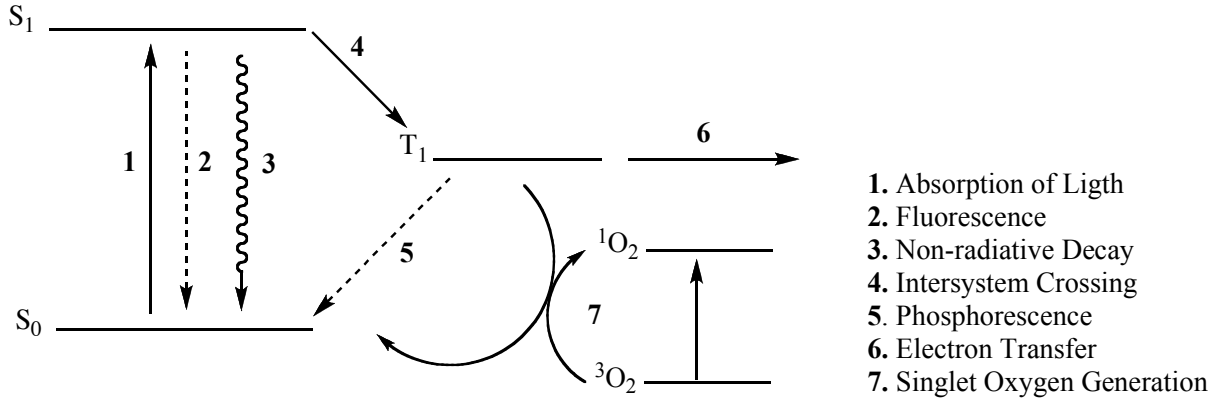

Figure 5.1 Simplified Jablonski diagram for the PDT process.

the sensititzer can undergo the non-radiative process of inter-system crossing to give the triplet state molecule (T_1) (**4**). Since the decay of the triplet to singlet state, phosphorescence (**5**), is forbidden, this transition is relatively slow. Therefore, the triplet state sensitizer has time to react with its chemical environment. The triplet sate sensitizer may react with biomolecules depending on the environment and concentration of species in two different ways known as Type I and Type II reactions.[6] The type I mechanism involves the formation of radical ions via direct electron transfer from the photosensitizer or electron abstraction from a substrate molecule such as endogenous amino acids and alcohols (**6**).[7] Formed radicals rapidly react with molecular oxygen resulting in production of highly reactive oxygen species such as peroxide anions and superoxide, which subsequently attack the cellular targets. The type II mechanism involves production of singlet oxygen, the lowest excited state of the molecular oxygen, by energy transfer from photosensitizer to ground state oxygen (**7**). Singlet oxygen is very toxic to tumor cells,[8] and it shows a limited radius of action (< 0.02 μm) with a life time shorter than 0.04 microseconds.[9] Thus, the toxicity of the photosensitizer is limited by its localized area. After the singlet oxygen production, the photosensitizer can return to its starting point where it is available to start the whole process again. The type II process is usually preferred at low concentration of substrate and high concentration of oxygen. In PDT, it is difficult to distinguish between two mechanisms. There is probably a contribution from both Type I and Type II mechanisms.

PDT has been used as an alternative method for treatment of cancer and it has been evaluated in various types of cancers including early stage head and neck,[10] esophageal,[11] lung,[12] bladder,[13] as well as brain tumors.[14] Currently, there are two drugs, Photofrin[15] and Visudyne,[16] approved by United States Food and Drug Administration (FDA) to be used in PDT. However, it is known that the Photofrin, a synthetic porphyrin, is not an ideal drug for PDT for the following reasons: 1) Since Photofrin consists of a mixture of porphyrins, an unknown chain length of

hematoporphyrin oligomer, the identity of the active component is debatable;[6] 2) the wavelength used to photoactivate the Photofrin, 630 nm, can only penetrate tissue to a depth of a few mm due to the endogenous chromophores and light scattering;[17] 3) dispersion of the Photofrin may take up to six weeks which makes the patient photosensitive to sunlight.[6] These drawbacks of the Photofrin have brought up a new research area regarding the synthesis and evaluation of next generations of photosensitizers that are more effective than the currently used FDA approved drugs.

A promising photosensitizer should be a pure compound and exhibit the following characteristics: 1) Strong absorption in the near-IR or IR region of the electromagnetic spectrum; 2) high quantum yield of triplet formation; 3) high singlet oxygen quantum yield; 4) low dark toxicity and strong phototoxicity upon irradiation with a specific wavelength of light; 5) high selectivity for a malignant tissue over a healthy tissue; 6) rapid clearance from the healthy tissue and blood stream. In addition, a practical and scalable synthesis of the drug is desirable. With the aim of the synthesis of a new generation of porphyrin- and Pc-based drugs for PDT, tremendous effort has been devoted over the last two decades.[18-21] Consequently, a number of porphyrin-and Pc-based drugs are being evaluated in clinical trials.[17] Recently, phase I clinical studies of SiPc for cutaneous malignancies were completed.[22] Also, phase I clinical trials of SiPc for PDT for the treatment of pre-malignant and malignant skin conditions are expected to be completed by the end of 2008.[23] Another Pc, tetra-sulfonated ZnPc, was evaluated in phase I clinical trials for PDT in dogs having naturally occurring tumors.[24] The tetra-sulfonated ZnPc gave promising results for further studies.

Phthalocyanines have attracted much interest due to the their red shifted Q band and large extinction coefficients relative to porphyrin analogues.[25] The red shifted absorption and excitation wavelength provide a significant advantage in increased tissue penetration. Their low

toxicity and high phototoxicity toward cells make them promising drug candidate for PDT. In this chapter, in vitro evaluation of oligoethyleneglycol-substituted Pcs is discussed.

5.2 Results and Discussion

Dark toxicity, phototoxicity, cellular uptake as well as intracellular localization of oligoethyleneglycol-substituted ZnPcs in human carcinoma HEp2 cells were evaluated. The structures of the Pcs used for in vitro studies are shown in Scheme 5.1. ZnPcs **3.8a**, **3.8b** and **3.10b** precipitated in the cell medium. Thus, the data is not presented for these compounds. While precipitation of the ZnPcs **3.8a** and **3.8b**, bearing octa-and hexa-benzyl rings, respectively,

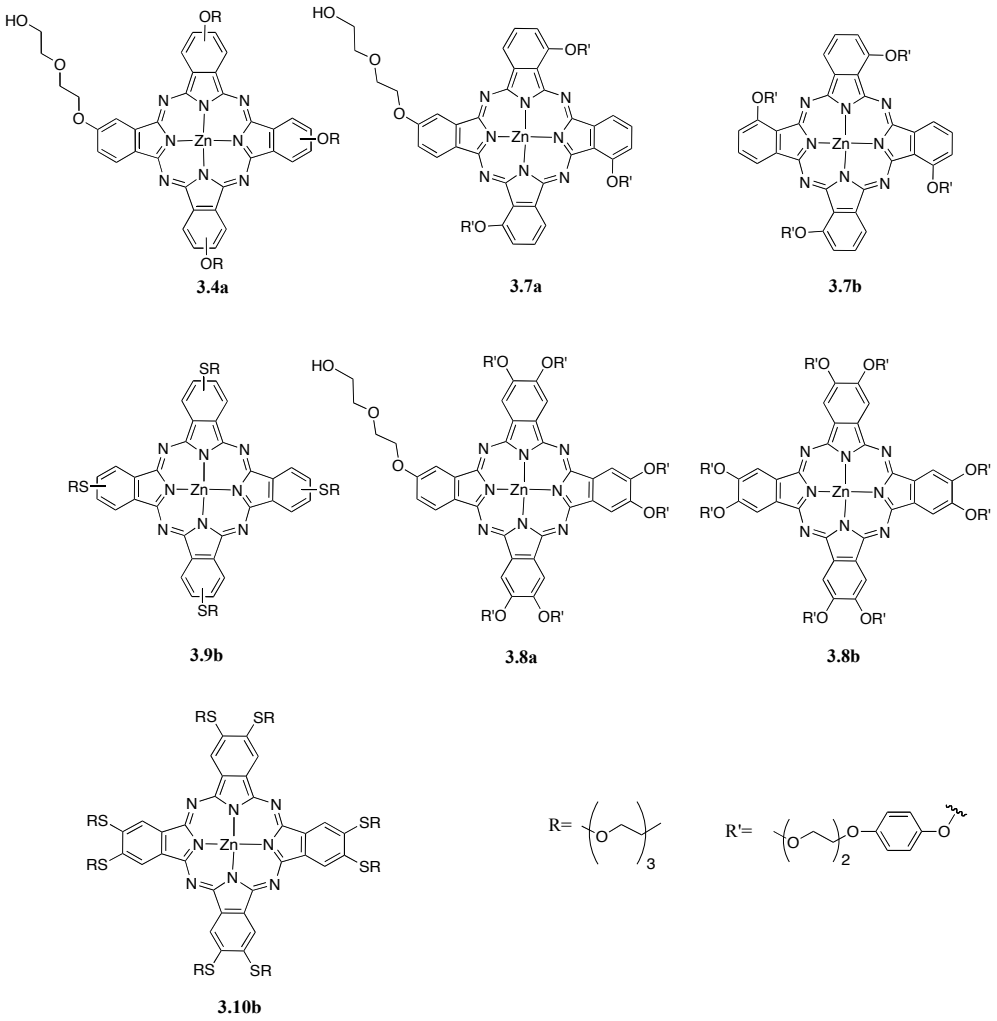

Scheme 5.1

could be due to the their hydrophobic nature and high tendency to aggregate, thio ether oligoethyleneglycol-substituted ZnPc **3.10b** could precipitate due to the having octa sulfur atoms which are much larger than oxygen.

5.2.1 Time-Dependent Cellular Uptake

The time-dependent cellular uptake of triethylene glycol-substituted ZnPcs **3.4a**, **3.9b** and **3.7a**, **3.7b,** decorated with dietyhlene glycol via benzyl linkage, were evaluated in human carcinoma HEp2 cells over a 24h time period. As shown in Figure 5.2, while ZnPcs **3.7a**, **3.7b** and **3.9b** were rapidly accumulated in the first 4h, ZnPc **3.4a,** bearing mono-hydroxyl and tri-triethylene glycol chains, continued to accumulate for 24h time period and was the most readily taken up by the cells. It is known that accumulation of porphyrinoids in cells is accentuated by increased amphiphilic character of them.[19,25-27] Consequently, the most hydrophobic ZnPc **3.7b**,

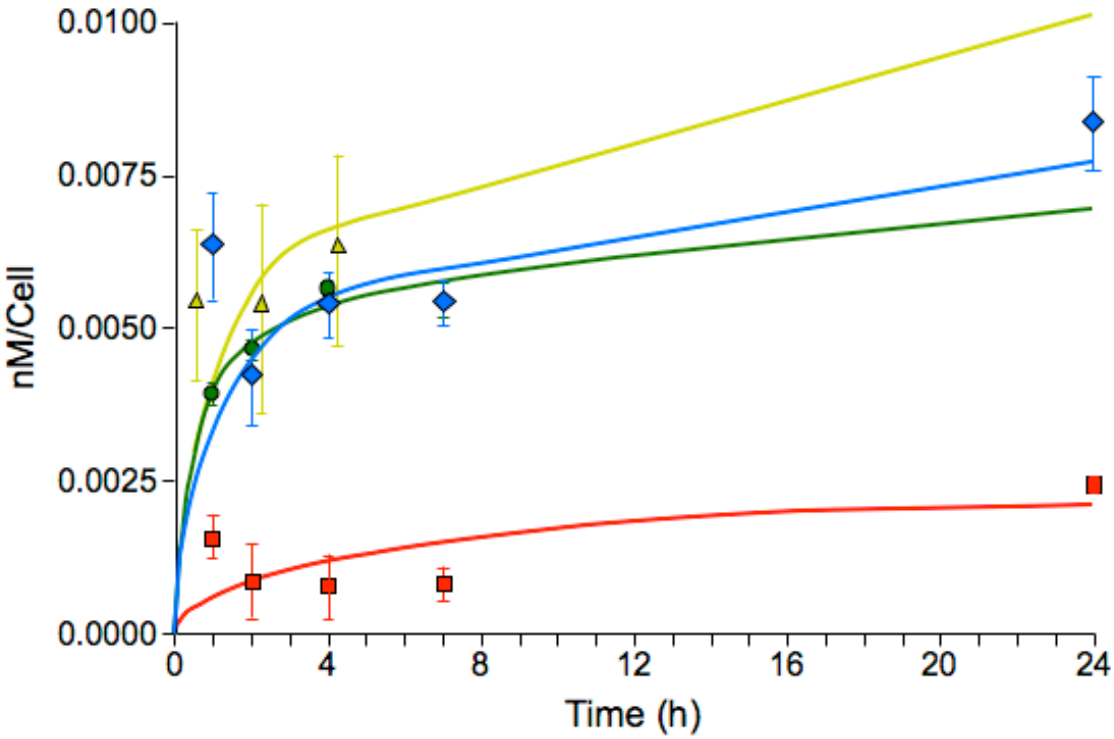

Figure 5.2 Time-dependent cellular uptake of ZnPcs into HEp2 cells at 10 µM concentration. **3.7b** (red), **3.9b** (green), **3.7a** (blue), and **3.4a** (yellow).

bearing four benzyl rings, accumulated in the cells approximately three times less than the asymmetrically substituted version ZnPc **3.7a** having tri-benzyl groups and mono-hydroxyl group.

5.2.2 Dark Cytotoxicity

Dark toxicity of short oligoethyleneglycol-substituted ZnPcs **3.4a**, **3.7a**, **3.7b** and **3.9b** toward human carcinoma HEp2 cells was evaluated. Figure 5.3 shows the dark toxicity of the ZnPcs **3.4a**, bearing mono-hydroxyl and tri-triethylene glycol units, and tetra-thio ether triethylene glycol-substituted **3.9b** at concentrations up to 100 µM. Dark toxicity of the ZnPcs **3.7a** and **3.7b**, bearing tri-and tetra benzyl units, respectively, at concentration up to 10 µM are shown in Figure 5.4. While the tetra- or tri-benzyl ether substituted ZnPcs **3.7a** and **3.7b** were found to be non-toxic to HEp2 cells under the test conditions up to 10 µM concentration

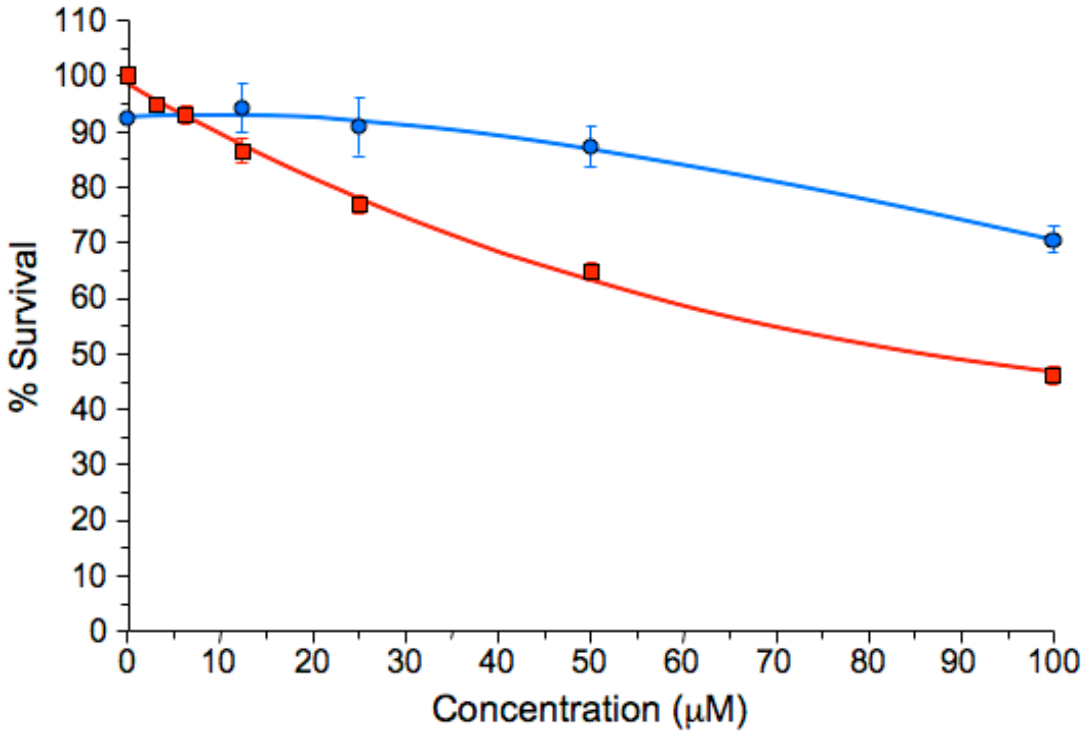

Figure 5.3 Dark cytotoxicity of ZnPcs toward HEp2 cells at 100 µM concentration. **3.4a** (blue), **3.9b** (red).

(Figure 5.4), tri-triethylene glycol bearing ZnPc **3.4a** exhibited low dark toxicity up to 20 µM concentration (Figure 5.3). Toxicity of **3.4a** increased with increasing concentration up to 100 µM. ZnPc **3.9b**, substituted with thio ether oligoethyleneglycol chains, was found to be the most toxic among the tested ZnPcs with measurable dark toxicity at an estimated IC_{50} of ~ 85 µM concentration (Figure 5.3).

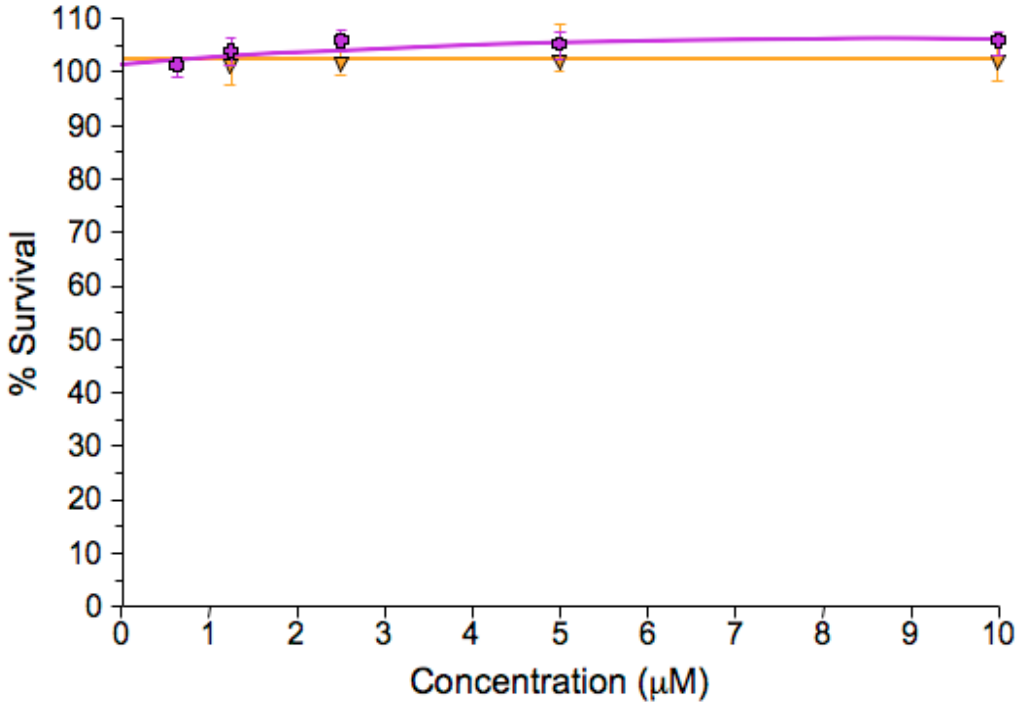

Figure 5.4 Dark cytotoxicity of ZnPcs toward HEp2 cells at 10 µM concentration. **3.7b** (yellow), **3.7a** (purple).

5.2.3 Phototoxicity

The HEp2 cells, loaded with short oligoethyleneglycol bearing ZnPcs **3.4a**, **3.7a**, **3.7b** and **3.9b,** were exposed to light. The total light exposure was approximately 0.5 J/cm^2. Figure 5.5 shows the phototoxicity of the ZnPcs to 10 µM concentration. Tri-triethylene glycol-substituted ZnPc **3.4a**, which was the most taken up by cells, exhibited high phototoxicity with an estimated IC_{50} of ~ 1 µM up to 10 µM concentration. Benzyl ether bearing ZnPcs **3.7a** and **3.7b** showed

close phototoxicity results with an estimated IC_{50} of ~ 0.6 µM and of ~ 0.8 µM concentrations, respectively. Vicente et. al., published similar results with cationic ZnPc, peripherally decorated with octa-triethylene glycol chains.[26] The ZnPc was highly phototoxic toward human HEp2 cells with an IC_{50} of ~2.2 µM.[26] In another paper, Vicente et al., evaluated hexadeca-carboxylate substituted ZnPc toward human HEp2 cells.[28] Water-soluble ZnPc found to be phototoxic toward human HEp2 cells with an IC_{50} of 4.6 µM. Short oligoethyleneglycol chains bearing ZnPcs **3.7a** and **3.7b**, having a similar substituent pattern with the published cationic ZnPc, were found to be more phototoxic toward human carcinoma cells with IC_{50} < 1 µM (Figure 5.5).

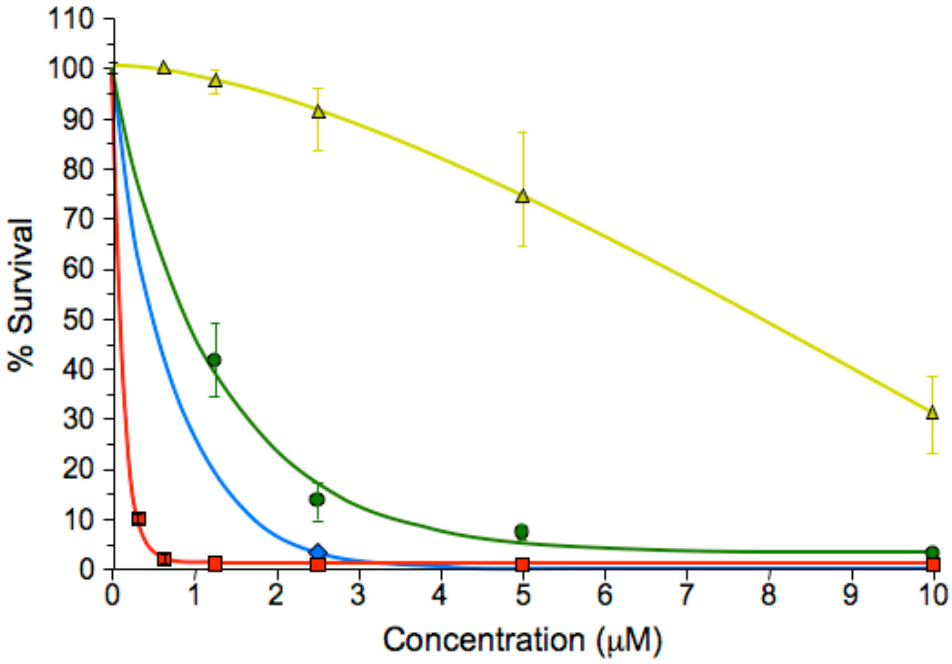

Figure 5.5 Phototoxicity of ZnPcs toward HEp2 cells at 10 µM concentration. **3.7a** (red), **3.7b** (blue), **3.4a** (green), and **3.9a** (yellow).

Comparison of the phototoxicity results of the tri-triethylene glycol-substituted ZnPc **3.4a** with tetra-benzyl ether bearing ZnPc **3.7b** suggested that the phototoxicity of the Pcs is not proportional to extent of accumulation of them in the cells. ZnPc **3.4a**, decorated with triethylene glycol chains, with the highest cellular uptake value is found to be less toxic than the

tetra-benzyl ether bearing ZnPc **3.7b**. As previously observed,[27] this result indicates that probably short oligoethyleneglycol-substituted ZnPc **3.4a** has the most enhanced amphiphilic character to cross the HEp2 cell membrane, which results in higher accumulation in the cells. Since phototoxicity of Pcs is also related with the ability of them to generate reactive oxygen species, it can be concluded that the ZnPc **3.7b**, decorated with tetra-benzyl ether, is capable of generating the toxic species in high concentrations to destroy the higher percentage of the human HEp2 cells.

Among the short Polyethylene glycol (PEG) chains bearing Pcs, thio ether oligoethyleneglycol-substituted ZnPc **3.9b** was found to be the least phototoxic with an estimated IC_{50} of ~ 8 μM. The low phototixicty of the thio ether bearing ZnPc **3.9b** can be due to the low cellular uptake as well as low concentration of generated reactive oxygen species.

5.2.4 Intracellular Localization

Fluorescence microscopy was used to evaluate the preferential sites of subcellular localization of short oligoethyleneglycol bearing ZnPcs **3.4a**, **3.7a**, **3.7b** and **3.9b**. The HEp2 cells were exposed to 10 μM Pc concentrations overnight. The fluorescence patterns of the Pcs were presented in Figures 5.6-5.9. For co-localization experiments, the cells were incubated concurrently with the specific organelle tracers. All Pcs are mainly localized in lysosomes and endoplasmic reticulum. It is known that hydrophilic and/or aggregated porphyrinoids are taken up into the cells by pinocystosis and/or endocytosis in which the compound travels within small vesicles.[1] Since these vesicles are fused with lysosomes and endosomes, and the light exposure permeabilize the lysosomes, the porphyrinoid derivatives are most likely be localized in lysosomes. Our results are in agreement with the previously reported subcellular localization of Pc-peptide conjugates and PEG containing porphyrins.[19,29,30]

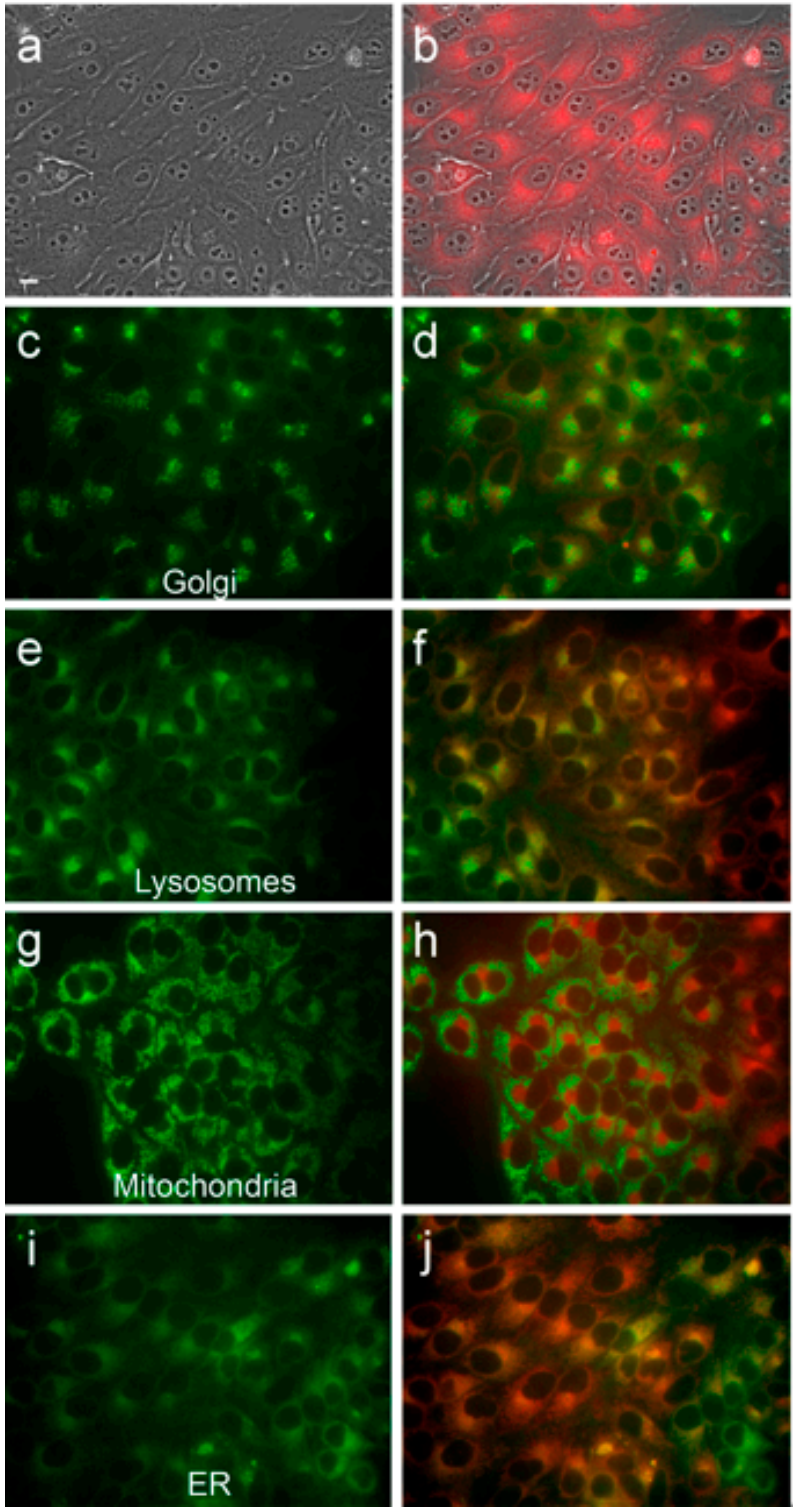

Figure 5.6 Intracellular localization of ZnPc **3.4a** in HEp2 cells at 10 μM for 24 h. (a) phase contrast; (b) Pc fluorescence; (c) BODIPY FL- C5-Ceramide fluorescence (Golgi label); (d) overlay with Pc; (e) LysoSensor fluorescence (lysosome label); f: overlay; (g) MitoTracker fluorescence (mitochondria label); (h) overlay; (i) ERTracker Green FM fluorescence (ER label); (j) overlay. Scale bar: 10 μm.

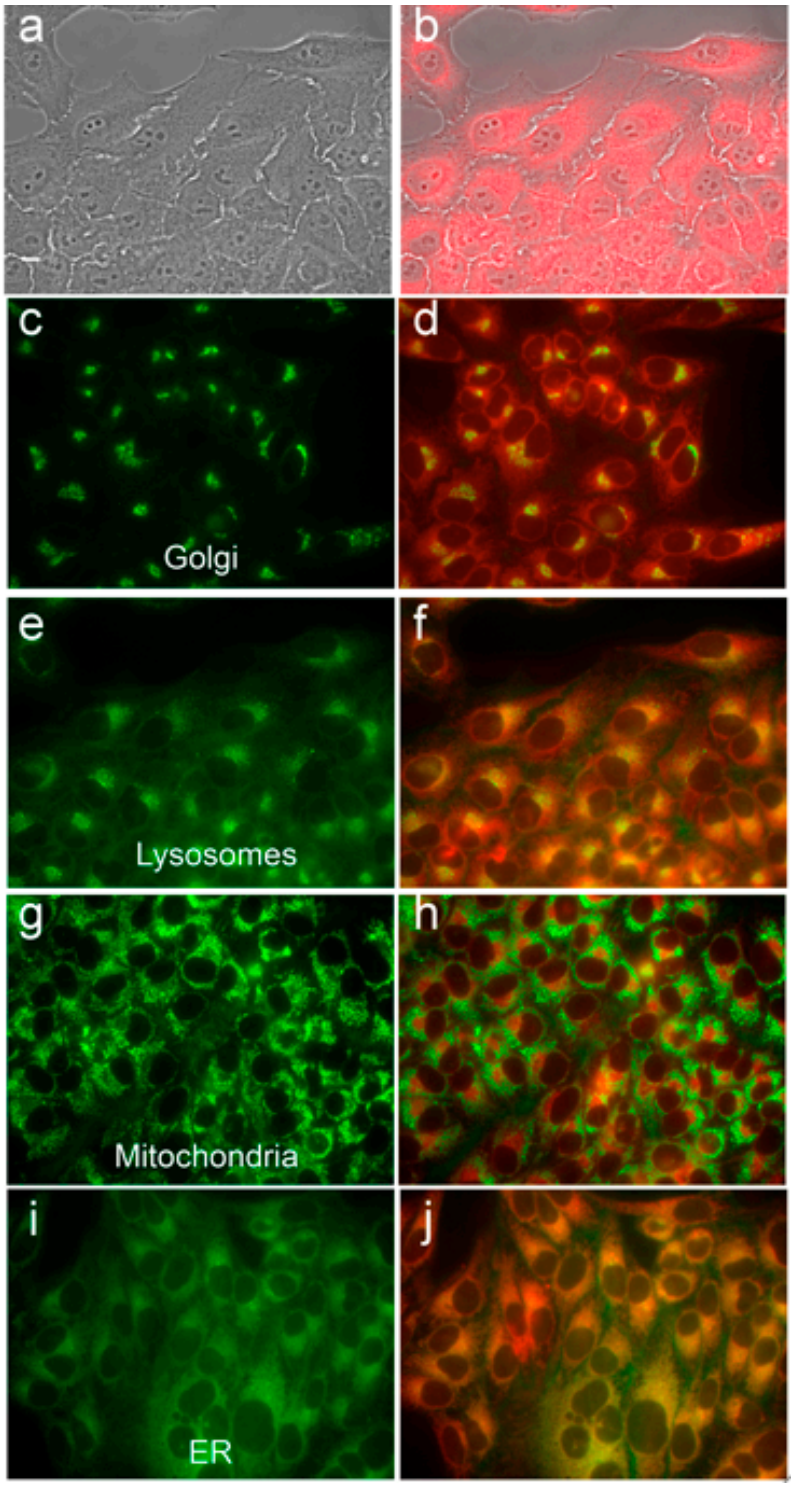

Figure 5.7 Intracellular localization of ZnPc **3.7a** in HEp2 cells at 10 μM for 24 h. (a) phase contrast; (b) Pc fluorescence; (c) BODIPY FL- C5-Ceramide fluorescence (Golgi label); (d) overlay with Pc; (e) LysoSensor fluorescence (lysosome label); f: overlay; (g) MitoTracker fluorescence (mitochondria label); (h) overlay; (i) ERTracker Green FM fluorescence (ER label); (j) overlay. Scale bar: 10 μm.

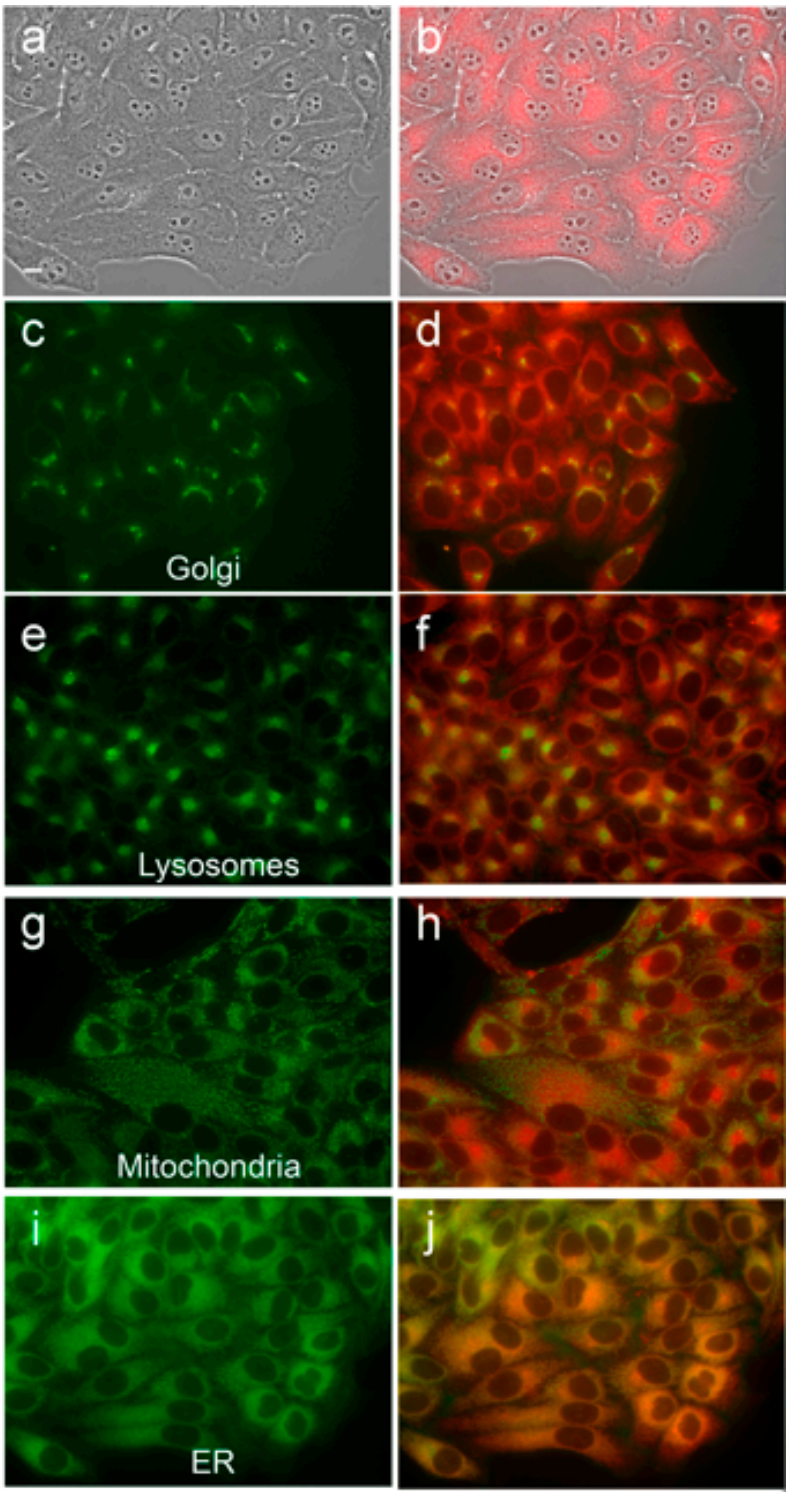

Figure 5.8 Intracellular localization of ZnPc **3.7b** in HEp2 cells at 10 μM for 24 h. (a) phase contrast; (b) Pc fluorescence; (c) BODIPY FL- C5-Ceramide fluorescence (Golgi label); (d) overlay with Pc; (e) LysoSensor fluorescence (lysosome label); f: overlay; (g) MitoTracker fluorescence (mitochondria label); (h) overlay; (i) ERTracker Green FM fluorescence (ER label); (j) overlay. Scale bar: 10 μm.

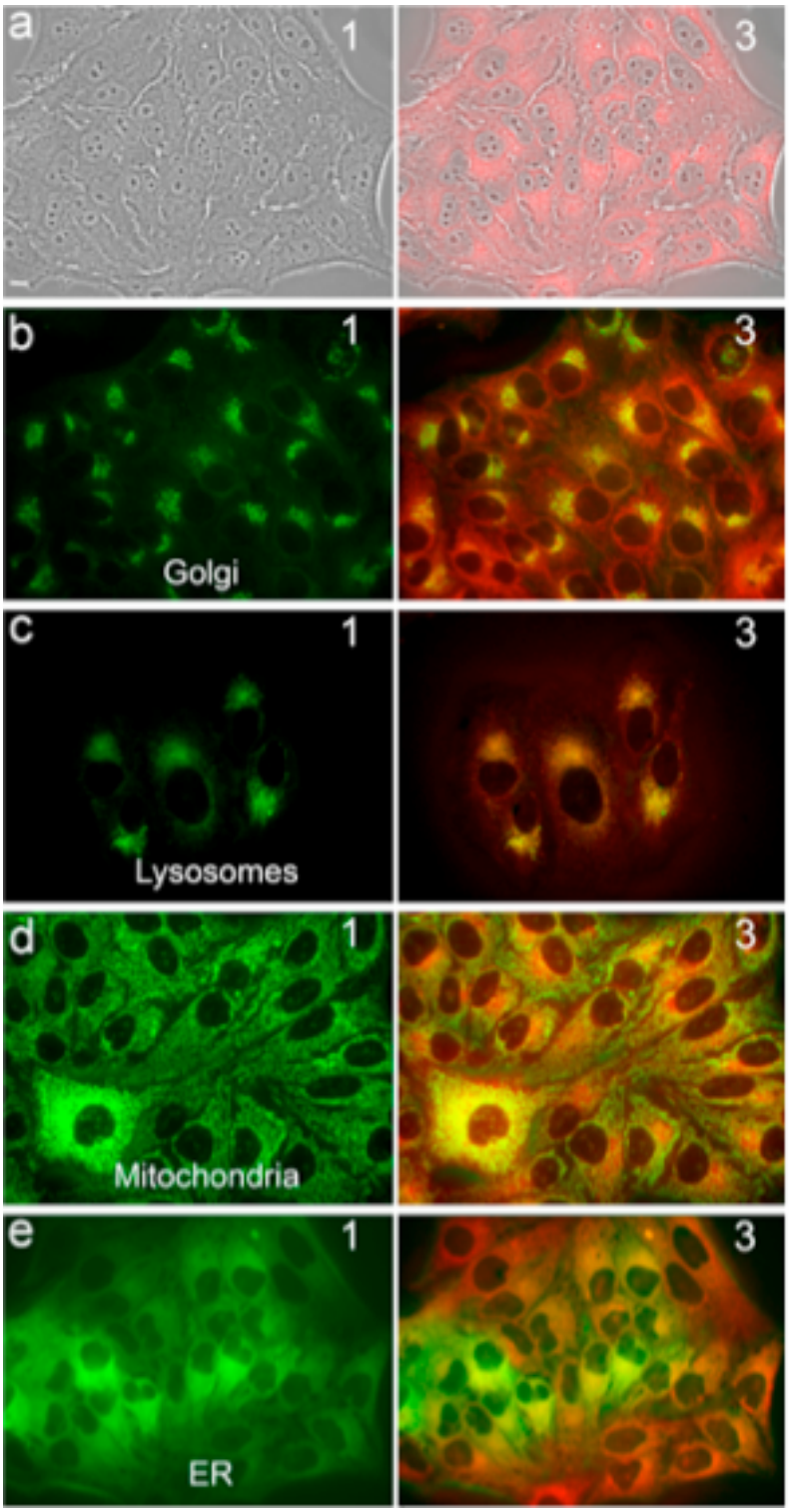

Figure 5.9 Intracellular localization of ZnPc **3.9b** in HEp2 cells at 10 μM for 24 h. (a) phase contrast; (b) Pc fluorescence; (c) BODIPY FL- C5-Ceramide fluorescence (Golgi label); (d) overlay with Pc; (e) LysoSensor fluorescence (lysosome label); f: overlay; (g) MitoTracker fluorescence (mitochondria label); (h) overlay; (i) ERTracker Green FM fluorescence (ER label); (j) overlay. Scale bar: 10 μm.

5.3 Conclusion

While benzyl ether bearing ZnPcs **3.7a** and **3.7b** were non-toxic to the human HEp2 cells, short oligoethyleneglycol-substituted ZnPcs **3.4a** and **3.9b** exhibited measurable toxicity to the cells. The ZnPc **3.7a**, bearing mono-hydroxyl and tri-diethylene glycol benzyl ether, was found to be the most phototoxic with an estimated IC_{50} of~0.6 μM. Tetra diethylene glycol benzyl ether substituted ZnPc **3.9b**, the least taken up by the cells, was the least phototoxic ($IC_{50\ of}$ ~ 8 μM) and the most toxic (IC_{50} of ~ 85 μM) to the carcinoma cells. The preferential sites of subcellular localization of the Pcs were found to be lysosomes and endoplasmic reticulum.

5.4 Experimental

Oligoethyleneglycol-substituted ZnPcs were evaluated in vitro by Mr. Tim Jensen in the Life Science Building at Louisiana State University.

Cell Culture

All tissue culture media and reagents were obtained from Invitrogen. HEp2 cells were obtained from ATCC and maintained in a 50:50 mixture of DMEM:Advanced MEM containing 5% FBS. Cells were subcultured biweekly to maintain subconfluent stocks.

Time-dependent Cellular Uptake

HEp2 cells were plated at 10000 per well in a Costar 96 well plate and allowed to grow overnight. Compound stocks were prepared in DMSO at a concentration of 10 mM. Compound was then diluted in medium to final working concentrations. Cells were exposed to 10 μM compound for 0, 1, 2, 4, 8, and 24 hours. Uptake was stopped by removing the loading medium and washing the cells with PBS. Cells were solubilized by the addition of 100 μL of 0.25% Triton X-100 (Calbiochem) in PBS. To determine compound concentration, fluorescence emission was read at 670/700 nm (excitation/emission) using a BMG FLUO star plate reader. Cell numbers were quantified using CyQuant reagent (Molecular Probes).

Cytotoxicity Assay

HEp2 cells were plated as described above and allowed 36-48h to attach. Cells were then exposed to various concentrations of compound up to 100 μM and incubated overnight. The loading medium was then removed and the cells fed medium containing CellTitre Blue (Promega) as per manufacturer's instructions. Cell viability was then measured by reading the fluorescence at 520/584 nm using a BMG FLUOstar plate reader. Signal was normalized to 100% viable (untreated cells) and 0% viable (cells treated with 0.2% saponin (Sigma)).

Phototoxicity Assay

HEp2 cells were prepared as per the cytotoxicity assay. After compound loading, the medium was removed and replaced with medium containing 50 mM HEPES pH 7.4. Cells were then placed on ice and exposed to light from a 100W halogen lamp filtered through a 610nm long pass filter (Chroma) for 10 minutes. An inverted plate lid filled with water to a depth of 5mm acted as an IR filter. The total light exposure was approximately 0.5 J/cm2. Cells were then returned to the incubator overnight and assayed for viability as described for the cytotoxicity assay.

Intracellular Localization

HEp2 cells were plated on LabTek 2 chamber coverslips and incubated overnight. Cells were then exposed to 10 μM of each Pc overnight. For co-localization experiments using organelle tracers, cells were incubated concurrently with compound the following morning for 30 minutes with the following organelle tracers: MitoTracker Green (Molecular Probes) 250 nM, LysoSensor Green (Molecular Probes) 50nM, DiOC6 (Molecular Probes) 5 μg/ml. Slides were then washed 3 times with growth medium and fed medium containing 50 mM HEPES pH 7.4. Fluorescent microscopy was performed using a Zeiss Labovert 200M inverted fluorescent microscope fitted with a standard FITC filter set (Ex/Em 470nm/540nm) for organelle tracers

and a 660nm/687nm set for compound detection (Chroma). Images were acquired with a Zeiss Axiocam MRM CCD camera fitted to the microscope.

5.5 References

(1) Dougherty, T. J. G., C. J.; Henderson, B. W.; Jori, G.; Kessel, D.; Koberlik, M.; Moan, J.; Peng Photodynamic Therapy *J. Natl. Cancer Inst.* **1998**, *90*, 889-905.

(2) Gray, M. J.; Lipson, R.; Maeck, J. V.; Parker, L.; Romeyn, D. Use of Hematoporphyrin Derivative in Detection and Management of Cervical Cancer - a Preliminary Report *Am. J. Obstet. Gynecol.* **1967**, *99*, 766-771.

(3) Ruiz-Moreno, J. M.; Tavolato, M.; Montero, J. A.; Alio, J. L. Choroidal neovascularization in myopic eyes after phakic refractive lens and iris-claw lens implantation *Eur. J. Ophthalmol.* **2004**, *14*, 159-162.

(4) Shah, A. R.; Del Priore, L. V. Progressive visual loss in subfoveal exudation in age-related macular degeneration: A meta-analysis using Lineweaver-Burke plots *Am. J. Ophthalmol.* **2007**, *143*, 83-89.

(5) Henderson, B. W.; Dougherty, T. J. How Does Photodynamic Therapy Work *Photochem. Photobiol.* **1992**, *55*, 145-157.

(6) Sternberg, E. D.; Dolphin, D.; Bruckner, C. Porphyrin-based photosensitizers for use in photodynamic therapy *Tetrahedron* **1998**, *54*, 4151-4202.

(7) Ochsner, M. Photophysical and photobiological processes in the photodynamic therapy of tumours *J. Photochem. Photobiol. B-Biol.* **1997**, *39*, 1-18.

(8) Anderson, C.; Hrabovsky, S.; McKinley, Y.; Tubesing, K.; Tang, H. P.; Dunbar, R.; Mukhtar, H.; Elmets, C. A. Phthalocyanine photodynamic therapy: Disparate effects of pharmacologic inhibitors on cutaneous photosensitivity and on tumor regression *Photochem. Photobiol.* **1997**, *65*, 895-901.

(9) Moan, J.; Berg, K. The Photodegradation of Porphyrins in Cells Can Be Used to Estimate the Lifetime of Singlet Oxygen *Photochem. Photobiol.* **1991**, *53*, 549-553.

(10) Biel, M. Photodynamic therapy and the treating of head and neck cancers *J. Clin. Laser Radia. Sur.* **1996**, *14*, 239-244.

(11) Lightdale, C. J.; Heier, S. K.; Marcon, N. E.; McCaughan, J. S.; Gerdes, H.; Overholt, B. F.; Sivak, M. V.; Stiegmann, G. V.; Nava, H. R. Photodynamic Therapy with Porfimer Sodium Versus Thermal Ablation Therapy with Nd-Yag Laser for Palliation of Esophageal Cancer - a Multicenter Randomized Trial *Gastrointest. Endosc.* **1995**, *42*, 507-512.

(12) Furuse, K.; Fukuoka, M.; Kato, H.; Horai, T.; Kubota, K.; Kodama, N.; Kusunoki, Y.; Takifuji, N.; Okunaka, T.; Konaka, C.; Wada, H.; Hayata, Y. A Prospective Phase-Ii Study

on Photodynamic Therapy with Photofrin-Ii for Centrally Located Early-Stage Lung-Cancer *J. Clin. Oncol.* **1993**, *11*, 1852-1857.

(13) Nseyo, U. O.; DeHaven, J.; Dougherty, T. J.; Potter, W. R.; Merrill, D. L.; Lundahl, S. L.; Lamm, D. L. Photodynamic therapy (PDT) in the treatment of patients with resistant superficial bladder cancer: A long term experience *J. Clin. Laser Med. Sur.* **1998**, *16*, 61-68.

(14) Muller, P. J.; Wilson, B. C. Photodynamic Therapy for Recurrent Supratentorial Gliomas *Semin. Surg. Oncol.* **1995**, *11*, 346-354.

(15) Dougherty, T. J. Studies on the Structure of Porphyrins Contained in Photofrin-Ii *Photochem. Photobiol.* **1987**, *46*, 569-573.

(16) Allison, B. A.; Crespo, M. T.; Jain, A. K.; Richter, A. M.; Hsiang, Y. N.; Levy, J. G. Delivery of benzoporphyrin derivative, a photosensitizer, into atherosclerotic plaque of watanabe heritable hyperlipidemic rabbits and balloon-injured New Zealand rabbits *Photochem. Photobiol.* **1997**, *65*, 877-883.

(17) Pandey, R. K. Recent advances in photodynamic therapy *J. Porphyr. Phthalocyanines* **2000**, *4*, 368-373.

(18) Moser, J. G. Porphyrins and phthalocyanines as model compounds for detoxification of tumor chemotherapeutic drugs *J. Porphyr. Phthalocyanines* **2000**, *4*, 129-135.

(19) Sibrian-Vazquez, M.; Jensen, T. J.; Fronczek, F. R.; Hammer, R. P.; Vicente, M. G. H. Synthesis and characterization of positively charged porphyrin-peptide conjugates *Bioconjugate Chem.* **2005**, *16*, 852-863.

(20) Gottumukkala, V.; Ongayi, O.; Baker, D. G.; Lomax, L. G.; Vicente, M. G. H. Synthesis, cellular uptake and animal toxicity of a tetra(carboranylphenyl)-tetrabenzoporphyrin *Bioorg. Med. Chem.* **2006**, *14*, 1871-1879.

(21) Sibrian-Vazquez, M.; Jensen, T. J.; Hammer, R. P.; Vicente, M. G. H. Peptide-mediated cell transport of water soluble porphyrin conjugates *J. Med. Chem.* **2006**, *49*, 1364-1372.

(22) Natioanal Cancer Institute Phase I Study of Photodynamic Therapy With Silicon Phthalocyanine 4 in Patients With Cutaneous Malignancies **2006**, 01/19/2006, http://www.cancer.gov/search/ViewClinicalTrials.aspxcdrid=68862&version=HealthProfessional&protocolsearchid=5481603.

(23) Natioanal Cancer Institute Phase I Study of Photodynamic Therapy Using Silicon Phthalocyanine 4 in Patients With Actinic Keratosis, Bowen's Disease, Squamous Cell or Basal Cell Skin Cancer, or Stage IA, IB, IIA, or IIB Mycosis Fungoides **2008,** http://www.cancer.gov/search/ViewClinicalTrials.aspx?cdrid=410675&version=HealthProfessional&protocolsearchid=5481603.

(24) Borgatti-Jeffreys, A.; Hooser, S. B.; Miller, M. A.; Lucroy, M. D. Phase I clinical trial of the use of zinc phthalocyanine tetrasulfonate as a photosensitizer for photodynamic therapy in dogs *Am. J. Vet. Res.* **2007**, *68*, 399-404.

(25) Hu, M.; Brasseur, N.; Yildiz, S. Z.; van Lier, J. E.; Leznoff, C. C. Hydroxyphthalocyanines as potential photodynamic agents for cancer therapy *J. Med. Chem.* **1998**, *41*, 1789-1802.

(26) Li, H. R.; Jensen, T. J.; Fronczek, F. R.; Vicente, M. G. H. Syntheses and properties of a series of cationic water-soluble phthalocyanines *J. Med. Chem.* **2008**, *51*, 502-511.

(27) Cauchon, N.; Tian, H. J.; Langlois, J.; La Madeleine, C.; Martin, S.; All, H.; Hunting, D.; van Lier, J. E. Structure-photodynamic activity relationships of substituted zinc trisulfophthalocyanines *Bioconjugate Chem.* **2005**, *16*, 80-89.

(28) Liu, W.; Jensen, T. J.; Fronczek, F. R.; Hammer, R. P.; Smith, K. M.; Vicente, M. G. H. Synthesis and cellular studies of nonaggregated water-soluble phthalocyanines *J. Med. Chem.* **2005**, *48*, 1033-1041.

(29) Sibrian-Vazquez, M.; Ortiz, J.; Nesterova, I. V.; Fernandez-Lazaro, F.; Sastre-Santos, A.; Soper, S. A.; Vicente, M. G. H. Synthesis and properties of cell-targeted Zn(II)-phthalocyanine-peptide conjugates *Bioconjugate Chem.* **2007**, *18*, 410-420.

(30) Sibrian-Vazquez, M.; Jensen, T. J.; Vicente, M. G. H. Synthesis and cellular studies of PEG-functionalized meso-tetraphenylporphyrins *J. Photochem. Photobiol. B-Biol.* **2007**, *86*, 9-21.

Appendix A- X-Ray Diffraction Data

A.1 Single Crystal X-ray Diffraction Data

N-(3,4-Dicyanophenyl)-4-nitrobenzamide (2.6)

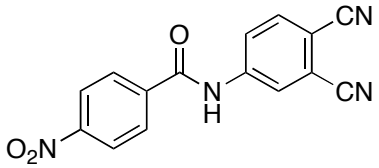

Crystal data

$C_{15}H_8N_4O_3 \cdot C_3H_6O_1$
$M_r = 350.33$

$F_{000} = 364$
$D_x = 1.387$ Mg m^{-3}

Triclinic, $P\bar{1}$

Mo $K\alpha$ radiation
$\lambda = 0.71073$ Å

Hall symbol: -P 1
$a = 7.901$ (5) Å
$b = 10.006$ (6) Å
$c = 11.698$ (10) Å
$\alpha = 107.47$ (2)°
$\beta = 100.06$ (2)°
$\gamma = 100.96$ (2)°
$V = 839.1$ (10) Å^3
$Z = 2$

Cell parameters from 2870 reflections

$\theta = 2.5$–26.0°
$\mu = 0.10$ mm^{-1}
$T = 110$ K

Lath, colorless
0.50 × 0.22 × 0.01 mm

Data collection

KappaCCD (with Oxford Cryostream) Diffractometer 3207 independent reflections

Radiation source: fine-focus sealed tube
Monochromator: graphite

$T = 110$ K
$P =$ kPa
ω scans with κ offsets
Absorption correction: none
10559 measured reflections

1196 reflections with $I > 2\sigma(I)$
$R_{int} = 0.125$
$\theta_{max} = 26.1$°
$\theta_{min} = 2.7$°
$h = -9 \rightarrow 9$
$k = -12 \rightarrow 12$
$l = -14 \rightarrow 14$

Refinement

Refinement on F^2 — Secondary atom site location: difference Fourier map
Least-squares matrix: full — Hydrogen site location: inferred from neighbouring sites
$R[F^2 > 2\sigma(F^2)] = 0.105$ — H-atom parameters constrained

$wR(F^2) = 0.317$ — $w = 1/[\sigma^2(F_o^2) + (0.0878P)^2 + 2.757P]$ where $P = (F_o^2 + 2F_c^2)/3$

$S = 1.05$ — $(\Delta/\sigma)_{max} < 0.001$
3207 reflections — $\Delta\rho_{max} = 0.34$ e Å^{-3}
237 parameters — $\Delta\rho_{min} = -0.35$ e Å^{-3}
Extinction correction: none
Primary atom site location: structure-invariant direct methods

Refinement: Refinement of F^2 against ALL reflections. The weighted R-factor wR and goodness of fit S are based on F^2, conventional R-factors R are based on F, with F set to zero for negative F^2. The threshold expression of $F^2 > 2\text{sigma}(F^2)$ is used only for calculating R-factors(gt) etc. and is not relevant to the choice of reflections for refinement. R-factors based on F^2 are statistically about twice as large as those based on F, and R- factors based on ALL data will be even larger.

Fractional atomic coordinates and isotropic or equivalent isotropic displacement parameters (Å^2)

	x	*y*	*z*	U_{iso}*/U_{eq}
O1	0.2820 (7)	0.7646 (6)	0.5841 (5)	0.0445 (15)
O2	0.6866 (8)	0.8975 (7)	0.1425 (6)	0.0650 (19)
O3	0.5433 (8)	0.6875 (7)	0.0143 (6)	0.0632 (18)
N1	0.2723 (7)	0.5229 (6)	0.5089 (6)	0.0362 (17)
H1N	0.2897	0.4551	0.4473	0.043*
N2	0.5892 (10)	0.7803 (9)	0.1190 (8)	0.051 (2)
N3	−0.1028 (9)	0.0235 (8)	0.6149 (7)	0.057 (2)
N4	−0.0310 (10)	0.2994 (7)	0.9457 (8)	0.057 (2)
C1	0.3078 (10)	0.6611 (9)	0.5068 (8)	0.041 (2)
C2	0.3868 (9)	0.6832 (8)	0.4027 (7)	0.035 (2)
C3	0.4972 (10)	0.8172 (8)	0.4240 (8)	0.041 (2)
H3	0.5254	0.8891	0.5039	0.049*
C4	0.5672 (10)	0.8500 (9)	0.3345 (8)	0.042 (2)
H4	0.6461	0.9418	0.3511	0.050*
C5	0.5190 (9)	0.7450 (8)	0.2190 (8)	0.0349 (19)

C6	0.4094 (10)	0.6102 (8)	0.1892 (8)	0.045 (2)
H6	0.3806	0.5402	0.1084	0.054*
C7	0.3409 (10)	0.5803 (9)	0.2854 (8)	0.043 (2)
H7	0.2624	0.4885	0.2692	0.052*
C8	0.2106 (10)	0.4803 (9)	0.6010 (8)	0.040 (2)
C9	0.1234 (9)	0.3346 (8)	0.5721 (7)	0.0358 (19)
H9	0.1061	0.2673	0.4913	0.043*
C10	0.0637 (10)	0.2896 (8)	0.6599 (8)	0.037 (2)
C11	0.0864 (10)	0.3873 (8)	0.7795 (8)	0.040 (2)
C12	0.1759 (10)	0.5315 (8)	0.8095 (8)	0.045 (2)
H12	0.1961	0.5974	0.8913	0.054*
C13	0.2352 (10)	0.5793 (8)	0.7221 (8)	0.041 (2)
H13	0.2930	0.6787	0.7424	0.049*
C14	−0.0299 (11)	0.1393 (10)	0.6326 (8)	0.042 (2)
C15	0.0211 (12)	0.3379 (9)	0.8719 (9)	0.049 (2)
O4	0.3267 (7)	0.2759 (6)	0.3298 (5)	0.0450 (15)
C16	0.2448 (12)	0.1726 (9)	0.2362 (9)	0.043 (2)
C17	0.3360 (11)	0.0683 (8)	0.1711 (8)	0.050 (2)
H17A	0.4638	0.1013	0.2105	0.076*
H17B	0.3168	0.0619	0.0843	0.076*
H17C	0.2879	−0.0274	0.1752	0.076*
C18	0.0522 (12)	0.1477 (11)	0.1784 (9)	0.069 (3)
H18A	−0.0022	0.2053	0.2381	0.103*
H18B	−0.0078	0.0446	0.1540	0.103*
H18C	0.0401	0.1769	0.1052	0.103*

Atomic displacement parameters (Å²)

	U^{11}	U^{22}	U^{33}	U^{12}	U^{13}	U^{23}
O1	0.044 (3)	0.037 (3)	0.051 (4)	0.012 (3)	0.011 (3)	0.012 (3)
O2	0.075 (4)	0.057 (4)	0.056 (4)	−0.005 (4)	0.021 (4)	0.019 (4)
O3	0.078 (4)	0.050 (4)	0.052 (5)	0.003 (3)	0.016 (4)	0.011 (4)
N1	0.038 (4)	0.030 (4)	0.046 (5)	0.013 (3)	0.017 (3)	0.013 (3)
N2	0.051 (5)	0.044 (5)	0.058 (6)	0.013 (4)	0.010 (4)	0.019 (5)
N3	0.057 (5)	0.053 (5)	0.057 (6)	0.004 (4)	0.017 (4)	0.017 (4)
N4	0.074 (5)	0.035 (4)	0.065 (6)	0.011 (4)	0.030 (5)	0.014 (4)
C1	0.032 (5)	0.042 (5)	0.047 (6)	0.009 (4)	0.005 (4)	0.017 (5)
C2	0.030 (4)	0.032 (5)	0.036 (5)	0.004 (4)	0.006 (4)	0.006 (4)
C3	0.035 (4)	0.030 (5)	0.045 (6)	−0.002 (4)	0.005 (4)	0.006 (4)
C4	0.042 (5)	0.036 (5)	0.048 (6)	0.010 (4)	0.011 (4)	0.016 (5)
C5	0.031 (4)	0.034 (5)	0.047 (6)	0.011 (4)	0.016 (4)	0.020 (4)

C6	0.053 (5)	0.027 (5)	0.048 (6)	0.003 (4)	0.009 (5)	0.008 (4)
C7	0.041 (5)	0.034 (5)	0.051 (6)	0.003 (4)	0.006 (4)	0.018 (5)
C8	0.037 (5)	0.041 (5)	0.040 (6)	0.012 (4)	0.009 (4)	0.012 (4)
C9	0.040 (5)	0.030 (5)	0.030 (5)	0.007 (4)	0.008 (4)	0.002 (4)
C10	0.037 (5)	0.035 (5)	0.040 (6)	0.018 (4)	0.011 (4)	0.010 (4)
C11	0.033 (4)	0.030 (5)	0.051 (6)	−0.004 (4)	0.010 (4)	0.013 (4)
C12	0.043 (5)	0.036 (5)	0.047 (6)	0.005 (4)	0.011 (4)	0.006 (4)
C13	0.045 (5)	0.036 (5)	0.045 (6)	0.014 (4)	0.016 (4)	0.016 (4)
C14	0.046 (5)	0.038 (5)	0.043 (6)	0.003 (4)	0.007 (4)	0.021 (4)
C15	0.064 (6)	0.036 (5)	0.051 (6)	0.021 (4)	0.013 (5)	0.016 (5)
O4	0.055 (4)	0.034 (3)	0.051 (4)	0.013 (3)	0.015 (3)	0.020 (3)
C16	0.057 (6)	0.031 (5)	0.050 (6)	0.014 (4)	0.010 (5)	0.025 (5)
C17	0.052 (5)	0.033 (5)	0.057 (6)	0.006 (4)	0.017 (5)	0.005 (4)
C18	0.066 (7)	0.084 (8)	0.067 (7)	0.028 (6)	0.019 (6)	0.035 (6)

Geometric parameters (Å, °)

O1—C1	1.231 (9)	C8—C9	1.398 (10)
O2—N2	1.196 (8)	C8—C13	1.419 (11)
O3—N2	1.236 (9)	C9—C10	1.360 (10)
N1—C1	1.366 (9)	C9—H9	0.9500
N1—C8	1.400 (9)	C10—C11	1.404 (10)
N1—H1N	0.8800	C10—C14	1.455 (11)
N2—C5	1.484 (10)	C11—C12	1.387 (10)
N3—C14	1.131 (9)	C11—C15	1.449 (12)
N4—C15	1.152 (10)	C12—C13	1.368 (10)
C1—C2	1.515 (11)	C12—H12	0.9500
C2—C3	1.379 (10)	C13—H13	0.9500
C2—C7	1.382 (10)	O4—C16	1.227 (9)
C3—C4	1.360 (11)	C16—C17	1.480 (11)
C3—H3	0.9500	C16—C18	1.493 (12)
C4—C5	1.375 (11)	C17—H17A	0.9800
C4—H4	0.9500	C17—H17B	0.9800
C5—C6	1.364 (10)	C17—H17C	0.9800
C6—C7	1.415 (11)	C18—H18A	0.9800
C6—H6	0.9500	C18—H18B	0.9800
C7—H7	0.9500	C18—H18C	0.9800
C1—N1—C8	125.4 (7)	C10—C9—H9	120.1
C1—N1—H1N	117.3	C8—C9—H9	120.1
C8—N1—H1N	117.3	C9—C10—C11	121.1 (7)
O2—N2—O3	122.7 (8)	C9—C10—C14	121.3 (8)
O2—N2—C5	118.9 (8)	C11—C10—C14	117.6 (7)

O3—N2—C5	118.5 (8)	C12—C11—C10	119.4 (8)
O1—C1—N1	123.9 (7)	C12—C11—C15	120.1 (8)
O1—C1—C2	120.1 (7)	C10—C11—C15	120.5 (7)
N1—C1—C2	115.9 (7)	C13—C12—C11	120.4 (8)
C3—C2—C7	118.9 (7)	C13—C12—H12	119.8
C3—C2—C1	117.8 (7)	C11—C12—H12	119.8
C7—C2—C1	123.0 (7)	C12—C13—C8	120.0 (7)
C4—C3—C2	122.2 (8)	C12—C13—H13	120.0
C4—C3—H3	118.9	C8—C13—H13	120.0
C2—C3—H3	118.9	N3—C14—C10	177.9 (9)
C3—C4—C5	117.3 (8)	N4—C15—C11	179.5 (9)
C3—C4—H4	121.3	O4—C16—C17	120.9 (8)
C5—C4—H4	121.3	O4—C16—C18	122.9 (8)
C6—C5—C4	124.5 (8)	C17—C16—C18	116.2 (8)
C6—C5—N2	117.3 (8)	C16—C17—H17A	109.5
C4—C5—N2	118.1 (7)	C16—C17—H17B	109.5
C5—C6—C7	116.2 (8)	H17A—C17—H17B	109.5
C5—C6—H6	121.9	C16—C17—H17C	109.5
C7—C6—H6	121.9	H17A—C17—H17C	109.5
C2—C7—C6	120.8 (7)	H17B—C17—H17C	109.5
C2—C7—H7	119.6	C16—C18—H18A	109.5
C6—C7—H7	119.6	C16—C18—H18B	109.5
C9—C8—N1	118.4 (7)	H18A—C18—H18B	109.5
C9—C8—C13	119.3 (7)	C16—C18—H18C	109.5
N1—C8—C13	122.3 (7)	H18A—C18—H18C	109.5
C10—C9—C8	119.8 (8)	H18B—C18—H18C	109.5
C8—N1—C1—O1	−3.2 (12)	C1—N1—C8—C9	158.3 (7)
C8—N1—C1—C2	175.5 (7)	C1—N1—C8—C13	−22.5 (11)
O1—C1—C2—C3	28.2 (11)	N1—C8—C9—C10	179.3 (7)
N1—C1—C2—C3	−150.6 (7)	C13—C8—C9—C10	0.0 (11)
O1—C1—C2—C7	−146.0 (8)	C8—C9—C10—C11	0.6 (11)
N1—C1—C2—C7	35.2 (11)	C8—C9—C10—C14	179.0 (7)
C7—C2—C3—C4	−2.2 (12)	C9—C10—C11—C12	−1.9 (11)
C1—C2—C3—C4	−176.6 (7)	C14—C10—C11—C12	179.6 (7)
C2—C3—C4—C5	2.0 (12)	C9—C10—C11—C15	179.7 (8)
C3—C4—C5—C6	−1.4 (12)	C14—C10—C11—C15	1.2 (11)
C3—C4—C5—N2	178.1 (7)	C10—C11—C12—C13	2.6 (11)
O2—N2—C5—C6	−179.5 (7)	C15—C11—C12—C13	−178.9 (8)
O3—N2—C5—C6	1.1 (10)	C11—C12—C13—C8	−2.1 (12)
O2—N2—C5—C4	1.0 (10)	C9—C8—C13—C12	0.8 (11)
O3—N2—C5—C4	−178.4 (7)	N1—C8—C13—C12	−178.5 (7)

C4—C5—C6—C7	0.9 (12)	C9—C10—C14—N3	176 (100)
N2—C5—C6—C7	−178.6 (7)	C11—C10—C14—N3	−6(24)
C3—C2—C7—C6	1.6 (11)	C12—C11—C15—N4	35 (100)
C1—C2—C7—C6	175.7 (7)	C10—C11—C15—N4	−146 (100)
C5—C6—C7—C2	−1.0 (11)		

Hydrogen-bond geometry (Å, °)

D—H···*A*	*D*—H	H···*A*	*D*···*A*	*D*—H···*A*
N1—H1N···O4	0.88	2.01	2.879 (8)	168

A.2 Single Crystal X-ray Diffraction Data

3-(4-(2-(2-Methoxyethoxy)ethoxy)phenoxy)phthalonitrile (2.13)

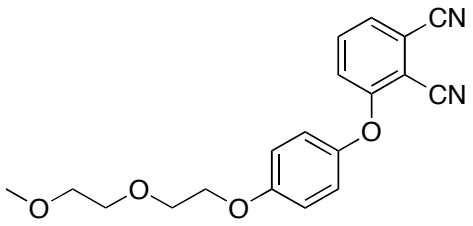

Crystal data

$C_{19}H_{18}N_2O_4$
$M_r = 338.35$

$D_x = 1.323$ Mg m^{-3}

Monoclinic, $P2_1/c$

Mo $K\alpha$ radiation
$\lambda = 0.71073$ Å

Hall symbol: -P 2ybc
$a = 9.297$ (3) Å
$b = 34.275$ (14) Å
$c = 10.672$ (4) Å
$\beta = 92.88$ (2)°
$V = 3396$ (2) Å^3
$Z = 8$
$F_{000} = 1424$

Cell parameters from 3513 reflections
$\theta = 2.5$–$25.6°$
$\mu = 0.09$ mm^{-1}
$T = 90$ K

Prism, colorless
0.23 × 0.12 × 0.07 mm

Data collection

Nonius KappaCCD (with Oxford Cryostream) Diffractometer
Radiation source: fine-focus sealed tube
Monochromator: graphite

$T = 90$ K
$P =$ kPa
ω scans with κ offsets
Absorption correction: none
12472 measured reflections

5664 independent reflections

3059 reflections with $I > 2\sigma(I)$
$R_{int} = 0.036$
$\theta_{max} = 25.7°$
$\theta_{min} = 2.6°$
$h = -11 \rightarrow 11$
$k = -26 \rightarrow 41$
$l = -13 \rightarrow 13$

Refinement

Refinement on F^2 — Secondary atom site location: difference Fourier map
Least-squares matrix: full — Hydrogen site location: inferred from neighbouring sites
$R[F^2 > 2\sigma(F^2)] = 0.076$ — H-atom parameters constrained
$w = 1/[\sigma^2(F_o^2) + (0.0636P)^2 + 4.2274P]$
where $P = (F_o^2 + 2F_c^2)/3$

$wR(F^2) = 0.183$
$S = 1.01$ — $(\Delta/\sigma)_{max} < 0.001$
5664 reflections — $\Delta\rho_{max} = 0.39$ e Å^{-3}
453 parameters — $\Delta\rho_{min} = -0.29$ e Å^{-3}
constraints — Extinction correction: none
Primary atom site location: — structure-invariant direct methods

Refinement: Refinement of F^2 against ALL reflections. The weighted R-factor wR and goodness of fit S are based on F^2, conventional R-factors R are based on F, with F set to zero for negative F^2. The threshold expression of $F^2 > 2$sigma(F^2) is used only for calculating R-factors(gt) etc. and is not relevant to the choice of reflections for refinement. R-factors based on F^2 are statistically about twice as large as those based on F, and R- factors based on ALL data will be even larger.

Fractional atomic coordinates and isotropic or equivalent isotropic displacement parameters (Å^2)

	x	*y*	*z*	U_{iso}*/U_{eq}
O1	0.4578 (3)	0.64053 (8)	0.6202 (2)	0.0189 (7)
O2	0.5984 (3)	0.51493 (8)	0.3219 (3)	0.0247 (7)
O3	0.5488 (3)	0.45068 (8)	0.1254 (3)	0.0237 (7)
O4	0.4278 (3)	0.39733 (8)	−0.0564 (3)	0.0247 (7)
O5	0.9424 (3)	0.64507 (8)	0.6236 (3)	0.0229 (7)
O6	1.1296 (3)	0.51786 (9)	0.3595 (3)	0.0277 (8)
O7	1.0284 (3)	0.44376 (9)	0.1386 (3)	0.0249 (7)
O8	0.9455 (3)	0.40452 (9)	−0.0927 (3)	0.0313 (8)
N1	0.2499 (4)	0.68983 (11)	0.8296 (4)	0.0265 (9)
N2	0.3336 (4)	0.80079 (11)	0.7586 (3)	0.0248 (9)
N3	0.7560 (4)	0.69481 (11)	0.8401 (4)	0.0282 (9)
N4	0.8383 (4)	0.80545 (11)	0.7626 (3)	0.0259 (9)
C1	0.4945 (4)	0.67772 (12)	0.5911 (4)	0.0141 (9)
C2	0.4286 (4)	0.70693 (11)	0.6599 (3)	0.0128 (9)
C3	0.4595 (4)	0.74624 (12)	0.6365 (4)	0.0160 (10)
C4	0.5560 (4)	0.75609 (12)	0.5470 (4)	0.0207 (10)
H4	0.5765	0.7827	0.5304	0.025*
C5	0.6222 (4)	0.72669 (12)	0.4818 (4)	0.0186 (10)

H5	0.6888	0.7334	0.4207	0.022*
C6	0.5935 (4)	0.68816 (12)	0.5038 (4)	0.0173 (10)
H6	0.6415	0.6685	0.4591	0.021*
C7	0.3296 (4)	0.69674 (12)	0.7536 (4)	0.0175 (10)
C8	0.3897 (4)	0.77667 (12)	0.7055 (4)	0.0178 (10)
C9	0.4947 (4)	0.60973 (12)	0.5395 (4)	0.0170 (10)
C10	0.4547 (4)	0.61082 (12)	0.4132 (4)	0.0215 (10)
H10	0.4056	0.6329	0.3783	0.026*
C11	0.4873 (4)	0.57906 (12)	0.3370 (4)	0.0197 (10)
H11	0.4613	0.5795	0.2497	0.024*
C12	0.5575 (4)	0.54722 (12)	0.3898 (4)	0.0183 (10)
C13	0.5927 (4)	0.54589 (12)	0.5166 (4)	0.0214 (10)
H13	0.6381	0.5234	0.5523	0.026*
C14	0.5616 (4)	0.57756 (13)	0.5923 (4)	0.0242 (11)
H14	0.5864	0.5769	0.6797	0.029*
C15	0.5795 (5)	0.51800 (13)	0.1867 (4)	0.0273 (11)
H15A	0.6259	0.5421	0.1574	0.033*
H15B	0.4757	0.5191	0.1614	0.033*
C16	0.6476 (5)	0.48277 (13)	0.1295 (4)	0.0271 (11)
H16A	0.6753	0.4891	0.0435	0.033*
H16B	0.7358	0.4755	0.1799	0.033*
C17	0.6189 (5)	0.41649 (12)	0.0838 (4)	0.0251 (11)
H17A	0.6875	0.4070	0.1510	0.030*
H17B	0.6742	0.4228	0.0096	0.030*
C18	0.5119 (5)	0.38546 (12)	0.0508 (4)	0.0241 (11)
H18A	0.5621	0.3607	0.0333	0.029*
H18B	0.4492	0.3810	0.1218	0.029*
C19	0.3481 (5)	0.36593 (13)	−0.1132 (4)	0.0314 (12)
H19A	0.4145	0.3475	−0.1504	0.047*
H19B	0.2808	0.3762	−0.1788	0.047*
H19C	0.2941	0.3525	−0.0495	0.047*
C20	0.9851 (4)	0.68163 (13)	0.5949 (4)	0.0189 (10)
C21	0.9266 (4)	0.71158 (12)	0.6650 (4)	0.0165 (10)
C22	0.9610 (4)	0.75067 (12)	0.6382 (4)	0.0155 (10)
C23	1.0545 (4)	0.75966 (12)	0.5447 (4)	0.0187 (10)
H23	1.0774	0.7860	0.5269	0.022*
C24	1.1135 (4)	0.72959 (13)	0.4785 (4)	0.0209 (10)
H24	1.1790	0.7355	0.4157	0.025*
C25	1.0794 (4)	0.69101 (13)	0.5013 (4)	0.0209 (10)
H25	1.1201	0.6708	0.4533	0.025*
C26	0.8315 (5)	0.70187 (12)	0.7620 (4)	0.0191 (10)

C27	0.8933 (4)	0.78140 (13)	0.7080 (4)	0.0190 (10)
C28	0.9907 (4)	0.61353 (12)	0.5514 (4)	0.0202 (10)
C29	1.1177 (5)	0.59547 (13)	0.5875 (4)	0.0262 (11)
H29	1.1747	0.6050	0.6573	0.031*
C30	1.1619 (5)	0.56336 (13)	0.5216 (4)	0.0255 (11)
H30	1.2507	0.5509	0.5446	0.031*
C31	1.0759 (4)	0.54941 (12)	0.4216 (4)	0.0231 (11)
C32	0.9472 (5)	0.56755 (13)	0.3882 (4)	0.0290 (12)
H32	0.8878	0.5578	0.3202	0.035*
C33	0.9045 (5)	0.60022 (13)	0.4545 (4)	0.0284 (11)
H33	0.8162	0.6130	0.4321	0.034*
C34	1.0415 (5)	0.50091 (14)	0.2631 (4)	0.0307 (12)
H34A	1.0263	0.5193	0.1922	0.037*
H34B	0.9465	0.4938	0.2945	0.037*
C35	1.1208 (5)	0.46483 (13)	0.2221 (4)	0.0299 (12)
H35A	1.2092	0.4724	0.1802	0.036*
H35B	1.1489	0.4485	0.2959	0.036*
C36	1.1006 (5)	0.41072 (13)	0.0911 (4)	0.0274 (11)
H36A	1.1469	0.3958	0.1616	0.033*
H36B	1.1768	0.4194	0.0359	0.033*
C37	0.9951 (5)	0.38516 (12)	0.0187 (4)	0.0255 (11)
H37A	1.0421	0.3603	−0.0028	0.031*
H37B	0.9127	0.3791	0.0706	0.031*
C38	0.8577 (5)	0.37946 (14)	−0.1711 (4)	0.0362 (13)
H38A	0.9160	0.3578	−0.2002	0.054*
H38B	0.8181	0.3942	−0.2436	0.054*
H38C	0.7786	0.3692	−0.1235	0.054*

Atomic displacement parameters (Å²)

	U^{11}	U^{22}	U^{33}	U^{12}	U^{13}	U^{23}
O1	0.0264 (16)	0.0137 (16)	0.0172 (16)	0.0018 (13)	0.0071 (13)	−0.0024 (13)
O2	0.0383 (18)	0.0171 (17)	0.0191 (17)	0.0052 (15)	0.0058 (14)	0.0002 (14)
O3	0.0265 (17)	0.0202 (17)	0.0245 (17)	0.0028 (14)	0.0026 (14)	−0.0061 (14)
O4	0.0334 (17)	0.0170 (16)	0.0233 (17)	−0.0009 (14)	−0.0039 (14)	−0.0031 (13)
O5	0.0314 (18)	0.0166 (17)	0.0217 (17)	−0.0039 (14)	0.0110 (14)	−0.0036 (13)
O6	0.0286 (17)	0.0236 (18)	0.0308 (18)	0.0033 (15)	0.0024 (15)	−0.0102 (15)
O7	0.0205 (15)	0.0265 (18)	0.0275 (18)	0.0061 (14)	−0.0016 (14)	−0.0121 (14)
O8	0.0352 (18)	0.0290 (19)	0.0290 (19)	−0.0048 (16)	−0.0043 (15)	−0.0079 (16)
N1	0.026 (2)	0.026 (2)	0.028 (2)	0.0026 (18)	0.0064 (19)	0.0016 (18)
N2	0.025 (2)	0.023 (2)	0.027 (2)	0.0005 (18)	0.0043 (17)	0.0020 (18)

N3	0.031 (2)	0.026 (2)	0.029 (2)	0.0033 (19)	0.0120 (19)	0.0016 (18)
N4	0.031 (2)	0.020 (2)	0.027 (2)	0.0026 (19)	0.0064 (18)	0.0026 (18)
C1	0.014 (2)	0.014 (2)	0.013 (2)	−0.0039 (18)	0.0001 (18)	0.0020 (18)
C2	0.012 (2)	0.013 (2)	0.013 (2)	0.0003 (18)	0.0022 (18)	0.0032 (18)
C3	0.014 (2)	0.019 (2)	0.014 (2)	−0.0018 (19)	−0.0014 (19)	−0.0017 (19)
C4	0.023 (2)	0.016 (2)	0.024 (3)	−0.005 (2)	0.001 (2)	0.000 (2)
C5	0.015 (2)	0.023 (3)	0.018 (2)	−0.003 (2)	0.0049 (19)	−0.001 (2)
C6	0.020 (2)	0.019 (2)	0.013 (2)	0.001 (2)	0.0038 (19)	−0.0066 (19)
C7	0.021 (2)	0.012 (2)	0.020 (2)	0.0025 (19)	0.000 (2)	−0.0043 (19)
C8	0.019 (2)	0.014 (2)	0.021 (2)	−0.002 (2)	0.002 (2)	0.002 (2)
C9	0.018 (2)	0.012 (2)	0.022 (3)	0.0012 (19)	0.0087 (19)	−0.0058 (19)
C10	0.025 (2)	0.020 (2)	0.020 (2)	0.004 (2)	0.001 (2)	0.001 (2)
C11	0.021 (2)	0.023 (2)	0.015 (2)	0.004 (2)	−0.0004 (19)	−0.007 (2)
C12	0.021 (2)	0.015 (2)	0.019 (2)	−0.001 (2)	0.0059 (19)	−0.0039 (19)
C13	0.031 (3)	0.013 (2)	0.021 (3)	0.004 (2)	0.003 (2)	0.001 (2)
C14	0.028 (3)	0.027 (3)	0.018 (2)	0.001 (2)	0.003 (2)	−0.003 (2)
C15	0.041 (3)	0.025 (3)	0.016 (2)	0.000 (2)	0.002 (2)	−0.004 (2)
C16	0.033 (3)	0.025 (3)	0.023 (3)	0.000 (2)	0.006 (2)	−0.009 (2)
C17	0.028 (3)	0.019 (2)	0.028 (3)	0.004 (2)	0.000 (2)	−0.007 (2)
C18	0.033 (3)	0.017 (2)	0.023 (3)	0.007 (2)	0.000 (2)	0.000 (2)
C19	0.037 (3)	0.026 (3)	0.031 (3)	−0.009 (2)	0.001 (2)	−0.008 (2)
C20	0.017 (2)	0.023 (3)	0.018 (2)	−0.001 (2)	0.0014 (19)	0.001 (2)
C21	0.014 (2)	0.021 (2)	0.015 (2)	0.0038 (19)	0.0023 (18)	−0.0011 (19)
C22	0.016 (2)	0.014 (2)	0.016 (2)	0.0021 (19)	−0.0029 (19)	−0.0012 (19)
C23	0.021 (2)	0.019 (2)	0.016 (2)	−0.002 (2)	0.003 (2)	0.0038 (19)
C24	0.020 (2)	0.027 (3)	0.016 (2)	−0.003 (2)	0.0033 (19)	0.001 (2)
C25	0.020 (2)	0.024 (3)	0.018 (2)	0.000 (2)	−0.001 (2)	0.001 (2)
C26	0.021 (2)	0.014 (2)	0.022 (3)	0.003 (2)	0.001 (2)	−0.002 (2)
C27	0.015 (2)	0.020 (3)	0.021 (3)	−0.001 (2)	−0.003 (2)	0.007 (2)
C28	0.020 (2)	0.020 (2)	0.021 (2)	−0.001 (2)	0.009 (2)	−0.001 (2)
C29	0.029 (3)	0.028 (3)	0.022 (3)	0.000 (2)	0.003 (2)	−0.004 (2)
C30	0.026 (2)	0.024 (3)	0.027 (3)	−0.002 (2)	−0.001 (2)	0.000 (2)
C31	0.022 (2)	0.015 (2)	0.032 (3)	0.004 (2)	0.007 (2)	−0.005 (2)
C32	0.031 (3)	0.026 (3)	0.029 (3)	0.000 (2)	−0.004 (2)	−0.010 (2)
C33	0.026 (3)	0.023 (3)	0.035 (3)	0.008 (2)	−0.003 (2)	−0.003 (2)
C34	0.026 (3)	0.033 (3)	0.032 (3)	0.004 (2)	−0.003 (2)	−0.009 (2)
C35	0.027 (3)	0.025 (3)	0.037 (3)	0.003 (2)	−0.001 (2)	−0.008 (2)
C36	0.025 (2)	0.026 (3)	0.031 (3)	0.012 (2)	0.001 (2)	−0.007 (2)
C37	0.031 (3)	0.016 (2)	0.030 (3)	0.000 (2)	0.006 (2)	−0.004 (2)
C38	0.034 (3)	0.038 (3)	0.037 (3)	−0.003 (2)	0.006 (2)	−0.021 (3)

Geometric parameters (Å, °)

O1—C1	1.359 (5)	C16—H16A	0.9900
O1—C9	1.416 (4)	C16—H16B	0.9900
O2—C12	1.386 (5)	C17—C18	1.487 (6)
O2—C15	1.448 (5)	C17—H17A	0.9900
O3—C17	1.423 (5)	C17—H17B	0.9900
O3—C16	1.432 (5)	C18—H18A	0.9900
O4—C18	1.413 (5)	C18—H18B	0.9900
O4—C19	1.425 (5)	C19—H19A	0.9800
O5—C20	1.354 (5)	C19—H19B	0.9800
O5—C28	1.414 (5)	C19—H19C	0.9800
O6—C31	1.375 (5)	C20—C21	1.397 (6)
O6—C34	1.408 (5)	C20—C25	1.399 (6)
O7—C35	1.406 (5)	C21—C22	1.410 (6)
O7—C36	1.423 (5)	C21—C26	1.434 (6)
O8—C37	1.418 (5)	C22—C23	1.390 (6)
O8—C38	1.427 (5)	C22—C27	1.452 (6)
N1—C7	1.150 (5)	C23—C24	1.379 (6)
N2—C8	1.143 (5)	C23—H23	0.9500
N3—C26	1.143 (5)	C24—C25	1.384 (6)
N4—C27	1.145 (5)	C24—H24	0.9500
C1—C6	1.389 (5)	C25—H25	0.9500
C1—C2	1.401 (5)	C28—C33	1.355 (6)
C2—C3	1.403 (5)	C28—C29	1.371 (6)
C2—C7	1.436 (6)	C29—C30	1.380 (6)
C3—C4	1.385 (6)	C29—H29	0.9500
C3—C8	1.449 (6)	C30—C31	1.386 (6)
C4—C5	1.386 (6)	C30—H30	0.9500
C4—H4	0.9500	C31—C32	1.380 (6)
C5—C6	1.370 (6)	C32—C33	1.393 (6)
C5—H5	0.9500	C32—H32	0.9500
C6—H6	0.9500	C33—H33	0.9500
C9—C14	1.372 (6)	C34—C35	1.516 (6)
C9—C10	1.381 (6)	C34—H34A	0.9900
C10—C11	1.401 (6)	C34—H34B	0.9900
C10—H10	0.9500	C35—H35A	0.9900
C11—C12	1.378 (6)	C35—H35B	0.9900
C11—H11	0.9500	C36—C37	1.500 (6)
C12—C13	1.376 (5)	C36—H36A	0.9900
C13—C14	1.392 (6)	C36—H36B	0.9900
C13—H13	0.9500	C37—H37A	0.9900

C14—H14	0.9500	C37—H37B	0.9900
C15—C16	1.506 (6)	C38—H38A	0.9800
C15—H15A	0.9900	C38—H38B	0.9800
C15—H15B	0.9900	C38—H38C	0.9800
C1—O1—C9	119.3 (3)	H19A—C19—H19B	109.5
C12—O2—C15	116.1 (3)	O4—C19—H19C	109.5
C17—O3—C16	109.8 (3)	H19A—C19—H19C	109.5
C18—O4—C19	112.4 (3)	H19B—C19—H19C	109.5
C20—O5—C28	118.6 (3)	O5—C20—C21	115.6 (4)
C31—O6—C34	117.6 (3)	O5—C20—C25	125.1 (4)
C35—O7—C36	110.5 (3)	C21—C20—C25	119.2 (4)
C37—O8—C38	111.3 (3)	C20—C21—C22	119.4 (4)
O1—C1—C6	125.3 (4)	C20—C21—C26	119.1 (4)
O1—C1—C2	115.4 (3)	C22—C21—C26	121.4 (4)
C6—C1—C2	119.3 (4)	C23—C22—C21	120.8 (4)
C1—C2—C3	119.7 (4)	C23—C22—C27	120.7 (4)
C1—C2—C7	120.2 (4)	C21—C22—C27	118.5 (4)
C3—C2—C7	120.1 (4)	C24—C23—C22	118.8 (4)
C4—C3—C2	120.1 (4)	C24—C23—H23	120.6
C4—C3—C8	119.8 (4)	C22—C23—H23	120.6
C2—C3—C8	120.0 (4)	C23—C24—C25	121.6 (4)
C3—C4—C5	119.2 (4)	C23—C24—H24	119.2
C3—C4—H4	120.4	C25—C24—H24	119.2
C5—C4—H4	120.4	C24—C25—C20	120.2 (4)
C6—C5—C4	121.3 (4)	C24—C25—H25	119.9
C6—C5—H5	119.3	C20—C25—H25	119.9
C4—C5—H5	119.3	N3—C26—C21	178.8 (5)
C5—C6—C1	120.3 (4)	N4—C27—C22	179.1 (5)
C5—C6—H6	119.9	C33—C28—C29	122.0 (4)
C1—C6—H6	119.9	C33—C28—O5	118.8 (4)
N1—C7—C2	177.8 (4)	C29—C28—O5	119.0 (4)
N2—C8—C3	179.2 (5)	C28—C29—C30	119.4 (4)
C14—C9—C10	121.1 (4)	C28—C29—H29	120.3
C14—C9—O1	117.9 (4)	C30—C29—H29	120.3
C10—C9—O1	120.8 (4)	C29—C30—C31	119.5 (4)
C9—C10—C11	119.4 (4)	C29—C30—H30	120.3
C9—C10—H10	120.3	C31—C30—H30	120.3
C11—C10—H10	120.3	O6—C31—C32	124.2 (4)
C12—C11—C10	119.3 (4)	O6—C31—C30	115.6 (4)
C12—C11—H11	120.3	C32—C31—C30	120.2 (4)
C10—C11—H11	120.3	C31—C32—C33	119.8 (4)

C13—C12—C11	120.8 (4)	C31—C32—H32	120.1
C13—C12—O2	115.4 (4)	C33—C32—H32	120.1
C11—C12—O2	123.7 (4)	C28—C33—C32	119.0 (4)
C12—C13—C14	119.9 (4)	C28—C33—H33	120.5
C12—C13—H13	120.0	C32—C33—H33	120.5
C14—C13—H13	120.0	O6—C34—C35	105.9 (3)
C9—C14—C13	119.4 (4)	O6—C34—H34A	110.6
C9—C14—H14	120.3	C35—C34—H34A	110.6
C13—C14—H14	120.3	O6—C34—H34B	110.6
O2—C15—C16	108.3 (3)	C35—C34—H34B	110.6
O2—C15—H15A	110.0	H34A—C34—H34B	108.7
C16—C15—H15A	110.0	O7—C35—C34	108.1 (3)
O2—C15—H15B	110.0	O7—C35—H35A	110.1
C16—C15—H15B	110.0	C34—C35—H35A	110.1
H15A—C15—H15B	108.4	O7—C35—H35B	110.1
O3—C16—C15	110.3 (4)	C34—C35—H35B	110.1
O3—C16—H16A	109.6	H35A—C35—H35B	108.4
C15—C16—H16A	109.6	O7—C36—C37	109.9 (3)
O3—C16—H16B	109.6	O7—C36—H36A	109.7
C15—C16—H16B	109.6	C37—C36—H36A	109.7
H16A—C16—H16B	108.1	O7—C36—H36B	109.7
O3—C17—C18	110.6 (3)	C37—C36—H36B	109.7
O3—C17—H17A	109.5	H36A—C36—H36B	108.2
C18—C17—H17A	109.5	O8—C37—C36	109.6 (4)
O3—C17—H17B	109.5	O8—C37—H37A	109.7
C18—C17—H17B	109.5	C36—C37—H37A	109.7
H17A—C17—H17B	108.1	O8—C37—H37B	109.7
O4—C18—C17	108.8 (3)	C36—C37—H37B	109.7
O4—C18—H18A	109.9	H37A—C37—H37B	108.2
C17—C18—H18A	109.9	O8—C38—H38A	109.5
O4—C18—H18B	109.9	O8—C38—H38B	109.5
C17—C18—H18B	109.9	H38A—C38—H38B	109.5
H18A—C18—H18B	108.3	O8—C38—H38C	109.5
O4—C19—H19A	109.5	H38A—C38—H38C	109.5
O4—C19—H19B	109.5	H38B—C38—H38C	109.5
C9—O1—C1—C6	−15.2 (5)	C28—O5—C20—C21	176.3 (3)
C9—O1—C1—C2	167.1 (3)	C28—O5—C20—C25	−2.8 (6)
O1—C1—C2—C3	−179.9 (3)	O5—C20—C21—C22	−177.7 (3)
C6—C1—C2—C3	2.3 (5)	C25—C20—C21—C22	1.6 (6)
O1—C1—C2—C7	−0.1 (5)	O5—C20—C21—C26	1.6 (5)
C6—C1—C2—C7	−177.9 (3)	C25—C20—C21—C26	−179.2 (4)

C1—C2—C3—C4	−0.8 (6)	C20—C21—C22—C23	−1.4 (6)
C7—C2—C3—C4	179.4 (3)	C26—C21—C22—C23	179.3 (3)
C1—C2—C3—C8	178.8 (3)	C20—C21—C22—C27	177.0 (3)
C7—C2—C3—C8	−1.0 (6)	C26—C21—C22—C27	−2.3 (6)
C2—C3—C4—C5	−0.5 (6)	C21—C22—C23—C24	0.0 (6)
C8—C3—C4—C5	179.9 (4)	C27—C22—C23—C24	−178.3 (4)
C3—C4—C5—C6	0.4 (6)	C22—C23—C24—C25	1.3 (6)
C4—C5—C6—C1	1.1 (6)	C23—C24—C25—C20	−1.1 (6)
O1—C1—C6—C5	180.0 (3)	O5—C20—C25—C24	178.8 (4)
C2—C1—C6—C5	−2.5 (6)	C21—C20—C25—C24	−0.3 (6)
C1—O1—C9—C14	130.9 (4)	C20—O5—C28—C33	−95.7 (5)
C1—O1—C9—C10	−54.0 (5)	C20—O5—C28—C29	89.4 (5)
C14—C9—C10—C11	−2.2 (6)	C33—C28—C29—C30	1.9 (7)
O1—C9—C10—C11	−177.1 (4)	O5—C28—C29—C30	176.6 (4)
C9—C10—C11—C12	0.6 (6)	C28—C29—C30—C31	−1.3 (7)
C10—C11—C12—C13	1.6 (6)	C34—O6—C31—C32	−6.0 (6)
C10—C11—C12—O2	−178.0 (4)	C34—O6—C31—C30	175.5 (4)
C15—O2—C12—C13	−172.2 (4)	C29—C30—C31—O6	178.7 (4)
C15—O2—C12—C11	7.4 (6)	C29—C30—C31—C32	0.1 (7)
C11—C12—C13—C14	−2.2 (6)	O6—C31—C32—C33	−177.7 (4)
O2—C12—C13—C14	177.4 (4)	C30—C31—C32—C33	0.7 (7)
C10—C9—C14—C13	1.6 (6)	C29—C28—C33—C32	−1.1 (7)
O1—C9—C14—C13	176.7 (4)	O5—C28—C33—C32	−175.8 (4)
C12—C13—C14—C9	0.6 (6)	C31—C32—C33—C28	−0.2 (7)
C12—O2—C15—C16	172.5 (3)	C31—O6—C34—C35	−174.2 (4)
C17—O3—C16—C15	−173.8 (3)	C36—O7—C35—C34	176.5 (4)
O2—C15—C16—O3	84.3 (4)	O6—C34—C35—O7	171.7 (3)
C16—O3—C17—C18	−167.0 (3)	C35—O7—C36—C37	171.1 (4)
C19—O4—C18—C17	165.2 (4)	C38—O8—C37—C36	173.3 (3)
O3—C17—C18—O4	67.3 (4)	O7—C36—C37—O8	68.2 (5)

A.3 Single Crystal X-ray Diffraction Data

4,5-Bis(4-(2-(2-methoxyethoxy)ethoxy)phenoxy)phthalonitrile (2.14)

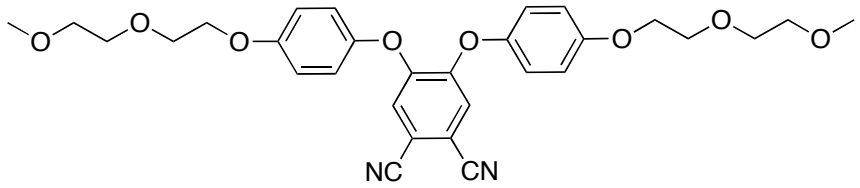

Crystal data

$C_{30}H_{32}N_2O_8$	$D_x = 1.304$ Mg m^{-3}
$M_r = 548.58$	
Monoclinic, $P2_1/c$	Mo $K\alpha$ radiation
	$\lambda = 0.71073$ Å
Hall symbol: -P 2ybc	Cell parameters from 4179 reflections
$a = 22.598$ (7) Å	$\theta = 2.5$–$26.7°$
$b = 16.029$ (5) Å	$\mu = 0.10$ mm^{-1}
$c = 7.7135$ (15) Å	$T = 90$ K
$\beta = 91.03$ (2)°	
$V = 2793.6$ (13) Å^3	Plate, colorless
$Z = 4$	0.42 × 0.23 × 0.03 mm
$F_{000} = 1160$	

Data collection

Nonius KappaCCD (with Oxford Cryostream) diffractometer	18124 measured reflections
Radiation source: fine-focus sealed tube	4666 independent reflections
Monochromator: graphite	2771 reflections with $I > 2\sigma(I)$
Detector resolution: pixels mm^{-1}	$R_{int} = 0.053$
$T = 90$ K	$\theta_{max} = 26.1°$
$P =$ kPa	$\theta_{min} = 2.9°$
ω scans with κ offsets	$h = -27 \rightarrow 27$
Absorption correction: multi-scan	
Denzo and Scalepack (Otwinowski & Minor, 1997)	$k = -18 \rightarrow 19$
$T_{min} = 0.961$, $T_{max} = 0.997$	$l = -7 \rightarrow 7$

Refinement

Refinement on F^2 Secondary atom site location: difference Fourier map
Least-squares matrix: full Hydrogen site location: inferred from neighbouring sites
$R[F^2 > 2\sigma(F^2)] = 0.050$ H-atom parameters constrained
$wR(F^2) = 0.105$ $w = 1/[\sigma^2(F_o^2) + (0.0397P)^2 + 0.4119P]$ where $P = (F_o^2 + 2F_c^2)/3$
$S = 1.03$ $(\Delta/\sigma)_{max} < 0.001$
4666 reflections $\Delta\rho_{max} = 0.28$ e Å^{-3}
364 parameters $\Delta\rho_{min} = -0.21$ e Å^{-3}
constraints Extinction correction: SHELXL, $Fc^* = kFc[1+0.001xFc^2\lambda^3/\sin(2\theta)]^{-1/4}$
Primary atom site location: structure-invariant direct methods
Extinction coefficient: 0.0045 (6)

Refinement: Refinement of F^2 against ALL reflections. The weighted R-factor wR and goodness of fit S are based on F^2, conventional R-factors R are based on F, with F set to zero for negative F^2. The threshold expression of $F^2 > 2\text{sigma}(F^2)$ is used only for calculating R-factors(gt) etc. and is not relevant to the choice of reflections for refinement. R-factors based on F^2 are statistically about twice as large as those based on F, and R- factors based on ALL data will be even larger.

Fractional atomic coordinates and isotropic or equivalent isotropic displacement parameters (Å^2)

	x	*y*	*z*	U_{iso}*/U_{eq}
O1	0.33722 (7)	0.46029 (10)	0.5207 (2)	0.0310 (5)
O2	0.52579 (7)	0.24106 (10)	0.5066 (2)	0.0255 (4)
O3	0.63993 (7)	0.16771 (10)	0.4376 (2)	0.0258 (4)
O4	0.58968 (8)	0.00017 (11)	0.4782 (2)	0.0333 (5)
O5	0.25403 (7)	0.56600 (10)	0.4853 (2)	0.0287 (5)
O6	0.10882 (7)	0.84017 (10)	0.3893 (2)	0.0251 (4)
O7	0.06051 (7)	0.97236 (10)	0.1935 (2)	0.0252 (4)
O8	0.05254 (8)	1.18146 (11)	0.0291 (2)	0.0368 (5)
N1	0.12026 (10)	0.45990 (14)	1.1054 (3)	0.0345 (6)
N2	0.25237 (10)	0.29694 (15)	1.1560 (3)	0.0383 (6)
C1	0.29497 (11)	0.45551 (15)	0.6432 (3)	0.0228 (6)
C2	0.24927 (11)	0.51451 (15)	0.6257 (3)	0.0220 (6)
C3	0.20406 (11)	0.51727 (15)	0.7445 (3)	0.0224 (6)
H3	0.1732	0.5572	0.7327	0.027*
C4	0.20450 (11)	0.46041 (15)	0.8821 (3)	0.0216 (6)
C5	0.24974 (11)	0.40144 (15)	0.8992 (3)	0.0212 (6)
C6	0.29508 (11)	0.39930 (15)	0.7785 (3)	0.0240 (6)
H6	0.3259	0.3592	0.7897	0.029*
C7	0.15724 (12)	0.46115 (15)	1.0054 (3)	0.0246 (6)

C8	0.25071 (11)	0.34289 (17)	1.0412 (4)	0.0274 (7)
C9	0.38449 (11)	0.40322 (16)	0.5274 (3)	0.0249 (6)
C10	0.37937 (11)	0.32773 (16)	0.4412 (3)	0.0270 (6)
H10	0.3430	0.3121	0.3869	0.032*
C11	0.42766 (11)	0.27584 (16)	0.4352 (3)	0.0255 (6)
H11	0.4247	0.2241	0.3755	0.031*
C12	0.48118 (11)	0.29853 (15)	0.5165 (3)	0.0218 (6)
C13	0.48554 (12)	0.37435 (15)	0.6019 (3)	0.0265 (6)
H13	0.5217	0.3903	0.6574	0.032*
C14	0.43675 (12)	0.42677 (16)	0.6058 (3)	0.0282 (7)
H14	0.4396	0.4791	0.6631	0.034*
C15	0.57970 (11)	0.25934 (15)	0.6019 (3)	0.0249 (6)
H15A	0.5705	0.2771	0.7214	0.030*
H15B	0.6013	0.3052	0.5448	0.030*
C16	0.61703 (11)	0.18207 (15)	0.6068 (3)	0.0265 (7)
H16A	0.6500	0.1890	0.6916	0.032*
H16B	0.5929	0.1338	0.6428	0.032*
C17	0.67116 (11)	0.09073 (15)	0.4231 (3)	0.0260 (6)
H17A	0.6875	0.0751	0.5386	0.031*
H17B	0.7048	0.0985	0.3443	0.031*
C18	0.63327 (12)	0.02150 (16)	0.3565 (3)	0.0291 (7)
H18A	0.6138	0.0387	0.2461	0.035*
H18B	0.6582	−0.0279	0.3329	0.035*
C19	0.55240 (13)	−0.06565 (16)	0.4150 (3)	0.0377 (7)
H19A	0.5335	−0.0486	0.3053	0.057*
H19B	0.5219	−0.0777	0.5002	0.057*
H19C	0.5763	−0.1158	0.3962	0.057*
C20	0.21397 (12)	0.63336 (15)	0.4668 (3)	0.0236 (6)
C21	0.15863 (12)	0.62118 (15)	0.3947 (3)	0.0258 (6)
H21	0.1457	0.5665	0.3650	0.031*
C22	0.12161 (11)	0.68929 (15)	0.3653 (3)	0.0242 (6)
H22	0.0833	0.6816	0.3150	0.029*
C23	0.14122 (11)	0.76837 (15)	0.4102 (3)	0.0203 (6)
C24	0.19755 (11)	0.77939 (15)	0.4825 (3)	0.0234 (6)
H24	0.2109	0.8338	0.5125	0.028*
C25	0.23401 (11)	0.71182 (16)	0.5109 (3)	0.0253 (6)
H25	0.2725	0.7192	0.5602	0.030*
C26	0.05186 (11)	0.83514 (15)	0.3073 (3)	0.0251 (6)
H26A	0.0259	0.7971	0.3726	0.030*
H26B	0.0554	0.8136	0.1876	0.030*
C27	0.02666 (11)	0.92127 (15)	0.3049 (3)	0.0273 (6)

H27A	−0.0150	0.9196	0.2632	0.033*
H27B	0.0275	0.9447	0.4236	0.033*
C28	0.03675 (11)	1.05430 (15)	0.1781 (3)	0.0270 (6)
H28A	0.0319	1.0794	0.2942	0.032*
H28B	−0.0024	1.0527	0.1184	0.032*
C29	0.07981 (12)	1.10464 (15)	0.0743 (3)	0.0297 (7)
H29A	0.1164	1.1149	0.1437	0.036*
H29B	0.0906	1.0738	−0.0318	0.036*
C30	0.09167 (14)	1.23311 (17)	−0.0674 (4)	0.0459 (8)
H30A	0.1274	1.2447	0.0026	0.069*
H30B	0.0718	1.2857	−0.0967	0.069*
H30C	0.1027	1.2043	−0.1742	0.069*

Atomic displacement parameters (Å²)

	U^{11}	U^{22}	U^{33}	U^{12}	U^{13}	U^{23}
O1	0.0321 (11)	0.0311 (11)	0.0303 (11)	0.0136 (9)	0.0114 (9)	0.0104 (8)
O2	0.0240 (10)	0.0260 (10)	0.0263 (10)	0.0057 (9)	−0.0034 (8)	−0.0044 (8)
O3	0.0307 (11)	0.0247 (10)	0.0220 (11)	0.0060 (9)	0.0027 (8)	−0.0011 (7)
O4	0.0388 (12)	0.0272 (11)	0.0341 (11)	−0.0075 (9)	0.0074 (9)	−0.0039 (8)
O5	0.0333 (11)	0.0246 (10)	0.0286 (11)	0.0119 (9)	0.0099 (8)	0.0110 (8)
O6	0.0264 (11)	0.0168 (10)	0.0320 (11)	0.0018 (8)	−0.0043 (8)	0.0011 (8)
O7	0.0314 (11)	0.0161 (10)	0.0283 (10)	0.0045 (8)	0.0038 (8)	0.0051 (7)
O8	0.0485 (13)	0.0233 (11)	0.0387 (11)	0.0047 (10)	0.0010 (9)	0.0058 (8)
N1	0.0326 (15)	0.0361 (15)	0.0352 (15)	0.0004 (12)	0.0065 (12)	0.0037 (11)
N2	0.0418 (16)	0.0353 (15)	0.0381 (16)	0.0017 (12)	0.0023 (12)	0.0075 (12)
C1	0.0233 (15)	0.0203 (15)	0.0249 (16)	0.0008 (12)	0.0040 (12)	0.0022 (12)
C2	0.0260 (15)	0.0174 (14)	0.0226 (16)	−0.0001 (12)	0.0005 (12)	0.0014 (11)
C3	0.0234 (15)	0.0172 (14)	0.0265 (16)	0.0001 (12)	−0.0016 (12)	0.0001 (11)
C4	0.0220 (15)	0.0216 (15)	0.0213 (15)	−0.0041 (12)	−0.0007 (12)	−0.0023 (11)
C5	0.0257 (16)	0.0165 (14)	0.0212 (15)	−0.0020 (12)	−0.0023 (12)	0.0016 (11)
C6	0.0226 (15)	0.0215 (15)	0.0279 (16)	0.0053 (12)	−0.0002 (12)	−0.0002 (12)
C7	0.0271 (16)	0.0198 (15)	0.0268 (16)	0.0000 (13)	−0.0027 (14)	0.0014 (12)
C8	0.0240 (16)	0.0254 (16)	0.0328 (18)	0.0011 (13)	0.0030 (13)	0.0005 (14)
C9	0.0247 (16)	0.0255 (16)	0.0247 (15)	0.0082 (13)	0.0075 (12)	0.0056 (12)
C10	0.0250 (16)	0.0300 (17)	0.0261 (16)	0.0006 (13)	−0.0006 (12)	0.0030 (12)
C11	0.0289 (17)	0.0221 (15)	0.0257 (16)	0.0027 (13)	0.0015 (12)	−0.0003 (11)
C12	0.0218 (15)	0.0225 (15)	0.0213 (15)	0.0064 (12)	0.0050 (12)	0.0028 (12)
C13	0.0275 (16)	0.0241 (16)	0.0278 (16)	0.0019 (13)	0.0006 (12)	−0.0030 (12)
C14	0.0357 (18)	0.0216 (15)	0.0276 (16)	0.0028 (14)	0.0069 (13)	−0.0003 (12)
C15	0.0265 (16)	0.0259 (16)	0.0224 (15)	−0.0008 (13)	−0.0010 (12)	−0.0029 (11)

C16	0.0338 (17)	0.0287 (16)	0.0169 (16)	0.0052 (13)	−0.0013 (12)	−0.0019 (11)
C17	0.0275 (16)	0.0271 (16)	0.0236 (16)	0.0072 (13)	0.0021 (12)	−0.0004 (12)
C18	0.0330 (17)	0.0287 (17)	0.0258 (16)	0.0058 (14)	0.0030 (13)	−0.0025 (12)
C19	0.0447 (19)	0.0274 (17)	0.0411 (18)	−0.0068 (15)	0.0016 (14)	−0.0060 (14)
C20	0.0292 (17)	0.0211 (15)	0.0207 (15)	0.0069 (13)	0.0063 (12)	0.0074 (11)
C21	0.0332 (17)	0.0139 (14)	0.0304 (16)	−0.0003 (13)	0.0050 (13)	0.0021 (11)
C22	0.0270 (16)	0.0199 (15)	0.0258 (15)	−0.0023 (13)	−0.0002 (12)	0.0018 (12)
C23	0.0263 (16)	0.0168 (14)	0.0181 (15)	0.0027 (12)	0.0056 (12)	0.0016 (11)
C24	0.0289 (16)	0.0170 (15)	0.0243 (15)	−0.0029 (12)	−0.0016 (12)	0.0018 (11)
C25	0.0245 (16)	0.0261 (16)	0.0253 (16)	0.0014 (13)	−0.0011 (12)	0.0050 (12)
C26	0.0254 (16)	0.0252 (15)	0.0249 (15)	−0.0009 (13)	0.0009 (12)	0.0033 (12)
C27	0.0259 (15)	0.0236 (15)	0.0325 (16)	0.0031 (13)	0.0040 (12)	0.0018 (12)
C28	0.0336 (17)	0.0203 (15)	0.0272 (16)	0.0073 (13)	−0.0015 (12)	−0.0030 (12)
C29	0.0449 (18)	0.0183 (15)	0.0259 (16)	0.0105 (13)	0.0028 (13)	0.0041 (12)
C30	0.065 (2)	0.0296 (18)	0.0438 (19)	−0.0068 (16)	0.0079 (16)	0.0102 (14)

Geometric parameters (Å, °)

O1—C1	1.358 (3)	C14—H14	0.9500
O1—C9	1.407 (3)	C15—C16	1.499 (3)
O2—C12	1.369 (3)	C15—H15A	0.9900
O2—C15	1.442 (3)	C15—H15B	0.9900
O3—C17	1.427 (3)	C16—H16A	0.9900
O3—C16	1.431 (3)	C16—H16B	0.9900
O4—C18	1.415 (3)	C17—C18	1.488 (3)
O4—C19	1.430 (3)	C17—H17A	0.9900
O5—C2	1.368 (3)	C17—H17B	0.9900
O5—C20	1.415 (3)	C18—H18A	0.9900
O6—C23	1.372 (3)	C18—H18B	0.9900
O6—C26	1.426 (3)	C19—H19A	0.9800
O7—C27	1.420 (3)	C19—H19B	0.9800
O7—C28	1.423 (3)	C19—H19C	0.9800
O8—C29	1.418 (3)	C20—C21	1.373 (3)
O8—C30	1.430 (3)	C20—C25	1.377 (3)
N1—C7	1.148 (3)	C21—C22	1.392 (3)
N2—C8	1.152 (3)	C21—H21	0.9500
C1—C6	1.379 (3)	C22—C23	1.385 (3)
C1—C2	1.405 (3)	C22—H22	0.9500
C2—C3	1.385 (3)	C23—C24	1.392 (3)
C3—C4	1.399 (3)	C24—C25	1.376 (3)
C3—H3	0.9500	C24—H24	0.9500

C4—C5	1.397 (3)	C25—H25	0.9500
C4—C7	1.443 (4)	C26—C27	1.493 (3)
C5—C6	1.397 (3)	C26—H26A	0.9900
C5—C8	1.442 (4)	C26—H26B	0.9900
C6—H6	0.9500	C27—H27A	0.9900
C9—C14	1.370 (3)	C27—H27B	0.9900
C9—C10	1.385 (3)	C28—C29	1.506 (3)
C10—C11	1.374 (3)	C28—H28A	0.9900
C10—H10	0.9500	C28—H28B	0.9900
C11—C12	1.400 (3)	C29—H29A	0.9900
C11—H11	0.9500	C29—H29B	0.9900
C12—C13	1.385 (3)	C30—H30A	0.9800
C13—C14	1.387 (3)	C30—H30B	0.9800
C13—H13	0.9500	C30—H30C	0.9800
C1—O1—C9	118.72 (18)	C18—C17—H17B	109.0
C12—O2—C15	116.83 (18)	H17A—C17—H17B	107.8
C17—O3—C16	113.44 (17)	O4—C18—C17	110.7 (2)
C18—O4—C19	111.40 (18)	O4—C18—H18A	109.5
C2—O5—C20	118.76 (18)	C17—C18—H18A	109.5
C23—O6—C26	118.69 (18)	O4—C18—H18B	109.5
C27—O7—C28	112.10 (18)	C17—C18—H18B	109.5
C29—O8—C30	111.1 (2)	H18A—C18—H18B	108.1
O1—C1—C6	124.9 (2)	O4—C19—H19A	109.5
O1—C1—C2	114.8 (2)	O4—C19—H19B	109.5
C6—C1—C2	120.3 (2)	H19A—C19—H19B	109.5
O5—C2—C3	125.0 (2)	O4—C19—H19C	109.5
O5—C2—C1	114.5 (2)	H19A—C19—H19C	109.5
C3—C2—C1	120.5 (2)	H19B—C19—H19C	109.5
C2—C3—C4	119.1 (2)	C21—C20—C25	121.5 (2)
C2—C3—H3	120.5	C21—C20—O5	120.6 (2)
C4—C3—H3	120.5	C25—C20—O5	117.7 (2)
C5—C4—C3	120.5 (2)	C20—C21—C22	119.7 (2)
C5—C4—C7	119.5 (2)	C20—C21—H21	120.2
C3—C4—C7	120.0 (2)	C22—C21—H21	120.2
C6—C5—C4	119.9 (2)	C23—C22—C21	119.2 (2)
C6—C5—C8	119.3 (2)	C23—C22—H22	120.4
C4—C5—C8	120.9 (2)	C21—C22—H22	120.4
C1—C6—C5	119.8 (2)	O6—C23—C22	124.8 (2)
C1—C6—H6	120.1	O6—C23—C24	115.0 (2)
C5—C6—H6	120.1	C22—C23—C24	120.2 (2)
N1—C7—C4	178.2 (3)	C25—C24—C23	120.3 (2)

N2—C8—C5	178.7 (3)	C25—C24—H24	119.8
C14—C9—C10	121.1 (2)	C23—C24—H24	119.8
C14—C9—O1	119.0 (2)	C24—C25—C20	119.1 (2)
C10—C9—O1	119.6 (2)	C24—C25—H25	120.5
C11—C10—C9	119.1 (2)	C20—C25—H25	120.5
C11—C10—H10	120.5	O6—C26—C27	107.1 (2)
C9—C10—H10	120.5	O6—C26—H26A	110.3
C10—C11—C12	120.5 (2)	C27—C26—H26A	110.3
C10—C11—H11	119.7	O6—C26—H26B	110.3
C12—C11—H11	119.7	C27—C26—H26B	110.3
O2—C12—C13	124.8 (2)	H26A—C26—H26B	108.5
O2—C12—C11	115.6 (2)	O7—C27—C26	109.3 (2)
C13—C12—C11	119.6 (2)	O7—C27—H27A	109.8
C12—C13—C14	119.5 (2)	C26—C27—H27A	109.8
C12—C13—H13	120.3	O7—C27—H27B	109.8
C14—C13—H13	120.3	C26—C27—H27B	109.8
C9—C14—C13	120.2 (2)	H27A—C27—H27B	108.3
C9—C14—H14	119.9	O7—C28—C29	107.0 (2)
C13—C14—H14	119.9	O7—C28—H28A	110.3
O2—C15—C16	108.34 (19)	C29—C28—H28A	110.3
O2—C15—H15A	110.0	O7—C28—H28B	110.3
C16—C15—H15A	110.0	C29—C28—H28B	110.3
O2—C15—H15B	110.0	H28A—C28—H28B	108.6
C16—C15—H15B	110.0	O8—C29—C28	108.3 (2)
H15A—C15—H15B	108.4	O8—C29—H29A	110.0
O3—C16—C15	108.84 (18)	C28—C29—H29A	110.0
O3—C16—H16A	109.9	O8—C29—H29B	110.0
C15—C16—H16A	109.9	C28—C29—H29B	110.0
O3—C16—H16B	109.9	H29A—C29—H29B	108.4
C15—C16—H16B	109.9	O8—C30—H30A	109.5
H16A—C16—H16B	108.3	O8—C30—H30B	109.5
O3—C17—C18	112.9 (2)	H30A—C30—H30B	109.5
O3—C17—H17A	109.0	O8—C30—H30C	109.5
C18—C17—H17A	109.0	H30A—C30—H30C	109.5
O3—C17—H17B	109.0	H30B—C30—H30C	109.5
C9—O1—C1—C6	1.3 (4)	C11—C12—C13—C14	0.0 (3)
C9—O1—C1—C2	−179.6 (2)	C10—C9—C14—C13	−0.9 (4)
C20—O5—C2—C3	7.2 (3)	O1—C9—C14—C13	−174.7 (2)
C20—O5—C2—C1	−173.1 (2)	C12—C13—C14—C9	0.7 (3)
O1—C1—C2—O5	1.5 (3)	C12—O2—C15—C16	167.72 (18)
C6—C1—C2—O5	−179.4 (2)	C17—O3—C16—C15	−173.8 (2)

O1—C1—C2—C3	−178.7 (2)	O2—C15—C16—O3	71.6 (2)
C6—C1—C2—C3	0.4 (4)	C16—O3—C17—C18	94.4 (2)
O5—C2—C3—C4	179.7 (2)	C19—O4—C18—C17	179.3 (2)
C1—C2—C3—C4	0.0 (3)	O3—C17—C18—O4	−67.3 (3)
C2—C3—C4—C5	−0.3 (3)	C2—O5—C20—C21	−82.9 (3)
C2—C3—C4—C7	−178.8 (2)	C2—O5—C20—C25	102.0 (3)
C3—C4—C5—C6	0.3 (4)	C25—C20—C21—C22	−0.1 (4)
C7—C4—C5—C6	178.8 (2)	O5—C20—C21—C22	−175.0 (2)
C3—C4—C5—C8	179.7 (2)	C20—C21—C22—C23	−0.3 (3)
C7—C4—C5—C8	−1.8 (4)	C26—O6—C23—C22	−3.5 (3)
O1—C1—C6—C5	178.6 (2)	C26—O6—C23—C24	176.6 (2)
C2—C1—C6—C5	−0.4 (4)	C21—C22—C23—O6	−179.4 (2)
C4—C5—C6—C1	0.1 (4)	C21—C22—C23—C24	0.5 (3)
C8—C5—C6—C1	−179.3 (2)	O6—C23—C24—C25	179.5 (2)
C1—O1—C9—C14	−96.5 (3)	C22—C23—C24—C25	−0.4 (3)
C1—O1—C9—C10	89.6 (3)	C23—C24—C25—C20	0.0 (3)
C14—C9—C10—C11	0.2 (4)	C21—C20—C25—C24	0.3 (4)
O1—C9—C10—C11	174.0 (2)	O5—C20—C25—C24	175.32 (19)
C9—C10—C11—C12	0.6 (3)	C23—O6—C26—C27	179.05 (18)
C15—O2—C12—C13	4.1 (3)	C28—O7—C27—C26	176.76 (19)
C15—O2—C12—C11	−174.7 (2)	O6—C26—C27—O7	66.9 (2)
C10—C11—C12—O2	178.2 (2)	C27—O7—C28—C29	173.8 (2)
C10—C11—C12—C13	−0.7 (3)	C30—O8—C29—C28	178.9 (2)
O2—C12—C13—C14	−178.7 (2)	O7—C28—C29—O8	169.29 (18)

A.4 Single Crystal X-ray Diffraction Data

4-(2-(2-(2-Methoxyethoxy)ethoxy)ethoxy)phthalonitrile (**2.15**)

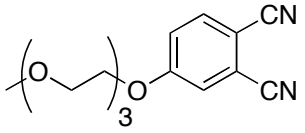

Crystal data

$C_{15}H_{18}N_2O_4$
$M_r = 290.31$

Triclinic, $P\bar{1}$

Hall symbol: -P 1

$a = 7.6600\ (10)$ Å
$b = 8.2470\ (12)$ Å
$c = 12.996\ (2)$ Å
$\alpha = 98.098\ (9)°$
$\beta = 97.453\ (9)°$
$\gamma = 111.584\ (8)°$
$V = 740.96\ (18)$ Å^3
$Z = 2$

$F_{000} = 308$
$D_x = 1.301$ Mg m^{-3}

Mo $K\alpha$ radiation
$\lambda = 0.71073$ Å
Cell parameters from 3714 reflections

$\theta = 2.5–32.0°$
$\mu = 0.10$ mm^{-1}
$T = 90$ K

Plate, colorless
0.30 × 0.25 × 0.10 mm

Data collection

KappaCCD (with Oxford Cryostream) diffractometer

Radiation source: fine-focus sealed tube
Monochromator: graphite

$T = 90$ K
$P =$ kPa
ω scans with κ offsets
Absorption correction: none
19427 measured reflections

4287 independent reflections

3252 reflections with $I > 2\sigma(I)$
$R_{int} = 0.023$
$\theta_{max} = 32.0°$
$\theta_{min} = 2.7°$
$h = -10 \rightarrow 11$
$k = -11 \rightarrow 11$
$l = -18 \rightarrow 18$

Refinement

Refinement on F^2	Secondary atom site location: difference Fourier map
Least-squares matrix: full	Hydrogen site location: inferred from neighbouring sites
$R[F^2 > 2\sigma(F^2)] = 0.042$	H-atom parameters constrained
$wR(F^2) = 0.108$	$w = 1/[\sigma^2(F_o^2) + (0.044P)^2 + 0.2446P]$ where $P = (F_o^2 + 2F_c^2)/3$
$S = 1.04$	$(\Delta/\sigma)_{max} < 0.001$
4287 reflections	$\Delta\rho_{max} = 0.35$ e Å^{-3}
192 parameters	$\Delta\rho_{min} = -0.24$ e Å^{-3}
	Extinction correction: SHELXL, $Fc^*=kFc[1+0.001xFc^2\lambda^3/\sin(2\theta)]^{-1/4}$
Primary atom site location:	structure-invariant direct methods

Refinement: Refinement of F^2 against ALL reflections. The weighted R-factor wR and goodness of fit S are based on F^2, conventional R-factors R are based on F, with F set to zero for negative F^2. The threshold expression of $F^2 > 2\text{sigma}(F^2)$ is used only for calculating R-factors(gt) etc. and is not relevant to the choice of reflections for refinement. R-factors based on F^2 are statistically about twice as large as those based on F, and R- factors based on ALL data will be even larger.

Fractional atomic coordinates and isotropic or equivalent isotropic displacement parameters (Å^2)

	x	*y*	*z*	U_{iso}*/U_{eq}
O1	0.47228 (12)	0.34743 (10)	0.71857 (6)	0.01772 (18)
O2	0.39249 (12)	0.22250 (10)	0.49455 (6)	0.01872 (18)
O3	0.56577 (12)	0.16393 (11)	0.31934 (7)	0.0204 (2)
O4	0.95490 (13)	0.39555 (12)	0.37622 (7)	0.0245 (2)
N1	0.75301 (17)	1.06277 (14)	0.99575 (9)	0.0284 (3)
N2	0.95232 (17)	0.83050 (15)	1.20380 (9)	0.0299 (3)
C1	0.57267 (16)	0.45562 (15)	0.81273 (8)	0.0161 (2)
C2	0.60104 (16)	0.63448 (15)	0.84001 (9)	0.0172 (2)
H2	0.5514	0.6892	0.7908	0.021*
C3	0.70346 (16)	0.73193 (14)	0.94073 (9)	0.0168 (2)
C4	0.77827 (16)	0.65282 (15)	1.01422 (9)	0.0174 (2)
C5	0.75085 (17)	0.47426 (15)	0.98455 (9)	0.0190 (2)
H5	0.8021	0.4196	1.0331	0.023*
C6	0.64993 (17)	0.37692 (15)	0.88523 (9)	0.0182 (2)
H6	0.6326	0.2558	0.8657	0.022*

C7	0.73034 (17)	0.91628 (16)	0.97058 (9)	0.0203 (2)
C8	0.87695 (18)	0.75260 (16)	1.11931 (9)	0.0208 (2)
C9	0.38154 (17)	0.42055 (15)	0.64364 (9)	0.0184 (2)
H9A	0.4798	0.5182	0.6209	0.022*
H9B	0.2971	0.4692	0.6769	0.022*
C10	0.26646 (17)	0.27359 (15)	0.54994 (9)	0.0188 (2)
H10A	0.1797	0.1701	0.5741	0.023*
H10B	0.1874	0.3148	0.5022	0.023*
C11	0.29004 (17)	0.09387 (15)	0.39944 (9)	0.0202 (2)
H11A	0.2350	0.1494	0.3485	0.024*
H11B	0.1835	−0.0054	0.4154	0.024*
C12	0.42262 (18)	0.02375 (15)	0.35138 (9)	0.0210 (2)
H12A	0.4840	−0.0249	0.4039	0.025*
H12B	0.3492	−0.0736	0.2893	0.025*
C13	0.7150 (2)	0.11537 (17)	0.28910 (11)	0.0256 (3)
H13A	0.6655	0.0264	0.2215	0.031*
H13B	0.7622	0.0615	0.3441	0.031*
C14	0.87530 (18)	0.27854 (17)	0.27613 (10)	0.0240 (3)
H14A	0.9745	0.2452	0.2484	0.029*
H14B	0.8263	0.3378	0.2252	0.029*
C15	1.1129 (2)	0.5529 (2)	0.37304 (11)	0.0305 (3)
H15A	1.2133	0.5206	0.3478	0.046*
H15B	1.1635	0.6280	0.4443	0.046*
H15C	1.0708	0.6184	0.3248	0.046*

Atomic displacement parameters (Å²)

	U^{11}	U^{22}	U^{33}	U^{12}	U^{13}	U^{23}
O1	0.0224 (4)	0.0159 (4)	0.0141 (4)	0.0086 (3)	−0.0007 (3)	0.0018 (3)
O2	0.0199 (4)	0.0186 (4)	0.0153 (4)	0.0078 (3)	0.0000 (3)	−0.0016 (3)
O3	0.0228 (4)	0.0192 (4)	0.0230 (4)	0.0111 (3)	0.0060 (3)	0.0068 (3)
O4	0.0227 (4)	0.0259 (4)	0.0228 (4)	0.0068 (4)	0.0040 (3)	0.0061 (4)
N1	0.0367 (6)	0.0200 (5)	0.0270 (6)	0.0116 (5)	0.0022 (5)	0.0033 (4)
N2	0.0328 (6)	0.0319 (6)	0.0210 (5)	0.0120 (5)	−0.0016 (5)	0.0011 (5)
C1	0.0164 (5)	0.0174 (5)	0.0139 (5)	0.0060 (4)	0.0032 (4)	0.0027 (4)
C2	0.0196 (5)	0.0188 (5)	0.0147 (5)	0.0086 (4)	0.0028 (4)	0.0057 (4)
C3	0.0183 (5)	0.0157 (5)	0.0162 (5)	0.0062 (4)	0.0040 (4)	0.0039 (4)
C4	0.0186 (5)	0.0188 (5)	0.0144 (5)	0.0073 (4)	0.0024 (4)	0.0029 (4)
C5	0.0215 (6)	0.0207 (5)	0.0168 (5)	0.0102 (5)	0.0027 (4)	0.0059 (4)
C6	0.0220 (6)	0.0172 (5)	0.0169 (5)	0.0093 (5)	0.0033 (4)	0.0045 (4)
C7	0.0229 (6)	0.0208 (6)	0.0161 (5)	0.0082 (5)	0.0006 (4)	0.0038 (4)

C8	0.0221 (6)	0.0219 (6)	0.0179 (5)	0.0087 (5)	0.0018 (4)	0.0048 (4)
C9	0.0231 (6)	0.0180 (5)	0.0159 (5)	0.0114 (5)	0.0003 (4)	0.0032 (4)
C10	0.0191 (5)	0.0200 (5)	0.0176 (5)	0.0093 (5)	0.0011 (4)	0.0022 (4)
C11	0.0224 (6)	0.0167 (5)	0.0160 (5)	0.0040 (5)	0.0000 (4)	0.0000 (4)
C12	0.0279 (6)	0.0154 (5)	0.0189 (5)	0.0080 (5)	0.0041 (5)	0.0026 (4)
C13	0.0269 (6)	0.0226 (6)	0.0298 (7)	0.0134 (5)	0.0066 (5)	0.0026 (5)
C14	0.0252 (6)	0.0270 (6)	0.0225 (6)	0.0133 (5)	0.0056 (5)	0.0038 (5)
C15	0.0244 (7)	0.0318 (7)	0.0317 (7)	0.0059 (6)	0.0058 (5)	0.0092 (6)

Geometric parameters (Å, °)

O1—C1	1.3522 (13)	C6—H6	0.9500
O1—C9	1.4468 (13)	C9—C10	1.4995 (16)
O2—C10	1.4219 (14)	C9—H9A	0.9900
O2—C11	1.4267 (13)	C9—H9B	0.9900
O3—C13	1.4248 (15)	C10—H10A	0.9900
O3—C12	1.4260 (15)	C10—H10B	0.9900
O4—C14	1.4151 (15)	C11—C12	1.5003 (17)
O4—C15	1.4222 (16)	C11—H11A	0.9900
N1—C7	1.1473 (16)	C11—H11B	0.9900
N2—C8	1.1470 (16)	C12—H12A	0.9900
C1—C2	1.3948 (16)	C12—H12B	0.9900
C1—C6	1.4034 (15)	C13—C14	1.4998 (18)
C2—C3	1.3957 (15)	C13—H13A	0.9900
C2—H2	0.9500	C13—H13B	0.9900
C3—C4	1.4053 (15)	C14—H14A	0.9900
C3—C7	1.4447 (16)	C14—H14B	0.9900
C4—C5	1.3974 (16)	C15—H15A	0.9800
C4—C8	1.4393 (16)	C15—H15B	0.9800
C5—C6	1.3787 (16)	C15—H15C	0.9800
C5—H5	0.9500		
C1—O1—C9	117.54 (9)	O2—C10—H10B	109.8
C10—O2—C11	111.24 (9)	C9—C10—H10B	109.8
C13—O3—C12	112.80 (9)	H10A—C10—H10B	108.3
C14—O4—C15	112.88 (10)	O2—C11—C12	109.75 (10)
O1—C1—C2	124.19 (10)	O2—C11—H11A	109.7
O1—C1—C6	115.73 (10)	C12—C11—H11A	109.7
C2—C1—C6	120.08 (10)	O2—C11—H11B	109.7
C1—C2—C3	119.04 (10)	C12—C11—H11B	109.7
C1—C2—H2	120.5	H11A—C11—H11B	108.2
C3—C2—H2	120.5	O3—C12—C11	109.61 (9)
C2—C3—C4	121.06 (10)	O3—C12—H12A	109.7

C2—C3—C7	119.50 (10)	C11—C12—H12A	109.7
C4—C3—C7	119.44 (10)	O3—C12—H12B	109.7
C5—C4—C3	118.91 (10)	C11—C12—H12B	109.7
C5—C4—C8	120.51 (10)	H12A—C12—H12B	108.2
C3—C4—C8	120.56 (10)	O3—C13—C14	109.09 (10)
C6—C5—C4	120.44 (10)	O3—C13—H13A	109.9
C6—C5—H5	119.8	C14—C13—H13A	109.9
C4—C5—H5	119.8	O3—C13—H13B	109.9
C5—C6—C1	120.45 (10)	C14—C13—H13B	109.9
C5—C6—H6	119.8	H13A—C13—H13B	108.3
C1—C6—H6	119.8	O4—C14—C13	108.48 (10)
N1—C7—C3	178.99 (13)	O4—C14—H14A	110.0
N2—C8—C4	178.64 (14)	C13—C14—H14A	110.0
O1—C9—C10	107.97 (9)	O4—C14—H14B	110.0
O1—C9—H9A	110.1	C13—C14—H14B	110.0
C10—C9—H9A	110.1	H14A—C14—H14B	108.4
O1—C9—H9B	110.1	O4—C15—H15A	109.5
C10—C9—H9B	110.1	O4—C15—H15B	109.5
H9A—C9—H9B	108.4	H15A—C15—H15B	109.5
O2—C10—C9	109.31 (9)	O4—C15—H15C	109.5
O2—C10—H10A	109.8	H15A—C15—H15C	109.5
C9—C10—H10A	109.8	H15B—C15—H15C	109.5
C9—O1—C1—C2	−2.98 (16)	C4—C5—C6—C1	−0.27 (18)
C9—O1—C1—C6	176.78 (10)	O1—C1—C6—C5	−178.42 (10)
O1—C1—C2—C3	178.44 (10)	C2—C1—C6—C5	1.35 (17)
C6—C1—C2—C3	−1.31 (17)	C1—O1—C9—C10	−175.40 (9)
C1—C2—C3—C4	0.22 (17)	C11—O2—C10—C9	−174.83 (9)
C1—C2—C3—C7	−178.74 (11)	O1—C9—C10—O2	−67.87 (12)
C2—C3—C4—C5	0.84 (17)	C10—O2—C11—C12	−171.90 (9)
C7—C3—C4—C5	179.80 (11)	C13—O3—C12—C11	170.29 (10)
C2—C3—C4—C8	−177.47 (11)	O2—C11—C12—O3	−64.77 (12)
C7—C3—C4—C8	1.49 (17)	C12—O3—C13—C14	−169.69 (10)
C3—C4—C5—C6	−0.81 (17)	C15—O4—C14—C13	178.15 (10)
C8—C4—C5—C6	177.50 (11)	O3—C13—C14—O4	65.11 (13)

A.5 Single Crystal X-ray Diffraction Data

4-(2-(2-Hydroxyethoxy)ethoxy)phthalonitrile (**2.16**)

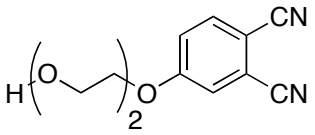

Crystal data

$C_{12}H_{12}N_2O_3$	$D_x = 1.334$ Mg m^{-3}
$M_r = 232.24$	
Monoclinic, $P2_1/c$	Mo $K\alpha$ radiation
	$\lambda = 0.71073$ Å
Hall symbol: -P 2ybc	Cell parameters from 3600 reflections
$a = 11.3397$ (14) Å	$\theta = 2.5$–$30.8°$
$b = 14.4892$ (15) Å	$\mu = 0.10$ mm^{-1}
$c = 7.3662$ (10) Å	$T = 90$ K
$\beta = 107.136$ (5)°	
$V = 1156.6$ (2) Å^3	Needle fragment, yellow
$Z = 4$	0.22 × 0.20 × 0.15 mm
$F_{000} = 488$	

Data collection

Nonius KappaCCD (with Oxford Cryostream) diffractometer	3575 independent reflections
Radiation source: fine-focus sealed tube	2978 reflections with $I > 2\sigma(I)$
Monochromator: graphite	$R_{int} = 0.019$
	$\theta_{max} = 30.8°$
$T = 90$ K	$\theta_{min} = 2.8°$
$P =$ kPa	$h = -16 \rightarrow 16$
ω scans with κ offsets	$k = -20 \rightarrow 19$
Absorption correction: none	$l = -10 \rightarrow 10$
24325 measured reflections	

Refinement

Refinement on F^2	Secondary atom site location: difference Fourier map
Least-squares matrix: full	Hydrogen site location: inferred from neighbouring sites

$R[F^2 > 2\sigma(F^2)] = 0.039$ H atoms treated by a mixture of independent and constrained refinement

$wR(F^2) = 0.107$ $w = 1/[\sigma^2(F_o^2) + (0.0552P)^2 + 0.3131P]$ where $P = (F_o^2 + 2F_c^2)/3$

$S = 1.03$ $(\Delta/\sigma)_{max} < 0.001$

3575 reflections $\Delta\rho_{max} = 0.39$ e Å^{-3}

157 parameters $\Delta\rho_{min} = -0.24$ e Å^{-3}

Primary atom site location: structure-invariant direct methods

Refinement: Refinement of F^2 against ALL reflections. The weighted R-factor wR and goodness of fit S are based on F^2, conventional R-factors R are based on F, with F set to zero for negative F^2. The threshold expression of $F^2 > 2$sigma(F^2) is used only for calculating R-factors(gt) etc. and is not relevant to the choice of reflections for refinement. R-factors based on F^2 are statistically about twice as large as those based on F, and R- factors based on ALL data will be even larger.

Fractional atomic coordinates and isotropic or equivalent isotropic displacement parameters (Å^2)

	x	*y*	*z*	U_{iso}*/U_{eq}
O1	0.16462 (6)	0.42958 (5)	0.46645 (10)	0.01642 (15)
O2	0.08440 (6)	0.59153 (5)	0.24915 (9)	0.01604 (15)
O3	0.11344 (7)	0.52376 (5)	−0.11014 (11)	0.02049 (16)
H3O	0.0398 (15)	0.5004 (10)	−0.150 (2)	0.031*
N1	0.62049 (8)	0.25375 (7)	0.95088 (14)	0.0255 (2)
N2	0.44703 (9)	0.02248 (7)	0.73726 (16)	0.0299 (2)
C1	0.22720 (8)	0.35086 (6)	0.52970 (13)	0.01384 (17)
C2	0.34780 (8)	0.34833 (6)	0.65229 (13)	0.01464 (18)
H2	0.3915	0.4038	0.6966	0.018*
C3	0.40245 (8)	0.26247 (7)	0.70807 (13)	0.01475 (18)
C4	0.33990 (8)	0.18017 (6)	0.64055 (13)	0.01560 (18)
C5	0.21935 (8)	0.18406 (7)	0.51777 (14)	0.01594 (18)
H5	0.1761	0.1287	0.4711	0.019*
C6	0.16351 (8)	0.26852 (7)	0.46466 (13)	0.01547 (18)
H6	0.0812	0.2709	0.3833	0.019*
C7	0.52491 (9)	0.25855 (7)	0.84107 (14)	0.0181 (2)
C8	0.39929 (9)	0.09246 (7)	0.69475 (15)	0.0201 (2)
C9	0.22619 (8)	0.51656 (6)	0.52827 (13)	0.01518 (18)
H9A	0.2977	0.5239	0.4783	0.018*
H9B	0.2561	0.5193	0.6687	0.018*
C10	0.13226 (9)	0.59158 (7)	0.45162 (13)	0.01570 (18)
H10A	0.0630	0.5839	0.5065	0.019*
H10B	0.1709	0.6522	0.4936	0.019*
C11	0.16700 (9)	0.63002 (7)	0.15498 (13)	0.01658 (18)

H11A	0.2478	0.5983	0.1974	0.020*
H11B	0.1802	0.6964	0.1860	0.020*
C12	0.11053 (9)	0.61771 (7)	−0.05626 (13)	0.0182 (2)
H12A	0.0240	0.6395	−0.0933	0.022*
H12B	0.1564	0.6557	−0.1246	0.022*

Atomic displacement parameters (Å²)

	U^{11}	U^{22}	U^{33}	U^{12}	U^{13}	U^{23}
O1	0.0133 (3)	0.0126 (3)	0.0203 (3)	0.0004 (2)	0.0001 (2)	0.0020 (2)
O2	0.0142 (3)	0.0169 (3)	0.0160 (3)	−0.0017 (2)	0.0028 (2)	0.0021 (2)
O3	0.0178 (3)	0.0183 (4)	0.0240 (4)	−0.0030 (3)	0.0041 (3)	−0.0047 (3)
N1	0.0160 (4)	0.0333 (5)	0.0251 (5)	0.0004 (3)	0.0028 (3)	0.0072 (4)
N2	0.0236 (4)	0.0211 (5)	0.0424 (6)	0.0045 (3)	0.0056 (4)	0.0050 (4)
C1	0.0130 (4)	0.0144 (4)	0.0136 (4)	0.0008 (3)	0.0033 (3)	0.0022 (3)
C2	0.0126 (4)	0.0154 (4)	0.0151 (4)	−0.0015 (3)	0.0027 (3)	0.0014 (3)
C3	0.0115 (4)	0.0182 (4)	0.0146 (4)	0.0002 (3)	0.0040 (3)	0.0027 (3)
C4	0.0146 (4)	0.0154 (4)	0.0174 (4)	0.0021 (3)	0.0055 (3)	0.0033 (3)
C5	0.0153 (4)	0.0151 (4)	0.0172 (4)	−0.0014 (3)	0.0047 (3)	0.0004 (3)
C6	0.0124 (4)	0.0172 (4)	0.0154 (4)	−0.0008 (3)	0.0019 (3)	0.0014 (3)
C7	0.0149 (4)	0.0202 (5)	0.0194 (4)	0.0009 (3)	0.0053 (3)	0.0045 (3)
C8	0.0161 (4)	0.0192 (5)	0.0247 (5)	0.0005 (3)	0.0055 (4)	0.0019 (4)
C9	0.0143 (4)	0.0139 (4)	0.0160 (4)	−0.0018 (3)	0.0024 (3)	0.0004 (3)
C10	0.0168 (4)	0.0147 (4)	0.0155 (4)	0.0005 (3)	0.0046 (3)	0.0003 (3)
C11	0.0174 (4)	0.0148 (4)	0.0171 (4)	−0.0035 (3)	0.0043 (3)	0.0005 (3)
C12	0.0204 (4)	0.0164 (4)	0.0164 (4)	0.0004 (3)	0.0034 (3)	0.0019 (3)

Geometric parameters (Å, °)

O1—C1	1.3515 (11)	C4—C8	1.4386 (13)
O1—C9	1.4477 (11)	C5—C6	1.3804 (13)
O2—C10	1.4289 (11)	C5—H5	0.9500
O2—C11	1.4327 (11)	C6—H6	0.9500
O3—C12	1.4211 (12)	C9—C10	1.5102 (13)
O3—H3O	0.868 (16)	C9—H9A	0.9900
N1—C7	1.1477 (13)	C9—H9B	0.9900
N2—C8	1.1486 (14)	C10—H10A	0.9900
C1—C2	1.3998 (12)	C10—H10B	0.9900
C1—C6	1.4038 (13)	C11—C12	1.5086 (13)
C2—C3	1.3965 (13)	C11—H11A	0.9900
C2—H2	0.9500	C11—H11B	0.9900

C3—C4	1.4016 (13)	C12—H12A	0.9900
C3—C7	1.4456 (13)	C12—H12B	0.9900
C4—C5	1.4005 (13)		
C1—O1—C9	118.07 (7)	O1—C9—H9A	110.4
C10—O2—C11	113.81 (7)	C10—C9—H9A	110.4
C12—O3—H3O	111.6 (10)	O1—C9—H9B	110.4
O1—C1—C2	123.95 (8)	C10—C9—H9B	110.4
O1—C1—C6	115.75 (8)	H9A—C9—H9B	108.6
C2—C1—C6	120.29 (8)	O2—C10—C9	113.51 (8)
C3—C2—C1	118.54 (8)	O2—C10—H10A	108.9
C3—C2—H2	120.7	C9—C10—H10A	108.9
C1—C2—H2	120.7	O2—C10—H10B	108.9
C2—C3—C4	121.27 (8)	C9—C10—H10B	108.9
C2—C3—C7	119.26 (8)	H10A—C10—H10B	107.7
C4—C3—C7	119.45 (8)	O2—C11—C12	108.30 (8)
C5—C4—C3	119.37 (8)	O2—C11—H11A	110.0
C5—C4—C8	120.19 (9)	C12—C11—H11A	110.0
C3—C4—C8	120.43 (8)	O2—C11—H11B	110.0
C6—C5—C4	119.85 (9)	C12—C11—H11B	110.0
C6—C5—H5	120.1	H11A—C11—H11B	108.4
C4—C5—H5	120.1	O3—C12—C11	111.32 (8)
C5—C6—C1	120.65 (8)	O3—C12—H12A	109.4
C5—C6—H6	119.7	C11—C12—H12A	109.4
C1—C6—H6	119.7	O3—C12—H12B	109.4
N1—C7—C3	177.63 (11)	C11—C12—H12B	109.4
N2—C8—C4	179.62 (12)	H12A—C12—H12B	108.0
O1—C9—C10	106.70 (7)		
C9—O1—C1—C2	0.37 (13)	C3—C4—C5—C6	−0.01 (14)
C9—O1—C1—C6	−179.67 (8)	C8—C4—C5—C6	−179.25 (9)
O1—C1—C2—C3	179.80 (8)	C4—C5—C6—C1	1.20 (14)
C6—C1—C2—C3	−0.17 (13)	O1—C1—C6—C5	178.92 (8)
C1—C2—C3—C4	1.37 (14)	C2—C1—C6—C5	−1.12 (14)
C1—C2—C3—C7	−177.34 (8)	C1—O1—C9—C10	−175.03 (8)
C2—C3—C4—C5	−1.29 (14)	C11—O2—C10—C9	−76.94 (10)
C7—C3—C4—C5	177.41 (9)	O1—C9—C10—O2	−59.71 (10)
C2—C3—C4—C8	177.94 (9)	C10—O2—C11—C12	174.83 (7)
C7—C3—C4—C8	−3.36 (14)	O2—C11—C12—O3	−71.58 (10)

Hydrogen-bond geometry (Å, °)

D—H···*A*	*D*—H	H···*A*	*D*···*A*	*D*—H···*A*
O3—H3O···O2^{i}	0.868 (16)	1.920 (16)	2.7420 (10)	157.5 (14)

Symmetry codes: (i) −*x*, −*y*+1, −*z*.

A.6 Single Crystal X-ray Diffraction Data

3,6-Bis(2-(2-(2-methoxyethoxy)ethoxy)ethoxy)phthalonitrile (2.17)

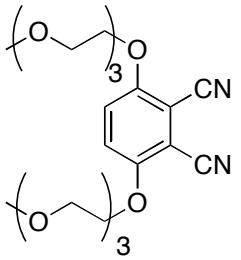

Crystal data

$C_{22}H_{32}N_2O_8$
$M_r = 452.40$

$D_x = 1.303$ Mg m^{-3}

Monoclinic, $P2_1/n$

Mo $K\alpha$ radiation
$\lambda = 0.71073$ Å

Hall symbol: -P 2yn
$a = 7.4919$ (14) Å
$b = 43.065$ (8) Å
$c = 7.9930$ (15) Å
$\beta = 116.541$ (8)°
$V = 2307.1$ (7) Å^3
$Z = 4$
$F_{000} = 968$

Cell parameters from 3585 reflections
$\theta = 2.5$–$26.7°$
$\mu = 0.10$ mm^{-1}
$T = 90$ K

Lath fragment, colorless
0.45 × 0.30 × 0.03 mm

Data collection

Nonius KappaCCD (with Oxford Cryostream) diffractometer 13077 measured reflections

Radiation source: fine-focus sealed tube
Monochromator: graphite

$T = 90$ K
ω scans with κ offsets
Absorption correction: multi-scan
Denzo and Scalepack (Otwinowski & Minor, 1997)
$T_{min} = 0.957$, $T_{max} = 0.997$

4715 independent reflections
3648 reflections with $I > 2\sigma(I)$
$R_{int} = 0.028$
$\theta_{max} = 26.7°$
$h = -9 \rightarrow 9$
$k = -43 \rightarrow 54$
$l = -9 \rightarrow 9$

Refinement

Refinement on F^2 — Secondary atom site location: difference Fourier map
Least-squares matrix: full — Hydrogen site location: inferred from neighbouring sites
$R[F^2 > 2\sigma(F^2)] = 0.047$ — H-atom parameters constrained
$wR(F^2) = 0.126$ — $w = 1/[\sigma^2(F_o^2) + (0.0596P)^2 + 1.0054P]$
where $P = (F_o^2 + 2F_c^2)/3$
$S = 1.03$ — $(\Delta/\sigma)_{max} = 0.001$
4715 reflections — $\Delta\rho_{max} = 0.50$ e Å^{-3}
292 parameters — $\Delta\rho_{min} = -0.24$ e Å^{-3}
Extinction correction: SHELXL, $Fc^*=kFc[1+0.001xFc^2\lambda^3/\sin(2\theta)]^{-1/4}$
Primary atom site location: structure-invariant direct method
Extinction coefficient: 0.0030 (8)

Refinement: Refinement of F^2 against ALL reflections. The weighted R-factor wR and goodness of fit S are based on F^2, conventional R-factors R are based on F, with F set to zero for negative F^2. The threshold expression of $F^2 > 2$sigma(F^2) is used only for calculating R-factors(gt) etc. and is not relevant to the choice of reflections for refinement. R-factors based on F^2 are statistically about twice as large as those based on F, and R- factors based on ALL data will be even larger.

Fractional atomic coordinates and isotropic or equivalent isotropic displacement parameters (Å^2)

	x	*y*	*z*	U_{iso}*/U_{eq}
O1	0.50055 (17)	0.81241 (3)	0.44353 (15)	0.0197 (3)
O2	0.75293 (17)	0.86391 (3)	0.44483 (15)	0.0189 (3)
O3	1.14881 (17)	0.88710 (3)	0.60838 (16)	0.0237 (3)
O4	1.4186 (3)	0.93878 (4)	0.7756 (2)	0.0477 (5)
O5	0.47120 (17)	0.68475 (3)	0.51017 (15)	0.0183 (3)
O6	0.55863 (17)	0.61746 (3)	0.54604 (15)	0.0208 (3)
O7	0.6130 (2)	0.53833 (3)	0.70674 (18)	0.0326 (3)
O8	0.7554 (2)	0.47426 (3)	1.0265 (2)	0.0386 (4)
N1	0.4667 (2)	0.80263 (4)	0.8599 (2)	0.0257 (4)
N2	0.4544 (2)	0.71319 (4)	0.9110 (2)	0.0230 (3)
C1	0.4775 (2)	0.76791 (4)	0.6002 (2)	0.0168 (4)
C2	0.4720 (2)	0.73547 (4)	0.6182 (2)	0.0160 (3)
C3	0.4778 (2)	0.71574 (4)	0.4813 (2)	0.0164 (3)
C4	0.4873 (2)	0.72911 (4)	0.3265 (2)	0.0182 (4)
H4	0.4912	0.7161	0.2322	0.022*
C5	0.4912 (2)	0.76106 (4)	0.3080 (2)	0.0184 (4)
H5	0.4953	0.7695	0.2001	0.022*
C6	0.4893 (2)	0.78102 (4)	0.4448 (2)	0.0165 (4)
C7	0.4715 (2)	0.78771 (4)	0.7429 (2)	0.0185 (4)

C8	0.4622 (2)	0.72255 (4)	0.7799 (2)	0.0177 (4)
C9	0.4884 (2)	0.82716 (4)	0.2756 (2)	0.0201 (4)
H9A	0.3509	0.8256	0.1734	0.024*
H9B	0.5803	0.8169	0.2344	0.024*
C10	0.5460 (2)	0.86056 (4)	0.3227 (2)	0.0194 (4)
H10A	0.5133	0.8723	0.2061	0.023*
H10B	0.4674	0.8695	0.3828	0.023*
C11	0.8731 (2)	0.86487 (4)	0.3473 (2)	0.0193 (4)
H11A	0.8533	0.8849	0.2807	0.023*
H11B	0.8331	0.8479	0.2537	0.023*
C12	1.0887 (2)	0.86120 (4)	0.4849 (2)	0.0208 (4)
H12A	1.1070	0.8418	0.5570	0.025*
H12B	1.1717	0.8599	0.4174	0.025*
C13	1.3539 (3)	0.88505 (5)	0.7397 (2)	0.0255 (4)
H13A	1.4375	0.8847	0.6727	0.031*
H13B	1.3777	0.8656	0.8123	0.031*
C14	1.4101 (3)	0.91224 (5)	0.8694 (3)	0.0280 (4)
H14A	1.3104	0.9150	0.9178	0.034*
H14B	1.5417	0.9085	0.9770	0.034*
C15	1.4659 (4)	0.96565 (6)	0.8939 (3)	0.0562 (7)
H15A	1.3695	0.9676	0.9451	0.084*
H15B	1.4600	0.9842	0.8208	0.084*
H15C	1.6006	0.9635	0.9967	0.084*
C16	0.4574 (3)	0.66438 (4)	0.3602 (2)	0.0197 (4)
H16A	0.5874	0.6637	0.3560	0.024*
H16B	0.3560	0.6724	0.2388	0.024*
C17	0.4008 (3)	0.63256 (4)	0.3918 (2)	0.0209 (4)
H17A	0.2821	0.6339	0.4154	0.025*
H17B	0.3645	0.6200	0.2774	0.025*
C18	0.5133 (3)	0.58521 (4)	0.5461 (2)	0.0226 (4)
H18A	0.5132	0.5750	0.4351	0.027*
H18B	0.3789	0.5828	0.5395	0.027*
C19	0.6657 (3)	0.57018 (4)	0.7208 (3)	0.0264 (4)
H19A	0.8012	0.5727	0.7301	0.032*
H19B	0.6632	0.5796	0.8328	0.032*
C20	0.7196 (3)	0.52234 (5)	0.8781 (3)	0.0360 (5)
H20A	0.6899	0.5316	0.9763	0.043*
H20B	0.8649	0.5241	0.9185	0.043*
C21	0.6578 (3)	0.48882 (5)	0.8499 (3)	0.0373 (5)
H21A	0.5112	0.4870	0.8008	0.045*
H21B	0.6974	0.4790	0.7596	0.045*

C22	0.7276 (4)	0.44177 (5)	1.0151 (3)	0.0461 (6)
H22A	0.5847	0.4371	0.9603	0.069*
H22B	0.7945	0.4328	1.1408	0.069*
H22C	0.7844	0.4329	0.9365	0.069*

Atomic displacement parameters (Å^2)

	U^{11}	U^{22}	U^{33}	U^{12}	U^{13}	U^{23}
O1	0.0273 (6)	0.0185 (7)	0.0150 (6)	−0.0027 (5)	0.0108 (5)	0.0011 (5)
O2	0.0186 (6)	0.0241 (7)	0.0144 (5)	−0.0027 (5)	0.0076 (5)	−0.0016 (5)
O3	0.0182 (6)	0.0250 (7)	0.0231 (6)	−0.0007 (5)	0.0048 (5)	−0.0057 (5)
O4	0.0705 (12)	0.0284 (9)	0.0276 (8)	−0.0075 (8)	0.0070 (8)	0.0008 (6)
O5	0.0239 (6)	0.0176 (6)	0.0131 (5)	−0.0001 (5)	0.0079 (5)	−0.0015 (5)
O6	0.0233 (6)	0.0187 (6)	0.0169 (6)	−0.0002 (5)	0.0057 (5)	0.0011 (5)
O7	0.0439 (8)	0.0218 (7)	0.0248 (7)	−0.0032 (6)	0.0087 (6)	0.0014 (6)
O8	0.0470 (9)	0.0272 (8)	0.0325 (8)	−0.0052 (7)	0.0095 (7)	0.0031 (6)
N1	0.0337 (9)	0.0240 (9)	0.0202 (8)	0.0007 (7)	0.0128 (7)	−0.0005 (7)
N2	0.0293 (8)	0.0235 (8)	0.0178 (7)	0.0003 (6)	0.0120 (6)	−0.0008 (6)
C1	0.0152 (8)	0.0216 (9)	0.0132 (7)	−0.0002 (7)	0.0060 (6)	−0.0016 (7)
C2	0.0136 (7)	0.0209 (9)	0.0124 (7)	−0.0003 (6)	0.0048 (6)	−0.0003 (7)
C3	0.0132 (7)	0.0194 (9)	0.0139 (7)	0.0000 (6)	0.0038 (6)	−0.0007 (7)
C4	0.0179 (8)	0.0235 (9)	0.0128 (8)	−0.0008 (7)	0.0064 (6)	−0.0030 (7)
C5	0.0172 (8)	0.0261 (10)	0.0118 (7)	−0.0011 (7)	0.0065 (6)	0.0005 (7)
C6	0.0137 (7)	0.0193 (9)	0.0147 (8)	−0.0013 (6)	0.0047 (6)	0.0005 (7)
C7	0.0184 (8)	0.0200 (9)	0.0161 (8)	−0.0007 (7)	0.0068 (7)	0.0026 (7)
C8	0.0169 (8)	0.0183 (9)	0.0158 (8)	0.0005 (7)	0.0054 (7)	−0.0029 (7)
C9	0.0199 (8)	0.0261 (10)	0.0113 (7)	−0.0025 (7)	0.0043 (6)	0.0029 (7)
C10	0.0182 (8)	0.0227 (9)	0.0175 (8)	0.0026 (7)	0.0080 (7)	0.0040 (7)
C11	0.0203 (8)	0.0231 (9)	0.0168 (8)	−0.0024 (7)	0.0103 (7)	−0.0004 (7)
C12	0.0217 (8)	0.0212 (9)	0.0197 (8)	−0.0006 (7)	0.0095 (7)	−0.0020 (7)
C13	0.0201 (9)	0.0303 (11)	0.0219 (9)	−0.0025 (7)	0.0057 (7)	0.0010 (8)
C14	0.0244 (9)	0.0334 (11)	0.0238 (9)	−0.0017 (8)	0.0087 (8)	0.0009 (8)
C15	0.0735 (18)	0.0265 (13)	0.0441 (13)	−0.0039 (12)	0.0044 (13)	−0.0072 (11)
C16	0.0245 (9)	0.0205 (9)	0.0125 (7)	0.0016 (7)	0.0067 (7)	−0.0032 (7)
C17	0.0210 (8)	0.0228 (10)	0.0146 (8)	0.0002 (7)	0.0040 (7)	−0.0009 (7)
C18	0.0259 (9)	0.0192 (9)	0.0229 (9)	−0.0025 (7)	0.0109 (8)	−0.0022 (7)
C19	0.0337 (10)	0.0190 (10)	0.0258 (9)	−0.0016 (8)	0.0126 (8)	−0.0015 (8)
C20	0.0421 (12)	0.0284 (11)	0.0297 (10)	−0.0004 (9)	0.0092 (9)	0.0035 (9)
C21	0.0457 (13)	0.0279 (12)	0.0305 (11)	−0.0047 (9)	0.0099 (9)	0.0032 (9)
C22	0.0540 (14)	0.0272 (12)	0.0418 (12)	−0.0070 (10)	0.0078 (11)	0.0089 (10)

Geometric parameters (Å, °)

O1—C6	1.354 (2)	C10—H10B	0.9900
O1—C9	1.4509 (19)	C11—C12	1.502 (2)
O2—C10	1.423 (2)	C11—H11A	0.9900
O2—C11	1.430 (2)	C11—H11B	0.9900
O3—C12	1.423 (2)	C12—H12A	0.9900
O3—C13	1.424 (2)	C12—H12B	0.9900
O4—C14	1.384 (2)	C13—C14	1.494 (3)
O4—C15	1.435 (3)	C13—H13A	0.9900
O5—C3	1.359 (2)	C13—H13B	0.9900
O5—C16	1.4515 (19)	C14—H14A	0.9900
O6—C17	1.428 (2)	C14—H14B	0.9900
O6—C18	1.430 (2)	C15—H15A	0.9800
O7—C20	1.418 (2)	C15—H15B	0.9800
O7—C19	1.418 (2)	C15—H15C	0.9800
O8—C22	1.411 (3)	C16—C17	1.489 (3)
O8—C21	1.414 (2)	C16—H16A	0.9900
N1—C7	1.148 (2)	C16—H16B	0.9900
N2—C8	1.149 (2)	C17—H17A	0.9900
C1—C6	1.403 (2)	C17—H17B	0.9900
C1—C2	1.407 (2)	C18—C19	1.499 (3)
C1—C7	1.441 (2)	C18—H18A	0.9900
C2—C3	1.401 (2)	C18—H18B	0.9900
C2—C8	1.439 (2)	C19—H19A	0.9900
C3—C4	1.395 (2)	C19—H19B	0.9900
C4—C5	1.385 (3)	C20—C21	1.502 (3)
C4—H4	0.9500	C20—H20A	0.9900
C5—C6	1.396 (2)	C20—H20B	0.9900
C5—H5	0.9500	C21—H21A	0.9900
C9—C10	1.501 (2)	C21—H21B	0.9900
C9—H9A	0.9900	C22—H22A	0.9800
C9—H9B	0.9900	C22—H22B	0.9800
C10—H10A	0.9900	C22—H22C	0.9800
C6—O1—C9	117.72 (13)	C14—C13—H13B	109.7
C10—O2—C11	112.77 (12)	H13A—C13—H13B	108.2
C12—O3—C13	111.46 (13)	O4—C14—C13	109.79 (15)
C14—O4—C15	111.51 (17)	O4—C14—H14A	109.7
C3—O5—C16	116.61 (12)	C13—C14—H14A	109.7
C17—O6—C18	109.73 (13)	O4—C14—H14B	109.7
C20—O7—C19	112.12 (14)	C13—C14—H14B	109.7
C22—O8—C21	112.33 (16)	H14A—C14—H14B	108.2

C6—C1—C2	120.43 (15)	O4—C15—H15A	109.5
C6—C1—C7	119.99 (15)	O4—C15—H15B	109.5
C2—C1—C7	119.58 (15)	H15A—C15—H15B	109.5
C3—C2—C1	120.64 (15)	O4—C15—H15C	109.5
C3—C2—C8	119.92 (16)	H15A—C15—H15C	109.5
C1—C2—C8	119.44 (15)	H15B—C15—H15C	109.5
O5—C3—C4	125.15 (15)	O5—C16—C17	109.68 (13)
O5—C3—C2	116.54 (14)	O5—C16—H16A	109.7
C4—C3—C2	118.31 (16)	C17—C16—H16A	109.7
C5—C4—C3	121.05 (15)	O5—C16—H16B	109.7
C5—C4—H4	119.5	C17—C16—H16B	109.7
C3—C4—H4	119.5	H16A—C16—H16B	108.2
C4—C5—C6	121.36 (15)	O6—C17—C16	112.16 (14)
C4—C5—H5	119.3	O6—C17—H17A	109.2
C6—C5—H5	119.3	C16—C17—H17A	109.2
O1—C6—C5	125.93 (15)	O6—C17—H17B	109.2
O1—C6—C1	115.89 (14)	C16—C17—H17B	109.2
C5—C6—C1	118.18 (16)	H17A—C17—H17B	107.9
N1—C7—C1	177.76 (18)	O6—C18—C19	109.71 (14)
N2—C8—C2	177.80 (18)	O6—C18—H18A	109.7
O1—C9—C10	107.17 (13)	C19—C18—H18A	109.7
O1—C9—H9A	110.3	O6—C18—H18B	109.7
C10—C9—H9A	110.3	C19—C18—H18B	109.7
O1—C9—H9B	110.3	H18A—C18—H18B	108.2
C10—C9—H9B	110.3	O7—C19—C18	105.92 (14)
H9A—C9—H9B	108.5	O7—C19—H19A	110.6
O2—C10—C9	111.87 (14)	C18—C19—H19A	110.6
O2—C10—H10A	109.2	O7—C19—H19B	110.6
C9—C10—H10A	109.2	C18—C19—H19B	110.6
O2—C10—H10B	109.2	H19A—C19—H19B	108.7
C9—C10—H10B	109.2	O7—C20—C21	108.60 (16)
H10A—C10—H10B	107.9	O7—C20—H20A	110.0
O2—C11—C12	109.32 (13)	C21—C20—H20A	110.0
O2—C11—H11A	109.8	O7—C20—H20B	110.0
C12—C11—H11A	109.8	C21—C20—H20B	110.0
O2—C11—H11B	109.8	H20A—C20—H20B	108.4
C12—C11—H11B	109.8	O8—C21—C20	106.81 (16)
H11A—C11—H11B	108.3	O8—C21—H21A	110.4
O3—C12—C11	109.21 (14)	C20—C21—H21A	110.4
O3—C12—H12A	109.8	O8—C21—H21B	110.4
C11—C12—H12A	109.8	C20—C21—H21B	110.4

O3—C12—H12B	109.8	H21A—C21—H21B	108.6
C11—C12—H12B	109.8	O8—C22—H22A	109.5
H12A—C12—H12B	108.3	O8—C22—H22B	109.5
O3—C13—C14	109.88 (16)	H22A—C22—H22B	109.5
O3—C13—H13A	109.7	O8—C22—H22C	109.5
C14—C13—H13A	109.7	H22A—C22—H22C	109.5
O3—C13—H13B	109.7	H22B—C22—H22C	109.5
C6—C1—C2—C3	−0.2 (2)	C7—C1—C6—C5	−178.86 (15)
C7—C1—C2—C3	−179.99 (15)	C6—O1—C9—C10	−168.61 (13)
C6—C1—C2—C8	179.31 (15)	C11—O2—C10—C9	85.10 (17)
C7—C1—C2—C8	−0.5 (2)	O1—C9—C10—O2	70.29 (17)
C16—O5—C3—C4	−5.1 (2)	C10—O2—C11—C12	−167.39 (14)
C16—O5—C3—C2	174.15 (13)	C13—O3—C12—C11	−178.84 (14)
C1—C2—C3—O5	−179.82 (14)	O2—C11—C12—O3	−64.54 (18)
C8—C2—C3—O5	0.7 (2)	C12—O3—C13—C14	−178.75 (15)
C1—C2—C3—C4	−0.5 (2)	C15—O4—C14—C13	178.09 (19)
C8—C2—C3—C4	−179.99 (14)	O3—C13—C14—O4	−72.2 (2)
O5—C3—C4—C5	179.27 (15)	C3—O5—C16—C17	−165.87 (14)
C2—C3—C4—C5	0.0 (2)	C18—O6—C17—C16	−167.88 (14)
C3—C4—C5—C6	1.2 (2)	O5—C16—C17—O6	−70.50 (17)
C9—O1—C6—C5	8.3 (2)	C17—O6—C18—C19	−172.89 (14)
C9—O1—C6—C1	−172.62 (13)	C20—O7—C19—C18	−168.17 (16)
C4—C5—C6—O1	177.28 (15)	O6—C18—C19—O7	−178.35 (14)
C4—C5—C6—C1	−1.8 (2)	C19—O7—C20—C21	−178.98 (18)
C2—C1—C6—O1	−177.87 (14)	C22—O8—C21—C20	−173.2 (2)
C7—C1—C6—O1	2.0 (2)	O7—C20—C21—O8	−175.61 (17)
C2—C1—C6—C5	1.3 (2)		

A.7 Single Crystal X-ray Diffraction Data

3,6-Bis(2-(2-methoxyethoxy)ethoxy)phthalonitrile (**2.18**)

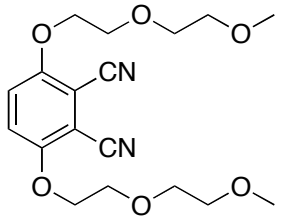

Crystal data

$C_{18}H_{24}N_2O_6$
$M_r = 364.39$

$D_x = 1.345$ Mg m^{-3}

Monoclinic, $P2_1$

Mo $K\alpha$ radiation
$\lambda = 0.71073$ Å

Hall symbol: P 2yb
$a = 4.6074$ (12) Å
$b = 26.513$ (8) Å
$c = 7.586$ (2) Å
$\beta = 103.904$ (12)°
$V = 899.5$ (4) Å^3
$Z = 2$
$F_{000} = 388$

Cell parameters from 1582 reflections
$\theta = 2.5$–$28.2°$
$\mu = 0.10$ mm^{-1}
$T = 90$ K

Plate fragment, colorless
0.45 × 0.25 × 0.12 mm

Data collection

Nonius KappaCCD (with Oxford Cryostream) diffractometer
Radiation source: fine-focus sealed tube
Monochromator: graphite

$T = 90$ K
$P =$ kPa
ω scans with κ offsets
Absorption correction: none
6074 measured reflections

2263 independent reflections

2159 reflections with $I > 2\sigma(I)$
$R_{int} = 0.018$
$\theta_{max} = 28.3°$
$\theta_{min} = 2.7°$
$h = -6 \rightarrow 6$
$k = -35 \rightarrow 22$
$l = -10 \rightarrow 10$

Refinement

Refinement on F^2 Hydrogen site location: inferred from neighbouring sites
Least-squares matrix: full H-atom parameters constrained
$R[F^2 > 2\sigma(F^2)] = 0.028$ $w = 1/[\sigma^2(F_o^2) + (0.0371P)^2 + 0.1419P]$ where $P = (F_o^2 + 2F_c^2)/3$
$wR(F^2) = 0.072$ $(\Delta/\sigma)_{max} < 0.001$

$S = 1.04$ $\Delta\rho_{max} = 0.22$ e Å^{-3}
2263 reflections $\Delta\rho_{min} = -0.18$ e Å^{-3}
238 parameters
Extinction correction: SHELXL, $Fc^*=kFc[1+0.001xFc^2\lambda^3/\sin(2\theta)]^{-1/4}$
constraints: Absolute
Primary atom site location: structure-invariant direct methods Flack parameter:
Extinction coefficient: 0.018 (3)
Secondary atom site location: difference Fourier map
parameter: Rogers

Refinement: Refinement of F^2 against ALL reflections. The weighted R-factor wR and goodness of fit S are based on F^2, conventional R-factors R are based on F, with F set to zero for negative F^2. The threshold expression of $F^2 > 2\text{sigma}(F^2)$ is used only for calculating R-factors(gt) etc. and is not relevant to the choice of reflections for refinement. R-factors based on F^2 are statistically about twice as large as those based on F, and R- factors based on ALL data will be even larger.

Fractional atomic coordinates and isotropic or equivalent isotropic displacement parameters (Å^2)

	x	*y*	*z*	U_{iso}*/U_{eq}
O1	−0.1720 (3)	0.33495 (5)	0.88536 (15)	0.0162 (2)
O2	−0.2020 (3)	0.23140 (5)	0.98747 (17)	0.0173 (2)
O3	−0.4165 (3)	0.10341 (5)	0.86286 (17)	0.0201 (3)
O4	0.4730 (2)	0.49502 (5)	0.70612 (15)	0.0153 (2)
O5	0.7157 (2)	0.60106 (5)	0.69229 (16)	0.0167 (2)
O6	0.9183 (3)	0.70876 (5)	0.45922 (18)	0.0221 (3)
N1	−0.4797 (3)	0.35446 (6)	0.4224 (2)	0.0201 (3)
N2	−0.0324 (3)	0.46404 (6)	0.2988 (2)	0.0204 (3)
C1	−0.0622 (3)	0.39243 (6)	0.6774 (2)	0.0133 (3)
C2	0.1023 (4)	0.43313 (6)	0.6318 (2)	0.0136 (3)
C3	0.3263 (3)	0.45648 (6)	0.7646 (2)	0.0136 (3)
C4	0.3784 (3)	0.43905 (6)	0.9433 (2)	0.0145 (3)
H4	0.5265	0.4549	1.0355	0.017*
C5	0.2164 (3)	0.39869 (6)	0.9882 (2)	0.0144 (3)

H5	0.2567	0.3873	1.1105	0.017*
C6	−0.0046 (3)	0.37463 (6)	0.8564 (2)	0.0135 (3)
C7	−0.2955 (4)	0.37011 (6)	0.5378 (2)	0.0151 (3)
C8	0.0343 (3)	0.45090 (6)	0.4477 (2)	0.0154 (3)
C9	−0.1327 (4)	0.31785 (7)	1.0706 (2)	0.0157 (3)
H9A	−0.1929	0.3446	1.1455	0.019*
H9B	0.0796	0.3093	1.1234	0.019*
C10	−0.3263 (4)	0.27187 (7)	1.0667 (2)	0.0166 (3)
H10A	−0.3363	0.2628	1.1918	0.020*
H10B	−0.5317	0.2789	0.9949	0.020*
C11	−0.3831 (4)	0.18715 (7)	0.9716 (2)	0.0177 (3)
H11A	−0.5860	0.1941	0.8959	0.021*
H11B	−0.4008	0.1759	1.0930	0.021*
C12	−0.2319 (4)	0.14712 (7)	0.8840 (2)	0.0184 (3)
H12A	−0.2084	0.1589	0.7644	0.022*
H12B	−0.0313	0.1394	0.9616	0.022*
C13	−0.3116 (4)	0.06553 (7)	0.7598 (2)	0.0229 (4)
H13A	−0.3262	0.0779	0.6363	0.034*
H13B	−0.4339	0.0351	0.7549	0.034*
H13C	−0.1026	0.0576	0.8174	0.034*
C14	0.6980 (3)	0.52110 (6)	0.8420 (2)	0.0154 (3)
H14A	0.8345	0.4964	0.9177	0.018*
H14B	0.6017	0.5412	0.9220	0.018*
C15	0.8708 (3)	0.55516 (6)	0.7449 (2)	0.0163 (3)
H15A	1.0690	0.5625	0.8259	0.020*
H15B	0.9031	0.5377	0.6358	0.020*
C16	0.8730 (4)	0.63003 (7)	0.5860 (2)	0.0174 (3)
H16A	0.8402	0.6154	0.4627	0.021*
H16B	1.0901	0.6293	0.6430	0.021*
C17	0.7616 (4)	0.68372 (7)	0.5737 (2)	0.0181 (3)
H17A	0.5432	0.6849	0.5208	0.022*
H17B	0.8050	0.6996	0.6954	0.022*
C18	0.8198 (4)	0.75920 (7)	0.4207 (3)	0.0245 (4)
H18A	0.6038	0.7594	0.3675	0.037*
H18B	0.9237	0.7741	0.3347	0.037*
H18C	0.8641	0.7789	0.5333	0.037*

Atomic displacement parameters (Å²)

	U^{11}	U^{22}	U^{33}	U^{12}	U^{13}	U^{23}
O1	0.0196 (5)	0.0158 (6)	0.0127 (5)	−0.0026 (4)	0.0028 (4)	0.0012 (4)

O2	0.0170 (5)	0.0133 (6)	0.0227 (6)	−0.0006 (4)	0.0068 (4)	−0.0012 (5)
O3	0.0225 (6)	0.0144 (6)	0.0248 (6)	−0.0028 (5)	0.0087 (5)	−0.0019 (5)
O4	0.0150 (5)	0.0150 (6)	0.0145 (5)	−0.0031 (4)	0.0008 (4)	0.0003 (4)
O5	0.0150 (5)	0.0147 (6)	0.0213 (5)	0.0015 (4)	0.0059 (4)	0.0023 (5)
O6	0.0253 (6)	0.0172 (6)	0.0265 (6)	0.0018 (5)	0.0111 (5)	0.0045 (5)
N1	0.0214 (7)	0.0201 (7)	0.0176 (6)	−0.0033 (6)	0.0024 (5)	0.0008 (6)
N2	0.0222 (7)	0.0192 (7)	0.0179 (7)	−0.0029 (6)	0.0012 (5)	0.0012 (6)
C1	0.0131 (7)	0.0137 (7)	0.0128 (6)	0.0016 (6)	0.0024 (5)	−0.0019 (6)
C2	0.0138 (7)	0.0144 (7)	0.0124 (7)	0.0025 (6)	0.0027 (5)	0.0007 (6)
C3	0.0118 (6)	0.0136 (8)	0.0157 (7)	0.0011 (5)	0.0041 (5)	−0.0010 (6)
C4	0.0136 (7)	0.0151 (8)	0.0138 (7)	0.0008 (6)	0.0015 (5)	−0.0015 (6)
C5	0.0155 (7)	0.0138 (8)	0.0133 (7)	0.0020 (6)	0.0023 (5)	0.0006 (6)
C6	0.0132 (7)	0.0128 (7)	0.0152 (7)	0.0020 (6)	0.0044 (5)	0.0002 (6)
C7	0.0165 (7)	0.0147 (8)	0.0148 (7)	0.0008 (6)	0.0052 (6)	0.0013 (6)
C8	0.0145 (7)	0.0139 (8)	0.0171 (7)	−0.0014 (6)	0.0025 (6)	−0.0020 (6)
C9	0.0171 (7)	0.0171 (8)	0.0133 (7)	0.0002 (6)	0.0044 (5)	0.0005 (6)
C10	0.0173 (7)	0.0140 (8)	0.0200 (7)	0.0008 (6)	0.0074 (6)	0.0017 (6)
C11	0.0175 (7)	0.0148 (8)	0.0211 (7)	−0.0017 (6)	0.0053 (6)	0.0020 (6)
C12	0.0188 (8)	0.0149 (8)	0.0223 (8)	−0.0015 (6)	0.0066 (6)	0.0008 (6)
C13	0.0288 (9)	0.0188 (9)	0.0214 (8)	0.0000 (7)	0.0067 (7)	−0.0018 (7)
C14	0.0118 (7)	0.0159 (8)	0.0166 (7)	−0.0017 (6)	−0.0001 (5)	−0.0007 (6)
C15	0.0129 (7)	0.0157 (8)	0.0198 (7)	0.0012 (6)	0.0030 (6)	0.0000 (6)
C16	0.0160 (7)	0.0172 (8)	0.0205 (8)	−0.0008 (6)	0.0072 (6)	0.0002 (6)
C17	0.0173 (7)	0.0184 (8)	0.0194 (7)	−0.0003 (6)	0.0059 (6)	0.0007 (7)
C18	0.0306 (9)	0.0165 (9)	0.0251 (9)	−0.0004 (7)	0.0040 (7)	0.0026 (7)

Geometric parameters (Å, °)

O1—C6	1.354 (2)	C9—H9A	0.9900
O1—C9	1.4458 (19)	C9—H9B	0.9900
O2—C10	1.416 (2)	C10—H10A	0.9900
O2—C11	1.428 (2)	C10—H10B	0.9900
O3—C12	1.424 (2)	C11—C12	1.509 (2)
O3—C13	1.426 (2)	C11—H11A	0.9900
O4—C3	1.357 (2)	C11—H11B	0.9900
O4—C14	1.4496 (18)	C12—H12A	0.9900
O5—C15	1.419 (2)	C12—H12B	0.9900
O5—C16	1.430 (2)	C13—H13A	0.9800
O6—C18	1.420 (2)	C13—H13B	0.9800
O6—C17	1.420 (2)	C13—H13C	0.9800
N1—C7	1.141 (2)	C14—C15	1.507 (2)
N2—C8	1.151 (2)	C14—H14A	0.9900

C1—C6	1.401 (2)	C14—H14B	0.9900
C1—C2	1.409 (2)	C15—H15A	0.9900
C1—C7	1.442 (2)	C15—H15B	0.9900
C2—C3	1.401 (2)	C16—C17	1.508 (2)
C2—C8	1.435 (2)	C16—H16A	0.9900
C3—C4	1.397 (2)	C16—H16B	0.9900
C4—C5	1.393 (2)	C17—H17A	0.9900
C4—H4	0.9500	C17—H17B	0.9900
C5—C6	1.398 (2)	C18—H18A	0.9800
C5—H5	0.9500	C18—H18B	0.9800
C9—C10	1.507 (2)	C18—H18C	0.9800
C6—O1—C9	117.30 (12)	H11A—C11—H11B	108.6
C10—O2—C11	111.75 (12)	O3—C12—C11	107.21 (13)
C12—O3—C13	111.29 (13)	O3—C12—H12A	110.3
C3—O4—C14	117.01 (12)	C11—C12—H12A	110.3
C15—O5—C16	109.28 (13)	O3—C12—H12B	110.3
C18—O6—C17	112.44 (14)	C11—C12—H12B	110.3
C6—C1—C2	120.54 (14)	H12A—C12—H12B	108.5
C6—C1—C7	120.51 (15)	O3—C13—H13A	109.5
C2—C1—C7	118.94 (14)	O3—C13—H13B	109.5
C3—C2—C1	120.59 (14)	H13A—C13—H13B	109.5
C3—C2—C8	120.36 (15)	O3—C13—H13C	109.5
C1—C2—C8	119.05 (14)	H13A—C13—H13C	109.5
O4—C3—C4	125.67 (14)	H13B—C13—H13C	109.5
O4—C3—C2	115.87 (14)	O4—C14—C15	108.06 (13)
C4—C3—C2	118.45 (15)	O4—C14—H14A	110.1
C5—C4—C3	120.94 (14)	C15—C14—H14A	110.1
C5—C4—H4	119.5	O4—C14—H14B	110.1
C3—C4—H4	119.5	C15—C14—H14B	110.1
C4—C5—C6	121.08 (15)	H14A—C14—H14B	108.4
C4—C5—H5	119.5	O5—C15—C14	111.23 (13)
C6—C5—H5	119.5	O5—C15—H15A	109.4
O1—C6—C5	125.71 (14)	C14—C15—H15A	109.4
O1—C6—C1	115.90 (14)	O5—C15—H15B	109.4
C5—C6—C1	118.39 (15)	C14—C15—H15B	109.4
N1—C7—C1	176.74 (19)	H15A—C15—H15B	108.0
N2—C8—C2	176.92 (18)	O5—C16—C17	109.31 (13)
O1—C9—C10	107.43 (13)	O5—C16—H16A	109.8
O1—C9—H9A	110.2	C17—C16—H16A	109.8
C10—C9—H9A	110.2	O5—C16—H16B	109.8
O1—C9—H9B	110.2	C17—C16—H16B	109.8

C10—C9—H9B	110.2	H16A—C16—H16B	108.3
H9A—C9—H9B	108.5	O6—C17—C16	105.28 (13)
O2—C10—C9	108.87 (13)	O6—C17—H17A	110.7
O2—C10—H10A	109.9	C16—C17—H17A	110.7
C9—C10—H10A	109.9	O6—C17—H17B	110.7
O2—C10—H10B	109.9	C16—C17—H17B	110.7
C9—C10—H10B	109.9	H17A—C17—H17B	108.8
H10A—C10—H10B	108.3	O6—C18—H18A	109.5
O2—C11—C12	107.03 (13)	O6—C18—H18B	109.5
O2—C11—H11A	110.3	H18A—C18—H18B	109.5
C12—C11—H11A	110.3	O6—C18—H18C	109.5
O2—C11—H11B	110.3	H18A—C18—H18C	109.5
C12—C11—H11B	110.3	H18B—C18—H18C	109.5
C6—C1—C2—C3	0.0 (2)	C2—C1—C6—O1	−179.11 (14)
C7—C1—C2—C3	178.63 (15)	C7—C1—C6—O1	2.3 (2)
C6—C1—C2—C8	−179.06 (15)	C2—C1—C6—C5	0.9 (2)
C7—C1—C2—C8	−0.4 (2)	C7—C1—C6—C5	−177.68 (15)
C14—O4—C3—C4	−1.7 (2)	C6—O1—C9—C10	−176.52 (13)
C14—O4—C3—C2	177.72 (14)	C11—O2—C10—C9	−177.18 (12)
C1—C2—C3—O4	179.44 (14)	O1—C9—C10—O2	70.38 (16)
C8—C2—C3—O4	−1.5 (2)	C10—O2—C11—C12	179.30 (13)
C1—C2—C3—C4	−1.1 (2)	C13—O3—C12—C11	172.49 (14)
C8—C2—C3—C4	177.91 (15)	O2—C11—C12—O3	−178.24 (12)
O4—C3—C4—C5	−179.28 (15)	C3—O4—C14—C15	169.47 (13)
C2—C3—C4—C5	1.4 (2)	C16—O5—C15—C14	−174.51 (13)
C3—C4—C5—C6	−0.4 (2)	O4—C14—C15—O5	81.64 (16)
C9—O1—C6—C5	4.1 (2)	C15—O5—C16—C17	−164.48 (13)
C9—O1—C6—C1	−175.85 (14)	C18—O6—C17—C16	174.94 (13)
C4—C5—C6—O1	179.32 (15)	O5—C16—C17—O6	−177.18 (13)
C4—C5—C6—C1	−0.7 (2)		

A.8 Single Crystal X-ray Diffraction Data

3-(2-(2-(2-Ethoxyethoxy)ethoxy)ethylthio)phthalonitrile (**2.20**)

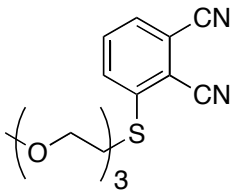

Crystal data

$C_{15}H_{18}N_2O_3S$
$M_r = 306.37$
Triclinic, $P\bar{1}$

Hall symbol: -P 1

$a = 7.947\ (5)$ Å
$b = 7.969\ (6)$ Å
$c = 13.704\ (11)$ Å
$\alpha = 95.09\ (3)°$
$\beta = 92.13\ (4)°$
$\gamma = 114.77\ (4)°$
$V = 782.3\ (10)$ Å^3
$Z = 2$

$F_{000} = 324$
$D_x = 1.301$ Mg m^{-3}

Mo $K\alpha$ radiation
$\lambda = 0.71073$ Å
Cell parameters from 1905 reflections
$\theta = 2.5–23.0°$
$\mu = 0.22$ mm^{-1}
$T = 100$ K

Plate, colorless
0.32 × 0.22 × 0.01 mm

Data collection

Nonius KappaCCD (with Oxford Cryostream) diffractometer
Radiation source: fine-focus sealed tube
Monochromator: graphite

$T = 100$ K
$P =$ kPa
ω scans with κ offsets
Absorption correction: multi-scan
Denzo and Scalepack (Otwinowski & Minor, 1997)
$T_{min} = 0.934$, $T_{max} = 0.998$

6918 measured reflections
2157 independent reflections
1731 reflections with $I > 2\sigma(I)$
$R_{int} = 0.064$
$\theta_{max} = 23.1°$
$\theta_{min} = 2.8°$
$h = -8 \rightarrow 8$
$k = -8 \rightarrow 8$
$l = -15 \rightarrow 15$

Refinement

Refinement on F^2 — Secondary atom site location: difference Fourier map
Least-squares matrix: full — Hydrogen site location: inferred from neighbouring sites
$R[F^2 > 2\sigma(F^2)] = 0.081$ — H-atom parameters constrained
$wR(F^2) = 0.258$ — $w = 1/[\sigma^2(F_o^2) + (0.1242P)^2 + 1.8912P]$ where $P = (F_o^2 + 2F_c^2)/3$
$S = 1.22$ — $(\Delta/\sigma)_{max} < 0.001$
2157 reflections — $\Delta\rho_{max} = 0.36$ e Å^{-3}
192 parameters — $\Delta\rho_{min} = -0.36$ e Å^{-3}
constraints — Extinction correction: SHELXL, $Fc^* = kFc[1+0.001xFc^2\lambda^3/\sin(2\theta)]^{-1/4}$
Primary atom site location: structure-invariant direct methods — Extinction coefficient: 0.094 (19)

Refinement: Refinement of F^2 against ALL reflections. The weighted R-factor wR and goodness of fit S are based on F^2, conventional R-factors R are based on F, with F set to zero for negative F^2. The threshold expression of $F^2 > 2\text{sigma}(F^2)$ is used only for calculating R-factors(gt) etc. and is not relevant to the choice of reflections for refinement. R-factors based on F^2 are statistically about twice as large as those based on F, and R- factors based on ALL data will be even larger.

Fractional atomic coordinates and isotropic or equivalent isotropic displacement parameters (Å^2)

	x	*y*	*z*	U_{iso}*/U_{eq}
S1	0.6219 (2)	0.5549 (3)	0.76187 (13)	0.0341 (7)
O1	0.7105 (6)	0.4146 (6)	0.5595 (3)	0.0303 (12)
O2	0.7187 (6)	0.1288 (6)	0.4182 (3)	0.0334 (13)
O3	0.9501 (6)	−0.0311 (7)	0.3199 (4)	0.0343 (13)
N1	0.2448 (9)	0.6511 (10)	0.8417 (5)	0.0455 (18)
N2	0.3483 (10)	0.8634 (10)	1.1182 (5)	0.0435 (17)
C1	0.6827 (9)	0.6539 (9)	0.8843 (5)	0.0280 (17)
C2	0.5540 (9)	0.7016 (10)	0.9336 (5)	0.0295 (17)
C3	0.5920 (9)	0.7785 (9)	1.0321 (5)	0.0304 (17)
C4	0.7605 (9)	0.8113 (10)	1.0826 (5)	0.0325 (18)
H4	0.7873	0.8631	1.1496	0.039*
C5	0.8891 (10)	0.7664 (10)	1.0329 (5)	0.0343 (18)
H5	1.0051	0.7904	1.0664	0.041*
C6	0.8518 (9)	0.6889 (10)	0.9372 (5)	0.0312 (17)
H6	0.9413	0.6581	0.9057	0.037*
C7	0.3800 (11)	0.6726 (11)	0.8818 (5)	0.0338 (18)

C8	0.4570 (10)	0.8233 (10)	1.0811 (5)	0.0331 (18)
C9	0.8446 (9)	0.5993 (10)	0.7138 (5)	0.0317 (17)
H9A	0.9398	0.7213	0.7442	0.038*
H9B	0.8844	0.5020	0.7298	0.038*
C10	0.8263 (9)	0.5988 (9)	0.6044 (5)	0.0293 (17)
H10A	0.7711	0.6846	0.5882	0.035*
H10B	0.9507	0.6425	0.5789	0.035*
C11	0.6828 (10)	0.4065 (10)	0.4564 (5)	0.0326 (17)
H11A	0.8043	0.4712	0.4293	0.039*
H11B	0.6048	0.4719	0.4410	0.039*
C12	0.5912 (9)	0.2116 (10)	0.4092 (5)	0.0324 (17)
H12A	0.4773	0.1411	0.4417	0.039*
H12B	0.5553	0.2091	0.3390	0.039*
C13	0.6526 (10)	−0.0440 (9)	0.3564 (6)	0.0333 (17)
H13A	0.6396	−0.0230	0.2869	0.040*
H13B	0.5292	−0.1300	0.3747	0.040*
C14	0.7903 (10)	−0.1281 (9)	0.3687 (5)	0.0352 (18)
H14A	0.8259	−0.1211	0.4395	0.042*
H14B	0.7321	−0.2608	0.3412	0.042*
C15	1.0742 (11)	−0.1178 (12)	0.3200 (6)	0.047 (2)
H15A	1.1834	−0.0461	0.2858	0.071*
H15B	1.0112	−0.2445	0.2862	0.071*
H15C	1.1136	−0.1224	0.3879	0.071*

Atomic displacement parameters (Å^2)

	U^{11}	U^{22}	U^{33}	U^{12}	U^{13}	U^{23}
S1	0.0232 (10)	0.0410 (11)	0.0343 (12)	0.0113 (8)	−0.0003 (8)	−0.0007 (8)
O1	0.033 (3)	0.029 (3)	0.027 (3)	0.011 (2)	−0.001 (2)	0.002 (2)
O2	0.027 (3)	0.031 (3)	0.038 (3)	0.011 (2)	−0.001 (2)	−0.005 (2)
O3	0.031 (3)	0.035 (3)	0.041 (3)	0.016 (2)	0.005 (2)	0.005 (2)
N1	0.031 (4)	0.060 (5)	0.048 (4)	0.021 (3)	0.002 (3)	0.008 (3)
N2	0.043 (4)	0.061 (5)	0.038 (4)	0.032 (4)	0.007 (3)	0.006 (3)
C1	0.021 (4)	0.023 (4)	0.038 (4)	0.007 (3)	0.001 (3)	0.004 (3)
C2	0.024 (4)	0.031 (4)	0.035 (4)	0.013 (3)	0.000 (3)	0.008 (3)
C3	0.026 (4)	0.029 (4)	0.039 (4)	0.015 (3)	0.004 (3)	0.007 (3)
C4	0.025 (4)	0.039 (4)	0.034 (4)	0.015 (3)	−0.002 (3)	0.003 (3)
C5	0.024 (4)	0.037 (4)	0.042 (5)	0.013 (3)	−0.001 (3)	0.007 (4)
C6	0.028 (4)	0.034 (4)	0.033 (4)	0.016 (3)	−0.001 (3)	0.002 (3)
C7	0.031 (4)	0.047 (5)	0.028 (4)	0.020 (4)	0.005 (3)	0.011 (3)
C8	0.032 (4)	0.031 (4)	0.036 (4)	0.013 (4)	−0.001 (3)	0.003 (3)

C9	0.020 (4)	0.032 (4)	0.038 (4)	0.008 (3)	0.002 (3)	0.000 (3)
C10	0.019 (3)	0.024 (4)	0.040 (4)	0.004 (3)	0.004 (3)	0.001 (3)
C11	0.030 (4)	0.033 (4)	0.037 (4)	0.015 (3)	0.002 (3)	0.002 (3)
C12	0.028 (4)	0.041 (4)	0.031 (4)	0.018 (3)	−0.002 (3)	0.000 (3)
C13	0.030 (4)	0.028 (4)	0.040 (4)	0.010 (3)	0.003 (3)	0.003 (3)
C14	0.038 (4)	0.023 (4)	0.037 (4)	0.007 (3)	0.002 (3)	0.000 (3)
C15	0.040 (5)	0.047 (5)	0.058 (6)	0.024 (4)	−0.002 (4)	−0.004 (4)

Geometric parameters (Å, °)

S1—C1	1.749 (7)	C6—H6	0.9500
S1—C9	1.815 (7)	C9—C10	1.500 (10)
O1—C11	1.413 (8)	C9—H9A	0.9900
O1—C10	1.431 (8)	C9—H9B	0.9900
O2—C12	1.429 (8)	C10—H10A	0.9900
O2—C13	1.430 (8)	C10—H10B	0.9900
O3—C14	1.411 (9)	C11—C12	1.483 (10)
O3—C15	1.421 (9)	C11—H11A	0.9900
N1—C7	1.127 (9)	C11—H11B	0.9900
N2—C8	1.158 (9)	C12—H12A	0.9900
C1—C2	1.406 (10)	C12—H12B	0.9900
C1—C6	1.409 (10)	C13—C14	1.515 (10)
C2—C3	1.400 (10)	C13—H13A	0.9900
C2—C7	1.449 (10)	C13—H13B	0.9900
C3—C4	1.395 (10)	C14—H14A	0.9900
C3—C8	1.436 (10)	C14—H14B	0.9900
C4—C5	1.397 (10)	C15—H15A	0.9800
C4—H4	0.9500	C15—H15B	0.9800
C5—C6	1.365 (10)	C15—H15C	0.9800
C5—H5	0.9500		
C1—S1—C9	103.3 (3)	O1—C10—H10B	109.7
C11—O1—C10	112.3 (5)	C9—C10—H10B	109.7
C12—O2—C13	110.3 (5)	H10A—C10—H10B	108.2
C14—O3—C15	111.9 (6)	O1—C11—C12	111.5 (6)
C2—C1—C6	117.7 (6)	O1—C11—H11A	109.3
C2—C1—S1	117.8 (5)	C12—C11—H11A	109.3
C6—C1—S1	124.5 (5)	O1—C11—H11B	109.3
C3—C2—C1	120.9 (6)	C12—C11—H11B	109.3
C3—C2—C7	119.2 (6)	H11A—C11—H11B	108.0
C1—C2—C7	119.8 (6)	O2—C12—C11	108.5 (5)
C4—C3—C2	120.1 (6)	O2—C12—H12A	110.0
C4—C3—C8	120.1 (6)	C11—C12—H12A	110.0

C2—C3—C8	119.8 (6)	O2—C12—H12B	110.0
C3—C4—C5	118.8 (7)	C11—C12—H12B	110.0
C3—C4—H4	120.6	H12A—C12—H12B	108.4
C5—C4—H4	120.6	O2—C13—C14	108.8 (6)
C6—C5—C4	121.5 (6)	O2—C13—H13A	109.9
C6—C5—H5	119.3	C14—C13—H13A	109.9
C4—C5—H5	119.3	O2—C13—H13B	109.9
C5—C6—C1	121.1 (6)	C14—C13—H13B	109.9
C5—C6—H6	119.5	H13A—C13—H13B	108.3
C1—C6—H6	119.5	O3—C14—C13	109.9 (6)
N1—C7—C2	179.6 (9)	O3—C14—H14A	109.7
N2—C8—C3	177.6 (8)	C13—C14—H14A	109.7
C10—C9—S1	109.2 (5)	O3—C14—H14B	109.7
C10—C9—H9A	109.8	C13—C14—H14B	109.7
S1—C9—H9A	109.8	H14A—C14—H14B	108.2
C10—C9—H9B	109.8	O3—C15—H15A	109.5
S1—C9—H9B	109.8	O3—C15—H15B	109.5
H9A—C9—H9B	108.3	H15A—C15—H15B	109.5
O1—C10—C9	109.6 (5)	O3—C15—H15C	109.5
O1—C10—H10A	109.7	H15A—C15—H15C	109.5
C9—C10—H10A	109.7	H15B—C15—H15C	109.5
C9—S1—C1—C2	158.5 (5)	C4—C5—C6—C1	1.0 (11)
C9—S1—C1—C6	−21.6 (7)	C2—C1—C6—C5	0.0 (10)
C6—C1—C2—C3	−1.0 (10)	S1—C1—C6—C5	−179.9 (6)
S1—C1—C2—C3	179.0 (5)	C1—S1—C9—C10	−155.8 (5)
C6—C1—C2—C7	178.5 (6)	C11—O1—C10—C9	178.0 (5)
S1—C1—C2—C7	−1.6 (9)	S1—C9—C10—O1	−68.3 (6)
C1—C2—C3—C4	0.9 (11)	C10—O1—C11—C12	170.0 (5)
C7—C2—C3—C4	−178.6 (6)	C13—O2—C12—C11	−167.7 (6)
C1—C2—C3—C8	−179.0 (7)	O1—C11—C12—O2	−68.6 (7)
C7—C2—C3—C8	1.5 (10)	C12—O2—C13—C14	−179.4 (6)
C2—C3—C4—C5	0.2 (11)	C15—O3—C14—C13	−173.4 (6)
C8—C3—C4—C5	−179.9 (7)	O2—C13—C14—O3	−74.5 (7)
C3—C4—C5—C6	−1.1 (11)		

Appendix B- Letter of Permission

Karen Buehler

RECEIVED

NOV - 7 2008

ACS COPYRIGHT OFFICE

From: S.Sibel Erdem [serdem1@lsu.edu]
Sent: Thursday, November 06, 2008 1:59 PM
To: Copyright
Subject: permission request

> Hello,
>
> Title: Solid-Phase Synthesis of Asymmetrically Substituted "AB3- Type"
> Phthalocyanines, Journal of Organic Chemistry, 73 (13), 5003– 5007,
> 2008 THG
>
> The above-referenced article has been accepteu for publication in the
> Journal of Organic Chemistry. I am the first author and would like
> permission to include the full text, results, discussion, tables and
> figures in my dissertation. Please email me a permission letter if
> this is acceptable.
>
>
>
> Thank you,
>
> S. Sibel Erdem
>
> Department of Chemistry
>
> Louisiana State University
>
> Baton Rouge, Louisiana 70803
>
> Email: serdem1@lsu.edu
>
> Tel: 225-578-4668
> Fax: 225-578-4424
>

American Chemical Society

Publications Division
Copyright Office

1155 Sixteenth Street, NW
Washington, DC 20036
Phone: (1) 202-872-4368 or -4367
Fax: (1) 202-776-8112 E-mail: copyright@acs.org

VIA FAX: 225-578-4424 DATE: November 12, 2008

TO: S. Sibel Erdem, Department of Chemistry
Louisiana State University, Baton Rouge, LA 70803

FROM: C. Arleen Courtney, Copyright Associate C. Arleen Courtney

Thank you for your request for permission to include **your** paper(s) or portions of text from **your** paper(s) in your thesis. Permission is now automatically granted; please pay special attention to the implications paragraph below. The Copyright Subcommittee of the Joint Board/Council Committees on Publications approved the following:

> Copyright permission for published and submitted material from theses and dissertations
> ACS extends blanket permission to students to include in their theses and dissertations their own articles, or portions thereof, that have been published in ACS journals or submitted to ACS journals for publication, provided that the ACS copyright credit line is noted on the appropriate page(s).
>
> Publishing implications of electronic publication of theses and dissertation material
> Students and their mentors should be aware that posting of theses and dissertation material on the Web prior to submission of material from that thesis or dissertation to an ACS journal may affect publication in that journal. Whether Web posting is considered prior publication may be evaluated on a case-by-case basis by the journal's editor. If an ACS journal editor considers Web posting to be "prior publication", the paper will not be accepted for publication in that journal. If you intend to submit your unpublished paper to ACS for publication, check with the appropriate editor prior to posting your manuscript electronically.

If your paper has **not** yet been published by ACS, we have no objection to your including the text or portions of the text in your thesis/dissertation in **print and microfilm formats**; please note, however, that electronic distribution or Web posting of the unpublished paper as part of your thesis in electronic formats might jeopardize publication of your paper by ACS. Please print the following credit line on the first page of your article: "Reproduced (or 'Reproduced in part') with permission from [JOURNAL NAME], in press (or 'submitted for publication'). Unpublished work copyright [CURRENT YEAR] American Chemical Society." Include appropriate information.

If your paper has already been published by ACS and you want to include the text or portions of the text in your thesis/dissertation in **print or microfilm formats**, please print the ACS copyright credit line on the first page of your article: "Reproduced (or 'Reproduced in part') with permission from [FULL REFERENCE CITATION.] Copyright [YEAR] American Chemical Society." Include appropriate information.

Submission to a Dissertation Distributor: If you plan to submit your thesis to UMI or to another dissertation distributor, you should not include the unpublished ACS paper in your thesis if the thesis will be disseminated electronically, until ACS has published your paper. After publication of the paper by ACS, you may release the entire thesis (**not the individual ACS article by itself**) for electronic dissemination through the distributor; ACS's copyright credit line should be printed on the first page of the ACS paper.

Use on an Intranet: The inclusion of your ACS unpublished or published manuscript is permitted in your thesis in print and microfilm formats. If ACS has published your paper you may include the manuscript in your thesis on an intranet that is not publicly available. Your ACS article cannot be posted electronically on a publicly available medium (i.e. one that is not password protected), such as but not limited to, electronic archives, Internet, library server, etc. The only material from your paper that can be posted on a public electronic medium is the article abstract, figures, and tables, and you may link to the article's DOI or post the article's author-directed URL link provided by ACS. This paragraph does not pertain to the dissertation distributor paragraph above. 06/07/06

Vita

Sultan Sibel Erdem was born in Istanbul, Turkey, in February, 1979. She graduated from Marmara University, Istanbul, Turkey, on July 2001, with a Bachelor of Science in chemistry education. During her undergraduate study, she received Turkish Government Prime Ministry Scholarship for four years (1997-2001) for her outstanding undergraduate studies. She taught high school chemistry for two years. In 2002, she received an Excellence in Teaching award for her outstanding teaching over five hundreds high school students. She enrolled at Louisiana State University to pursue her doctorate degree in August 2003, and joined Professor Robert P. Hammer's research group in January 2004. She is the recipient of the Colgate-Palmolive Teaching Award (2006) for excellence in teaching. To date, she has published one paper in the *Journal of Organic Chemistry* and several other manuscripts based on the dissertation are submitted or in preparation. She will receive her Doctor of Philosophy degree in chemistry on May 15th, 2009.